# Gene therapy strategies for Spinal Muscular Atrophy

Thesis submitted for the degree of Doctor of Philosophy at the University of London

by
Ellie Crompton

School of Life Sciences and the Environment
Department of Biological Sciences
Royal Holloway – University of London

July 2020

# Declaration of authorship

I, Ellie Crompton, hereby declare that this thesis and the work presented in it is entirely my own. Where I have consulted the work of others, this is always clearly stated.

Signed:

Date: 8th July 2020

# Acknowledgements

I am extremely grateful for the support from the many people who helped me complete my PhD.

Firstly, I would like to thank my supervisor, Rafael Yáñez-Muñoz, for his guidance in the development of this project and support throughout my time at Royal Holloway. I am also grateful to Philip Chen and Chris Wilkinson for their roles on my review committee. I am thankful to all the other academics at Royal Holloway who have provided help when needed throughout the years.

I would like to very much thank the members of the AGCT lab; Jamuna, Simona, Sahar, Versha, Ioanna, Ben and Katie, who have been present during my PhD, making lab work and office hours so much fun. Members of office 404 have also been a valuable source of enjoyment, encouragement and support, so I would like to thank them, especially Joe, Ellie and Judith. I am also grateful to Rob and all members of staff who make the Department of Biological Sciences run so smoothly.

I would like to thank Theo Hirst for sharing his expertise in pre-clinical meta-analyses, for teaching me these statistical techniques and data interpretation methods, and for his help and support throughout writing the meta-analysis presented here. I would also like to thank Evalyne Muiruri for writing the R script necessary to produce the graphs within the meta-analysis. I am grateful to Ke Ning, Vinay Godena, Melissa Bowerman and Tom Gillingwater who all contributed knowledge, materials or support to my project. Where used, the source of figures and tables from published literature were cited and permissions to use these were obtained.

I was very lucky to be granted a financial scholarship from Royal Holloway and funding from Hobson Charity Ltd, without which I would not have been able to complete my PhD, so for these generous donations I am extremely grateful.

Finally, I am indebted to my family for their love and support over the past three years. You have provided financial and emotional support and a place I could always de-stress. Sam, I could not have gone through this process without you by my side; cheering me up after a hard day in the lab, chattering about western blots like you know what one is and encouraging me to pursue my dreams.

# Abstract

Spinal muscular atrophy (SMA), the most common genetic disorder resulting in infantile death, is caused by defective production of the Survival Motor Neuron (SMN) protein encoded by *SMN1,* leading to degeneration of motor neurons (MNs) and neuromuscular dysfunction within months of birth in the most severe cases. Two licensed treatments are now available; one antisense oligonucleotide and one adeno-associated virus serotype 9 (AAV9) encoding *SMN1*. The pre-clinical development of these two therapies was investigated here in a systematic review and meta-analysis, showing an overall significant improvement in survival following the treatment of SMA models with these agents. Integration-deficient lentiviral vectors (IDLVs) are highly efficient tools for delivering therapeutic genes, representing an alternative therapeutic avenue. This thesis describes the *in vitro* characterisation of IDLVs expressing codon-optimised *SMN1* under three transcriptional controls (CMV, hSYN, hPGK). Neuronal cell lines and severe SMA fibroblasts showed significantly increased SMN protein levels following transduction with IDLVs, as well as significant increases in gem numbers (an endpoint suggestive of functional *SMN1* expression). Since MNs are the primary pathological target of SMA, a protocol to differentiate human induced pluripotent stem cells (iPSCs) to MNs was implemented, showing high transduction of the resulting MNs. SMA iPSC MNs recapitulate *in vivo* characteristics and hallmarks of SMA disease. It was possible to rescue SMN production to supraphysiological levels following transduction with IDLVs, something that was not able to be achieved using an AAV9 encoding an equivalent cassette. Moreover, IDLVs were able to restore gemin proteins in mutant MNs as well. Finally, the extent of DNA damage and apoptosis was examined in SMA cells, as well as attempting to rescue these with IDLV transduction. These findings suggest that IDLVs may be particularly effective tools and could be useful for novel SMA gene therapy approaches.

# Table of contents

# Index of figures

# Index of tables

# Abbreviations

| | |
|---|---|
| γH2AX | Phosphorylated H2A histone family member X |
| AAV | Adeno-associated virus |
| ACh | Acetylcholine |
| AChR | Acetylcholine receptor |
| Ad | Adenovirus |
| ALS | Amyotrophic lateral sclerosis |
| ASO | Antisense oligonucleotide |
| ATM | Ataxia Telangiectasia Mutated |
| BBB | Blood brain barrier |
| BDNF | Brain derived neurotrophic factor |
| bGH | Bovine growth hormone |
| BMP | Bone morphogenetic protein |
| bp | Base pairs |
| BSA | Bovine serum albumin |
| CAG | Chicken beta actin CMV hybrid promoter |
| CBA | Chicken beta actin |
| ChAT | Choline acetyltransferase |
| CHO | Chinese hamster ovary cell line |
| CHOP-INTEND | Children's Hospital of Philadelphia Infant Test of Neuromuscular Disorders |
| CI | Confidence interval |
| CMV | Cytomegalovirus |
| CNS | Central nervous system |
| CNTF | Ciliary neurotrophic factor |
| *Co-hSMN1* | Codon-optimised human *Survival Motor Neuron 1* |
| Cre | Cyclization recombinase enzyme |
| CRISPR | Clustered regularly interspaced short palindromic repeats |
| DAPI | 4,6-diamidino-2-phenylindole |
| DDR | DNA damage response |
| df | Degrees of freedom |
| DMEM | Dulbecco's modified Eagle's medium |
| DMSO | Dimethyl sulfoxide |
| DNA-PKcs | DNA protein kinase catalytic subunit |
| ds | Double stranded |
| DSB | Double strand break |
| E15 | Embryonic day 15 |
| EDTA | Ethylenediaminetetraacetic acid |
| EGF | Epidermal growth factor |
| eGFP | Enhanced green fluorescent protein |
| EMA | European Medicines Agency |
| Env | Envelope |
| ESC | Embryonic stem cell |
| ESE | Exonic splicing enhancer |
| FACS | Fluorescent associated cell sorting |
| FBS | Fetal bovine serum |
| FDA | US Food and Drug Administration |
| FGF2 | Fibroblast growth factor 2 |
| FL-SMN | Full length survival motor neuron |
| FMO | Fluorescent minus one |
| Gag | Group specific antigen |
| GDNF | Glial derived neurotrophic factor |
| H2AX | H2A histone family member X |

| | |
|---|---|
| HB9 | Homeobox 9 |
| HBSS | Hank's balanced salt solution |
| HDACi | Histone deacetylase inhibitor |
| HDR | Homology directed recombination |
| HEK293T | Human embryonic kidney cell line, SV40 large T-antigen |
| HEPES | 4-(2-hydroxyethyl)-1-piperazineethanesulfonic acid |
| HFMSE | Hammersmith Functional Motor Scale Expanded |
| HINE-2 | Hammersmith Infant Neurological Examination section 2 |
| HIV | Human immunodeficiency virus |
| hnRNP | Heterologous nuclear ribonucleoprotein |
| hPGK | Human phosphoglycerate kinase promoter |
| hPSC | Human pluripotent stem cell |
| HR | Homologous recombination |
| HSV | Herpes simplex virus |
| hSYN | Human Synapsin promoter |
| ICV | Intracerebroventricular |
| IDLV | Integration deficient lentiviral vector |
| IGF | Insulin-like growth factor |
| IM | Intramuscular |
| IP | Intraperitoneal |
| IPLV | Integration proficient lentiviral vector |
| iPSC | Induced pluripotent stem cell |
| IS | Intraspinal |
| ISS-N1 | Intronic splicing sequence-N1 |
| IT | Intrathecal |
| ITR | Inverse terminal repeat |
| IUGT | *In utero* gene therapy |
| IV | Intravascular |
| kB | Kilo base |
| kDa | Kilo-Dalton |
| LB | Luria-Bertani |
| LDLR | Low density lipoprotein receptor |
| LRT | Late reverse transcript |
| LTR | Long terminal repeats |
| LV | Lentiviral vector |
| MN | Motor neuron |
| MNP | Motor neuron progenitor |
| MO | Morpholino oligonucleotide |
| MOI | Multiplicity of infection |
| MSR | Median survival ratio |
| nAChR | Nicotinic acetylcholine receptor |
| NHEJ | Non-homologous end joining |
| NMJ | Neuromuscular junction |
| nt | Nucleotide |
| OLIG2 | Oligodendrocyte transcription factor 2 |
| ORF | Open reading frame |
| P1 | Post-natal day 1 |
| pATM | Phosphorylated ATM |
| PBS | Phosphate buffered saline |
| PCR | Polymerase chain reaction |
| PFA | Paraformaldehyde |
| PFU | Plaque forming unit |
| PMO | Phosphorodiamidate morpholino |
| Pol | Polymerase |
| qPCR | Quantitative polymerase chain reaction |

| | |
|---|---|
| RA | Retinoic acid |
| RIPA | Radioimmunoprecipitation assay buffer |
| RRE | Rev responsive element |
| RT | Reverse transcriptase |
| RT-PCR | Reverse transcriptase PCR |
| SAG | Smoothened agonist |
| SC | Subcutaneous |
| scAAV | Self-complementary adeno-associated viral vector |
| SDS | Sodium dodecyl sulfate |
| SDS-PAGE | Sodium dodecyl sulfate-polyacrylamide gel electrophoresis |
| SHH | Sonic hedgehog |
| SIN | Self-inactivating |
| SMA | Spinal muscular atrophy |
| SMI-32 | Neurofilament H |
| SMN | Survival motor neuron |
| SMNΔ7 | Survival motor neuron lacking exon 7 |
| snRNP | Small nuclear ribonucleoprotein |
| ss | Single stranded |
| ssAAV | Single stranded adeno-associated viral vector |
| SSB | Single stranded break |
| SSEA1 | Stage-specific embryonic antigen 1 |
| SSEA3 | Stage-specific embryonic antigen 3 |
| TAE | Tris-acetate EDTA buffer |
| TBS | Tris buffered saline |
| TE | Tris-EDTA |
| vg | Vector genomes |
| VSV-G | Vesicular stomatitis virus glycoprotein G |
| WPRE | Woodchuck hepatitis post-transcriptional regulatory element |
| WT | Wild type |

# 1 Introduction

## 1.1 Spinal muscular atrophy

Spinal muscular atrophy (SMA) is a neuromuscular disease chiefly characterised by degenerating alpha motor neurons (MNs) caused by defects in the gene *Survival Motor Neuron 1* (*SMN1*; see section 1.1.1 regarding genetics) (Lefebvre et al., 1995). SMA mostly affects children, with symptoms including muscle weakness, areflexia, difficulty swallowing and feeding, and in the most severe cases is fatal. MN loss results in atrophy of skeletal muscles, paralysis and denervation of neuromuscular junctions (NMJs) (Bowerman et al., 2017), with infantile death most commonly attributed to respiratory failure (Farrar et al., 2017). Although MNs are the cells primarily affected in this disease, we are becoming increasingly aware that systemic pathology exists. Systemic abnormalities such as cardiac defects (Wijngaarde et al., 2017) are beginning to be reported more widely, with an increasing number of body systems seeming to be involved.

SMA was first described in 1890 (Werdnig, 1890) and again the following year (Hoffman, 1891), where children presented with muscle weakness in the early months of their life. Later, a more mild form of the disease was also recorded (Kugelberg and Welander, 1956). These descriptions were the basis of the current types we use to classify SMA today (Table 1.1) that were agreed by international consensus and presented at the 1992 International SMA consortium meeting (Munsat and Davies, 1992). Type I SMA (also known as Werdnig-Hoffman disease) is the most severe form of the disease where children are affected from birth, requiring invasive ventilation and succumb to the disease by the age of two if left untreated. Type II and III (III: Kugelberg-Welander disease) are less severe forms where children are physically disabled (type II can sit unsupported but never walk, type III may acquire ability to walk unaided) but are able to live a relatively normal lifespan. Type IV onset occurs in adulthood where ambulation is maintained. A final class of SMA (type 0) can also be classified, however this exists with *in utero* onset and fetal death.

| | Type of SMA | | | | |
|---|---|---|---|---|---|
| | 0 | I | II | III | IV |
| ***SMN2* copy number*** | 1 | 2 | 3 | 3-5 | 3-5 |
| **Age of onset** | *In utero* | Majority by 6 months | 6-12 months | After 18 months (IIIa: <3 years, IIIb: >3 years) | Adulthood |
| **Key clinical features** | Widespread motor and sensory neuronal loss<br>Contractures<br>High incidence of congenital cardiac defects | Neonatal hypotonia<br>Poor feeding and head control<br>Respiratory insufficiency<br>Never develop ability to roll or sit unaided | Sit unsupported<br>Never walk<br>Respiratory muscle weakness | Walk unaided, even if briefly | Progressive proximal weakness<br>Lower limb predominance |
| **Natural history** | Peri-natal death | 50% death by 12 months<br>90% death by 24 months without invasive ventilation | Life expectancy 30-50 years depending on respiratory function | Loss of ambulation very variable (from childhood to late life)<br>Respiratory involvement uncommon<br>Life expectancy near normal | Slow progression<br>Ambulation maintained<br>Normal lifespan |

*All SMA patients, regardless of type have no functional copies of *SMN1*; the number of *SMN2* copies in unaffected individuals (carriers or non-carriers) can range from 2 to 5.

***Table 1.1 Classification of spinal muscular atrophy types.***

*SMA is classified into five sub-types based on* SMN2 *copy number and clinical presentation of the disease. Type 0 is the most severe form of SMA and as this results in fetal death, this type is sometimes not considered as one of the main clinical types of SMA. Types I-IV decrease in severity whilst increasing in the number of* SMN2 *copies and a range of symptoms can be seen in these types. Taken from Bowerman et al. (2017).*

### 1.1.1 Genetics of SMA

SMA is the second most common autosomal recessive disease after Cystic Fibrosis (Monani, 2005) and is also the most common genetic disease resulting in infantile death (Bowerman et al., 2017). Despite these statistics stating that this disease is common, SMA actually has rare disease status due to the fact it only affects 1 in 6000 births, with a 1 in 50 carrier rate (Pearn, 1980), a lower incidence rate than the 1 in 2000 needed for official rare disease classification (Rare Disease UK, 2020). Alternative, less common, forms of SMA without an autosomal recessive inheritance pattern do exist, but these are caused by mutations in genes other than *SMN1*. Autosomal dominant (Oates et al., 2012) and X linked forms (Dressman et al., 2007) are examples and are caused by mutations in the *TRPV4* and *UBA1* genes, respectively. These have been included here for completeness, but will not be the subject of this project.

The genetics of SMA were researched thoroughly in the early 1990s. Linkage analysis by several groups (e.g. Gilliam et al. (1990), Melki et al. (1990), Sheth et al. (1991) and others) revealed the SMA disease locus resided in the 5q13 region within a 500kb inverted duplication (Figure 1.1). The causative gene for SMA was identified and characterized soon after (Lefebvre et al., 1995). Lefebvre and colleagues narrowed the critical region in progressive steps to a 20kb telomeric

fragment where a candidate gene, which they named *SMN* for survival of motor neurons, was found to be absent in 93% of SMA patients. *SMN* was predicted to encode a novel 294 amino acid, 38kDa protein with no homology to already known proteins. Upstream *(*Figure 1.1), a duplicated centromeric form of this gene was found with only five differences in genomic sequence. Later these genes were re-named with the telomeric gene called *SMN1* and centromeric gene *SMN2*.

Within *SMN2*, a translationally-silent C to T mutation 6bp into exon 7 results in an alternatively spliced, truncated transcript known as *SMNΔ7 (*Figure 1.1), which, when translated, leads to a protein with a different C-terminus. Specifically, the C to T transition is necessary and sufficient to induce *SMNΔ7* production by disrupting a *cis*-acting exonic splicing enhancer (ESE) in exon 7 (Lorson et al., 1999, Monani et al., 1999) that normally promotes the inclusion of this exon. This disruption leads to the increased production of *SMNΔ7*, at the expense of full-length transcripts. Reciprocally, the correction of the T nucleotide back to C, rescues the production of full-length *SMN2* transcripts. *SMN2* pre-mRNA splicing is particularly complex with combinatorial action of both splice enhancers and silencers. A naturally occurring intronic splicing silencer located immediately downstream of the 5' splice site in intron 7 of *SMN2*, known as ISS-N1, also acts as a limiting factor for exon 7 inclusion. Negative splice factors such as hnRNPA1 and hnRNPA2 bind to ISS-N1 and prevent recognition of exon 7 by splicing machinery, resulting in its exclusion. The combination of the C to T transition disrupting the ESE that normally promotes exon 7 inclusion, as well as the strong inhibitory influence of the ISS-N1, leads to 90% of transcripts from *SMN2* lacking exon 7.

Northern blot analysis found the presence of a full length 1.7kb mRNA transcript encoded by *SMN1* in various tissues, within wild type samples, which also showed far less abundant truncated transcripts (Lefebvre et al., 1995). SMA patients showed a decrease in total RNA, the vast majority of which were truncated transcripts. The final hypothesis from Lefebvre and colleagues suggested that if this truncated transcript was translated to form a partially functional protein, there may be a gene dosage effect from *SMN2* responsible for delineating the SMA type I-III phenotypes.

95% of SMA patients show deletions of *SMN1* with the remaining 5% carrying mutations in this gene. Homozygous deletions or mutations cause no SMN protein

production from *SMN1*, however this can be partially compensated for by *SMN2.* As stated above, *SMN2* is alternatively spliced 90% of the time, resulting in a truncated protein which is rapidly degraded, however a very small amount of full-length protein is produced and is sufficient for survival. A study determined that approximately 15% of normal Smn acted as a threshold for survival in a mouse model, a level that could be achieved with two copies of *SMN2* (Bowerman et al., 2012). Both SMN and SMNΔ7 are normally degraded by the ubiquitin proteasome system, but via pulse-chase labelling, it has been found that degradation of SMNΔ7 occurs twice as fast as full length SMN (Burnett et al., 2009). The extent to which *SMN2* can rescue the SMA phenotype is tightly correlated to *SMN2* copy number. The genomic region in which these two genes lie has a complex organisation and is very unstable (Monani, 2005) causing variable copy numbers of the *SMN2* gene between individuals (Schmutz et al., 2004). So, as Lefebvre and colleagues predicted, *SMN2* copy number does play a vital role in SMA phenotypes.

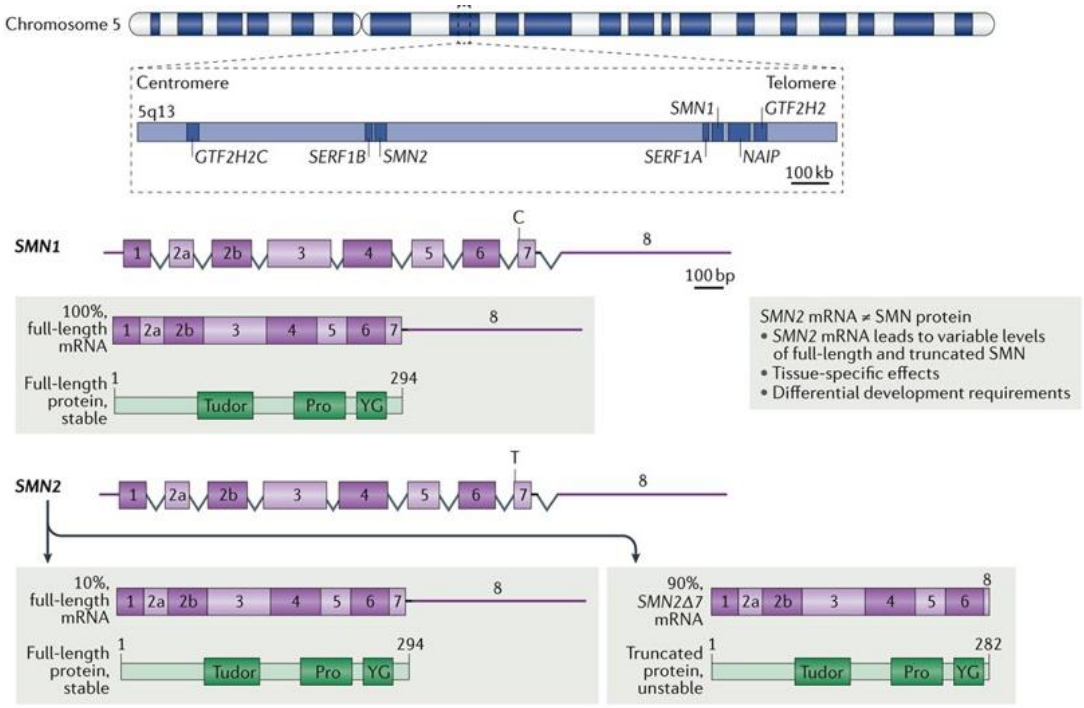


***Figure 1.1 Genetics of SMA.***

SMN1 *(telomeric) and* SMN2 *(centromeric) are located at the 5q13 locus and are encoded by 8 exons.* SMN1 *and* SMN2 *vary by only five nucleotide differences, the most important of which being a C to T transition 6bp in exon 7. This transition causes alternative splicing of the transcript encoded by* SMN2*, the formation of an exonic splice suppressor and the exclusion of exon 7 from 90% of mRNA transcripts, which when translated form a truncated, unstable protein. Adapted from (Groen et al., 2018).*

*In situ* hybridisation data from early studies showed widespread *SMN* expression in the CNS of humans, rats and monkeys (Battaglia et al., 1997). Signals were particularly strong in the ventral horn of the spinal cord and in specific neuronal subpopulations such as pyramidal neurons in layer V of the neocortex and MNs in the brainstem and spinal cord. Subcellular localisation of *SMN* transcript was located predominantly in the cytoplasm of neurons. This neuroanatomical data was the first link between *SMN* expression and the cells degenerating in SMA. Developmentally, SMN expression can be detected as early as 13 weeks gestation in human fetal forebrain and spinal cord samples with particularly intense signals within spinal cord anterior horn MNs and the basal nucleus of Meynert (a major source of cholinergic afferents to the cortex) (Briese et al., 2006).

#### 1.1.1.1 *SMN* homologues

*SMN1* homologues exist in all vertebrate species, but it has been found that *SMN2* is unique to humans (Lorson et al., 2011) and bonobos only (Swoboda, 2014). The murine homolog of *SMN1* was discovered in 1997 by three groups (Bergin et al., 1997, DiDonato et al., 1997, Viollet et al., 1997) all presenting data showing the same key information. Mouse *Smn* is located on chromosome 13, has 82% DNA sequence identity to *SMN1*, expresses a 1.3kb transcript encoding a 288 amino acid protein with 31.3kDa molecular weight. These groups also proved that only one *Smn* gene was present and that no alternative splicing was found. Later it was found that homozygous deletion of *Smn* is embryonic lethal (Schrank et al., 1997) due to the lack of a *SMN2* homolog, thus a simple knockout could not be used to mimic SMA in humans.

*SMN* homologues in other animal species have been studied to create models of SMA across multiple species. *Drosophila melanogaster Smn* exhibits 41% sequence homology and is found to cause a dominant negative developmental arrest or pupal lethality if expressed in a truncated form (Miguel-Aliaga et al., 2000), highlighting the necessity of *Smn* for *Drosophila* survival (Edens et al., 2015). Zebrafish (*Danio rerio*) have been popular SMA models due to a simple, but conserved nervous system (Edens et al., 2015). The *smn* gene was mapped using a radiation hybrid panel (Hukriede et al., 1999) and its expression has been confirmed as ubiquitous by *in situ* hybridisation (McWhorter et al., 2003). Furthemore, antisense morpholino knockdown of *smn* can recapitulate MN defects seen in SMA patients (McWhorter et al., 2003). Finally, non-human primates,

specifically chimpanzees, have been shown to have 2-7 copies of a *SMN* homolog per diploid genome and do not exhibit any signs of a *SMNΔ7*-like transcripts (Rochette et al., 2001), confirming the lack of *SMN2* in species other than humans.

### 1.1.2 Functions of the SMN protein

*SMN* encodes a 294 amino acid protein of approximately 38kDa (Monani, 2005). This protein has multiple domains including a nucleic acid and Gemin2 binding domains in the N terminal region (Figure 1.2A). Mutations have been mapped to all regions of the protein, suggesting that a specific tertiary structure is necessary for proper function (Singh et al., 2017c). SMN localises to both the nuclear and cytoplasmic compartments of the cell; in gems and associated with proteins such as coilin in Cajal bodies within the nucleus, and associated with microtubules and the Golgi network in the cytoplasm (Singh et al., 2017c). SMN oligomerisation (Monani, 2005) has been shown to be mediated by self-association domains encoded by exons 2 (Young et al., 2000), 6 (Lorson et al., 1998) and 7 (Burnett et al., 2009). Deletion of these exons reduces SMN protein stability, suggesting these oligomerisation domains are important for stability (Burnett et al., 2009), perhaps explaining why SMNΔ7 is degraded faster than its full length counterpart. Within development, SMN may have different roles than postnatally, as at least one isoform of the protein, axonal-SMN (a-SMN) has a different temporal expression pattern. The a-SMN isoform is encoded by *SMN1*, but differs from *FL-SMN1* transcripts due to retention of intron 3 caused an alternative splicing event (Setola et al., 2007). An in-frame stop codon within this intron leads to premature termination and a shorter splice variant (Locatelli et al., 2012). a-SMN has been shown to promote axonal growth, cell motility and regulation of chemokine and growth factor expression, but after birth this isoform is degraded by the nonsense mediated decay pathway (Locatelli et al., 2012).

SMN is a ubiquitously expressed protein that has many roles (Figure 1.2B), including well established housekeeping functions such as those involved in RNA metabolism. However, SMN is also involved in other processes such as cytoskeletal maintenance, transcription, translation, cell signaling, DNA repair and telomerase functions (Singh et al., 2017c). Although expressed in all cells, as well as the ubiquitous functions mentioned above, the extreme vulnerability of MNs to a lack of SMN is still largely not understood. It has been proposed that MN specific pathways (Monani, 2005), aberrant in SMA may account for this vulnerability, or that the

variety in tissue-specific vulnerability may be due to different abundance of SMN's interacting partners in each tissue (Singh et al., 2017c). Just some of these binding partners include small nucleolar ribonucleoproteins, RNA helicase A, RNA polymerase II, fibrillarin and profillin (Monani, 2005).

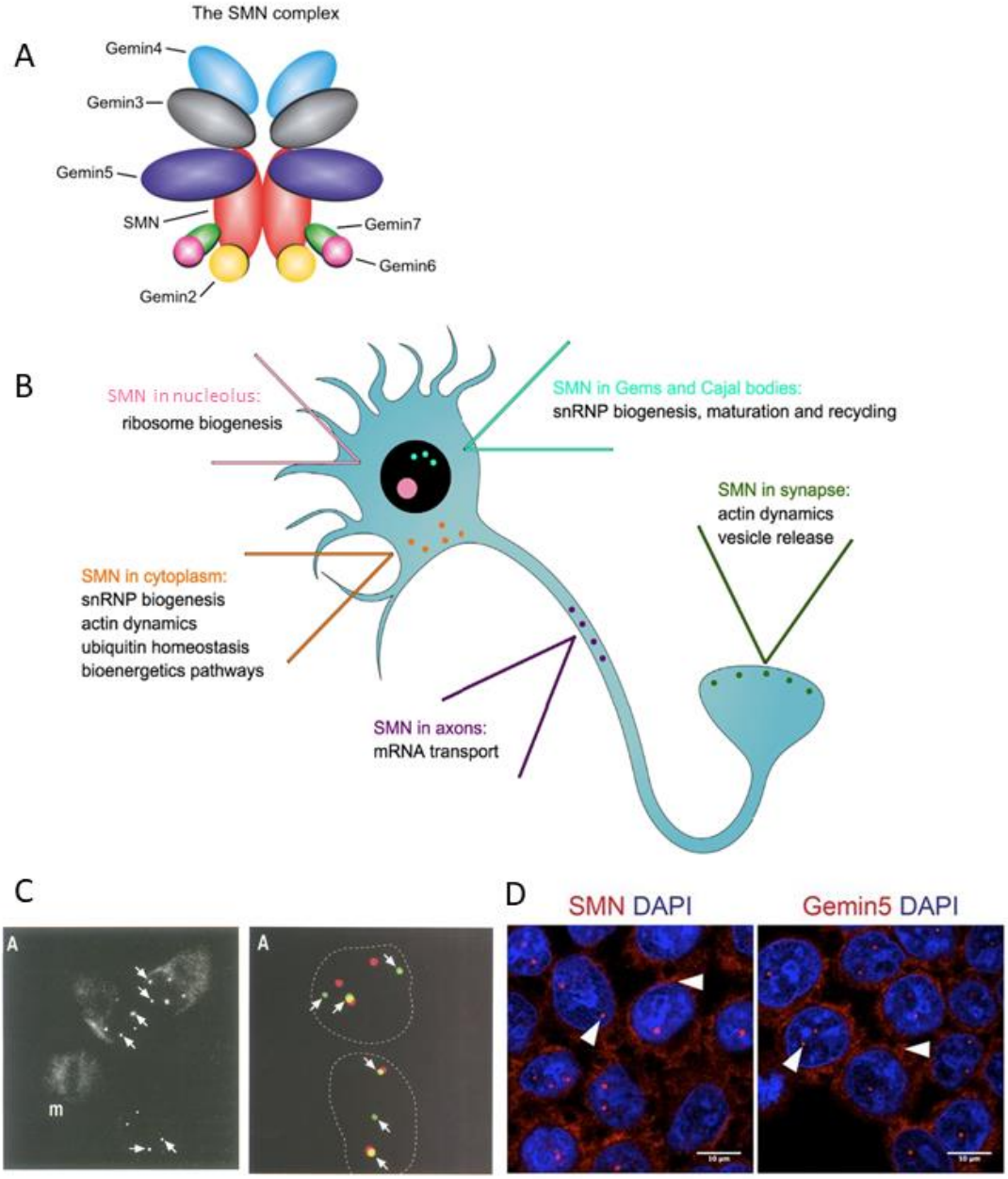


***Figure 1.2 SMN protein and its cellular functions.***

*(A) The SMN protein exists in a multiprotein complex with Gemin2-7 and a model representation of this based on protein interaction evidence is shown here, adapted from Gubitz et al. (2004). (B) Within the motor neuron, the SMN protein has many roles in different cellular compartments, such as small nuclear ribonucleoprotein (snRNP) biogenesis, perhaps the most well characterised role of SMN; adapted from Bowerman et al. (2017). (C) HeLa cells in which gems (labelled with arrows) were first identified with an antibody against SMN; gems are not visible in cells undergoing mitosis, labelled m (left image). Gems (labelled with arrows) often are*

*seen in very close proximity to Cajal bodies, but these are not the same structure (green = SMN, red = coilin in Cajal bodies, right image); adapted from Liu and Dreyfuss (1996). (D) Gems can now be identified with antibodies against SMN and gemin proteins (arrowhead represent SMN cytoplasmic and nuclear gem localisation); adapted from Prusty et al. (2017).*

Perhaps the most studied binding partners of SMN are the gemin proteins, so much so that an alternative name for SMN is Gemin1. The nuclear localisation of SMN protein was first identified in 1996 (Liu and Dreyfuss, 1996) where immunofluorescence of HeLa cells showed dot-like foci in the nucleus (Figure 1.2C). These foci appeared in similar sizes and numbers as Cajal bodies, however they were not the same, even though these two structures could often be found adjacent to, or in contact with one another (Figure 1.2C) (Liu and Dreyfuss, 1996). This novel nuclear structure was termed a "gem" due to the fact that they appeared like a twin, or gemini, of the Cajal body. It is true that SMN localises to Cajal bodies during snRNP biogenesis (discussed below), but this nuclear structure is more complex than a gem as it contains other proteins such as coilin. Within gems, multiple gemin proteins were later identified largely by the Dreyfuss laboratory; Gemin 2 (Liu et al., 1997), Gemin 3 (Charroux et al., 1999, Campbell et al., 2000), Gemin 4 (Charroux et al., 2000), Gemin 5 (Gubitz et al., 2002), Gemin 6 (Pellizzoni et al., 2002) and Gemin7 (Baccon et al., 2002). Now, antibodies against multiple gemin proteins, or SMN itself, can detect these nuclear structures (Figure 1.2D).

SMN and gemin proteins form gem complexes within the nucleus and together participate in SMN's most studied housekeeping role: RNA metabolism and more specifically spliceosomal small nuclear ribonucleoprotein (snRNP) assembly. SMN and gemin proteins form an assemblysome within the cytoplasm with snRNAs. snRNAs recognise critical splice signals at 5' and 3' ends of introns, acting as guides for splicing machinery. The assemblysome then further binds with immature heptameric Sm rings, which surround the snRNA molecule. The snRNP (now consisting of SMN, gemins 2-7, snRNAs and an Sm ring) translocates back to the nucleus to undergo final maturation steps within the Cajal body (Monani, 2005, Singh et al., 2017c). The mature snRNP then binds to pre-mRNA transcribed from any gene to form what is known as the spliceosome. This whole process is important and necessary for the cell because snRNP biogenesis is critical for the removal of introns from pre-mRNA and thus highlights SMN's critical role in splicing regulation. Furthermore, a correlation has been found between the degree of disrupted snRNP biogenesis and clinical severity of SMA (Gabanella et al., 2007).

SMN also has many other roles. These include a role in homologous recombination in DNA repair where SMN interacts with Gemin2 and RAD51 to promote homologous DNA strand pairing and exchange (Takaku et al., 2011). SMN has a prominent role when regulating the actin cytoskeleton through interactions with Profillin2a (Giesemann et al., 1999), an actin-binding protein found in neurons, the RhoA/ROCK pathways (Nölle et al., 2011) and Plastin3 (Delanote et al., 2005), all of which have been implicated in SMA pathology or as disease modifiers (Oprea et al., 2008). SMN has a role in ubiquitin homeostasis and this pathway is strongly dysregulated in SMA where UBA1, an E1 ubiquitin-activating enzyme (Ramser et al., 2008), levels are depleted causing accumulation of its downstream targets including β catenin (Wishart et al., 2014). Targeting of UBA1 may be a promising therapeutic avenue (Powis et al., 2016).

### 1.1.3 Pathophysiology

Despite the many roles of the SMN protein that have been described above and elsewhere, still the pathophysiology of this disease is not fully understood. However, SMA pathophysiology is known to involve defects in axonal transport and functionality of small nuclear RNAs, leading to aberrant pre-mRNA splicing and subsequently transcriptional dysregulation of genes involved in synaptogenesis and NMJ maintenance (Zhang et al., 2013). However, further work is required to gain a deeper understanding of why MNs are particularly susceptible when SMN is ubiquitously expressed (Monani, 2005) and systemic damage to peripheral tissues such as the heart and liver exists (Bowerman et al., 2017). Propositions that SMN deficiency causes a vulnerability-resistance spectrum along which all body tissues are located, place MNs at the very extreme of vulnerability (Sleigh et al., 2011), but it is unclear why.

#### 1.1.3.1 Motor neuron specific pathophysiology

MN pathology is a hallmark feature of SMA and is present in all patients. It is likely that MN-specific and non-neuronal cellular pathways combined cause the overt MN pathology seen in SMA patients and animal models. Theories have been proposed to explain the vulnerability of MNs. One example regards disrupted axonogenesis (Hamilton and Gillingwater, 2013) that potentially could be caused by deficient SMN/hnRNP-R-mediated delivery of β-actin to pre-synaptic sites (Mourelatos et al., 2001). This may be linked to SMN's protein trafficking role which has been

evidenced by bi-directional SMN-positive puncta moving along axons (Zhang et al., 2003). Lower levels of β-actin mRNA in primary motor neurons from severe Taiwanese model mice (discussed in section 1.3.2.1) correlated with a three-fold reduced growth cone size (Rossoll et al., 2003), highlighting axonal defects.

Pathologies associated with motor function can be found not only within the MNs themselves, but also at sites closely linked, such as the NMJ. Neuromuscular pathology has been found to occur prematurely to MN loss in SMA patients (Swoboda et al., 2005) and model mice (Murray et al., 2008). NMJ pathologies include a loss of nerve terminals with accumulation of neurofilament proteins in any remaining units, as well as impaired neurotransmitter release and improper maturation of post-synaptic acetylcholine receptor (AChR) clusters (Kong et al., 2009).

#### 1.1.3.2 Systemic nature of SMA

SMN depletion specifically in MNs does not lead to an SMA phenotype *in vivo*, instead presenting with dystrophic qualities (Park et al., 2010). This strengthens the argument that SMA is a systemic disease, and a lack of the ubiquitous SMN protein, does lead to disease pathogenesis in non-MN tissues. Here, the most common and well studies non-MN pathologies will be discussed (Figure 1.3), but other pathologies have been reported in a small number of publications and can also be found in Figure 1.3.

As stated above, NMJ pathology exists because MNs are closely linked to the musculature that they innervate. A reciprocal relationship between these cell types occurs where muscles secrete neurotrophic factors to promote MN neurite outgrowth towards potential NMJ sites, supporting MN survival, whilst the MNs themselves promote muscle connections by secreting neuregulin and agrin to increase AChR synthesis (Guo et al., 2010). Muscle tissue pathology in SMA is prevalent with delayed muscle growth in severe SMA fetuses (Martinez-Hernandez et al., 2009), represented by small myotubes, which correlates with reduced proliferative rate and fusion defects seen in myoblasts (Shafey et al., 2005). However, muscle defects are not consistently seen across all SMA models, as evidenced by a lack of muscle differentiation defects in zebrafish (McWhorter et al., 2003).

The second most prevalent body system to display pathological features is the cardiovascular system. Arrythmias (most commonly bradycardia) and dilated cardiomyopathy have been reported in both patients (Rudnik-Schoneborn et al., 2008) and in mouse models (Bevan et al., 2010). Vascular defects such as necrosis of digits in patients (Araujo et al., 2009, Rudnik-Schoneborn et al., 2010) or tails and ear tissue (Hsieh-Li et al., 2000, Passini et al., 2010, Foust et al., 2010, Valori et al., 2010) in SMA mouse models, respectively, have been observed. These phenotypes are more often seen following invasive ventilation or survival-prolonging treatment, suggesting these may be later emerging phenotypes that are not seen in untreated animals that succumb to the disease before their appearance.

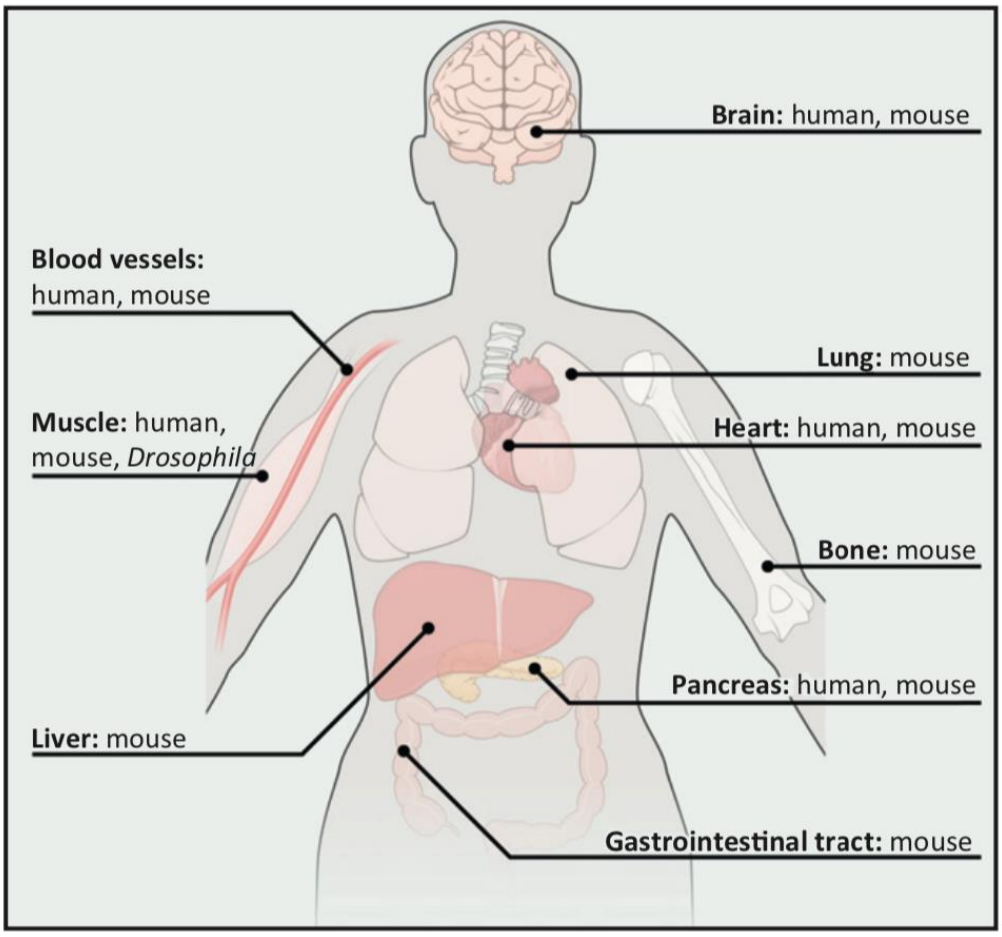


***Figure 1.3 Systemic pathologies known to be present in SMA.***

*Various non-neuronal pathologies have been found in SMA patients and animal models of SMA disease. Models in which each pathology has been identified are indicated. Taken from Hamilton and Gillingwater (2013).*

### 1.1.4 Treatments and emerging therapeutic strategies

Two treatments are now licensed for administration in the clinic to SMA patients, but many others are still in development at various stages of pre-clinical research and clinical trials (Figure 1.4). Within SMA therapeutic development, three strategies are simultaneously being developed; these are known as SMN-dependent, SMN-independent and SMN-plus strategies. The first of these strategies aims to augment SMN protein using viral vectors or correcting the aberrant splicing of *SMN2* to enhance full length SMN protein production (either using antisense oligonucleotides, or small molecules), generally taking into consideration the development of SMA and the body's normal SMN requirements (Figure 1.5).

The age at which a therapy is administered is crucial when determining potential therapeutic benefit. The requirement for SMN protein greatly increases during embryonic development and then remains plateaued at a high level during infancy (Figure 1.5). This highlights a time when neuromuscular maturation is occurring and infants are growing at a fast rate, and also when symptoms present in the most severe SMA patients. Thus, implementing SMN augmentation strategies here may have a larger benefit than later in life after these events have already occurred.

The second and third strategies aim to identify non-SMN targets for therapeutic intervention that can either be targeted alone, or in combination with SMN-dependent therapeutics. These often aim to provide supportive care to prevent SMA hallmarks such as neuromuscular degeneration, for example SRK-015 which (Figure 1.4) targets myostatin to prevent muscle atrophy.

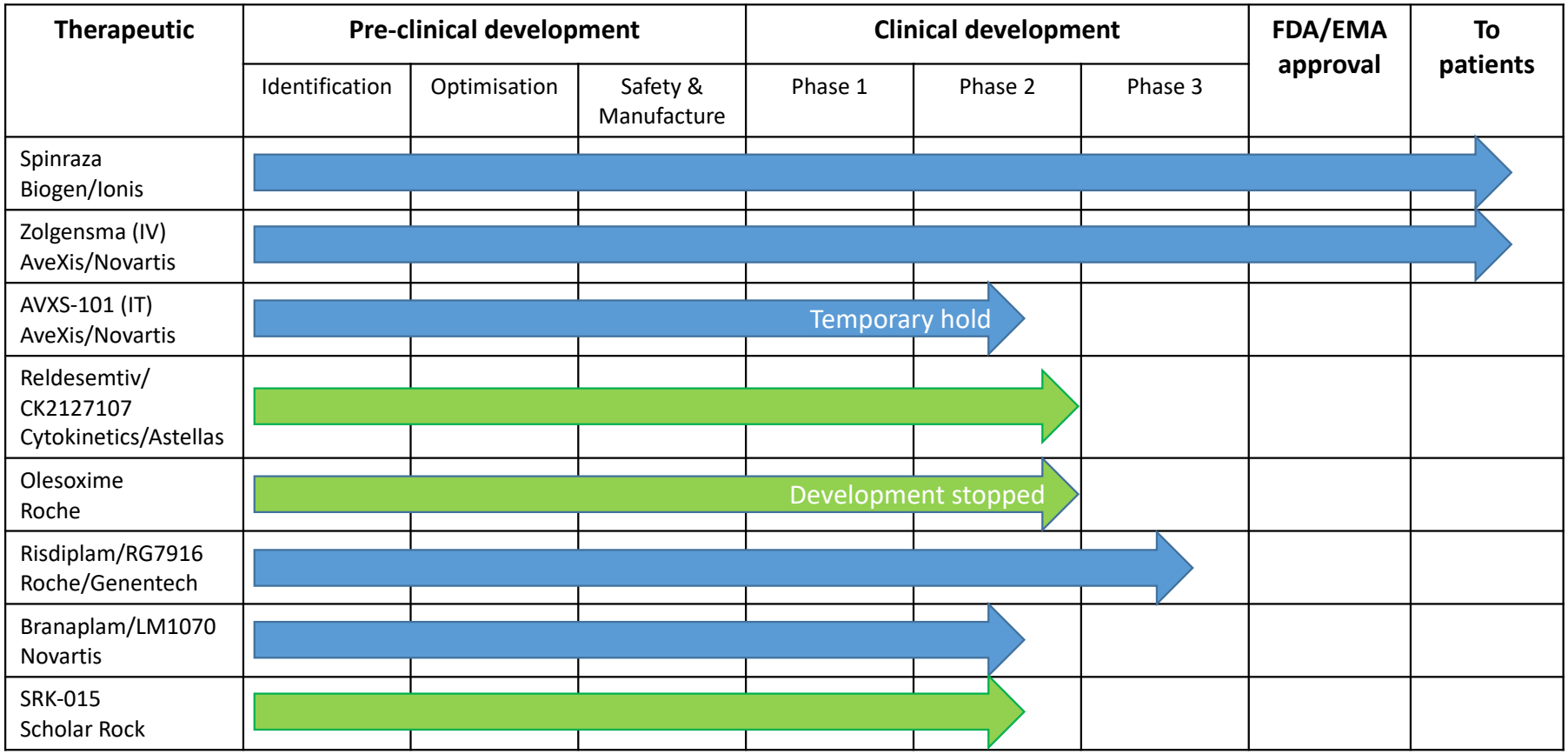


***Figure 1.4 The pipeline of SMA therapies in clinical development.***

*A substantial number of therapeutic strategies are in development for SMA with those in clinical development shown here. Spinraza and Zolgensma are the only two therapies licensed for administration in the clinic, whilst others are at various stages of clinical trials. A temporary hold has been placed on AVXS-101 delivered directly to the central nervous system due to toxicity concerns. Development of Olesoxime was halted at the 18 month stage of the OLEOS phase 2 trial. IV = intravenous delivery, IT = intrathecal delivery.*

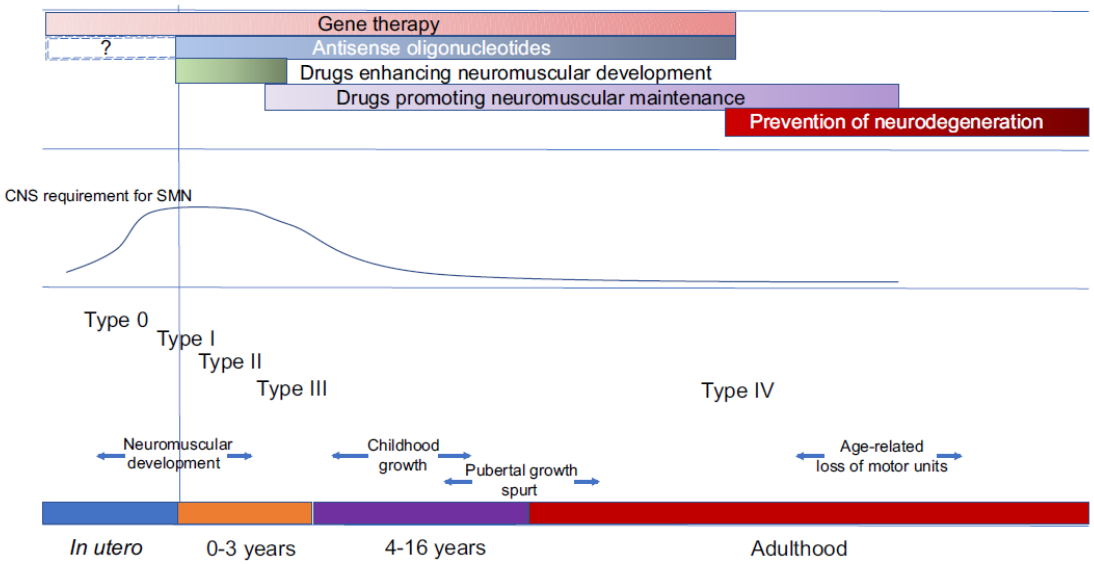


***Figure 1.5 SMN protein requirements at different stages of SMA development.***

*The requirements for SMN vary during development, affecting treatment strategies used at different stages of the disease. During healthy embryonic development the requirement for SMN, particularly in the CNS, increases until birth as the genesis and development of the neuromuscular system occurs. In severe SMA, this increase in SMN cannot be achieved and fetal death occurs in type 0 cases. Here, therapies that could mimic this endogenous increase would be optimal, such as genetic therapies including viral vectors and potentially antisense oligonucleotides, possibly preventing early defects in neuromuscular development. In infancy (0-3 years), the requirement for SMN remains relatively stable, albeit at a high level, and here the* SMN2 *copy number dictates the differences in onset between types I-III. This will alter the therapeutic strategy needed; gene therapies will continue to produce SMN protein whilst antisense oligonucleotides can enhance the production of full-length protein from* SMN2*, both providing the high level SMN required. Further drugs may be included in the treatment regimen to promote neuromuscular development and maintenance, attempting to prevent degeneration. Considerations of how many of these therapeutic strategies to employ together are important based on disease severity and efficacy of the treatments. Taken from Bowerman et al. (2017).*

#### 1.1.4.1 Spinraza

The antisense oligonucleotide (ASO) Spinraza (Nusinersen) aims to promote inclusion of exon 7 within *SMN2* mRNA transcripts and hence the synthesis of full-length SMN protein. Spinraza binds to *SMN2* pre-mRNA at the ISS-N1 splice silencing sequence discussed in section 1.1.1. This prevents negative splice factors such as hnRNPA1 and hnRNPA2 from binding this site (Figure 1.6C) (Talbot and Tizzano, 2017). This allows the recognition of exon 7 by the U1snRNP cellular splicing machinery (Figure 1.6C) and thus the inclusion of exon 7 in the mature *SMN2* mRNA transcript (Talbot and Tizzano, 2017). ISS-N1 has been termed the master checkpoint that regulates *SMN2* splicing since its deletion or masking with an ASO can abrogate the requirement for functional positive *cis*-elements such as the ESE that is disrupted by the C to T transition (Singh et al., 2017a).

The ISS-N1 was first discovered in 2004 by the Singh and Androphy laboratories (Singh et al., 2006) where they also found that the activity of this inhibitory element could be abrogated in a highly specific manner by ASOs at nanomolar concentrations. These results were later validated independently by Ionis Pharmaceuticals and the Krainer laboratory (Hua et al., 2007) with an ASO of a different chemistry, strengthening the value of this new therapeutic strategy. Spinraza was licensed later on as an 18-mer ASO with Ionis' proprietary chemistry (Singh et al., 2017b).

Spinraza has provided excellent results in type I SMA patients. Several clinical trials were conducted prior to the licensing of Spinraza in 2017 (more details regarding the use of Spinraza in clinical trials can be found in section 3.6). Licensing approval, however, was based heavily on the phase 3 ENDEAR trial which showed a significant 47% reduction in risk of death or permanent ventilation requirements (Finkel et al., 2017). Other clinical trials are continuing now even after approval to attempt to expand the use of Spinraza to other SMA patient populations. For example, NURTURE is an ongoing trial enrolling pre-symptomatic infants with SMA aiming to dose patients before 6 weeks of age.

The marketing approval of Spinraza was a dramatic development for SMA and the wider neuromuscular disease community. Spinraza was only licensed by the FDA in December 2016 and later by the European Medical Agency (EMA) in April 2017. Spinraza is delivered via intrathecal injection in repeated doses every few months,

however, this is one of the great limitations of this therapy. Intrathecal injections are invasive procedures that can be challenging in young children due to compliance issues, or may be technically difficult in patients presenting with scoliosis, rendering the injection site hard to access. Secondly, Spinraza is hugely expensive and the repeated nature of administration poses threats to drug accessibility for all patients that need it.

Long term effects of this treatment are still unknown. Initially only licensed for type I SMA patients, and only very recently approved for expanded access to all SMA types and patient ages, the effect of Spinraza on those with milder phenotypes is largely unknown. Due to the nature of intrathecal delivery, SMN protein levels will only be restored in spinal MNs, leaving all tissues outside of the CNS untreated. This treatment will prolong survival of SMA patients by preventing MN degeneration and the lethal consequences of this, but hitherto masked peripheral organ damage may now be at the forefront of the clinical phenotype presenting yet unknown burdens. Evidence of how the neuromuscular system will react to the presence of antisense oligonucleotides over the lifetime is a question that remains to be answered as children who received Spinraza in early clinical trials are only now reaching adolescence. It is possible that cells may become sensitised to this treatment and no longer respond. New targets for therapies may be needed to provide alternatives to Spinraza and Zolgensma and are explored in section 1.1.4.3.

#### 1.1.4.2 Zolgensma

This issue of systemic pathology not corrected by Spinraza leads on to the need for treatment options that can restore SMN levels throughout the body. Zolgensma (Onasemnogene Abeparvovec), a gene therapy strategy developed by Avexis (and recently purchased by Novartis), may solve this issue. Zolgensma is a self-complementary AAV9 vector that is delivered intravenously leading to systemic transgene expression. The *SMN1*-expressing construct is driven by a chicken β-actin hybrid promoter (Figure 1.6D) which replaces the missing endogenous *SMN1* gene. Impressive results described below have culminated in the recent FDA and EMA approval of Zolgensma. Zolgensma is indicated for the treatment of SMA patients with bi-allelic *SMN1* mutations, either with a clinical type I diagnosis, or up to 3 copies of *SMN2* (EMA, 2020).

A phase 1 clinical trial providing Zolgensma to SMA type I patients (Mendell et al., 2017) has produced outstanding results with 100% of patients surviving at 20 months of age, compared to 8% in a historical cohort. Patients exceed the natural history of the disease achieving motor milestones such as sitting unassisted, rolling and even in two cases, walking, achievements held by no patients in the historical cohort (Mendell et al., 2017). At the March 2019 data cut-off point for the STR1VE phase 3 clinical trial (recruitment now completed), results continued to be promising. 91% patients were alive without permanent ventilatory support, one patient died at 7.8 months of age and one withdrew from the clinical trial (AveXis, 2019). Improvement in motor functions were commonly seen with 50% patients sitting unaided and increases in CHOP INTEND score (AveXis, 2019). Data from the STR1VE clinical trial formed the basis of EMA approval of Zolgensma earlier this year. A number of other clinical trials using Zolgensma to treat SMA are currently ongoing (SPR1NT, START, STRONG and STR1IVE-EU).

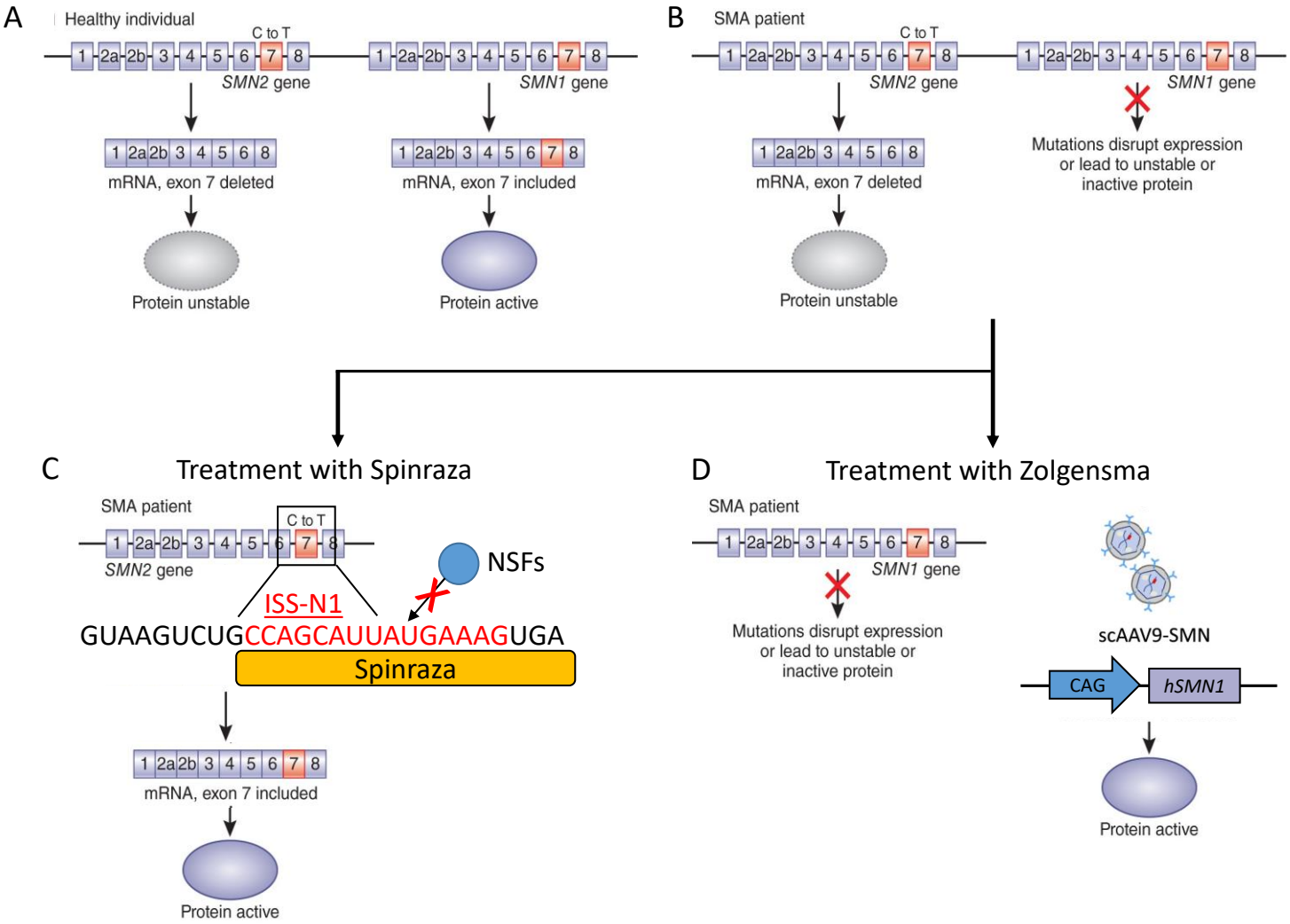


***Figure 1.6 The mechanisms of action of Spinraza and Zolgensma.***

*(A) Healthy individuals possess two* SMN *genes.* SMN1 *is transcribed to produce full length mRNA which is translated into a stable, active protein.* SMN2 *contains a C to T transition within exon 7, causing this to be excluded from mRNA transcripts by the action of negative splice factors (NSFs) binding to the ISS-N1 (intronic splicing silencer) in intron 7. This causes translation into a largely unstable protein, rapidly degraded. (B) SMA patients do not possess a* SMN1 *gene and as only 10% of SMN protein produced from* SMN2 *is stable, the SMA phenotype presides. (C) In SMA patients treated with Spinraza, the antisense oligonucleotide binds to ISS-N1, masking this from NSFs so they are unable to bind. Exon 7 is then able to be recognised by cellular splicing machinery and is included in the* SMN2 *mRNA transcript, translating into full length, active SMN protein. (D) Although Zolgensma does act through the manipulation of the endogenous SMN genes, it acts to replace* SMN1 *delivered by a self-complementary AAV9 vector encoding* SMN1 *under transcriptional control of the CAG promoter. This vector expresses full length, active SMN and can thus replace the missing endogenous* SMN1 *gene. Adapted from Corey (2017) and Kim and Monani (2018).*

#### 1.1.4.3 Other SMN-dependent and SMN-independent strategies

There is growing consensus in the SMA research community regarding the need for combinatorial therapy to fully address the disease phenotype (Bowerman et al., 2017). This is likely to include SMN-dependent and SMN-independent avenues. ASOs, gene therapy or small molecules can be used to increase SMN protein levels separately or together, whilst neuroprotective or muscle-targeted strategies could also be used.

Reldesemtiv, formerly known as CK-2127107, (Figure 1.4) targets muscles to reduce fatigue and weakness (Hwee et al., 2015) by slowing the release of calcium from skeletal muscle regulatory troponin complexes. The aim of this therapy is to increase skeletal muscle contractile ability despite a potential lack of MN innervation. This could improve the quality of life of SMA patients without attempting to correct the underlying SMN-dependent cause.

Olesoxime is an oral drug targeting mitochondria with the aim of preventing oxidative stress that might exacerbate motor neuron degeneration. This drug was performing well at the 12 month interim of the phase 2 OLEOS clinical trial with some evidence of functional improvements in non-ambulant type II or type III patients (Bertini et al., 2017). However, at the 18 month stage, Roche decided to withdraw Olesoxime from further development based on motor deterioration in patients despite drug administration, as well as problems including formulation and dosage of the compound.

Following the withdrawal of Olesoxime from Roche's therapeutic program, effort has been focused on the development of orally delivered, small molecules to augment full-length SMN production from *SMN2*. The first small molecule clinical trial (compound: RG7800, MOONFISH trial) was terminated following ophthalmological and skin-related toxicology results in the concurrent 39 week non-human primate study administering doses in excess of that in the MOONFISH trial (Ratni et al., 2018), despite no evidence of these issues seen in human subjects. Following analysis of RG7800 and resolution of these pre-clinical issues by adjustment of chemical structure, Risdiplam (formerly known as RG7916), in collaboration with Genentech was developed. This compound has a very similar mode of action to RG7800 and augments full-length *SMN2* transcription by promoting inclusion of exon 7 in transcripts. Multiple clinical trials administering Risdiplam are now ongoing (SUNFISH, FIREFISH, JEWELFISH, RAINBOWFISH), all of which are paying close attention for any potential toxicology.

Recent data presented at the Cure SMA 2020 annual conference has revealed promising data from FIREFISH, SUNFISH and JEWELFISH trials. The primary difference between the FISH trials lies in the SMA patient population enrolled. FIREFISH enrolled 1-7 month old SMA type I patients (2 *SMN2* copies), whilst SUNFISH enrolled patients between the ages of 2-25 with non-ambulant type II or III SMA. Finally, JEWELFISH enrollment was inclusive of a broad age range (6 months to 60 years) and also included non-treatment naïve patients. 12 month endpoint data from the FIREFISH trial where were treated has shown 29% of infants are now able to sit without support, something never occurring in the natural history of SMA type I (Servais, 2020). This study update also presented 85% event-free survival at 12 months, compared to only 50% survival at 8 months in a natural history cohort (Servais, 2020). The SUNFISH trial has shown that it improves or stabilises motor function (Day, 2020). Finally, the JEWELFISH trial assessing patients treated with Risdiplam after previous treatment with any of the MOONFISH, Spinraza, Olesoxime, or Zolgensma drugs found a sustained more than 2-fold increase in SMN protein levels from baseline (Chiriboga, 2020).

Branaplam, or LMI070, is a small molecule drug that is delivered by oral dosing and that targets alternative splicing of *SMN2*. Initial development of this drug was paused in 2016 after reports of nerve injury in pre-clinical animal trials (Shorrock et al., 2018), but research was resumed in 2017 (Novartis, 2017). A phase 1/2 clinical trial (NCT02268552) administering Branaplam to SMA type I patients is currently

active, but not recruiting, with some patients having received the drug for between 4 and 5 years.

## 1.2 Gene therapy

Gene therapy can be defined as the introduction of genetic material to host cells to prevent or correct disease (Verma and Weitzman, 2005) or as a technique to modify a person's genes with therapeutic intent (FDA, 2018). Gene addition, correction, silencing and cell elimination strategies are possible through using this group of techniques. Types of gene therapy agent include therapeutic genes encoded by plasmid DNA, viral or bacterial vectors (further information on specific viral vectors can be found in sections 1.2.3 and 1.2.4), gene editing technology such as CRISPR/Cas9, or cell therapy based products which have been corrected *ex vivo*, before being transfused back into patients (FDA, 2018). Agents such as ASOs are not classically defined as a gene therapy as they do not modify the genome sequence, instead modifying the RNA to provide therapeutic effects and as such are sometimes known as genetic therapies. However, for simplicity within this introduction, ASOs will be included within the gene therapy umbrella.

### 1.2.1 Advantages and disadvantages of gene therapy

Most genetic diseases currently lack treatment strategies that address the underlying cause of the disease, instead focusing on the use of conventional therapies to potentially alleviate symptoms and improve quality of life. Monogenic diseases have been the primary focus of *in vivo* gene therapy development, but treatment of human cancers both *in vivo* or *ex vivo* gene and cell therapy approaches have also provided very encouraging results. Some of the advantages and disadvantages of gene therapy applications can be found in Table 1.2 and Figure 1.7 details some licensed gene therapy products in.

| Advantages | Disadvantages |
|---|---|
| Potentially long-lasting effects | Costly |
| Potential to treat diseases that conventional medicine has failed | Potential for pre-existing immunity to viral vectors, precluding their use |
| Hope for patients with rare diseases that may not be appropriately targeted with pharmacological means | Access to widespread genetic testing is not readily available |
| Opportunity for personalised medicine | Difficult to use in polygenic or complex disorders |

***Table 1.2 Advantages and disadvantages of gene therapy approaches compared to conventional disease treatment.***

### 1.2.2 Licensed gene therapy products

Gene therapy products are increasingly becoming licensed for use in the clinic for both *in vivo* and *ex vivo* administration (Figure 1.7) with over twenty products approved, and many more in clinical trials (Shahryari et al., 2019). Gendicine was approved for the treatment of head and neck squamous cell carcinoma in China in 2003, Neovasculgen was approved in Russia in 2011 for peripheral artery disease and Glybera was licensed for the treatment of lipoprotein lipase deficiency in Europe and the US in 2012. Following this, rapid approval of further therapies such as Luxturna, a treatment for inherited retinal dystrophy that utilises an AAV2 expressing the deficient *RPE65* gene, or Kymriah and Yescarta, both *ex vivo*, autologous, CAR T cell therapies to treat acute lymphoblastic leukaemia, were also licensed (Butera, 2018). Since then, the number of licensed gene and cell therapy products has increased significantly within the last four years, now including two gene therapies for SMA (Spinraza and Zolgensma) within this roster.

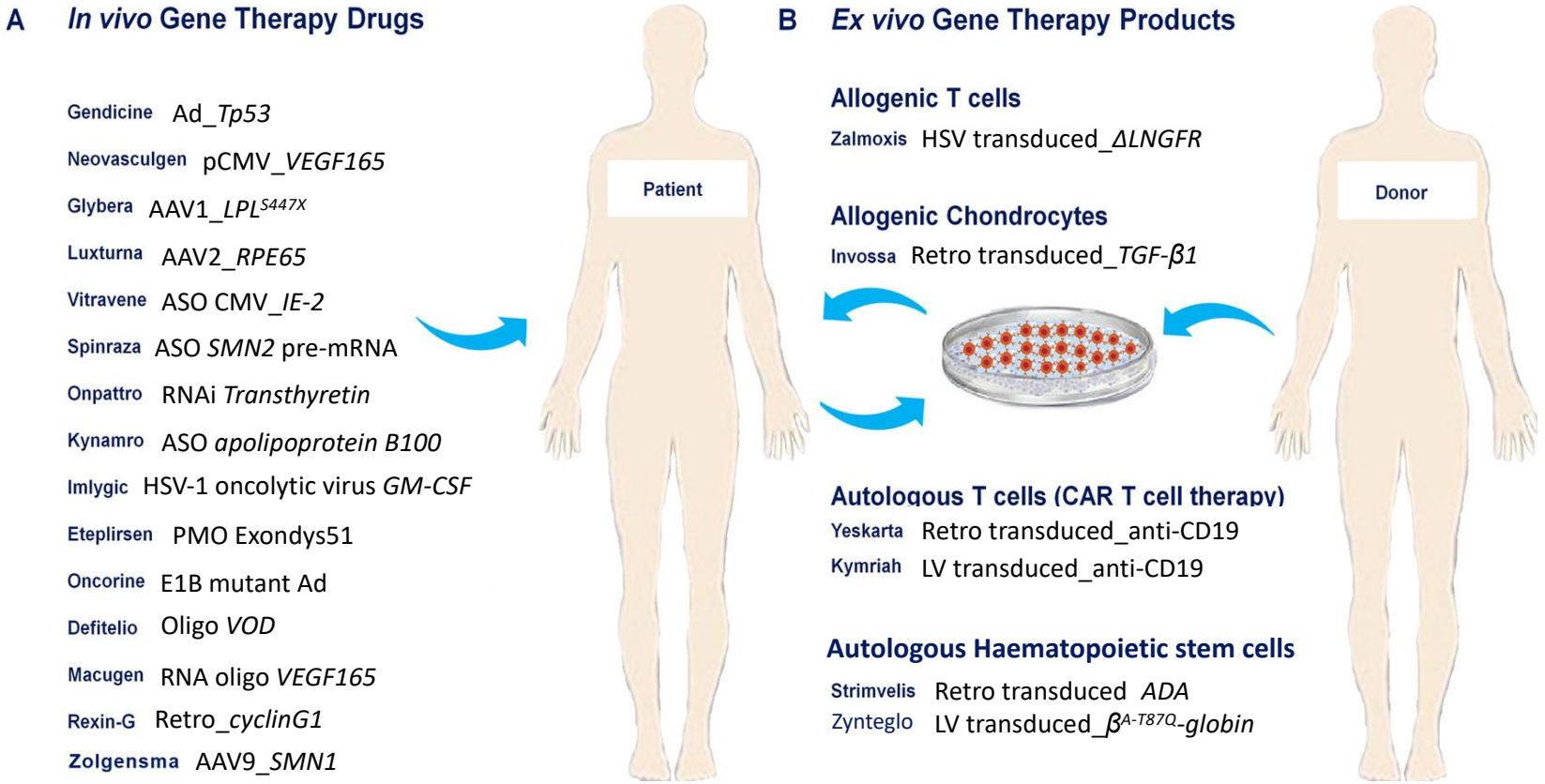


***Figure 1.7 Examples of licensed gene therapy products.***

*Over twenty gene therapy products have been licensed, examples of which are shown here, although this is not a complete list. Commercial names and a brief description of the gene therapy agent have been given. (A)* In vivo *and (B)* ex vivo *gene therapy products.* Ex vivo *products consist of cells that have been transduced outside of the body with a gene therapy agent, before being transfused into the same patient (autologous), or another patient (allogenic). Licensing may vary between countries. Adapted from Shahryari et al. (2019). Ad = adenoviral vector, AAV = adeno-associated viral vector, ASO = antisense oligonucleotide, RNAi = RNA intereference, HSV = Herpes Simplex viral vector, PMO = phosphorodiamidate morpholino, Retro = retroviral vector, LV = lentiviral vector.*

### 1.2.3 Lentiviral vectors

Lentivirus is a genus within the *Retroviridae* family, with several species exploited and manipulated to become lentiviral vectors. These include Human, Simian and Feline immunodeficiency viruses, Equine Infectious Anaemia, Caprine Arthritis Encephalitis and Jembrana Disease viruses. The lentiviral vectors used throughout this project descend from Human immunodeficiency virus 1 (HIV-1).

Lentiviruses exist as enveloped viral particles (Figure 1.8A) containing a single stranded RNA genome. These viral particles use envelope glycoproteins (GP120 in the case of wild type HIV-1) to bind to cell surface receptors (CD4 and CXCR4 for HIV-1) to initiate clathrin-mediated endocytosis. The viral genome and proteins such as reverse transcriptase and integrase are released into the host cell cytoplasm. Reverse transcription of viral RNA into DNA and subsequent nuclear import of this pro-viral DNA follows. Pro-viral DNA can be successfully integrated by the integrase protein into chromatin of the host genome leading to persistent gene expression. These qualities have been exploited to create highly efficient lentiviral vectors to deliver a gene of interest to a host, resulting in persistent expression with a host of other advantages ((A) Schematic of a HIV-1 enveloped viral particle containing the single stranded (ss) RNA genome and viral proteins such as reverse transcriptase and integrase. Adapted from https://old.abmgood.com/marketing/knowledge_base/The_Lentivirus_System.php. (B) Successive alterations have been made to the wild type HIV-1 provirus to improve biosafety by removing or separating viral genes. These alterations are known as lentiviral vector generations. 1st generation lentiviral vectors had endogenous LTRs and the HIV-1 envelope removed. 2nd generation vectors lacked accessory proteins such as VIF, R and U. Finally, 3rd generation vectors involve the separation of transgene, Rev and envelope constructs to prevent replication competent viruses forming. Taken from Vigna and Naldini (2000). (C) Configurations of self-inactivating (SIN) vectors compared to wild type. SIN vectors have a truncated U3 3' LTR, abrogating intrinsic promoter activity, and instead contain an external promoter such as CMV to drive transgene expression, but will not integrate itself. Advanced lentiviral vector transfer constructs also contain elements such as PPT to aid in reverse transcription, or WPRE to improve transgene expression. Taken from Sakuma et al. (2012) to be found at https://portlandpress.com/biochemj/article-abstract/443/3/603/80645/Lentiviral-vectors-basic-to-translational?redirectedFrom=PDF.

Table 1.3).

Lentiviral vectors are created by manipulating the parental viral genome, in this case HIV-1, to remove pathogenic and replicative genes and separate functional elements into several plasmids for vector manufacture (Verma and Weitzman, 2005). These genomic manipulations aim to increase biosafety of the resulting lentiviral vectors and have been implemented in successive generations (Figure 1.8B). The separated functional constructs that exist in the third generation lentiviral vectors used in this project include packaging (viral structural genes; *gag* and *pol*), Rev (required for *gag* and *pol* expression and nuclear export of viral transcripts), envelope and transfer (gene of interest flanked by cis-acting LTRs (long terminal repeats)) constructs. Finally, vectors can be made self-inactivating (SIN; Figure 1.8C) through the use of truncated LTRs lacking endogenous promoter activity, in which case an internal promoter such as the immediate early cytomegalovirus (CMV) promoter is used to drive transgenic expression, improving biosafety further. All the vectors in this project were classed as SIN vectors.

| **Advantages** | **Disadvantages** |
|---|---|
| High coding capacity of approximately 7.5-9Kb | Low titres |
| Low immunogenicity | Difficult to scale up production |
| Host immunologically naïve to vector | |
| Efficient transduction of mitotic and quiescent cells | |
| Non-integrating vectors available | |
| Stable and robust gene expression | |

To improve transgene expression in the target cell or tissue, transfer plasmids also contain a relevant promoter (in the case of SIN vectors) and possibly the mutated woodchuck hepatitis virus cis-acting post-transcriptional regulatory element (mWPRE) to improve transgene expression (Zufferey et al., 1999). Other elements may be included in advanced lentiviral vectors (Figure 1.8C, bottom) such as nuclear import and export signals or elements aiding in reverse transcription. Transgene expression can be targeted to a certain cell types, or can be kept broad, in a process known as pseudotyping. Here, the wild type HIV-1 envelope gene, *env*, is replaced with a gene from another virus, mitigating the need for HIV-1 envelope

binding to CD4 receptors. This allows retargeting of vector entry mediated by alternative envelope proteins in cells that do not express CD4. In some cases, the use of specific envelope proteins significantly improves transduction, for example baculovirus *GP64* for hepatocyte transduction (Markusic et al., 2004). Here, all vectors are pseudotyped with VSV-G from the Vesicular Stomatitis virus, allowing viral entry into a broad range of cells. When packaging, Rev and transfer constructs, along with a plasmid containing the alternative *env* gene, are co-transfected into a cell line like HEK293T cells, production of vector particles will result.

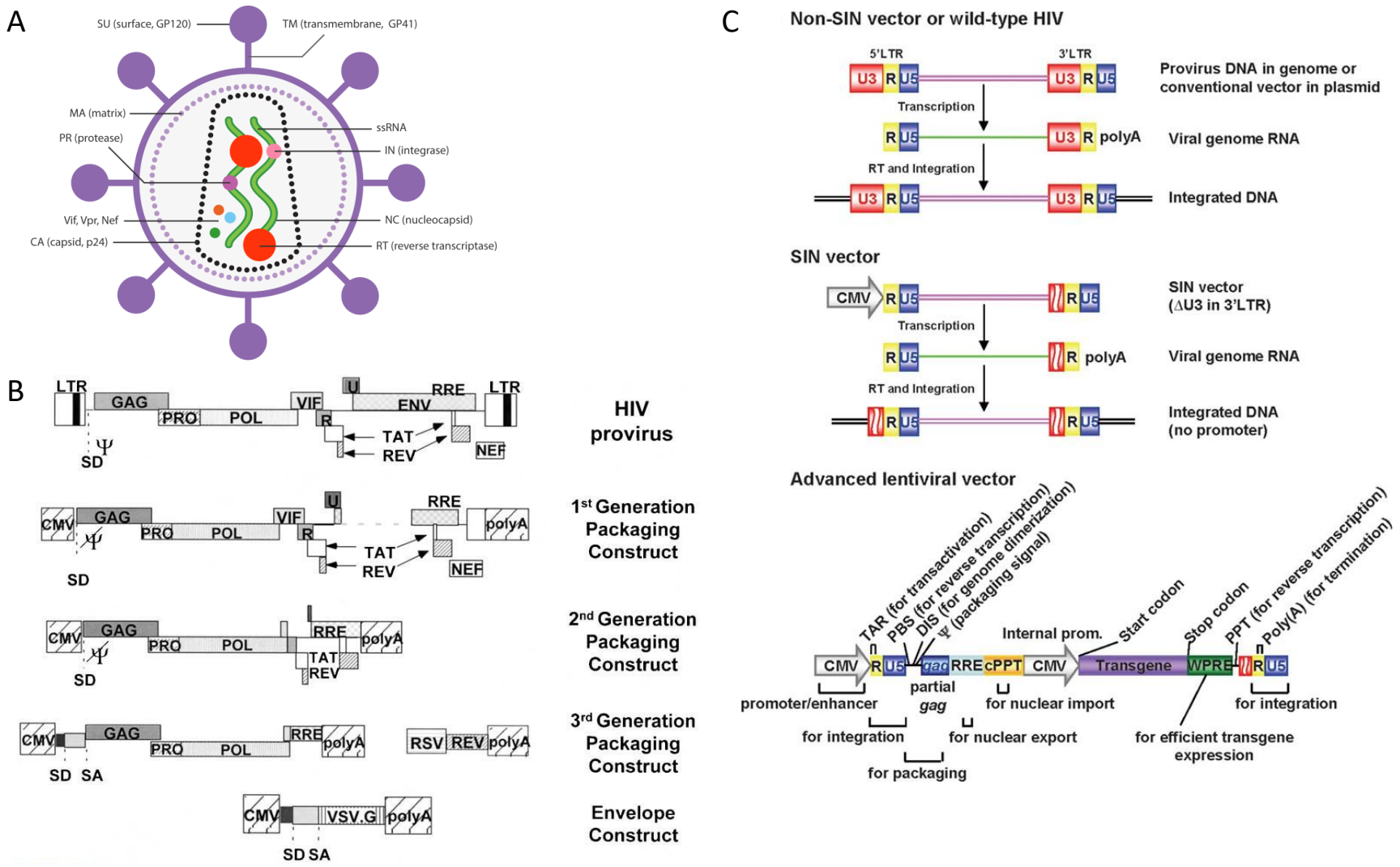


***Figure 1.8 Structure, genomic organisation and safety improvements of lentiviral vectors.***

*(A) Schematic of a HIV-1 enveloped viral particle containing the single stranded (ss) RNA genome and viral proteins such as reverse transcriptase and integrase. Adapted from https://old.abmgood.com/marketing/knowledge_base/The_Lentivirus_System.php. (B) Successive alterations have been made to the wild type HIV-1 provirus to improve biosafety by removing or separating viral genes. These alterations are known as lentiviral vector generations. 1st generation lentiviral vectors had endogenous LTRs and the HIV-1 envelope removed. 2nd generation vectors lacked accessory proteins such as VIF, R and U. Finally, 3rd generation vectors involve the separation of transgene, Rev and envelope constructs to prevent replication competent viruses forming. Taken from Vigna and Naldini (2000). (C) Configurations of self-inactivating (SIN) vectors compared to wild type. SIN vectors have a truncated U3 3' LTR, abrogating intrinsic promoter activity, and instead contain an external promoter such as CMV to drive transgene expression, but will not integrate itself. Advanced lentiviral vector transfer constructs also contain elements such as PPT to aid in reverse transcription, or WPRE to improve transgene expression. Taken from Sakuma et al. (2012) to be found at https://portlandpress.com/biochemj/article-abstract/443/3/603/80645/Lentiviral-vectors-basic-to-translational?redirectedFrom=PDF.*

| Advantages | Disadvantages |
|---|---|
| High coding capacity of approximately 7.5-9Kb | Low titres |
| Low immunogenicity | Difficult to scale up production |
| Host immunologically naïve to vector | |
| Efficient transduction of mitotic and quiescent cells | |
| Non-integrating vectors available | |
| Stable and robust gene expression | |

***Table 1.3 Advantages and disadvantages of lentiviral vectors in gene therapy applications.***

#### 1.2.3.1 Integration deficient lentiviral vectors

Lentiviral vectors with the ability to integrate viral DNA into the host genome pose a risk of insertional mutagenesis where nearby genes can become dysregulated. Early retroviral gene therapy trials (Hacein-Bey-Abina et al., 2003, Gaspar et al., 2004, Howe et al., 2008) aiming to treat SCID-X1 encountered problems when retroviral integration caused LTR enhancer activity to interact with the promoter of an endogenous oncogene (*LMO2*), causing hematological malignancies to occur in five patients. Therefore, non-integrating vectors (e.g. integration-deficient lentiviral vectors; IDLVs) are preferred. IDLVs are engineered with class I missense

mutations (Engelman, 1999) in the viral *pol* gene encoding integrase, the enzyme responsible for proviral insertion (Philippe et al., 2006, Yáñez-Muñoz et al., 2006). Defective integration results in the accumulation of episomal DNA circles in the host cell nucleus (Figure 1.9). Episomal gene expression activity is transient in dividing cells due a lack of episomal replication capacity, but quiescent cells show long-lasting, efficient expression. This is relevant here where cells of the central nervous system are targeted. Successful use of IDLVs for transduction of the eye, brain and spinal cord has previously been published with comparable efficacies of IDLVs and their integration-proficient counterparts when expressing the transgene of interest (Philippe et al., 2006, Yáñez-Muñoz et al., 2006, Hutson et al., 2012, Peluffo et al., 2013, Lu-Nguyen et al., 2014, Lu-Nguyen et al., 2015). Of particular relevance here, SMN overexpression can be detected in all cells transduced with IDLVs expressing *hSMN1* or a codon-optimised version (*Co-hSMN1)*, for instance in primary rat MN cultures with higher transgene expression occurring with *Co-hSMN1* (Ali Mohammadi Nafchi, 2017).

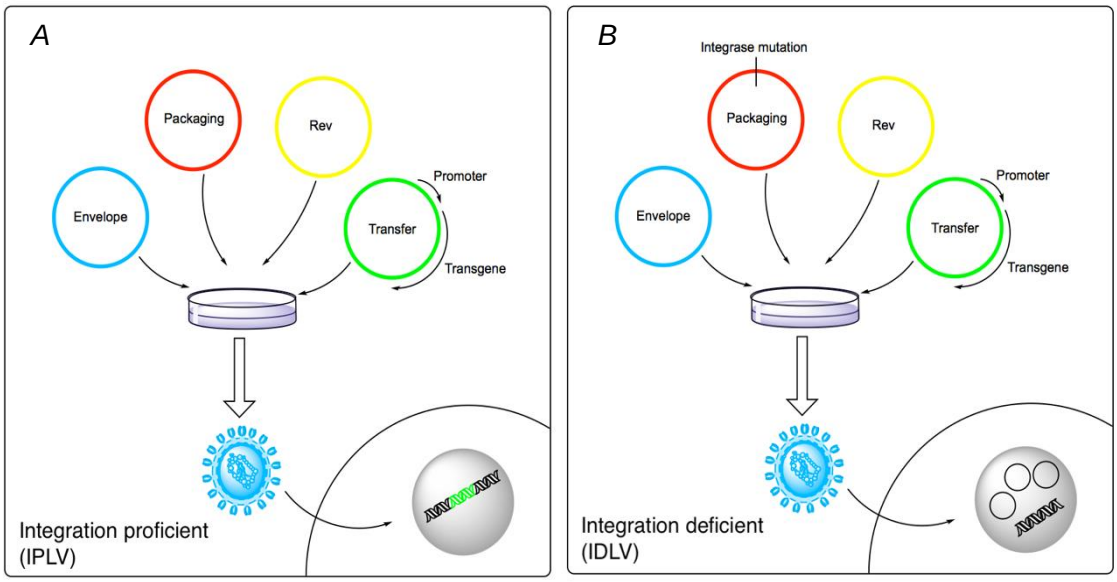


***Figure 1.9 Integration proficient and deficient lentiviral vectors.***

*Upon co-transfection of envelope, packaging, Rev and transfer plasmids into producer cells, viral vector particles will result. When these are used to transduce target cells transgene DNA will either be (A) integrated into the host cell genome or (B) retained within the nucleus as episomal circles.*

### 1.2.4 Adeno-associated virus vectors

Adeno-associated virus (AAV) vectors are derived from the wild type AAV *Dependoparvovirus* genus and exist as a single stranded DNA (ssDNA) genome encased in a capsid (Figure 1.10A) that occurs in a range of serotypes. The wild type ssDNA genome consists of two open reading frames (ORFs; the 5' encoding viral Rep proteins (rep), whilst the 3' encodes capsid VP1-3 proteins (cap)) flanked by 145bp inverted terminal repeats (ITRs; Figure 1.10B) (Buning et al., 2004). Naturally, expression of these two ORFs are driven by the action of three promoters; p5, p19 and p40. ITRs contain all *cis*-acting elements necessary for the replication and packaging of an AAV.

Again, the AAV genome has been manipulated to remove viral genes and make it suitable for use as a gene therapy vector. AAV vector genomes consist of ITRs flanking an up to 4.5Kb of transgene cassette, replacing the rep and cap ORFs (Figure 1.10C). To improve biosafety, a transient transfection system of multiple plasmids is required to produce AAV vectors (Warnock et al., 2011). This is due to a lack of VP protein-encoding genes in the AAV genome, so a helper virus or plasmid expressing these must be introduced to producer cells as well as the separate transfer construct. AAV vector production also involves the use of Rep protein supplied *in trans*, further improving biosafety. Capsid serotypes (known as 1-9) direct the vector's cellular tropism (Warnock et al., 2011) and it is possible to change AAV vector serotype by mixing capsids and genomes from different serotypes to improve transduction efficacy or alter tropism. Most AAV vectors used for gene therapy use an AAV2 genome with a relevant capsid, for example serotype 9 (notation: AAV2/9) for transduction of the CNS.

The nature of the ssDNA AAV vector genome means that the host's cellular machinery is needed to synthesise a second DNA strand upon transduction of a cell following uncoating of AAV vector particles (Figure 1.10D). This is a rate limiting step before expression of the transgene can occur (McCarty et al., 2003). ITRs serve as replications origins for host cell DNA polymerases to begin *de novo* second strand synthesis. Strand annealing is an alternative method to obtain a double stranded genome which relies on sense and antisense DNA strands from different viral particles annealing (Figure 1.10D). To overcome this, self-complementary AAV (scAAV) vectors have been developed (McCarty et al., 2003). A mutation in one ITR

causes a failure in the Rep protein being able to nick the terminal resolution site within the ITR, resulting in maintenance of the ITR hairpin structure, rather than resolution into a linear strand. This maintained hairpin ITR structure results in a dimeric genome structure with an ITR at each of the 5' and 3' ends, but also one central ITR that mediates strand complementation (Figure 1.10D).

Therefore, the ORF within scAAV vectors contains the transgene cassette, and a sequence complementary to this within the dimeric genome. Following transduction, these complementary sequences spontaneously anneal, producing dsDNA without the need for synthesis. This vastly improves speed of transgene expression onset, but requires that the coding capacity of the ORF is halved to accommodate the complementary sequence. A compromise must be drawn between very fast gene expression onset and a very small coding capacity of approximately 2.5Kb. As with any viral vector system, AAVs are subject to further advantages and disadvantages and some of these can found in Table 1.4.

Similarly to IDLVs, the genomes of AAVs and their derived vectors exist primarily as episomes within the target cell's nucleus. Second order interactions including end to end joining mediated by strand annealing is able to cause the generation of concatemeric episomes (McCarty, 2008), stabilising the genome. However, wild type AAVs can integrate at very low levels as well as forming episomes. Integration preferentially occurs into the AAVS1 site on chromosome 19 (Samulski et al., 1991) as this site has sequence similarity to that of ITRs as well as it containing an active Rep binding element (McCarty et al., 2004). In the cases of AAV vectors were Rep was supplied *in trans* during production, AAV vector genome integrations is further reduced (Wang et al., 2019).

AAVs have been commonly used *in vivo* to transduce a variety of tissues taking advantage of different tropisms and serotypes (Gao et al., 2004). AAV9 is a particularly relevant serotype when conducting CNS research as this has been shown to cross the blood brain barrier (BBB) (Foust et al., 2009). Concurrently with Kaspar's group reporting BBB crossing, the Barkats' laboratory replicated this and also showed the first successful transduction of MNs *in vivo* following AAV9 intravenous delivery in adult mice (Duque et al., 2009). More recently, the biodistribution of AAV9 transduction has been demonstrated using an AAV9_*GFP* vector delivered intravenously at postnatal day 1 (P1) to wild type mice (Powis et al., 2016). Strong *GFP* expression in the heart and liver was visible 48 hours post-

transduction and this expression level was sustained from P3-P60, whereas expression in brain, muscle and spinal cord showed a delayed, linear increase in expression over time (Powis et al., 2016).

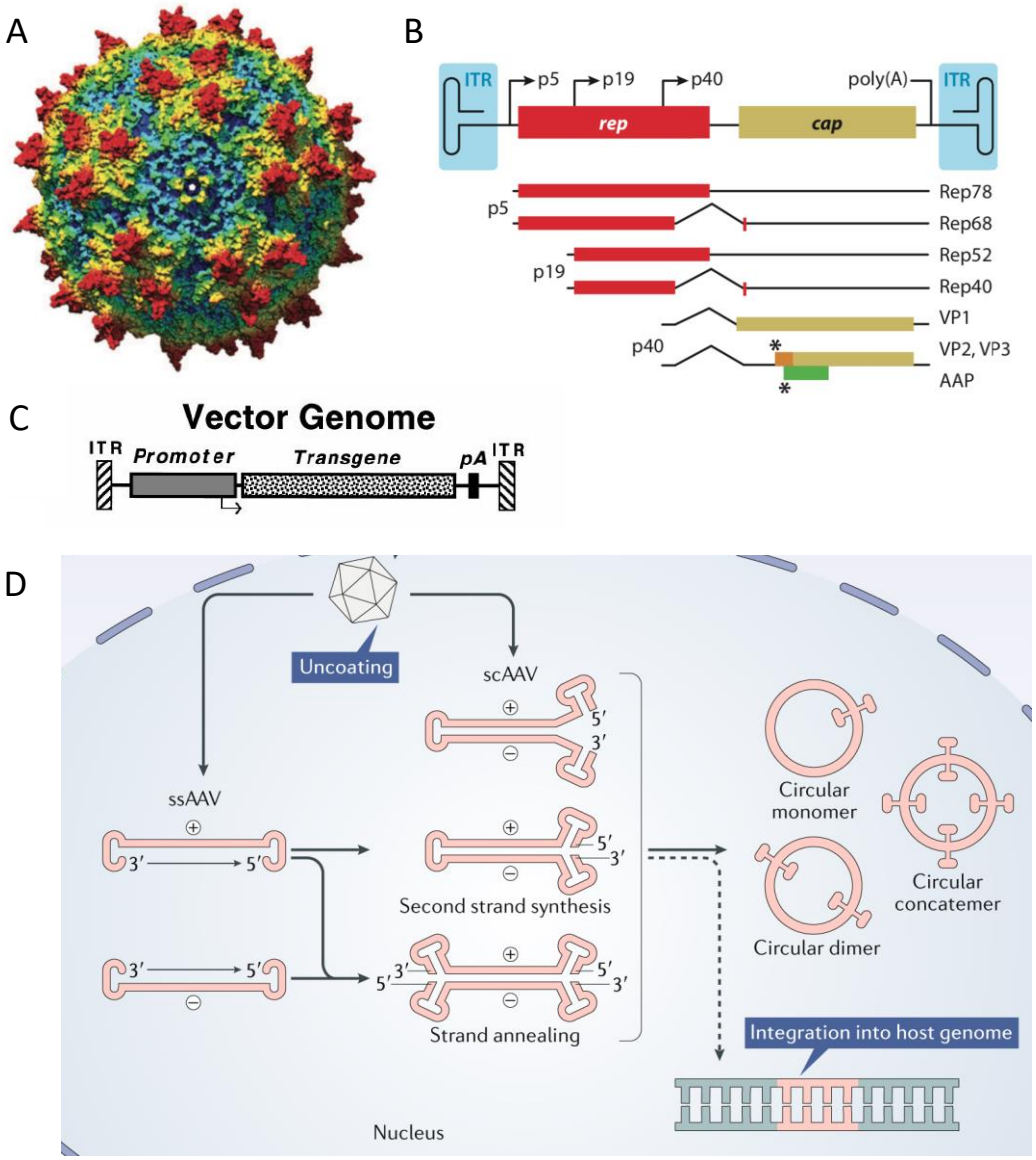


***Figure 1.10 AAV vector particle structure and genomic organisation.***

*(A) A model of the AAV vector capsid surface. (B) The wild type AAV genome consists of two open reading frames (rep and cap) with three promoters (p5, p19 and p40), flanked by inverse terminal repeats (ITRs).* Rep *encodes four proteins that function in genome replication (rep78/68) and packaging (rep52/40).* Cap *encodes three proteins (VP1/2/3) that form the viral capsid. AAP is a support protein that promotes maturation of capsid an is encoded by an alternative open reading frame. (A,B) Taken from Samulski and Muzyczka (2014). (C) AAV vector genomes contain a promoter, transgene and polyA signal instead of rep and cap open reading frames. Adapted from Russell and Kay (1999). (D) Upon entry to the nucleus, the AAV vector genome is released by capsid uncoating. AAV vector genomes are classed as single stranded (ssAAV) or self-complementary (scAAV). ssAAV genomes contain single strands of DNA in either sense (+) or antisense (-) formats, that undergo second strand synthesis to form double stranded DNA. scAAV genomes bypass this second strand synthesis as they are already double stranded by design. Strands anneal and then are transcribed. Inter- or intra-molecular recombination of transcripts can occur to form circularised episomes or integrate into the host genome, albeit at a lower frequency. Adapted from Wang et al. (2019).*

| Advantages | Disadvantages |
|---|---|
| High titres with easier large scale production | Helper virus/plasmid-dependent production |
| Wide range of serotypes provides broad cellular tropisms | Small packaging capacity of approximately 4.5-5Kb |
| Transduce both dividing and non-dividing cells | Slow onset gene expression unless self-complementary system is used |
| Strong and sustained transgene expression | Possible pre-existing immunity |
| Low immunogenicity | |

***Table 1.4 Advantages and disadvantages of AAVs in gene therapy applications.***

## 1.3 Gene therapy in SMA models

### *1.3.1 In vitro*

#### 1.3.1.1 Primary cells and cell lines

Much of the early gene therapy work finding SMA therapeutic strategies was completed in primary SMA fibroblasts or cell lines whose SMN protein was knocked down. The first study attempting gene addition for SMA used adenoviral vectors encoding *SMN* to transduce SMA fibroblasts resulting in increased levels of functional SMN protein (DiDonato et al., 2003). Fibroblasts and lymphoblasts have also been used to study how histone deacetylase inhibitors can increase *FL-SMN* transcripts and SMN protein (Andreassi et al., 2004, Andreassi et al., 2001, Also-Rallo et al., 2011, Farrelly-Rosch et al., 2017). Vast amounts of research aiming to modulate *SMN2* exon 7 splicing was completed *in vitro* with analysis of U7 snRNAs (Madocsai et al., 2005, Marquis et al., 2009, Nlend and Schumperli, 2012), ASOs and phosphorodiamidate morpholinos (PMOs) (Singh et al., 2013, Pao et al., 2014, Singh et al., 2015b, Touznik et al., 2017, Touznik et al., 2018, Maruyama et al., 2018), as examples.

#### 1.3.1.2 Induced pluripotent stem cells

Induced pluripotent stem cells (iPSCs) are somatic cell-derived pluripotent cells similar to embryonic stem cells (ESCs). iPSCs will indefinitely self-renew whilst also

retaining the capacity to differentiate into cell types from all three germ layers, highlighted by their ability to form teratomas (Takahashi et al., 2007). iPSCs have become popular *in vitro* pathophysiological disease models (Takahashi and Yamanaka, 2006) when derived from patient biopsies then differentiated into relevant cell types. The use of iPSCs as a source of pluripotent stem cells obviates the ethical concerns of using ESCs which necessarily involve the destruction of a blastocyst, as no fertilised embryos are required for iPSC production (Frattini et al., 2015).

iPSCs were first produced by retroviral transduction of mouse (Takahashi and Yamanaka, 2006) and subsequently human (Takahashi et al., 2007, Yu et al., 2007) fibroblasts. The retroviral vectors used to induce pluripotency in these three studies encoded the transcription factors OCT4 and SOX2 along with KLF4 and C-MYC (Takahashi et al., 2007) or NANOG and LIN28 (Yu et al., 2007). The transcription factors used reprogrammed the cells from an epidermal fate to that of an embryonic one by masking transcription of skin genes and promoting ESC gene transcription by binding to these promoters (Frattini et al., 2015).

However, the use of retroviral vectors to encode transcription factors poses safety concerns so several adaptations to this protocol have been created to improve biosafety. Firstly, the re-expression of KLF4 or C-MYC oncogenes in iPSC progeny could produce tumours so this re-expression can be prevented through Cre-loxP excision. The retroviral reprogramming cassette is flanked by loxP sites which is then excised in iPSC progeny upon expression of the Cre recombinase. Secondly, non-integrating vectors, such as the Sendai virus, or episomal methods can be used to deliver the transcription factors. These methods are of relevance here as they were used to reprogram the AD3-CL1 and 19-9-7T, SMA-13 and SMA-32 iPSC lines, respectively, used within this project. Non-integrating methods of reprogramming offer opportunity to switch transcriptional profile of the cells being targeting, without the safety concerns that integrated oncogenes bring.

It is now possible to replace some or all of these transcription factors with small molecules (Lin and Wu, 2015). Forskolin is a small molecule that can replace OCT4 whilst some TGF-β inhibitors can replace SOX2 through induction of Nanog transcription (Ichida et al., 2009). WNT signaling regulators or valproic acid could replace C-MYC (Huangfu et al., 2008) and KLF4 could be substituted for Kenpaullone (Lyssiotis et al., 2009). Chemical cocktails have been shown to

generate mouse iPSCs in combination with OCT4 transduction (Li et al., 2011b). Increasing the number of small molecules within these cocktails, as well as supplementing culture media with growth factors such as bFGF has proven that mouse embryonic fibroblasts can be reprogrammed into iPSCs without any use of transcription factors, calling for these cells to be termed chemical iPSCs (CiPSCs) (Hou et al., 2013).

Recent advances have shown that cells other than fibroblasts obtained by patient biopsy have now been reprogrammed into iPSCs. Examples of cells now used include keratinocytes from hair samples (Umegaki-Arao et al., 2014, Re et al., 2018) and renal tubule epithelial cells isolated from urine (Feng et al., 2018). These solutions provide more convenient sources of cells that are isolated in a non-invasive, cost-effective manner (Yi et al., 2018).

iPSCs from SMA patients are now common with these cells retaining comparable SMN protein levels to the fibroblasts from which they were reprogrammed and alternatively spliced *SMN2* transcripts (Ebert et al., 2009). Direct conversion of SMA fibroblasts to MNs, bypassing the iPSC stage, has also been achieved as an SMA model (Zhang et al., 2017) with reduced neurite growth rate and degeneration recapitulating phenotypes seen in *in vivo* models and human patients. Many groups have now been able to differentiate iPSCs into MNs (Ebert et al., 2009, Corti et al., 2012, Du et al., 2015, Yoshida et al., 2015, Fuller et al., 2016, Powis et al., 2016, Bhinge et al., 2017, Yi et al., 2018), the cell type primarily affected in SMA and other motor neuron diseases such as ALS. Modulation of SMN has been explored in SMA iPSC MNs using histone deacetylase inhibitors to increase *SMN2* expression, genome editing to convert *SMN2* to a *SMN1*-like gene by correction of the C to T point mutation in exon 7 and other RNA therapeutics. However, in comparison to the vast amount of papers exploring SMN modulation *in vivo*, far less research has actually been published regarding gene therapy in SMA iPSC MNs, something that has been investigated in this thesis. The differentiation of SMA iPSC MNs and the modulation of SMN within SMA iPSC MNs will be discussed in more detail in chapters 5 and 6.

### *1.3.2 In vivo*

#### 1.3.2.1 SMA mouse models

The mouse is a very valuable model because of anatomical and physiological similarities to human neuromuscular systems as well as an easy to manipulate genome. There is 82% amino acid identity between *Smn* and *hSMN1*. *Smn* knockout is embryonic lethal and approximately 85% loss of Smn protein is required to reflect SMA phenotypes (Bowerman et al., 2017), therefore introduction of human *SMN2* to *Smn*$^{-/-}$ mice produces a severely affected SMA phenotype while allowing survival for up to two post-natal weeks, modelling severe infantile SMA. Among the many SMA mouse models (please see Table 1.5 for more details), one progressively gaining acceptance is the Taiwanese model, with two *SMN2* copies on *Smn* null background.

| SMA model common name | Genotype | Severity | Notes | Reference(s) |
|---|---|---|---|---|
| *Smn* knockout | *Smn*$^{-/-}$ | ++++ | Death of embryo occurs prior to uterine implantation. | Schrank et al., 1997 |
| *Smn* heterozygote | *Smn*$^{+/-}$ | + | Early acute loss of lumbar spinal cord motor neurons (~28% within 5 weeks), with subsequent slowly progressive reduction over an extended time scale. | Jablonka et al., 2000; Balabanian et al., 2007 |
| Taiwanese | *Smn*$^{-/-}$; *SMN2(2Hung)*$^{+/+}$ | + to +++ | Transgene including human *SMN2*, *SERF1* and part of *NAIP*; rescues embryonic lethality of *Smn*$^{-/-}$. Transgene copy number correlates with disease severity, which ranges from death within 1 week to normal survival. | Hsieh-Li et al., 2000 |
| SMNΔ7 | *Smn*$^{-/-}$; *SMN2(89Ahmb)*$^{+/+}$ ; *SMNΔ7*$^{+/+}$ | +++ | Transgene containing human *SMNΔ7*, the predominant isoform produced by *SMN2*; improves the phenotype of *Smn*$^{-/-}$; *SMN2*$^{+/+}$. Mean lifespan: 13.3±0.3 days. | Le et al., 2005 |
| *Smn*$^{2B/-}$ | *Smn*$^{2B/-}$ | ++ | *Smn* transgene harbouring three nucleotide substitutions within the exonic splicing enhancer of exon 7. Mean lifespan: 28 days. | Bowerman et al, 2009 |
| Burghes' severe | *Smn*$^{-/-}$; *SMN2(89Ahmb)*$^{+/+}$ | + to +++ | Transgene containing only the *SMN2* locus, rescues *Smn*$^{-/-}$ embryonic lethality. 42/56 mice with one or two transgene copies were stillborn or died before 6 hours, with the remainder dying between 4-6 days. Mice with eight copies of the transgene reach adulthood. | Monani et al., 2000 |
| Neuronal *Smn* exon 7 deletion | *NSE-Cre*$^{+}$; *Smn*$^{F7/F7}$ | ++ | *Smn*$^{F7/F7}$ (also written as *Smn*$^{+/+}$) mice with Cre-*loxP*-mediated deletion of *Smn* exon 7 in neuronal tissue. Mean lifespan: 31±2 days. | Ferri et al., 2004 |

***Table 1.5 Comparison of frequently used SMA mouse models.***

*Genotypes, phenotypes and specific characteristics of SMA mouse models vary widely. Presented here are the most commonly used SMA mouse models within the literature. Adapted from Sleigh et al. (2011), please see therein for details of further SMA mouse models not included here for brevity. Severity scale: + mild, ++ moderate, +++ severe, ++++ embryonic lethal.*

#### 1.3.2.2 Gene therapy in SMA mouse models

Proof of principle for the use of lentiviral vectors for the delivery of *SMN* in an *in vivo* model was obtained whereby intramuscular injection of an Equine Infectious Anaemia-derived lentivirus increased SMN protein levels, decreased MN death and extended the life of SMA$\Delta$7 mice by 3-5 days (Azzouz et al., 2004). Further to this, gene therapy research in mouse models of SMA rapidly increased in 2010-11 where several leaders of the field published research all suggesting AAV-mediated expression of *SMN1 in vivo* on the day of birth provides amelioration of SMA phenotype, specifically improving survival (up to 340 days compared to 13-15 in untreated mice), motor function, neuromuscular physiology and prevention for MN death (Foust et al., 2010, Passini et al., 2010, Valori et al., 2010, Dominguez et al., 2011).

Many strategies pertaining to the implementation of *in vivo* gene therapy for SMA have been developed. The vast amount of research in this field necessitates comparisons between studies to gain a detailed consensus of how gene therapy for SMA should be implemented. Only a very brief overview of SMA *in vivo* gene therapy has been given above as an extensive analysis of this subject and the necessary comparisons, as highlighted in the first objective of this thesis, is presented in chapter 3.

### *1.3.3 In utero*

Despite the current licensed and pipeline therapies, no strategies address the genesis of SMA *in utero*. It is recognised that the translation of fetal gene therapy to humans is a challenging feat, but the technology is becoming more common and *in utero* gene therapy (IUGT) remains the best possible avenue for the treatment of genetic diseases arising during gestation (Almeida-Porada et al., 2019). IUGT is simply the delivery of relevant genes to the developing fetus to correct genetic defects (Chauhan et al., 2004). Prevention of disease onset is only one of the advantages of this technology. Immune tolerance to the transgene product due to an immature immune system (Waddington et al., 2004), increased vector biodistribution due to small body size and the possibility of transducing stem cells leading to the permanent genetic correction are all also highly beneficial qualities (Waddington et al., 2005).

IUGT in rodents and large animal models is becoming increasingly studied in a wide variety of diseases, including Parkinson's disease (Chansel-Debordeaux et al., 2017), X-Linked Hypohidrotic Ectodermal Dysplasia (Hermes et al., 2014), hereditary tyrosinemia type I (mice: (Nicolas et al., 2017, Rossidis et al., 2018), pigs: (Nicolas et al., 2018)), Thalassemia (mice: (Shangaris et al., 2017, Ricciardi et al., 2018), macaques: (Mattar et al., 2011, Mattar et al., 2017, Chan et al., 2019)) and Gaucher disease (Massaro et al., 2018) and fetal growth restriction (sheep: (Carr et al., 2014, Mehta et al., 2012, Mehta et al., 2014, David et al., 2008) and guinea pigs: (Swanson et al., 2016)).

Prospective clinical studies to inform design of the upcoming EVERREST phase I/IIa clinical trial (NCT02097667) are now ongoing (Spencer et al., 2017). Further *in utero* interventions in humans include treatment of three second trimester X-Linked Hypohidrotic Ectodermal Dysplasia patients (Schneider et al., 2018) and *in utero* surgeries to correct Spina Bifida at Great Ormond Street Hospital. Lastly, the BOOSTB4 phase I/II clinical trial (NCT03706482; started May 2019) aims to deliver allogeneic fetal mesenchymal stem cells intravenously for the treatment of severe Osteogenesis Imperfecta between 16 and 35 weeks of gestation.

Preclinical studies in mice aiming to restore SMN protein levels using gene therapy have derived a therapeutic window consisting of postnatal days 0-3 (P0-3) where treatment is effective at improving motor function, neuromuscular physiology and life span (Farrar et al., 2017). Pre-symptomatic delivery of treatment may prevent development of the SMA phenotype and the irreversible damage that accompanies this, perhaps due to the deficiency being corrected during the period of NMJ maturation (Farrar et al., 2017). In light of this, *in utero* delivery is an attractive opportunity to prevent any development of symptoms and potentially allow healthy offspring to be born.

More recently, a laboratory has published the first use of IUGT in SMA mice (Rashnonejad et al., 2019) to investigate the efficacy of fetal gene therapy for this disease. This study compared intracerebroventricular (ICV) and intraplacental routes of administration, as well as both single-stranded and self-complementary AAV9_*SMN1* vectors, concluding that ICV injection of scAAV9 vectors was optimal. SMN$\Delta$7 fetuses injected in this manner at E15 resulted in 43.8% full-term gestation births, with these pups going on to survive for a median of 105 days, compared to

12 days in untreated pups (Rashnonejad et al., 2019). Supraphysiological levels of SMN protein were found in CNS samples, but not in muscles. Despite this, atrophied muscle present in untreated SMA mice had been rescued in IUGT treated animals, which also showed increased numbers of MNs in spinal cord sections (Rashnonejad et al., 2019). This study provides proof of principle that IUGT for SMA may be a viable option and should be explored further, however a comparison between the phenotypic benefits of *in utero* and post-natal gene therapy for SMA should also be considered.

## 1.4 Objectives

The overall aim of this project was to study the phenotype of SMA models *in vitro* upon transgenic expression of the novel transgene, *Co-hSMN1,* using viral vectors. This thesis assessed aspects that were possible to rescue and those which may need revising with alternative strategies. It was hypothesised that expressing a codon-optimised version of the *SMN1* gene (*Co-hSMN1*) in MNs, would rescue SMN protein levels, leading to an improved phenotype which could become a viable therapeutic strategy for pre-clinical translation. The overall aim of this project could be broken down into four, more specific, objectives.

Objective 1: Analyse current data from literature of *in vivo* gene therapy in SMA models using meta-analytic techniques.

Objective 2: Apply *in vitro* delivery of lentiviral and AAV vectors expressing *Co-hSMN1* in cell lines.

Objective 3: Establish an iPSC-derived model of SMA MNs.

Objective 4: Apply *in vitro* delivery of lentiviral vectors expressing *Co-hSMN1* within SMA iPSC MNs and assess downstream phenotypic effects.

# 2 Materials and methods

## 2.1 Materials

### 2.1.1 Cell lines and primary cells

A number of different cell lines and primary cells were used throughout this project. Table 2.1 describes their origin, the media used to culture each cell type as well as a brief description of how these cells were used.

| **Cell line or primary cells** | **Origin** | **Media** | **Use** |
|---|---|---|---|
| HEK293T/17 | Human embryonic kidney cell line | DMEM+Glutamax<br>10% FBS<br>1% Penicillin/ Streptomycin | Lentiviral vector production and preliminary tests |
| HeLa | Human adenocarcinoma cell line | DMEM+Glutamax<br>10% FBS<br>1% Penicillin/ Streptomycin | Lentiviral vector titration |
| Neuro2a | Murine neuroblastoma cell line | *Undifferentiated state:*<br>DMEM+Glutamax<br>10% FBS<br>1% Penicillin/ Streptomycin<br><br>*Differentiated:*<br>DMEM+Glutamax<br>1% FBS<br>1X Non-essential amino acids<br>0.7M NaCO3<br>20µM Retinoic acid | Validation of IDLV_*eGFP* and IDLV_*Co-hSMN1* in a neuronal cell line |
| SH-SY5Y | Human neuroblastoma cell line | *Undifferentiated state:*<br>DMEM+Glutamax<br>10% FBS<br>1% Penicillin/ Streptomycin<br><br>*Differentiated:*<br>DMEM+Glutamax<br>1% FBS<br>1X Non-essential amino acids | Validation of IDLV_*eGFP* and IDLV_*Co-hSMN1* in a human neuronal cell line |

| | | | |
|---|---|---|---|
| | | 20μM Retinoic acid | |
| CHO | Chinese hamster ovary cell line | DMEM+Glutamax<br>10% FBS<br>1% Penicillin/ Streptomycin<br>0.02g/l L-proline<br><br>*Growth arrest:*<br>Methionine-free DMEM + Glutamax<br>2% FBS<br>1% Penicillin/ Streptomycin<br>0.02g/l L-proline | AAV9 vector characterisation |
| Wild type fibroblasts | Primary human skin fibroblasts obtained from healthy donor. Provided by Dr. Eduardo Tizzano (Barcelona, Spain) | 65% DMEM+Glutamax<br>21% M199<br>10% FBS<br>10ng/ml FGF2<br>25ng/ml EGF<br>1μg/ml gentamicin | Validation of IDLV_*Co-hSMN1* |
| GM04603 wild type fibroblasts | Primary human fibroblasts obtained from healthy donor. Obtained for Coriell Institute for Medical Research | 65% DMEM+Glutamax<br>21% M199<br>10% FBS<br>10ng/ml FGF2<br>25ng/ml EGF<br>1μg/ml gentamicin | Validation of IDLV_*Co-hSMN1* |
| SMA type I fibroblasts | Patient skin fibroblasts obtained from Dr Eduardo Tizzano (Barcelona, Spain) | 65% DMEM+Glutamax<br>21% M199<br>10% FBS<br>10ng/ml FGF2<br>5ng/ml EGF<br>1μg/ml gentamicin | Validation of IDLV_*Co-hSMN1* |
| GM00232 SMA type I fibroblasts | Primary fibroblasts obtained from an SMA type I donor. Obtained for Coriell Institute for Medical Research | 65% DMEM+Glutamax<br>21% M199<br>10% FBS<br>10ng/ml FGF2<br>5ng/ml EGF<br>1μg/ml gentamicin | Validation of IDLV_*Co-hSMN1* |
| C2C12 | Mouse myoblast cell line | *Undifferentiated state:*<br>DMEM+Glutamax<br>10% FBS<br>1% Penicillin/ Streptomycin<br><br>D*ifferentiated:*<br>DMEM+Glutamax<br>2% horse serum<br>1% Penicillin/ Streptomycin | Establishment of co-culture system with iPSC MNs |

| | | | |
|---|---|---|---|
| Wild type iPSC lines:<br><br>4603<br>19-9-7T<br>AD3-CL1 | Wild type iPSCs derived from healthy fibroblasts | *Undifferentiated state:*<br>mTESR1, grown on Matrigel matrix<br><br>*Differentiated:*<br>See section 2.3.1.7 | MN differentiation and testing of IDLV_*Co-hSMN1* in wild type backgrounds |
| SMA iPSC lines:<br><br>CS13iSMAI-nxx SMA-19<br>CS32iSMAI-nxx | iPSCs derived from SMA type I patient fibroblasts | *Undifferentiated state:*<br>mTESR1, grown on Matrigel matrix<br><br>*Differentiated:*<br>See section 2.3.1.7 | MN differentiation and testing of IDLV_*Co-hSMN1* in patient specific backgrounds |

***Table 2.1: Summary of cell lines used.***

*Various cell lines were used throughout this project. Here, the media use to culture cells, as well as a brief description of the cells and their uses here are given. For more information regarding iPSC clones, please see section 5.3.1.*

### 2.1.2 Plasmids

A number of plasmids were used within this project for molecular cloning, production of lentiviral and AAV vectors. These are detailed in Table 2.2.

| Plasmid number | Plasmid name | Vector | Use |
|---|---|---|---|
| pRY_397 | pMDLg_pRREintD64V | LV | Packaging |
| pRY_399 | pMD2_VSV-G | LV | Envelope |
| pRY_400 | pRSV_Rev | LV | Rev |
| pRY_396 | pRRLsin_PPT_CMV_*eGFP*_WPRE | LV | Transfer |
| pRY_543 | pRRLsc_CMV _*Co-hSMN1*_mWPRE | LV | Transfer |
| pRY_544 | pRRLsc_hSYN _*Co-hSMN1*_mWPRE | LV | Transfer |
| pRY_552 | pRRLsc_hPGK_*Co-hSMN1*_mWPRE | LV | Transfer |
| pRY_586 | 121_AAV9_CAG_*eGFP* | AAV | Transfer |
| pRY_587 | 701_pAAV_CAG_*Co-hSMN1*_mWPRE | AAV | Transfer |

***Table 2.2 Plasmids used throughout this project.***

*Plasmid numbers and names are given for each of the plasmids used throughout this project. Transfer plasmids carry the transgene cassette containing a gene of interest, whilst packaging, envelope and Rev plasmids are used in the production of lentiviral vectors. LV = lentiviral vector, AAV = adeno-associated viral vector.*

### 2.1.3 Molecular biology buffers

Various molecular biology buffers were used for agarose gel electrophoresis, western blotting and immunofluorescence staining. The composition of these buffers is shown in Table 2.3.

| Use | Buffer | Ingredients |
|---|---|---|
| Agarose gel electrophoresis | 50X TAE | 2M Tris Acetate, 0.05M EDTA, pH 8.2-8.4, made up to 1 litre with distilled water |
| | Running buffer | 1X TAE, 0.5µg/ml Ethidium Bromide (Sigma) |
| Western blotting | 10X TBS | 200mM Tris, 1.5M NaCl, made up to 1 litre with distilled water |
| | 10X running buffer | 250mM Tris, 1.9M glycine, 1% SDS, pH 8.3, made up to 1 litre with distilled water |
| | 10X transfer buffer | 250mM Tris, 1.9M glycine, made up to 1 litre with distilled water. 20% methanol was added to buffer when diluted to 1X immediately before use |
| | 20X running buffer | NuPAGE™ Tris-Acetate SDS Thermo Fisher Scientific |
| | 20X transfer buffer | NuPAGE™ Thermo Fisher Scientific |
| | Wash solutions | 0.1% Tween-20 in PBS or TBS |
| Immunofluorescence staining | Fixation solution | 4% paraformaldehyde (PFA). |
| | Wash solution | 0.1% Tween-20 in PBS |
| | Blocking solution | 1% bovine serum albumin (BSA) in PBS, 3% BSA, 0.25% Triton X-100 in PBS or 5% normal goat serum, 0.25% Triton X-100 in PBS |

***Table 2.3 Molecular biology buffers and their composition.***

### 2.1.4 Antibodies

Antibodies were used in this project for western blotting, immunofluorescence staining and flow cytometry (for protocols please see sections 2.3.4, 2.3.5 and 2.3.6.3, respectively). The following antibodies were used within these protocols depending on the target required (Table 2.4, Table 2.5 and Table 2.6, respectively).

#### 2.1.4.1 Western blot antibodies

| Western blot antibody | Stock concentration | Working concentration | Dilution | Source and catalogue |
|---|---|---|---|---|
| Mouse monoclonal anti-Gemin2 | 1mg/ml | 0.5µg/ml | 1:2000 | Abcam, ab6084 |
| Mouse monoclonal anti-SMN | 250µg/ml | 0.05µg/ml | 1:5000 | BD Biosciences, 610646 |
| Rabbit polyclonal anti-alpha tubulin | 0.66mg/ml | 0.33µg/ml | 1:2000 | Abcam, ab4074 |
| Mouse monoclonal anti-ATM | 1mg/ml | 0.5µg/ml | 1:2000 | Abcam, ab78 |
| Rabbit monoclonal anti-ATM | 0.12mg/ml | 0.12µg/ml | 1:1000 | Abcam, ab32420 |
| Rabbit monoclonal anti-ATM (phospho S1981) | 0.56mg/ml | 0.28µg/ml | 1:2000 | Abcam, ab81292 |
| Polyclonal IRDye 800 CW goat anti-mouse | 1mg/ml | 0.5µg/ml | 1:2000 | LiCor, 926-32210 |
| Polyclonal Goat anti-rabbit Alexa Fluor 680 | 2mg/ml | 0.4µg/ml | 1:5000 | Invitrogen, A-21076 |

***Table 2.4: Summary of western blot antibodies used.***

#### 2.1.4.2 Immunofluorescence antibodies

| Immunofluorescence antibody | Stock concentration | Working concentration | Dilution | Source and catalogue |
|---|---|---|---|---|
| Mouse monoclonal anti-Gemin2 | 1mg/ml | 2.5-5µg/ml | 1:200-400 | Abcam, ab6084 |
| Mouse monoclonal anti-SMN | 250µg/ml | 0.6µg/ml | 1:400 | BD Biosciences, 610646 |
| Mouse monoclonal anti-OLIG2 | 200µg/ml | 2µg/ml | 1:100 | Santa Cruz, sc-515947 |
| Mouse monoclonal anti-neurofilament heavy SMI-32 | 1mg/ml | 10µg/ml | 1:100 | Biolegend, 801701 |
| Rabbit polyclonal anti-βIII tubulin | 0.6mg/ml | 10µg/ml | 1:60 | Sigma, T2200 |
| Rabbit monoclonal anti-choline acetyltransferase | 0.54mg/ml | 5.4µg/ml | 1:100 | Abcam, ab181023 |

| | | | | |
|---|---|---|---|---|
| Mouse monoclonal anti-HB9 | Unknown | Unknown | 1:50 | DSHB, 81.5c10 |
| Polyclonal, Goat anti-mouse Alexa Fluor 488 | 2mg/ml | 2µg/ml | 1:1000 | Invitrogen, A-11001 |
| Polyclonal, Goat anti-mouse Alexa Fluor 555 | 2mg/ml | 2µg/ml | 1:1000 | Invitrogen, A-21424 |
| Polyclonal, Goat anti-rabbit Alexa Fluor 488 | 2mg/ml | 2µg/ml | 1:1000 | Invitrogen, A-11034 |

***Table 2.5: Summary of immunofluorescence antibodies used.***

#### 2.1.4.3 Flow cytometry antibodies

| Flow cytometry antibody | Stock concentration | Optimal dilution | Source | Catalogue number |
|---|---|---|---|---|
| Mouse monoclonal anti-human/mouse SSEA1 PE-Cy7 conjugated | 0.5mg/ml | 10µl for $5x10^5$ cells | Biolegends | 125602 |
| Rat monoclonal anti-human/mouse SSEA3 Alexa Fluor® 647 conjugated | Unknown | 7.5µl for $5x10^5$ cells | Biolegends | 330308 |
| Mouse monoclonal anti-human TRA-181 PE conjugated | Unknown | 15µl for $5x10^5$ cells | Biolegends | 330708 |

***Table 2.6: Summary of flow cytometry antibodies used.***

### 2.1.5 Kits

Various commercial kits were used throughout this project to extract DNA and RNA from cell pellets, purify DNA from bacterial colonies, purify molecular biology reactions, synthesise cDNA and quantify protein concentration in samples. Details of the kits used for these reactions can be found in Table 2.7.

| Kit | Use | Source | Catalogue number |
|---|---|---|---|
| DNeasy Blood and Tissue Kit | DNA extraction from mammalian cells | Qiagen | 69506 |
| QIAprep Spin Miniprep Kit | DNA extraction from bacterial mini-cultures | Qiagen | 27104 |
| EndoFree Plasmid Maxi Kit | DNA extraction from bacterial maxi-cultures | Qiagen | 12362 |

| | | | |
|---|---|---|---|
| QIAquick PCR purification Kit | Purification of PCR products from amplification reactions | Qiagen | 28104 |
| QIAquick Gel Extraction Kit | Extraction of DNA fragments from agarose gels, used in cloning experiments | Qiagen | 28704 |
| RNeasy Mini Kit | Purification of total RNA from mammalian cells | Qiagen | 74104 |
| High Capacity cDNA Reverse Transcription | Synthesis of cDNA from RNA, for use in RT-PCRs | Applied Biosystems | 4368814 |
| DC protein assay | Determining protein concentration from lysed cells | BioRad | 5000112 |
| hPSC Genetic Analysis Kit | qPCR analysis kit for detecting karyotypic abnormalities in iPSCs | STEMCELL Technologies | 07550 |

***Table 2.7: Summary of kits used.***

## 2.2 Data source and meta-analytical methods

### 2.2.1 Study identification

The electronic databases PubMed and Web of Science were searched for relevant published studies between 1950 and 12th June 2020. Keyword strings “gene therapy AND spinal muscular atrophy” and “antisense oligonucleotide AND spinal muscular atrophy” were used. Despite literature often colloquially referring to the use of oligonucleotide-based approaches in gene therapy experiments, oligonucleotides are not officially classed as gene therapies by the FDA, or Advanced Therapy Medicinal Products by EMA. Therefore, the term genetic therapies was used for the remainder of this analysis, with the exception of the search criteria. To avoid missing studies, a broad search string including the words gene therapy was used, as well as a more specific oligonucleotide-containing string. All languages were included in the search and relevant papers were translated if necessary. No restriction concerning type of publication was used. Manual searching of the bibliographies of each of the electronically identified studies revealed references for additional studies which were then retrieved.

### 2.2.2 Study selection criteria

Primary studies found from the electronic and manual searches were screened for eligibility based on the following inclusion criteria; (1) genetic therapy was

administered *in vivo*; (2) a rodent model of SMA was used; (3) median survival data were reported in text, or were calculable form Kaplan-Meier plots; and (4) the number of animals in control and treated groups were reported. Here, *in vivo* genetic therapy was defined as the introduction of genetic material (DNA, RNA, oligonucleotides, viral vectors, bacterial vectors or genome editing technology) directly into an animal. All studies using pharmacological means to manipulate gene expression, for example histone deacetylase inhibitors, were excluded. No restrictions on the type of SMA rodent model were enforced.

### 2.2.3 Data extraction of primary studies

Survival data and aspects of experimental design for each comparison were extracted from included publications. Experimental design characteristics included the type of genetic therapy agent used, rodent model, therapeutic target route and time of administration. Here, P1 was designated as the day of birth. Disparity was observed in the reporting of viral vector dose, with some studies using the total number of vector genomes (vg) administered per animal and others using vector genomes per kilogram (vg/kg). Here, all doses were converted to vg/kg using an approximate birth weight of 1g per pup. Outcome data were recorded as median survival (the number of days at which 50% of animals were alive), and the number of animals in both control and experimental cohorts was recorded. If no median survival data were reported in text, these were measured from figures or sought through contact with authors. If more than 50% of animals survived at the end of the reported time period, the median survival value was recorded as the last time point of assessment. If studies presented multiple control groups, the following hierarchy was implemented and data were extracted from that of the highest relevance; (1) reporter gene (if viral vector) or scrambled ASO (if oligonucleotide), (2) sham surgery or saline injection, (3) untreated. If data were presented from both heterozygous and homozygous SMA animal models, data were extracted from that of homozygous comparisons. If any data were not reported within the study, or if clarification was necessary, study authors were contacted; if no reply was received after two weeks, corresponding studies were excluded.

### 2.2.4 Data analysis

Standard meta-analysis techniques could not be employed here given that no standard error or deviation is associated with median survival data. Therefore, the

meta-analysis workflow used here was adapted using techniques presented in (Vesterinen et al., 2014). This approach has proven successful in other recent pre-clinical meta-analyses (Hirst et al., 2013) and has shown to be comparable to standard (hazard or odds ratio) techniques (Michiels et al., 2005).

Median survival ratios (MSR), equivalent to the survival of treated animals divided by survival of control animals, were calculated to summarise the median survival data that were extracted. This approach was used to maximise consistency with the hazard ratio method commonly used in meta-analyses (Tierney et al., 2007, Michiels et al., 2005). Log-transformed MSRs were entered into a random effects model adapted from DerSimonian and Laird (DerSimonian and Laird, 1986, DerSimonian and Laird, 2015) with the number of animals used as a measure of precision to weight each study. The number of animals was calculated as the sum of treated and true control (number of control animals divided by the number of treatment groups per control group) animals. To achieve an estimate of variance from data that do not contain an inherent error or deviation value, a fixed effect size with associated measure of heterogeneity, denoted by tau, was first calculated. This was then substituted into the random effects model. Finally, the overall MSR (a measure of whether treatment provided a therapeutic benefit or not) was calculated with associated 95% confidence intervals and a final random effects standard error. An MSR of 1 represents a neutral treatment effect, <1 suggested genetic therapy was detrimental to survival, >1 suggests genetic therapy provided a survival advantage.

A stratified meta-analysis was undertaken so that the effect of different experimental intervention conditions could be analysed. The effect of heterogeneity across strata was identified using the $\chi^2$ statistic to determine a threshold level of significance to compare all individual stratifications to. Seven strata were used in this review; type of genetic therapy, dosage of viral vector, overall therapeutic target and *SMN1*-versus *SMN2*-based approaches, mouse model and finally route and time of administration. The $\chi^2$ statistic with degrees of freedom equal to the number of sub-strata minus 1 was adjusted to account for stratifications using the Bonferroni correction. The threshold level of significance calculated was equal to P=0.0073. Stratifications that produced a Bonferroni adjusted P value less than P=0.0073 suggested that heterogeneity between sub-strata, and thus the MSR, was significantly different from one another.

Publication bias was assessed using funnel plots, Egger regression (Egger et al., 1997) and Trim and Fill analysis (Duval and Tweedie, 2000) using the number of animals as a measure of precision. The number of animals was used here, instead of inverse variance, as previously described (Hirst et al., 2013, Vesterinen et al., 2014). The approach here also avoids potential correlation between standard error and effect sizes that can cause the appearance of funnel plot asymmetry (Peters et al., 2006).

#### 2.2.4.1 Statistical formulae

The formulae used when calculating meta-analytic statistics are shown here. Equations marked with an asterisk give a single summary value for all comparisons combined whilst equations without give a value for every comparison. Equations were used in a sequential manner to produce a meaningful endpoint.

$$Eq.1\ Median\ survival\ ratio\ (MSR) = \frac{treated\ median\ survival}{control\ median\ survival}$$

$$Eq.2\ Weight\ (W) = N\ treated\ animals + \left(\frac{N\ total\ control\ animals}{number\ of\ treatment\ groups\ served}\right)$$

$$Eq.3\ Weighted\ effect\ size\ (WES) = W\ x\ (ln\left(\frac{treated\ median\ survival}{control\ median\ survival}\right))$$

$$Eq.4^{*}\ ES_{fixed} = \frac{\sum WES}{\sum W}$$

$$Eq.5\ Heterogeneity = W\ x\ (WES - ES_{fixed})^2$$

$$Eq.6^{*}\ \tau = \sum heterogeneity - (N\ comparisons - 1)$$

$$Eq.7\ W_{random} = \frac{1}{\left(\frac{1}{W} + \tau\right)}$$

$$Eq.8^{*}\ ES_{random} = \left(\frac{\sum(WES\ x\ W_{random})}{\sum W_{random}}\right)$$

$$Eq.9\ WD_{random} = \left(\frac{W_{random}}{\sum W_{random}}\right) x\ (WES - ES_{random})^2$$

$$Eq.10^{*}\ SE_{random} = \left(\frac{\sum WD_{random}}{N\ comparisons}\right)^{0.5}$$

$$Eq.11^{*}\ Overall\ MSR = exponential\left(\frac{\sum(WES\ x\ W_{random})}{\sum W_{random}}\right)$$

$$Eq.12^{*}\ 95\%\ CI = exponential(ES_{random} \pm (1.959963985\ x\ SE_{random}))$$

### 2.2.5 Software

Searches were uploaded to the Collaborative Approach to Meta-Analysis and Review of Animal Data from Experimental Studies (CAMARADES) tool to screen studies for inclusion or exclusion. Data extraction and statistical calculations were performed in Microsoft Excel and Stata. Graphical results were created using the ggplot2 package within R and Microsoft Excel.

## 2.3 Laboratory-based methods

### 2.3.1 Cell culture

All cell lines and primary cells were cultured using the following techniques, with the exception of iPSCs and iPSC-derived MNs, whose techniques are described in sections 2.3.1.6 and 2.3.1.7. The medium in which each individual cell type grows is shown in Table 2.1, FBS and horse serum were both heat inactivated at 65°C for 30 minutes prior to medium addition. All cells were cultured in 37°C incubator at 5% $CO_2$.

#### 2.3.1.1 Resuscitation of frozen cells

Cells that were stored in liquid nitrogen were thawed quickly in a 37°C water bath before being resuspended in 9ml medium, centrifuged at 300xg to remove freezing medium containing DMSO and then seeded into medium in appropriate cultureware.

#### 2.3.1.2 Passaging of cells

Cells were grown until 80-90% confluency before being passaged using trypsin digestion or EDTA clump passaging.

Trypsin digestion required briefly washing cells in PBS, before adding an appropriate volume of trypsin for the culture vessel. Trypsin was inactivated by the addition of appropriate medium. The suspended cells were then centrifuged at 300xg for 5 minutes. A 10µl aliquot of cells was counted in the presence of trypan blue using a haemocytometer to determine the number of live cells in the whole sample. After centrifugation, the cell pellet was resuspended in 1ml medium before the appropriate number of cells were re-seeded.

EDTA (Ethylenediaminetetraacetic acid) clump passaging was used in situations where a single cell suspension was not appropriate and lifting clusters of cells from the culture vessel was needed. Adherent cells were washed with PBS before 0.5mM EDTA was added to the culture vessel and incubated for 5-8 minutes at room temperature. EDTA was aspirated and the addition of medium to the culture vessel was lifted cells from the surface. An appropriate dilution of cells were immediately added in a drop-wise fashion to new cultureware without pipetting up and down to dissociate cells.

#### 2.3.1.3 Freezing of cells for long-term storage

Between 1 and 1.5x$10^6$ cells were frozen in cryovials for long-term storage in appropriate freezing medium for that cell type, also containing DMSO as a preservative. These were stored at -80°C overnight in an isopropanol freezing chamber before being transferred to liquid nitrogen.

| Cell type | Freezing medium |
|---|---|
| HEK293T/17 | 40% DMEM, 50% FBS, 10% DMSO |
| HeLa | 40% DMEM, 50% FBS, 10% DMSO |
| Neuro2a | 40% DMEM, 50% FBS, 10% DMSO |
| CHO | 40% DMEM, 50% FBS, 10% DMSO |
| C2C12 | 40% DMEM, 50% FBS, 10% DMSO |
| SH-SY5Y | 95% culture medium, 5% DMSO |
| Fibroblasts | 90% culture medium, 10% DMSO |
| iPSCs | 100% Cryostor (STEMCELL Technologies) |
| iPSC-MNPs | 90% basal medium, 10% DMSO |

***Table 2.8 Freezing media for long term cell storage in liquid nitrogen.***

*Culture media stated for SH-SY5Y and fibroblast cells are stated in Table 2.1. Basal medium for iPSC storage is stated in Table 2.9.*

#### 2.3.1.4 C2C12 culture

Passaging of C2C12 cells varied from the above protocol due to the requirement for low seeding densities and frequent passages to prevent onset of differentiation. C2C12 cells were seeded at low density ($0.06x10^4$ cells/$cm^2$) during growth phases and were passaged every two days. Differentiation of myoblasts to myotubes was initiated by seeding cells at high density ($1.75x10^4$ cells/$cm^2$) in combination with serum starvation (2% horse serum compared to 10% FBS in growth media).

#### 2.3.1.5 CHO cell cycle arrest

To induce exit from the cell cycle CHO cells were switched from standard medium to growth arrest medium (Table 2.1). Growth arrest medium contained DMEM lacking methionine and low serum concentrations. Cells were cultured in growth arrest medium for four days before cellular DNA content was measured using flow cytometry (see section 2.3.6.1 for details) to confirm that cells had successfully exited the cell cycle.

#### 2.3.1.6 iPSC culture

Six iPSC lines were used in this project; three wild type (4603, 19-9-7T, AD3-CL1) and three SMA type I (CS13iSMAI-nxx, SMA-19 and CS32iSMAI-nxx). For general culture and prior to the start of differentiation iPSCs were seeded at a density of 20,000 cells/$cm^2$ onto Matrigel-coated cultureware in mTESR1 medium. For more information regarding individual iPSC clones, see Table 2.9.

#### 2.3.1.7 iPSC MN differentiation

iPSCs were grown until 90% confluent in 6 well plates then clump EDTA passaged to matrix-coated 10cm dishes until 60-70% confluent. A published protocol (Maury et al., 2015), with some adaptions, was used to differentiate iPSCs into MNs (see section 5.4 and Figure 5.7). The 28-day cell culture protocol was divided into stages. Days 0-9: iPSCs were grown in basal medium (Table 2.9) whilst undergoing neural induction and patterning. Specific media alterations such as additions of retinoic acid and SAG (Smoothened agonist) at day 3 and removal of Chir99021 and Compound C at day 4 were used to mimic signaling pathways present in embryogenesis (see section 5.4). Days 9-16: single cell passaging (on day 9 and 13 with 1:3 split ratio) was performed using Accutase and cells were re-seeded onto matrix-coated cultureware in the presence of Rock inhibitor (Y27632) for 24 hours. During days 9-16 MN progenitors (MNPs) expanded and subsequently acquired

OLIG2 positivity. Day 16: OLIG2+ MNPs were passaged again and seeded for the final time onto matrix-coated cultureware appropriate for the desired assay (e.g. 6 well plates for protein analysis). The addition of DAPT into media from day 16 encourages maturation of MNPs into to post-mitotic MNs highlighted by the appearance of neuronal morphology and axon sprouting. Laminin and a cocktail of growth factors (IGF1, CNTF, BDNF and GDNF) were also added to media to supplement maturation. Day 23: DAPT was removed from the media.

| **Basal medium component** | **Differentiation element** | |
|---|---|---|
| | **Supplement** | **Timing of addition** |
| 1X DMEM/F12 | 3μM Chir99021 | Days 0-3 |
| 1X Neurobasal | 1μM Compound C | Days 0-3 |
| 1X B27 | 1μM Retinoic Acid | Day 3 onwards |
| 1X N2 | 500nM SAG | Day 3 onwards |
| 1X Antibiotic-Antimycotic | 0.5μg/ml Laminin | Day 16 onwards |
| 1X β-mercaptoethanol | 10ng/ml BDNF | Day 16 onwards |
| 0.5μM Ascorbic Acid | 10ng/ml GDNF | Day 16 onwards |
| | 10ng/ml CNTF | Day 16 onwards |
| | 10ng/ml IGF1 | Day 16 onwards |
| | 10μM DAPT | Days 16-23 |

***Table 2.9 Media for MN differentiation.***

*Basal medium consisted of the elements in the first column and was used throughout the differentiation protocol. Basal medium was supplemented at specific time points with differentiation elements.*

## 2.3.2 Bacterial culture and molecular cloning

### 2.3.2.1 Bacterial culture

LB agar plates (20mg/ml LB, 15mg/ml agar, both Sigma) and LB broth (2%w/v) were prepared freshly for each session of bacterial work. Antibiotics (ampicillin and kanamycin at working concentrations of 100μg/ml) were added to LB agar plates when poured or to LB broth immediately before mini-culture set up. Bacterial (*E. coli*) glycerol stocks were removed from -80°C and immediately placed on ice to prevent thawing before being streaked onto set LB agar plates in serial dilutions to obtain single colonies. These were incubated at 37°C overnight then stored at 4°C.

Mini-cultures were set up by picking a single colony with a pipette tip and dropping this into 5ml LB broth containing the appropriate antibiotic. Overnight incubation at 37°C with 225rpm shaking allowed mini-cultures to grow. Maxi-cultures were set up

using the final 1ml of mini-culture. 1:1000 dilution of mini-culture to LB broth (with antibiotic) was cultured overnight at 37°C with 225rpm shaking.

#### 2.3.2.2 Glycerol stocks

1ml of mini-culture was used to make glycerol stocks, if needed, by diluting this 1:1 with 50% glycerol to give a final 25% glycerol concentration. Glycerol stocks were stored at -80°C.

#### 2.3.2.3 Mini-prep DNA extraction

Mini-cultures can be used to extract low concentration yields of plasmid DNA for diagnostic testing. 3ml of mini-culture was used for DNA extraction using QIAprep Spin Miniprep Kit (Qiagen) according to kit instructions. Briefly, bacteria were pelleted then resuspended in 250µl each P1 and P2 buffers to lyse cells. 350µl N3 buffer was added to neutralise lysis reactions before centrifugation at 13,000rpm for 10 minutes to pellet cell debris. The supernatant was applied to the spin column and spun to bind DNA to membrane. Bound DNA was washed sequentially with 500µl PB and 750µl PE. DNA was eluted in 50µl EB twice, or if a high concentration was required the first eluate was used again. The ND1000 Nanodrop Spectrophotometer (Thermo Fisher Scientific) was used to determine DNA concentration and purity in each sample.

#### 2.3.2.4 Maxi-prep DNA extraction

A bacterial cell pellet is obtained by centrifuging maxi-cultures at 4°C, 3240xg for 45 minutes. The EndoFree Plasmid Maxi Kit (Qiagen) was used to obtain sterile, purified plasmid DNA to be used in transfection experiments or to make viral vectors, according to kit instructions. Briefly, the bacterial cell pellet was resuspended in 10ml P1, lysed with 10ml P2 for 5 minutes, then neutralised with 10ml chilled P3 buffer. The lysate was filtered using a QIAfilter Cartridge to remove cell debris. 2.5ml buffer ER was added to the filtered lysate and incubated on ice for 30 minutes, before applying to an equilibrated QIAGEN-tip 500 to bind DNA. This was washed twice with 30ml buffer QC before eluting DNA in 15ml buffer QN. DNA was precipitated using isopropanol then pelleted by centrifuging at 6000rpm for 1 hour at 4°C. DNA was washed with endotoxin-free 70% ethanol, then re-pelleted by centrifugation at 6000rpm for 30 minutes at 4°C. The pellet was air dried in a tissue culture hood to maintain sterility then dissolved in a suitable volume of endotoxin-

free, sterile TE. The concentration of this purified DNA was determined, then restriction digested to confirm the expected fragment pattern was present.

#### 2.3.2.5 Ligation of plasmid DNA

Ligation of plasmid DNA was prepared in microcentrifuge tubes on ice using the T4 DNA Ligase (NEB) protocol. For a 20µl reaction, 2µl 10X T4 DNA Ligase buffer, 1µl T4 DNA Ligase, vector and insert DNA fragments at an appropriate molar ratio and nuclease-free water were combined. The reaction was gently mixed before incubating at 16°C overnight. Following this, the reaction was chilled on ice before being stored at -20°C until use.

#### 2.3.2.6 Transformation of plasmid DNA

Transformation of ligated or control plasmid DNA was performed using chemically competent Top10 or XL10 Gold Ultracompetent (Stratagene) bacterial cells using similar heat shock protocols. Appropriate controls such as a supercoiled plasmid (pUC18), uncut vector and digested vector were used during the transformation procedures. Top10 *E. coli* were thawed on ice then aliquoted into 50µl samples. 1-5µl ligated DNA (corresponding to 10pg-100ng DNA) was added to the aliquot of cells then incubated on ice for 2 minutes. Heat shock transformation of each tube was conducted by placing each in a 42°C water bath for 30 seconds. Immediately following heat shock, tubes were placed on ice for 2 minutes. 900µl pre-warmed antibiotic-free LB broth was added to each tube before plating 100µl onto Ampicillin-containing LB agar plates and incubated at 37°C again overnight.

XL10 Gold Ultracompetent cells (Stratagene) were thawed on ice then aliquoted into 50µl samples before adding 2µl β-mercapthoethanol and incubated for 10 minutes on ice. 2µl ligated DNA was added to one aliquot of cells, whilst the pUC18 control plasmid was diluted 1:10 then 1µl added to a second aliquot. These were incubated on ice for 30 minutes then administered a heat shock by placing tubes in a 42°C water bath for 30 seconds. Immediately following heat shock, tubes were placed on ice for 2 minutes. 450µl pre-warmed SOC media (Fisher Scientific) was added per tube and were incubated at 37°C for 1 hour with 225rpm shaking to provide time for the synthesis of antibiotic resistance proteins. 200µl of cells transformed with the ligation or 5µl of pUC18 transformed cells were plated onto Ampicillin-containing LB agar plates and incubated at 37°C again overnight.

### 2.3.3 Molecular biology

#### 2.3.3.1 DNA extraction

The Qiagen DNeasy Blood and Tissue Kit was used to extract DNA from cultured cell samples following kit instructions. Briefly, a cell pellet containing a maximum of $5x10^6$ cells was resuspended in 200µl PBS before adding 20µl proteinase K. 200µl buffer AL was added and samples incubated at 56°C for 10 minutes to allow complete lysis of cells. 200µl of 96-100% ethanol was used to precipitate DNA before application of the cell lysate and DNA precipitate onto the spin column. Centrifugation at >6000xg was used to bind DNA to the membrane. A series of washes (500µl AW1, 500µl AW2) was used to remove impurities and residual ethanol from DNA. DNA was eluted twice in 200µl buffer AE. The ND1000 Nanodrop Spectrophotometer (Thermo Fisher Scientific) was used to determine DNA concentration and purity in each sample.

#### 2.3.3.2 RNA extraction

The Qiagen RNeasy Mini Kit was used to extract total RNA from cultured cell samples following kit instructions. Cells were lysed as either pellets or directly in the culture vessel by adding 350µl or 600µl buffer RLT (350µl for $<5x10^6$ cells or 650µl for $5x10^6$-$1x10^7$ cells). Samples were lysed and homogenized using a pipette and/or vortexing for a 1 minute. 1 volume of 70% ethanol was added to precipitate RNA. Lysates were transferred to a spin column and centrifuged at >8000xg for 15 seconds to allow RNA to bind to the membrane. A series of washes (700µl RW1, 500µl RPE, 500µl RPE) was used to remove impurities, residual ethanol from RNA and dry membrane. RNA was eluted twice in 30µl RNase-free water, or by re-using the first eluate if a high concentration was required. The ND1000 Nanodrop Spectrophotometer (Thermo Fisher Scientific) was used to determine RNA concentration and purity in each sample.

#### 2.3.3.3 cDNA synthesis

Single stranded complementary DNA (cDNA) was synthesised from total RNA using the Applied Biosystems High Capacity cDNA Reverse Transcription Kit. Up to 2µg total RNA was used per 20µl reaction. A 2X reverse transcription (RT) master mix

was first prepared on ice using 2µl 10X RT buffer, 0.8µl 25X 100mM dNTP mix, 2µl 10X random primers, 1µl MultiScribe™ Reverse Transcriptase and nuclease-free water up to 10µl per reaction needed. To this, 10µl of RNA extract (containing a maximum of 2µg RNA) was added to each thin-walled PCR tube already containing 10µl of master mix. Briefly, tubes were centrifuged to collect all material at the bottom and eliminate air bubbles. Reactions were placed into the Techne 512 thermocycler and the following program was set; 25°C 10 minutes, 37°C 2 hours, 85°C 5 minutes, 4°C hold. Resulting cDNA was stored at 4°C if synthesised up to 24 hours before use, or at -20°C for long-term storage.

#### 2.3.3.4 PCR

Polymerase chain reaction (PCR) was performed using the following reaction components and cycling conditions in the Techne 512 thermocycler. Temperature gradient PCRs were performed to find optimal primer annealing temperature. All PCR reactions were set up on ice. Primer sequences can be seen in Table 2.10. PCR products were visualised on agarose gels with an appropriate molecular weight marker. Two PCR protocols were followed depending on the DNA polymerase used in per experiment.

The first protocol details procedures for GoTaq G2 Flexi DNA polymerase (Promega). 1X GoTaq Flexi Green buffer, 1.5mM $Mg^{2+}$, 0.3µM each forward and reverse primers, 0.2mM dNTPs, 0.05U/µl GoTaq G2 Flexi DNA Polymerase and an appropriate amount of starting genomic or plasmid DNA were included per reaction in a final volume of either 25µl or 50µl. Initial denaturation 95°C 2 minutes, 35 cycles of denaturation 95°C 30 seconds, annealing optimal°C 30 seconds, extension 72°C (extension time varies based on expected product length, 1 minute for 1kb using GoTaq), final extension 5 minutes then 4°C hold.

The second protocol details procedures for Q5 High-Fidelity DNA polymerase (NEB). 1X Q5 reaction buffer, 0.5µM each forward and reverse primers, 0.2mM dNTPs, 0.02U/µl Q5 High-Fidelity DNA Polymerase and an appropriate amount of starting genomic or plasmid DNA were included per reaction in a final volume of either 25µl or 50µl. Optionally, 1X Q5 High GC Enhancer was added to reactions containing template DNA with a high GC content. Initial denaturation 98°C 30 seconds, 35 cycles of denaturation 98°C 10 seconds, annealing optimal°C 30

seconds, extension 72°C (extension time varies based on expected product length, 30 seconds for 1kb using Q5), final extension 2 minutes then 4°C hold.

| Name | Purpose | Sequence (5' to 3') |
|---|---|---|
| Exon6_F_Gaby | Origins of SMN transcript RT-PCR | CTCCCATATGTCCAGATTCTCTTG |
| Exon8_R_Gaby | | CTACAACACCCTTCTCACAG |
| pRY_586/7_CAG_Sequencing_F1 | Sequencing of CAG promoter region in AAV plasmids pRY_586 and pRY_587 | CAATACGCAAACCGCCTCTC |
| pRY_586/7_CAG_Sequencing_F2 | | TATGCCAAGTACGCCCCCTA |
| pRY_586/7_CAG_Sequencing_F3 | | CTGACTGACCGCGTTACTCC |
| pRY_586/7_CAG_Sequencing_F4 | | CCGCAGCCATTGCCTTTTAT |
| pRY_586/7_CAG_Sequencing_R4 | | CCTTGATCAGGGCGGTGTC |
| pRY_586/7_CAG_Sequencing_R5 | | CAGATGTCGCCGTTCTTCAG |
| 189_mGapdhex4_Fw | Origins of SMN transcript RT-PCR | AAAGGGTCATCATCTCCGCC |
| 190_mGapdhex4-5_Rv | | ACTGTGGTCATGAGCCCTTC |
| B-actin_F | Origins of SMN transcript RT-PCR | TCACCCACACTGTGCCCATCTACGA |
| B-actin_R | | CAGCGGAACCGCTCATTGCCAATGG |
| B-actin_F | Lentiviral titration qPCR | TCACCCACACTGTGCCCATCTACGA |
| B-actin_R | | CAGCGGAACCGCTCATTGCCAATGG |
| 2d-LRT_F | Lentiviral titration qPCR | AACTAGAGATCCCTCAGACCCTTTT |
| 2d-LRT_R | | CTTGTCTTCGTTGGGAGTGAATT |
| Endog_SMN_F | Amplifies exons 1-4 of endogenous SMN genes | CAGGAGGATTCCGTGCTGTT |
| Endog_SMN_R | | GGGTGGTGGAGGGAGAAAAG |
| pRY_587_Co-hSMN1_F | Transgene specific amplification for RT-PCR | CCCGAGCAGGAAGATAGCGT |
| pRY_587_Co-hSMN1_R | | CTGCAGGTCAGTTCAGGCT |

***Table 2.10 Primers used throughout this project.***

#### 2.3.3.5 Reverse transcriptase-PCR (RT-PCR)

RT-PCR was performed as above for general PCRs, but with the exception that starting genomic material was not genomic or plasmid DNA, but was cDNA synthesised from RNA. Please see sections 2.3.3.2 and 2.3.3.3 for RNA extraction and cDNA synthesis protocols.

#### 2.3.3.6 Quantitative PCR and RT-PCR (qPCR and qRT-PCR)

qPCR reactions were set up on ice and utilised the SensiMix SYBR No-ROX Mix mastermix containing all necessary reaction components except target primers. Mastermixes for each target were prepared by multiplying the volumes stated by the number of each reaction needed. An appropriate volume of mastermix was aliquotted per qPCR tube. Reactions were analysed using the Qiagen Rotorgene Q qPCR machine with the following cycling conditions: 50°C 2 minutes, 95°C 10 minutes, then 50 cycles of 95°C 15 seconds, 60°C 1 minute. Where appropriate, the ΔΔCt method of qPCR analysis was used to determine gene expression fold-change.

##### 2.3.3.6.1 Preparation of qPCR standards

qPCR standards were prepared from plasmid DNA for LRT lentiviral titration qPCR reactions using the pRY_396 plasmid. The average molecular weight of the plasmid was calculated as 660g/mol multiplied by total length of plasmid. The number of molecules in 1µg of each plasmid was calculated using Avogadro's number and adjusted to calculate number of molecules/µl. Dilutions of this plasmid were prepared to achieve $10^2$-$10^7$ molecules in 6.25µl for input into qPCR reactions.

qPCR standards using genomic DNA were prepared for β actin standards for lentiviral titration. HeLa cells were cultured and genomic DNA was extracted from $1x10^6$ cells using the Qiagen Blood and Tissue DNeasy kit as per kit instructions. This genomic DNA was serially diuluted to a $1x10^1$-$10^6$ range of molecules. 5µl of this was used per qPCR reaction.

##### 2.3.3.6.2 hPSC Genetic Analysis qPCR assay

The hPSC Genetic Analysis Kit (STEMCELL Technologies) provided all reagents necessary for the analysis, except target cell DNA. Provided reagents included

qPCR mastermix (2X), genomic DNA control, TE buffer and probes specific to the following chromosomal regions: 1q, 4p, 8q, 10p, 12p, 17q, 20q, Xp. All reactions were set up on ice.

Genomic DNA was harvested from undifferentiated iPSC lines using the Qiagen Blood and Tissue DNeasy kit as per kit instructions. qPCR reaction set up was conducted as per hPSC Genetic Analysis Kit instructions, briefly described here. Genomic DNA control and harvested DNA from target cells was diluted in nuclease free water to a final concentration of 5ng/µl in a total of 58µl. qPCR mastermix was vortexed on high for 5 seconds, then 145µl was added to each genomic DNA sample and mixed by pipetting up and down. These were protected from light and stored on ice until needed. Stock solutions of primer-probe mixes were prepared by resuspension of powdered probe in 33µl TE buffer. These were then diluted in nuclease-free water by a factor of 1:6. Dilute genomic DNA and dilute primer-probe mixes were then combined by adding 14µl DNA and 6µl primer-probe mixes to a total of 20µl reaction volume possible in the Qiagen Rotorgene Q qPCR machine. Reactions were analysed with the following cycling conditions: 95°C 3 minutes then 40 cycles of 95°C 15 seconds, 60°C 1 minute. Values were analysed using the ΔΔCt method described below.

#### 2.3.3.6.3 ΔΔCt analysis of expression

Average Ct values for each sample (both housekeeping or control gene and gene of interest) were first calculated. ΔCt values were then calculated by subtracting the average gene of interest Ct value from the average housekeeping or control Ct value within the same sample. This normalises data within samples to account for any differences in starting material concentration. Next, ΔΔCt values were calculated by subtracting the average ΔCt value from the sample of interest from the average ΔCt value of an external control sample (e.g. wild type cells, or control genomic DNA). Expression fold change was then calculated by $2^{-\Delta\Delta Ct}$, or chromosomal copy number by 2 multiplied by $2^{-\Delta\Delta Ct}$.

### 2.3.3.7 Restriction digests

Restriction digests of mini-prep DNA were completed using the following reaction volume: 2.5µl 10x buffer, 2.5µl 10mg/ml BSA, 500ng plasmid DNA, 10 units restriction enzyme, sterile water up to 25µl. Reactions were incubated at appropriate

temperatures for cleavage (e.g. 37°C) for 1 hour then heat inactivated (e.g. 65°C) for 20 minutes. Loading dye was added to samples before agarose gel electrophoresis with an appropriate molecular weight marker for reference. Gels and running buffer contained ethidium bromide to intercalate into DNA. Gels were imaged using a Gel Doc under UV light.

#### 2.3.3.8 Blunting

If DNA were required to be blunt ended prior to a procedure such as blunt end ligation for example, the following procedure were used. T4 DNA ligase buffer, 50uM dNTPs, 1 unit Klenow (NEB) per 1µg plasmid DNA were incubated at 25°C for 15 mins before the addition of 10mM EDTA and a further incubation at 75°C for 20 minutes.

#### 2.3.3.9 Agarose gel electrophoresis

An appropriate mass of agarose (depending on percentage of gel desired) was dissolved in 1x TAE by microwaving in short bursts. Once fully dissolved, the mixture was cooled under running water and ethidium bromide added to a final concentration of 0.5µg/ml. The molten gel was poured into a tank containing a well comb of appropriate size and left to set for 30 minutes. Following this, buffer dams and combs were removed and the tank filled with running buffer before samples were loaded. If samples did not contain a coloured buffer, 5x or 6x loading dye was added as appropriate before loading onto the gel. Gels were run at 1V/cm, generally at 50V for 60 minutes in most cases. DNA bands were visualized using the Bio-Rad Gel Doc 2000 UV Transilluminator. If necessary, Image J was used to quantify visible bands.

#### 2.3.3.10 Gel extraction and PCR purification

The QIAquick Gel Extraction Kit (Qiagen) was used to retrieve desired DNA fragments following agarose gel electrophoresis of either PCR amplicons or restriction digested DNA. The desired fragment was excised from the gel with a scalpel, minimizing the amount of excess gel. The weight of the excised gel was used to calculate the volume of buffer QG to add (100mg gel ~100µl). 3 volumes buffer QG (or 6 volumes if >2% agarose gel used) was added and incubated for 10 minutes at 50°C, vortexing every few minutes, to dissolve the gel. 1 volume isopropanol was added to precipitate DNA and the solution was transferred to a spin

column. Centrifugation at full speed (~17,900xg) was used to bind DNA to the column membrane. Washes with 500µl buffer QG and 750µl buffer PE were used to wash DNA, particularly important steps for downstream salt-sensitive applications such as blunt end ligation and sequencing. DNA was eluted in 30µl buffer EB (EB was left to stand in the column for up to 4 minutes to increase yield) then concentration was determined.

PCR purification was performed using the QIAquick PCR Purificatin Kit (Qiagen) to remove primers, nucleotides, polymerases and salts from PCR products of interest. 5 volumes of buffer PB was added to 1 volume PCR sample and mixed, pH was adjusted if necessary using 3M sodium acetate. The sample was applied to a spin column and centrifuged for 1 minute at full speed (~17,900xg). One wash using 750µl buffer PE removes impurities before a further spin to remove residual ethanol. DNA was eluted in 30µl buffer EB twice, or re-using the first eluate if a high concentration was required. Concentration and purity were determined using a Nanodrop Spectrophotometer.

### 2.3.4 Protein analysis

Cells of interest were lysed using RIPA (radioimmunoprecipitation assay; Fisher Scientific) buffer in the presence of protease inhibitor cocktail, and phosphatase inhibitors if needed, for 5 minutes on ice. This lysate was gathered, transferred to an eppendorf and centrifuged for 15 minutes at 14,000xg (4°C) to pellet cell debris. The supernatant was then stored at -80°C until use. The concentration of total protein in this supernatant was determined using the microplate BioRad DC protein assay according to kit instructions. Briefly, BSA standards (0-2mg/ml) and samples of unknown concentration were incubated in the presence of alkaline copper tartrate, dilute folin and surfactant solution for 15 minutes before the absorbance of these samples was measured at 750nm using a plate reader (BioTek).

Western blotting protocols were optimised individually for the detection of each protein of interest, therefore detailed protocols for these proteins can be found below. Whilst all possible attempts were made for consistency and reproducibility between western blots completed throughout this project, inherent variation will be present. Therefore, the comparison of protein signals across all western blots within this thesis should not be undertaken, but only within experiments that were completed concurrently.

#### 2.3.4.1 Standard western blots

Western blots were undertaken as soon as possible after protein extraction to avoid loss of protein immunoreactivity over time (Hunter et al., 2014). SDS-PAGE was undertaken using 4-15% Tris-Glycine pre-cast gels (Bio-Rad) in the presence of 1x running buffer (see Table 2.3 for 10X recipe). 8µg protein (unless otherwise stated), loading buffer (Invitrogen) containing Coomassie G250 and Phenol Red tracking dyes and a reducing agent (Invitrogen) were denatured by heating to 95°C for 5 minutes. Samples were then loaded into gels and run at 200V for 30 minutes to allow protein separation, along with 5µl PageRuler™ Plus Prestained Protein Ladder. Gels were removed from cassettes and immediately placed in 1x transfer buffer (see Table 2.3 for 10X recipe) to avoid dehydration. Transfer cassettes were assembled with nitrocellulose membranes (Sigma) then placed into the transfer tank with an ice block to prevent excessive heat, then run at 100V for 1 hour.

Following transfer of protein samples obtained from MNs, nitrocellulose membranes were washed once in PBS then incubated for 5 minutes in REVERT Total Protein Stain then washed twice for 30 seconds each with REVERT Total Protein Wash (LiCor). Membranes were then immediately imaged using the Odyssey CLx (LiCor) in the 700nm channel.

Following total protein staining or transfer for all other experiments not using protein samples from MNs, membranes were blocked in Odyssey blocking buffer (LiCor) 1:1 PBS for 1 hour at room temperature with gentle agitation. Primary and secondary antibodies (Table 2.4) were diluted in Odyssey blocking buffer 1:1 0.1% PBST. Primary antibody incubation of membranes took place overnight at 4°C, whilst secondary antibody incubation occurred at room temperature for 1 hour, both with gentle agitation. Following each antibody incubation, four 5 minute 0.1% PBST washes were used to remove antibody residue and prevent high background signal. Membranes were imaged using the Odyssey CLx in 700nm and 800nm channels. Quantification of protein signals was achieved using Image Studio Lite (LiCor).

#### 2.3.4.2 ATM and phosphorylated ATM western blots

SDS-PAGE was undertaken using NuPAGE™ 3-8% Tris-Acetate pre-cast gels in the presence of 1X running buffer containing 1X antioxidant (NuPAGE™). 10µg

protein (unless otherwise stated) and loading buffer (NuPAGE™) containing Coomassie G250 and Phenol Red tracking dyes (NuPAGE™) denatured by heating to 70°C for 10 minutes, following which reducing agent (NuPAGE™) was added immediately prior to loading. Samples were then loaded into gels and run at 150V for 70 minutes to allow protein separation, along with 10µl HiMark Pre-stained protein standard. Gels were removed from cassettes and immediately placed in 1X transfer buffer plus 10% methanol to avoid dehydration. Transfer cassettes were assembled with nitrocellulose membranes (Sigma) then placed into the transfer tank, buffer and an ice block to prevent excessive heat, then run at 30V for 2 hours.

Following total protein staining or transfer for all other experiments not using protein samples from MNs, membranes were blocked in blocking buffer (Table 2.11) for 1 hour at room temperature with gentle agitation. Primary and secondary antibodies (Table 2.4) were diluted in antibody dilution buffer (Table 2.11). Primary antibody incubation of membranes took place overnight at 4°C, whilst secondary antibody incubation occurred at room temperature for 1 hour, both with gentle agitation. Following each antibody incubation, four 5 minute washes (Table 2.11) were used to remove antibody residue and prevent high background signal. Membranes were imaged using the Odyssey CLx in 700nm and 800nm channels. Quantification of protein signals was achieved using Image Studio Lite (LiCor).

| Reagent | ATM-probed membranes | Phosphorylated ATM-probed membranes |
|---|---|---|
| Blocking buffer | 5% milk in PBS | 5% BSA in TBS |
| Antibody dilution buffer | 5% milk in 0.1% PBS-T | 5% BSA in 0.1% TBS-T |
| Wash buffer | 0.1% PBS-T | 0.1% TBS-T |

***Table 2.11 Buffers used in ATM and pATM western blots***

### 2.3.5 Immunofluorescence staining

Cells to be immunostained were fixed by washing twice with ice-cold PBS then incubated in 4% PFA for 10 minutes at room temperature, followed by two further ice-cold PBS washes. If not being stained immediately, samples were stored at 4°C. Cells were then permeabilised to allow binding of antibodies to intracellular target proteins. This step was combined with blocking to prevent unspecific binding when cells were incubated with 5% normal goat serum (Fisher Scientific) in PBS with

0.25% Triton X-100 for 45 minutes. Antibodies (see Table 2.5) were also diluted in the same solution. Primary antibody incubation occurred at 4°C overnight before three 5 minute PBS washes with gentle agitation removed the excess. Cells were incubated with the secondary antibody at room temperature for 1 hour before three further 5 minute PBS washes. Cells were counterstained with DAPI (Sigma) at 1µg/ml for 5 minutes then rinsed once with PBS. Cells were imaged using a Zeiss Axio Observer D1 fluorescent microscope with consistent exposure settings for all corresponding experiments.

#### 2.3.5.1 Immunofluorescence staining of motor neurons

Immunofluorescence staining was used to assess expression of markers indicating MN maturity. For this, MNs were seeded at a density of 25,000 cells on day 16 of differentiation (see 2.2.2.4) onto 13mm coverslips coated with 15µg/ml poly-ornithine and Matrigel. Primary antibodies against SMI32 (a component of neurofilament heavy chains), βIII-tubulin (a pan-neuronal marker), choline acetyltransferase (ChAT; the enzyme responsible for recycling the neurotransmitter choline) and HB9 (a MN-specific transcription factor) were used to assess maturity. Antibodies used and their corresponding working concentrations can be found in Table 2.5.

Due to the fragile nature of MNs are the likelihood of detachment from coverslips, an adjusted immunofluorescence protocol was used to avoid cell loss. Coverslips were removed from cultureware using sharp forceps and dipped into a clean well of ambient temperature PBS to wash off excess cell culture media, before being dipped in a clean well of pre-warmed 4% PFA, then a second clean PBS well. At all times coverslips were gently held in forceps and were only in contact with each new solution for a few seconds. These were transferred into a 24 well plate containing 5% normal goat serum in PBS with 0.25% Triton X-100 for blocking (45 minutes). All solutions removed or added to the coverslips were done so very gently to avoid MN loss. Primary antibody incubation occurred at ambient temperature for 2 hours before three 5 minute PBS washes removed the excess. Cells were incubated with the secondary antibody at room temperature for 1 hour before three further 5 minute PBS washes. Cells were counterstained with DAPI at 1µg/ml for 5 minutes then rinsed once with PBS. Coverslips were mounted onto glass slides using Fluoromount (Sigma) to preserve fluorescence, slides were stored 4°C in the dark.

Cells were imaged using a Zeiss Axio Observer D1 fluorescent microscope with consistent exposure settings for all corresponding experiments.

#### 2.3.5.2 iPSC MN neurite length measurement

Neurite length was assessed using an ImageJ plugin called NeuriteTracer (Pool et al., 2008). Briefly, MNs immunostained against βIII-tubulin and counterstained with DAPI were fluorescently imaged in separate channels for the nuclear marker and the neuronal marker. These were adapted into grey-scale images and loaded into the NeuriteTracer plugin, multiple pairs of images were analysed simultaneously. Thresholds were set that ensured that all neurite outgrowths and nuclei were framed in each channel, without background signals. The diameter of a number of nuclei were measured to determine a size range of visible nuclei, which is then inputted into the program. The scale of the image is inputted into the plugin to allow calculation of absolute neurite lengths in micrometers. The total length of all neurites in the image, as well as the number of nuclei present, is presented. This total length was divided by the number of nuclei to calculate an average neurite length per cell.

### 2.3.6 Flow cytometry

Cells to be assessed by fluorescent associated cell sorting (FACS) were harvested by trypsin or Accutase digestion then pelleted by centrifugation at 1000rpm for 5 minutes. If samples were to be assessed immediately the cell pellet was resuspended in PBS, but if samples were to be stored prior to analysis the cell pellet was resuspended in 1% PFA. The FACS Canto II (BD Biosciences) and associated FACS Diva software were used for all flow cytometry. Cell samples were mixed prior to loading onto the machine to achieve a homogeneous suspension. Appropriate lasers containing relevant excitation and emission bandpass filters were used depending on the experiment. *eGFP* expression was detected using the blue laser and FITC channel with 488nm excitation and 530/30 bandpass filter.

#### 2.3.6.1 Cellular DNA content measurement

Samples containing approximately $1x10^6$ cells were harvested by trypsin digestion, pelleted then resuspended in 1% PFA for 10 minutes on ice. Samples were then centrifuged, PFA discarded and cells resuspended in 0.1% (v/v) Triton X-10 in PBS to allow permeabilisation for 10 minutes. 10µl of 10mg/ml RNase A was added to 1ml of cell suspension (final concentration 100µg/ml) to prevent measurement of

RNA rather than DNA content. Samples were incubated for 5 minutes at room temperature. The nucleic acid stain DAPI (1µg/ml final concentration) was added to samples which were then incubated in the dark for 10 minutes. To collect DAPI fluorescence, the violet laser with Pacific Blue channel was used (401nm excitation and 450/50 bandpass filter).

#### 2.3.6.2 Survival of iPSC-derived MNs

Survival and longevity of mature MNs was analysed using a flow cytometry-based assay. MNs were harvested with Accutase digestion then stained with 20µg/ml propidium iodide (Sigma) on ice for 10 minutes or 1µM SYTOX AADvanced dead cell stain (Thermo Fisher Scientific) at 37ºC for 5 minutes to label dead cells, with CellEvent Caspase 3/7 Green Detection Reagent (Thermo Fisher Scientific) at 37ºC for 30 minutes to label apoptotic cells, without PFA-mediated fixation. Propidium iodide fluorescence was collected in the PE channel, SYTOX AADvanced fluorescence in PerCP-Cy5.5 channel (488nm excitation and 695/40 bandpass filter) and CellEvent fluorescence in FITC channel (488nm excitation and 530/30 bandpass filter). The percentage of cells expressing each marker was calculated.

#### 2.3.6.3 Direct antibody staining

Cells were harvested and counted before the total number of cells needed were resuspended in 0.1% BSA in PBS. No fixation was used in direct antibody staining experiments. 50µl of cell suspension was used per sample. Samples were kept on ice at all times to prevent antigen internalisation. To determine the appropriate volume of antibody to add to each sample, a titration was performed that maximized number of positive cells without creating high background signal. Antibodies were added directly to tubes containing 50µl cell suspension, then incubated on ice in the dark for 30 minutes. Two washes (700rpm centrifugation for 3 minutes) using 500µl 0.1% BSA/PBS were used to remove excess, unbound antibody. Cell suspensions were transferred to FACS tubes before being analysed on the flow cytometer.

Antibodies used for flow cytometry can be seen in Table 2.6. Appropriate controls were used to exclude background signal from results. Unstained samples are used to detect autofluorescent cells, whilst single stained samples help to reveal spectral overlap between fluorophores. In samples stained with more than two antibodies,

fluorescent minus one (FMO) controls detect spillover induced background and allow for compensation calculations.

### 2.3.7 Viral vectors

#### 2.3.7.1 Production of lentiviral vectors

A 3rd-generation lentiviral system was used to produce IDLVs. This involved transient calcium phosphate co-transfection of HEK293T/17 cells with four plasmids (1:1:1:2 ratio) encoding the packaging constructs (pMDL_D64V), replication and transcriptional machinery (pRSV_REV), envelope proteins (pMD2_VSV-G) and the transfer plasmid encoding the transgene of interest (see Table 2.2). Transgene cassettes are driven by relevant promoters (CMV, hSYN or hPGK) and are coupled to mWPRE. Packaging plasmids contain a D64V point mutation (Yáñez-Muñoz et al., 2006) in the catalytic active site of the integrase enzyme to prevent viral integration into the host cell genome. The co-transfection of all four plasmids was undertaken in the presence of 2.5M $CaCl_2$ and HBS (100mM HEPES, 281mMM NaCl, 1.5mM $Na_2HPO_4$, pH 7.12). Ultracentrifugation (23,400 rpm for 2 hours) of the supernatant collected from each HEK293T plate at 48 and 72 hours post-transfection was used to concentrate vectors. These vectors were resuspended in DMEM without supplements, centrifuged briefly to remove debris then adjusted to a concentration of 10mM $MgCl_2$ as well as DNase I added. For long term storage and future use these were frozen at -80°C as whole samples. Both 48 and 72 hour samples for each vector produced were thawed fully and combined together so that harvests are mixed. This combined sample was then aliquotted and stored at -80°C.

##### 2.3.7.1.1 Titration of lentiviral vectors

Titration of lentiviral vectors was performed by qPCR and in addition flow cytometry for vectors expressing eGFP. HeLa cells were transduced with vectors of unknown titre in serial dilutions in the presence of 8µg/ml polybrene. Vector stock was diluted at both 1:2000 and 1:20000 for transductions for qPCR titration, whilst serial dilutions ranging from $1x10^{-3}$ to $1x10^{-7}$ were used for FACS titrations.

##### 2.3.7.1.2 qPCR

For qPCR analysis, $1x10^5$ HeLa cells transduced with serial dilutions (A 1:2000 or B 1:20000) of the vector(s) of interest were harvested by trypsin digestion, pelleted and subjected to DNA extraction using DNeasy Blood and Tissue Kit (Qiagen), 24 hours post-transduction. This HeLa DNA containing viral genomes was used to set up qPCR reactions. All DNA extractions and qPCR set up were performed in a laminar flow hoods to avoid contamination from DNA sources wherever possible. Water and AE DNA elution buffer (from DNeasy Blood and Tissue kit) were used as no template controls. DNA from HeLa cells mock transduced with vector was used as a negative control. LRT standards ($10^2$, $10^3$, $10^4$, $10^5$, $10^6$, $10^7$ copies of the pHR'SIN-cPPT-SEW plasmid) and β-actin standards ($10^1$, $10^2$, $10^3$, $10^4$, $10^5$, $10^6$ HeLa cell genomes) were used in standard curves. See section 2.3.3.6.1 for details of qPCR standard production. Control and standard reactions were performed in triplicate, whilst viral DNA reactions were performed in duplicate.

qPCR reactions were set up on ice using the components stated in

Table 2.12. A mastermix for both LRT and β-actin reactions were prepared, following which 13.75µl of LRT mastermix or 15µl of β-actin mastermix was aliquoted per qPCR tube. 6.25µl or 5µl control, standard or DNA was added to LRT and β-actin reaction tubes, respectively, to a total of 20µl per tube. Reactions were analysed using the Qiagen Rotorgene Q qPCR machine with the following cycling conditions: 50°C 2 minutes, 95°C 10 minutes, then 50 cycles of 95°C 15 seconds, 60°C 1 minute.

| **Component** | **LRT reaction (µl)** | **β-actin reaction (µl)** |
|---|---|---|
| SensiMix SYBR No-ROX Mix | 10 | 10 |
| Forward primer (LRT_F/ β-actin _F;10µM) | 0.2 | 0.2 |
| Forward primer (LRT_R/ β-actin _R;10µM) | 0.2 | 0.2 |
| Sterile water | 3.35 | 4.6 |
| Total | 13.75 | 15 |

***Table 2.12 Reaction components used in LRT and β-actin qPCR lentiviral titration reactions.***

Samples were analysed in the Cycling A. Green channel with an automatic threshold set. The signal values (copies/µl) for LRT and β-actin were exported and viral titres calculated based on the following equations. The total LRT signal from each viral dilution was calculated by multiplying the average LRT signal by 64 (representing the proportion of total eluted DNA (400µl) added to LRT reactions (6.25µl)) then dividing this by the average β-actin signal. The total LRT value was multiplied by either 2000 or 20000 (the dilution factor used at transduction stage), then also by 100000 (to account for $1x10^5$ HeLa cells seeded prior to transduction). This equation gives the viral titre for dilution A and B, which are then averaged to give a final titre. Titres were measured in vector genomes per milliliter (vg/ml).

$$Total\ LRT = \frac{(Average\ LRT\ signal\ x\ 64)}{Average\ \beta\ actin\ signal}$$

$$Viral\ titre\ \ (vg/ml) = Total\ LRT\ x\ dilution\ factor\ x\ 100000$$

2.3.7.1.3 Flow cytometry

Flow cytometric analysis was performed 72 hours post-transduction. Cells transduced with fluorescent vectors to be analysed by flow cytometry were harvested, pelleted and resuspended in PBS or 1% PFA, if not being subjected to FACS immediately. The percentage of *eGFP*-positive cells in each sample was determined before the following calculation was used to determine titre, based on the dilution in which 1-10% cells were *eGFP*-positive.

$$eGFP\ transducing\ units = \frac{\%\ eGFP\ positive\ cells}{100}\ x\ 10^5\ x\ \frac{1}{vector\ dilution}$$

Flow cytometric analysis reveals a value of functional vectors measured in transducing units per milliliter (TU/ml). Functional vectors exist where the viral genome is packaged correctly, subsequently forming a virion which is able to transduce cells. qPCR titres are more accurate and reliable than flow cytometric titres, which often do not distinguish between cells containing single or multiple viral copies (Barczak et al., 2015), thus qPCR values were used when calculating the MOI used in subsequent experiments.

2.3.7.2 Production of AAV vectors

Two AAV9 vectors were commercially produced by Atlantic Gene Therapies. These vectors were designed to have equivalent expression cassettes to the lentiviral vectors used in this project. Therefore, a single stranded conformation expressing either *eGFP* or *Co-hSMN1* coupled to mWPRE under transcriptional control of the CAG promoter was designed. To achieve this goal 100µg of the pRY_543 IDLV_CMV_*Co-hSMN1* plasmid was sent with instructions to release a 1483bp fragment containing both *Co-hSMN1* and mWPRE by digestion with *Age*I and *Acc65*I or *Kpn*I. From this, AAV9 vectors were produced and titrated by Atlantic Gene Therapies using qPCR against viral ITRs (inverse terminal repeats).

### 2.3.8 Transduction and transfection

#### 2.3.8.1 Lentiviral and AAV9 transduction

24 hours prior to transduction, cells were seeded into 6, 12 or 24 well plates. The number of cells seeded varies based on the experiment being conducted and the cell type, but commonly $5x10^5$ cells/6 well for protein analysis, $1x10^5$ cells/12 well for flow cytometry and $5x10^4$ cells/24 well for *Co-hSMN1* transduction and subsequent immunofluorescence were used. Seeding cells 24 hours prior to transduction allows them to settle and encourages higher transduction efficacy. The appropriate volume of vector was diluted in fresh media according to a calculation that takes into account cell number, the desired MOI and the vector titre obtained by qPCR. Once dilutions were made, medium in the plate was aspirated and replaced with the minimum volume of diluted vector needed to cover the cells (500µl/6 well plate, 300µl/12 well plate, 100µl/24 well plate).

For lentiviral vector transductions, minimal media containing the vector was left for 1 hour so the cells are in presence of concentrated vector, then after this hour, fresh medium was topped up (1.5ml/6 well, 700µl/12 well, 400µl/24 well). For AAV9 vector transductions, serum-free medium was used to dilute the vectors and the minimal volume was left in the cells presence for 5 hours before topping up with media containing serum. All cells were incubated for 72 hours post-transduction before analysis.

#### 2.3.8.2 Transfection of plasmid DNA using Lipofectamine 2000

Cells were seeded 24 hours prior to transfection at a density that allowed 70-90% confluency upon addition of transfection reagents. Media was changed to serum- and antibiotic-free media 45 minutes before transfection. Separately, Lipofectamine 2000 and plasmid DNA were diluted in Opti-MEM media at required concentrations. Equal volumes (150µl/6 well plate, 25µl/24 well plate) of each diluted reagent were then combined and incubated at room temperature for 5 minutes. DNA-lipid complexes were then added to cells and left for 48 hours before analysis.

### 2.3.9 Statistical analyses

Experimental data were collated using Microsoft Excel then analysed using GraphPad Prism. Data are presented as mean ± standard deviation. For all experiments where replicate data were presented, n = 3 replicates were used, unless otherwise stated in specific sections. A range of statistical tests were used throughout this thesis, with the most appropriate test for each dataset being determined individually. Data were tested for a normal distribution wherever possible, and appropriate parametric and non-parametric tests were used accordingly. Individual statistical tests used are highlighted for each experiment.

Common statistical tests employed included one-and two-tailed t-tests and one- and two-way ANOVAs. Post-hoc tests including Dunnett's and Bonferroni corrections were applied to one- and two-way ANOVAs. T-tests were used to directly compare data from two samples, with two-tailed tests used as default to better detect an effect in a particular direction. One-tailed t-tests with higher power to detect a statistical difference were only performed after preliminary data were collected that informed the direction of effect. To avoid multiple t-tests on the same dataset, ANOVAs were used to assess multi-sample data. One-way ANOVAs were used to analyse datasets with more than one sample compared to a control (for example, transduction of one cell line with three different vectors, all compared to the same mock sample). Two-way ANOVAs were used to analyse more complex datasets with two variables to be compared in multiple samples (for example, multiple cell lines were transduced with multiple MOIs, all compared to mock). In some instances, if an ANOVA with a very large number of comparisons did not reveal significance of a sample with a very clear fold-difference, compared to control, a second statistical test may have been applied with fewer comparisons to detect a true effect.

Significance was determined where $P<0.05$ and is represented on graphs in the following manner: * $P<0.05$, ** $P<0.01$, *** $P<0.001$, **** $P<0.0001$. Individual P values will be stated wherever possible, but in some cases GraphPad only indicated if a comparison was significant or not, without stating the actual P value.

# 3 Systematic review and meta-analysis determining the benefits of in vivo gene therapy in SMA rodent models

The data presented in this chapter were obtained with help from Theodore Hirst and Evalyne Muiruri. TH provided expertise on pre-clinical statistical meta-analyses. EM provided R script used for data transformation and visualisation.

## 3.1 Introduction

### 3.1.1 Benefits of conducting meta-analyses

Meta-analyses were first introduced by Glass (1976) and aim to integrate findings of individual studies into a statistical framework allowing meaningful conclusions to be drawn. The use of meta-analyses has increased in popularity in medical and clinical research recently, with the DerSimonian and Laird random-effects model employed here, gaining over 20,000 citations since its publication in 1986 (according to Web of Science Core Collection). Often, data from individual studies of a small number of participants or animals can contradict that of other studies, but due to low statistical power it can be hard to identify true patterns or conclusions. Findings from pooled analyses may provide increased precision and validity of estimates of treatment effect than any individual contributing study (Haidich, 2010).

### 3.1.2 Pre-clinical meta-analyses

Although traditionally meta-analyses are conducted using randomised, controlled clinical trial publications, it is becoming an increasingly used technique for pre-clinical studies too. The CAMARADES (Collaborative Approach to Meta-Analysis and Review of Animal Data from Experimental Studies) consortium was launched to promote pre-clinical meta-analyses as a tool to investigate the common translational failure between promising animal trial data that were not replicated in clinical trials. Part of the NC3Rs initiative to prevent excessive use of animals in research, combining data from multiple pre-clinical studies may help to compute estimates of risk factors or treatment effect, without new animal studies being undertaken.

Examples of existing pre-clinical systematic reviews and meta-analyses have investigated pharmacological improvement of stem cell implantation after myocardial infarction (Dai et al., 2015), the benefits of histone deacetylase inhibitors after acute brain injury (Gibson and Murphy, 2010) and cell based therapies for chronic kidney disease (Papazova et al., 2015) as just a few examples.

### 3.1.3 Relevance to SMA

SMA has been the subject of a few systematic reviews and meta-analyses over the past decade. Systematic reviews have assessed the health and wellbeing of adult SMA patients (Wan et al., 2020), the quality of life of patients (Vaidya and Boes, 2018, Landfeldt et al., 2019), and the evidence available to support the use of Spinraza in clinical trials (Meylemans and De Bleecker, 2019). Those that also included a quantitative meta-analysis component assessed the effects of long-term non-invasive ventilation in infants (Bedi et al., 2018), or the efficacy and safety of valproic acid as a therapeutic target (Elshafay et al., 2019). The publications mentioned above focused on human data, only two reviews have included pre-clinical SMA as a subject of investigation. The first assessed genome editing for a variety of monogenic neuromuscular diseases (Long et al., 2016), whilst the second investigated ASO delivery in heritable neurodegenerative and neuromuscular disorders (van der Bent et al., 2018). To my knowledge, no systematic review or meta-analysis has investigated gene therapy for SMA as is done here.

Two treatments have been approved to treat SMA within the last three years. Spinraza is an antisense oligonucleotide targeting *SMN2* splicing, aiming to promote inclusion of exon 7 within transcripts and hence the synthesis of full-length SMN protein. Spinraza binds to *SMN2* pre-mRNA at an intronic splicing sequence in intron 7, preventing negative splice factors from binding this site. This causes recognition of exon 7 by U1 snRNP and inclusion in the mature *SMN2* mRNA transcript (Talbot and Tizzano, 2017). A second treatment called Zolgensma is a self-complementary AAV9 vector encoding *SMN1*. This therapy aims to replace the missing *SMN1* gene in SMA patients, thus restoring normal SMN protein function (Mendell et al., 2017). Both of these therapies were extensively tested in pre-clinical experiments before progressing to clinical trials. The approval of Spinraza was largely underpinned by data from ENDEAR and CHERISH clinical trials, whist only

one clinical trial using Zolgensma has been completed. Data from these studies will be reviewed in this chapter.

Here, studies that have used a gene therapy approach to treat SMA rodent models were reviewed using meta-analytic techniques to provide quantitative data pertaining to treatment efficacy. The hypothesis stated that application of gene therapy would likely lead to a prolonging of survival in treated SMA animals, but the efficacy of this was affected by the type of gene therapy used and the severity of the SMA model it is administered to, amongst other factors. Together, this information is useful as it can provide insights into the most successful strategies in pre-clinical data, avoiding unnecessary and unethical repetition of animal experimentation (Vesterinen et al., 2014), or identify gaps in knowledge that can be addressed in the future.

## 3.2 Aims

In this chapter I aimed to systematically review and analyse existing *in vivo* SMA gene therapy studies from a literature search and assess any benefits of this. Specifically, my objectives were:

(A) Systematically identify literature pertaining to *in vivo* SMA gene therapy.
(B) Assess how gene therapy impacts overall survival and how experimental design affects this.
(C) Explore potential sources of bias and heterogeneity in pre-clinical studies.
(D) Identify how well pre-clinical data can predict clinical trial outcome.

## 3.3 Publication identification

Electronic and manual searching retrieved 1,737 publications, 469 of which were duplicates found from more than one database search. 1,268 publications were screened to determine if they met inclusion criteria, 1,179 of these were excluded. Reasons for exclusion included: reviews or non-primary literature, non-SMA, non-genetic therapy intervention, non-rodent model, clinical only data. Of the 89 publications that were deemed relevant, data extraction were completed successfully for 51. The remaining 38 were excluded due to missing, incalculable or irrelevant data. From the included publications, 155 individual comparisons were used in statistical analysis, corresponding to 2,573 animals in total. This information

is summarised in Figure 3.1, with characteristics of included publications in Table 3.1. Figure 3.2 shows the distribution of publications and individual comparisons across the years, highlighting a large increase from 2009 onwards.

N = 23 publications contained comparisons using an oligonucleotide-based approach, n = 26 used a viral vector and n = 2 used a combination of both. Genetic therapy agents were delivered between P1 and P25 into a range of models including Taiwanese (n = 14 studies) and SMN$\Delta$7 (n = 28 studies) mice, via local (intrathecal, intramuscular and intracranial), systemic (intravascular, subcutaneous and intraperitoneal), or multiple routes of administration. The different characteristics of each study provided the basis of the stratified meta-analysis.

On pooling the 155 comparisons in meta-analysis, it was found that SMA animals treated with a genetic therapy to survive over 3 times as long as controls (MSR: 3.23, 95% CI 2.75-3.79; $\chi^2 = 2671.65$, df = 154; $P < 0.0073$).

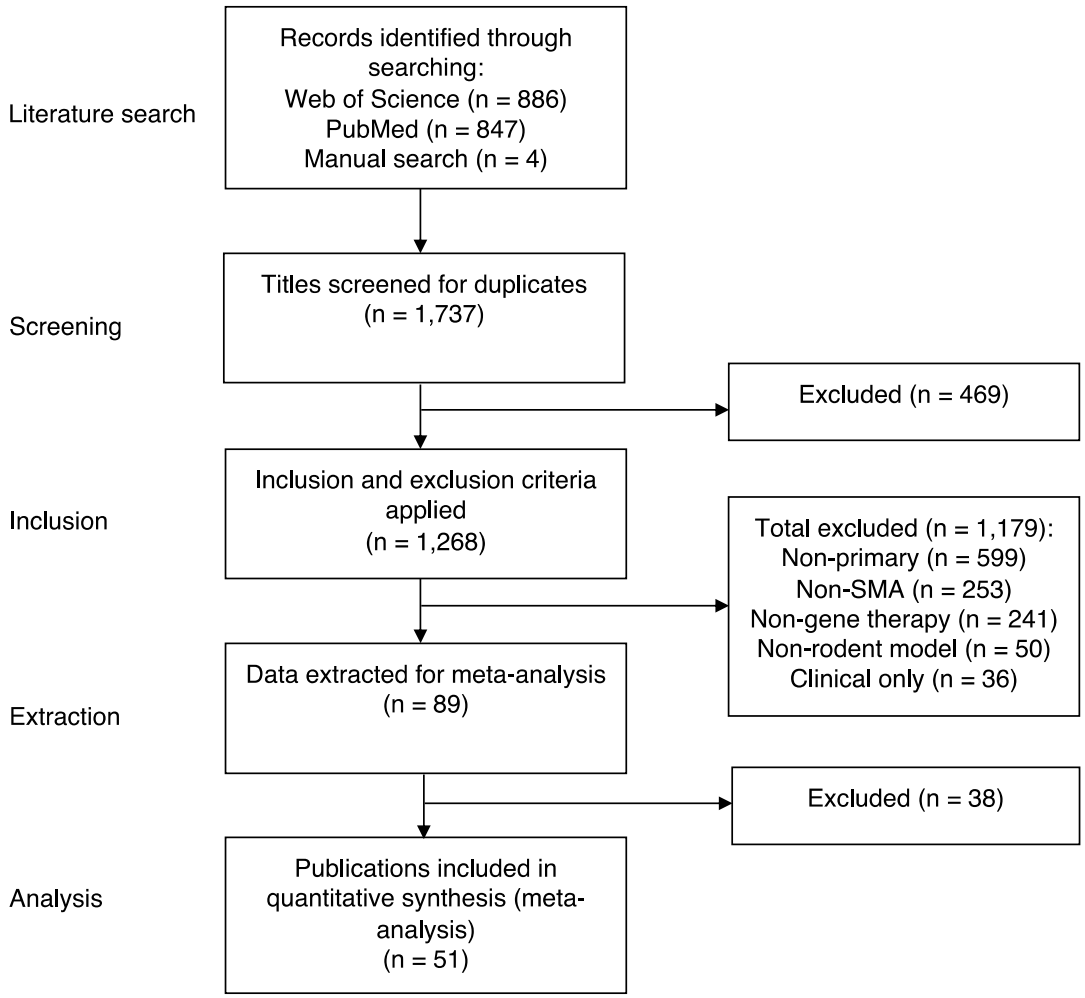


***Figure 3.1 Flow chart illustrating steps in study identification and assessment of eligibility for inclusion in the meta-analysis.***

*This meta-analysis was conducted in five stages; literature search, screening, inclusion, extraction and analysis. Publications were excluded from the screening stage onwards, with the largest number excluded when strict inclusion criteria were applied. At this stage, the reason for exclusion is shown, the most common reason being the publication was not primary research. 38 studies were excluded at data extraction due to missing, incalculable or irrelevant data on close inspection. n = number of studies.*

| Study | Genetic therapy | Target and/or transgene | SMA model | Administration | | Dosage | Median survival (days) | |
|---|---|---|---|---|---|---|---|---|
| | | | | Time | Route | | Treated | Control |
| **Oligonucleotide-based approaches:** | | | | | | | | |
| Baughan et al, 2009 | RNA | *SMN2* | Burghes' severe | P2+P4 | ICV | 6 µg | 7 | 5 |
| Coady and Lorson, 2010 | ASO | *SMN2* | Burghes' severe | P1 | ICV | Not reported | 7 | 4 |
| Shababi et al, 2011 | RNA | *SMN2* | Burghes' severe | P2+P3+P4 | ICV | 10 µg | 6 | 4 |
| | | *IGF1* | | | | | 7 | |
| | | *SMN2+IGF1* | | | | | 8 | |
| Hua et al, 2011 | ASO | *SMN2* | Taiwanese | P1 | ICV | 20 µg | 16 | 10 |
| | | | | P1+P3 | SC | 50 µg/g | 108 | 9 |
| | | | | P1+P3+P5+P7 | SC | 50µg/g | 137 | 9 |
| | | | | P1+P3 | ICV+SC | 20 µg+50 µg/g | 173 | 10 |
| | | | | P1+P3 | SC | 40 µg/g | 84 | 10 |
| | | | | P1+P3 | SC | 80 µg/g | 170 | 10 |
| | | | | P1+P3 | SC | 160 µg/g | 248 | 10 |
| | | | | P5+P7 | SC | 100 µg/g | 16 | 11 |
| | | | | P1+P3 | IP | 80 µg/g | 118 | 11 |
| Passini et al, 2011 | ASO | *SMN2* | SMNΔ7 | P1 | ICV | 8 µg | 23 | 16 |
| | | | | | | 4 µg | 25 | |
| | | | | | | 2 µg | 23 | |
| | | | | | | 1 µg | 20 | |
| | | | | | | 0.5 µg | 17 | |
| Osman et al, 2012 | ASO | *SMN2* | SMNΔ7 | P1 | ICV | 6 µg | 16.5 | 12 |
| | RNA 1 | | | | | | 19 | |
| | RNA 2 | | | | | | 20 | |
| Porensky et al, 2012 | MO | *SMN2* | SMNΔ7 | P1 | ICV | 27 µg | 83 | 15 |
| | | | | | ICV | 54 µg | 104 | |
| | | | | | ICV | 81 µg | 112 | |
| | | | | | IV | 50 µg/g | 35 | |
| | | | | | IV + ICV | 54 µg | 93 | |
| | | | | P4 | ICV | 54 µg | 41 | |
| | | | | P4 | IV | 81 µg | 21 | |
| Zhou et al, 2013 | PMO 18 | *SMN2* | Taiwanese | P1 | ICV | 20 µg/g | 12 | 9.5 |
| | PMO 25 | | | | | 40 µg/g | 32 | |
| | | | | | | 20 µg/g | 43 | |
| | | | | | | 40 µg/g | 85.5 | |
| | | | | | IV | | 230 | |
| | | | | P1+P3 | IV + SC/IP | 40 µg/g | 93.5 | |
| | VPMO 25 | | | | IV + IP | 7 µg/g | 16 | |

*Table continued on next page.*

| Study | Genetic therapy | Target and/or transgene | SMA model | Administration | | Dosage | Median survival (days) | |
|---|---|---|---|---|---|---|---|---|
| | | | | Time | Route | | Treated | Control |
| Keil et al, 2014 | ASO | *SMN2* | Taiwanese | P1+P5+P10 | IP | 20 µg/g | 8 | 10 |
| | | | | | | 80 µg/g | 13 | 10 |
| | | | Hemi-hybrid | | | 80 µg/g | 50 | 16 |
| Nizzardo et al, 2014 | MO (modified) | *SMN2* | SMNΔ7 | P1+P3 | ICV+SC | 2 nM | 42.5 | 17 |
| | MO (unmodified) | | | | | 10 nM | 40 | |
| | | | | | | 5 nM | 46 | |
| | | | | | | 2 nM | 40 | |
| Osman et al, 2014 | ASO | *SMN2* | SMNΔ7 | P2 | IP | 2 mM | 14 | 10 |
| | | | | | ICV | | 39 | |
| | | | | | ICV+ICV | | 54 | |
| | | | SMNRT | | ICV+IP | | 54 | |
| | | | | | ICV | | 175 | 17 |
| Bogdanik et al, 2015 | ASO | *SMN2* | II/III Burgheron | P10 | IP | 80 µg/g twice | 169.5 | 125.5 |
| | | | | P25 | | | 100 | |
| Hua et al, 2015 | ASO | *SMN2* | Taiwanese | P1+P3 | SC | 120 mg/kg | 237 | 10 |
| | | | | | ICV+SC | 120 mg/kg + 30 µg decoy | 212 | 10 |
| Zhou et al, 2015 | PMO 25 | *SMN2* | Taiwanese | P1 | ICV | 40 µg/g | 212 | 9.5 |
| | | | | | SC | | 261 | |
| | | | | | ICV | 20 µg/g | 43 | |
| | | | | | SC | | 58 | |
| | | | | | ICV | 10 µg/g | 22 | |
| | | | | | SC | | 25 | |
| Olivan et al, 2016 | Plasmid | *SMN* | Type II | P1 | IM | 50 µg in two muscles | 8 | 8 |
| Hammond et al, 2016 | PMO | *SMN2* | Taiwanese | P1 | IV | 10 µg/g | 167 | 12 |
| Hosseinibarkooie et al, 2016 | ASO | *SMN2* | Taiwanese | P1+P2 | SC | 30 µg | 25 | 12.5 |
| Lin et al, 2016 | ASO | *SMN2* | Taiwanese | P1 | SC | 80 µg/g | 19.7 | 7.7 |
| Osman et al, 2016 | ASO E1 MO | *SMN2* | SMNΔ7 | P1 | ICV | 2 µl of 40nM | 47.8 | 12.3 |
| | ASO $E1^{MOv1}$ | | | | | | 15.8 | |
| | ASO $E1^{MOv2}$ | | | | | | 10.2 | |
| | ASO $E1^{MOv3}$ | | | | | | 19 | |
| | ASO $E1^{MOv4}$ | | | | | | 19.5 | |
| | ASO $E1^{MOv5}$ | | | | | | 15.3 | |
| | ASO $E1^{MOv6}$ | | | | | | 18.8 | |
| | ASO $E1^{MOv7}$ | | | | | | 15.8 | |
| | ASO $E1^{MOv8}$ | | | | | | 18.3 | |
| | ASO $E1^{MOv9}$ | | | | | | 17.5 | |
| | ASO $E1^{MOv10}$ | | | | | | 30.8 | |
| | ASO $E1^{MOv11}$ | | | | | | 50.9 | |
| | ASO $E1^{MOv12}$ | | | | | | 19.2 | |

*Table continued on next page.*

| Study | Genetic therapy | Target and/or transgene | SMA model | Administration | | Dosage | Median survival (days) | |
|---|---|---|---|---|---|---|---|---|
| | | | | Time | Route | | Treated | Control |
| Arnold et al, 2016 | ASO | *SMN2* | SMNΔ7 | P4 | ICV | 40 µg | 60 | 16.5 |
| | | | | P6 | | | 22 | |
| Riessland et al, 2017 | ASO | *SMN2* | Taiwanese | P1 | SC | 30 µg | 180 | 17 |
| Shabanpoor et al, 2017 | PMO (naked) | *SMN2* | Taiwanese | P1+P2 | IV | 10 µg/g | 29 | 14 |
| | PMO (Br-ApoE) | | | | | | 78 | |
| d'Ydewalle et al, 2017 | ASO | *SMN2* | SMNΔ7 | P1+P3 | SC | 400 mg/kg | 18 | 18 |
| | SSO | | | | | 50 mg/kg | 25 | |
| | ASO + SSO | | | | | 400 mg/kg + 50 mg/kg | 37 | |
| **Viral vector-based approaches:** | | | | | | | | |
| Lesbordes et al, 2003 | Ad | *CT1* | NSE-Cre+ $Smn^{F7/F7}$ | P5-7 | IM | 10e8 pfu/mouse | 44.4 | 33.7 |
| Azzouz et al, 2004 | EIAV SIN LV | *SMN1* | SMNΔ7 | P2 | IM | 1.2e8 vg/mouse | 18 | 13 |
| Passini et al, 2010 | ssAAV8 | *SMN1* | SMNΔ7 | P1 | ICV+IS | 5e10 vg/mouse | 50 | 15 |
| | scAAV8 | | | | | 1.7e10 vg/mouse | 157 | 16 |
| Valori et al, 2010 | scAAV9 | *Codon optimised SMN1* | SMNΔ7 | P1 | IV | 10e11 vg/mouse | 69.1 | 11.2 |
| Foust et al, 2010 | scAAV9 | *SMN1* | SMNΔ7 | P1 | IV | 5e11 vg/mouse | 250 | 15.5 |
| Dominguez et al, 2011 | scAAV9 | *SMN1* | SMNΔ7 | P1 | IV | 4.5e10 vg/mouse | 160 | 13.7 |
| Glascock et al, 2012a | scAAV9 | *SMN1* | Burghes' severe | P1 | ICV | 2e11 vg/mouse | 17 | 7 |
| | | | | | IV | | 10 | |
| Glascock et al, 2012b | scAAV9 | *SMN1* | SMNΔ7 | P2 | IV | 2e10 vg/mouse | 34.9 | 11 |
| | | | | P2+P3 | ICV | | 126.7 | |
| Shababi et al, 2012 | scAAV9 | *SMN1* | SMNΔ7 | P2 | IV | 1e11 vg/mouse | 23.5 | 12 |
| Benkhelifa-Ziyyat et al, 2013 | scAAV9 | *Codon optimised SMN1* | SMNΔ7 | P1+P2 | IM (2 limbs) | 5e13 vg/kg | 26 | 12 |
| | | | | | IM (4 limbs) | | 163 | |
| Tsai et al, 2014 | AAV1 | *IGF1* | Burghes' severe | P1 | IV | 3.4e9 vg/mouse | 12 | 9 |
| Passini et al, 2014 | scAAV9 | *SMN1* | SMNΔ7 | P1 | ICV+IT | 5e10 vg/mouse | 153 | 17 |
| | | | | | | 1e10 vg/mouse | 70 | |
| | | | | | | 1e9 vg/mouse | 18 | |
| Robbins et al, 2014 | scAAV9 | *SMN1* | SMNΔ7 | P2 | ICV | 1e11 vg/mouse | 204 | 14 |
| | | | | P3 | | | 75 | |
| | | | | P4 | | | 167 | |
| | | | | P5 | | | 37 | |
| | | | | P6 | | | 34 | |
| | | | | P7 | | | 28 | |
| | | | | P8 | | | 18 | |
| Little et al, 2015 | scAAV9 | *PTEN* | SMNΔ7 | P1 | IV | 10e10 vg/mouse | 23.5 | 10 |
| Powis et al, 2016 | ssAAV9 | *Uba1* | Taiwanese | P1 | IV | 2.4e11 vg/mouse | 12 | 9 |

*Table continued on next page.*

| Study | Genetic therapy | Target and/or transgene | SMA model | Administration | | Dosage | Median survival (days) | |
|---|---|---|---|---|---|---|---|---|
| | | | | Time | Route | | Treated | Control |
| Odermatt et al, 2016 | scAAV9 | *SMN2 via U7-ESE-B* | SMNΔ7 | P1+P2 | ICV | 4.07e12 vg/kg | 22 | 12 |
| | | | | | | 1.75e13 vg/kg | 25.5 | |
| | | | | | | 3.21e13 vg/kg | 33 | |
| | | | | | | 4.34e13 vg/kg | 34 | |
| | | | | | | 2.27e14 vg/kg | 195 | |
| Armbruster et al, 2016 | scAAV9 | *Codon optimised SMN1* | SMNΔ7 | P1 | ICV | 1.9e13 vg/kg | 201 | 16 |
| | | | | | | 3e13 vg/kg | 346 | |
| | | | | | | 7.5e13 vg/kg | 154 | |
| | | | | | | 1.9e13 vg/kg | 283 | |
| | | | | | ICV+IV | 3e13 vg/kg | 188 | |
| | | | | | | 7.5e13 vg/kg | 262 | |
| Alrafiah et al, 2018 | ssAAV9 | *Plastin3* | SMNΔ7 | P1 | IT | 5e10 vg/mouse | 17.5 | 12.5 |
| Villalon et al, 2019 | scAAV9 | *Stathmin1* | Smn2B/- | P2 | ICV | 1e11 vg/mouse | 27.02 | 19.04 |
| Donadon et al, 2019 | AAV9 | *SMN2 via ExSpeU1s* | Taiwanese | P1+P3 | IP | 1.5e12 vg/mouse | 219 | 10 |
| | | | | P1 | | | 150 | |
| | | | | P1+P3 | | 1.5e11 vg/mouse | 13.56 | |
| Rashnonejad et al, 2019 | ssAAV9 | *SMN1* | SMNΔ7 | E14-15 | ICV | 4e10 vg/mouse | 63 | 12 |
| | scAAV9 | | | | | | 105 | |
| Simon et al, 2019 | scAAV9 | *Stasimon* | SMNΔ7 | P1 | ICV | 1e11 vg/mouse | 15.03 | 14.12 |
| Osman et al, 2019 | scAAV9 | *SMN1* | SMNΔ7 | P2 | ICV | 1e11 vg/mouse | 70 | 10 |
| | | *D. rerio Smn* | | | | | 70 | |
| | | *X. laevis Smn* | | | | | 38 | |
| | | *D. melanogaster Smn* | | | | | 13 | |
| | | *C. elegans Smn* | | | | | 11 | |
| | | *S. pombe Smn* | | | | | 9 | |
| | | *SMN_236* | | | | | 15 | 13 |
| | | | Smn2B/- | | | | 36 | 25 |
| Ahlskog et al, 2020 | scAAV8 | *Klf15* | Taiwanese | P1 | IV | 2e10 vg/mouse | 13.8 | 12.82 |
| | | | | | | 1e10 vg/mouse | 7.88 | |
| | | | Smn2B/- | | | 2e10 vg/mouse | 21.73 | 20.7 |
| Besse et al, 2020 | AAV9 | *Codon optimised SMN1 (hSYN)* | SMNΔ7 | P1 | ICV | 4.5e10 vg/mouse | 15.5 | 16 |
| | | | | | | 1.2e11 vg/mouse | 39.5 | |
| | | *Codon optimised SMN1 (hPGK)* | | | | 4.5e10 vg/mouse | 221 | |
| | | | | | IV | | 142 | |
| Nizzardo et al, 2020 | AAV9 | *Syt13* | SMNΔ7 | P1 | IM | 5e10 vg/mouse | 18 | 12 |

*Table continued on next page.*

| Study | Genetic therapy | Target and/or transgene | SMA model | Administration | | Dosage | Median survival (days) | |
|---|---|---|---|---|---|---|---|---|
| | | | | Time | Route | | Treated | Control |
| **Combinatorial approaches:** | | | | | | | | |
| Kaifer et al, 2017 | scAAV9 | *Plastin3* | SMNΔ7 | P1 | IV | 1e11 vg/mouse | 15 | 15 |
| | ASO | *Plastin3* | | | ICV | 1 nmol | 17 | 15 |
| | ASO+ scAAV9 | *SMN2 + Plastin3* | | | ICV+IV | 1 nmol+1e11 vg/mouse | 14 | 15 |
| | ASO | *SMN2* | | | ICV | 2 nmol | 20 | 17 |
| | ASO+scAAV9 | *SMN2 + Plastin3* | Smn2B/- | | ICV+IV | 2 nmol+1e11 vg/mouse | 43.5 | 17 |
| | scAAV9 | *Plastin3* | | | IV | 1e11 vg/mouse | 43.75 | 30 |
| | scAAV9 | *Plastin3* | | | IV | 3e11 vg/mouse | 45 | 30 |
| Zhou et al, 2020 | AAV | *Myostatin* | Taiwanese | P1 | SC | 2.5e10 vg/mouse | 12 | 10 |
| | PMO 25 | *SMN2* | | | | 40 µg/g | 261 | |
| | PMO + AAV | *SMN2 + Myostatin* | | | | 40 µg/g + 2.5e10 vg/mouse | 166 | |

***Table 3.1 Overview of pre-clinical gene therapy applications in SMA mice models.***

*51 publications were included in this meta-analysis, as highlighted by the first column. However, some studies incorporated multiple relevant comparisons within the publication, for example with different treatment dosages, so were included as part of the 155 individual comparisons analysed here. Details of each comparison are highlighted in the table, including the type of genetic therapy and its target, the mouse model in which this was administered, the dosage, time and route of administration and finally the median survival. ASO = antisense oligonucleotide, MO = morpholino, PMO = phosphorodiamidate morpholino, AAV = adeno-associated viral vector, EIAV = equine infectious anaemia virus, SIN = self-inactivating, LV = lentiviral vector, IV = intravascular, IT = intrathecal, ICV = intracerebral ventricular, IS = intraspinal, IM = intramuscular, IP = intraperitoneal, SC = subcutaneous, P1 = post-natal day 1, vg = vector genomes, pfu = plaque forming unit.*

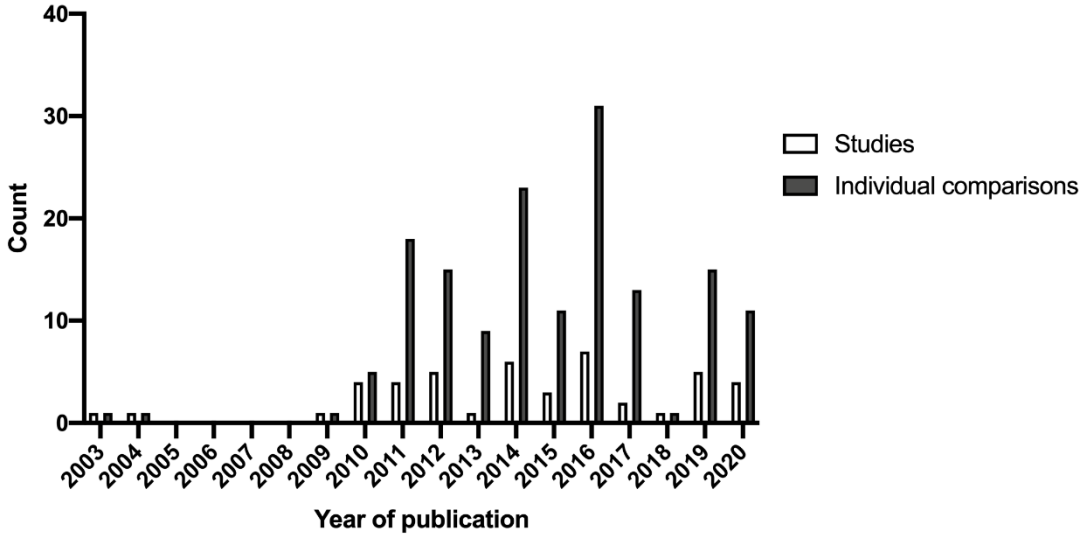


***Figure 3.2 Distribution of studies and the individual comparisons they contain.***

*Within the last 18 years, 51 eligible studies were included in this meta-analysis. Some publications contained multiple comparisons within the main study; together 155 individual comparisons were assessed here.*

## 3.4 Stratification of data

### 3.4.1 Type of genetic therapy

Three categories of genetic therapy agents were compared; oligonucleotide-based approaches (including antisense oligonucleotides (ASO), peptide morpholinos and naked DNA/RNA), viral vector-based approaches (including AAVs, adenoviruses and lentiviruses) and oligonucleotide plus viral vector combinatorial approaches. Oligonucleotide-based approaches led to the development of Spinraza, whilst viral vector-based approaches, specifically AAV, led to the development of Zolgensma. Therefore, this allows direct comparison of the efficacy of two drugs' rationale, and how successfully these translated to human clinical trials.

All three types of genetic therapy were associated with a significant increase in median survival ($\chi^2 = 38.54$, df = 2; $P < 0.0073$). Both oligonucleotide and viral vector approaches provided just over three-fold survival advantage (oligonucleotide: MSR: 3.18, 95% CI 2.58-3.93; n comparisons = 85; Figure 3.3A, viral vector: MSR: 3.33, 95% CI 2.60-4.27; n = 66; Figure 3.3A). Efficacy was very similar, if slightly increased, when oligonucleotide and viral vectors were combined within a single treatment (MSR: 3.41, 95% CI 0.89-13.08; n = 3; Figure 3.3A). However, only two publications (Kaifer et al., 2017, Zhou et al., 2020), containing three individual comparisons, used a combinatorial treatment so efficacy may be overestimated.

#### 3.4.1.1 Viral vector dosage

Within the different types of genetic therapy, an attempt was made to further stratify by dosage of genetic therapy agent. This was possible for those studies that used viral vector-based approaches as raw data presented in total vector genomes per mouse, or vector genomes (vg)/kg could be delineated into discreet groups by conversion of all to vg/kg. However, dosage delineation for oligonucleotide-based approaches was not possible due to disparity in the presentation of dose. Some publications presented dose as weight-based measures (either absolute µg or µg/g) or in molar concentrations. Therefore, only sub-stratification by viral vector dosage is shown here.

Of the 69 comparisons that administered viral vectors, alone or in combination with an oligonucleotide, significant differences between efficacy were observed ($\chi^2$ = 1817.93, df = 2; P < 0.0073). A minority of comparisons used ≤e12vg/kg leading to a small, but significant increase in survival (MSR: 1.29, 95% CI 1.14-1.45; n = 5; Figure 3.3B). These comparisons either used ≤e12vg/kg as a low dose comparison to others in e13vg/kg or ≥e14vg/kg categories, or vector titre may have been limited due to the nature of virus used, as in the case of lentiviral vectors (Azzouz et al., 2004) and adenoviral vectors (Lesbordes et al., 2003). Approximately equal numbers of comparisons implemented either e13vg/kg or ≥e14vg/kg viral dosages. e13vg/kg was associated with the largest survival advantage (MSR: 4.83, 95% CI 3.32-7.03; n = 30; Figure 3.3B). Finally, the highest dose of viral vector (≥e14vg/kg) produced a larger increase in survival than ≤e12vg/kg, but not as high as e13vg/kg (MSR: 2.72, 95% CI 1.98-3.74; n = 34; Figure 3.3B).

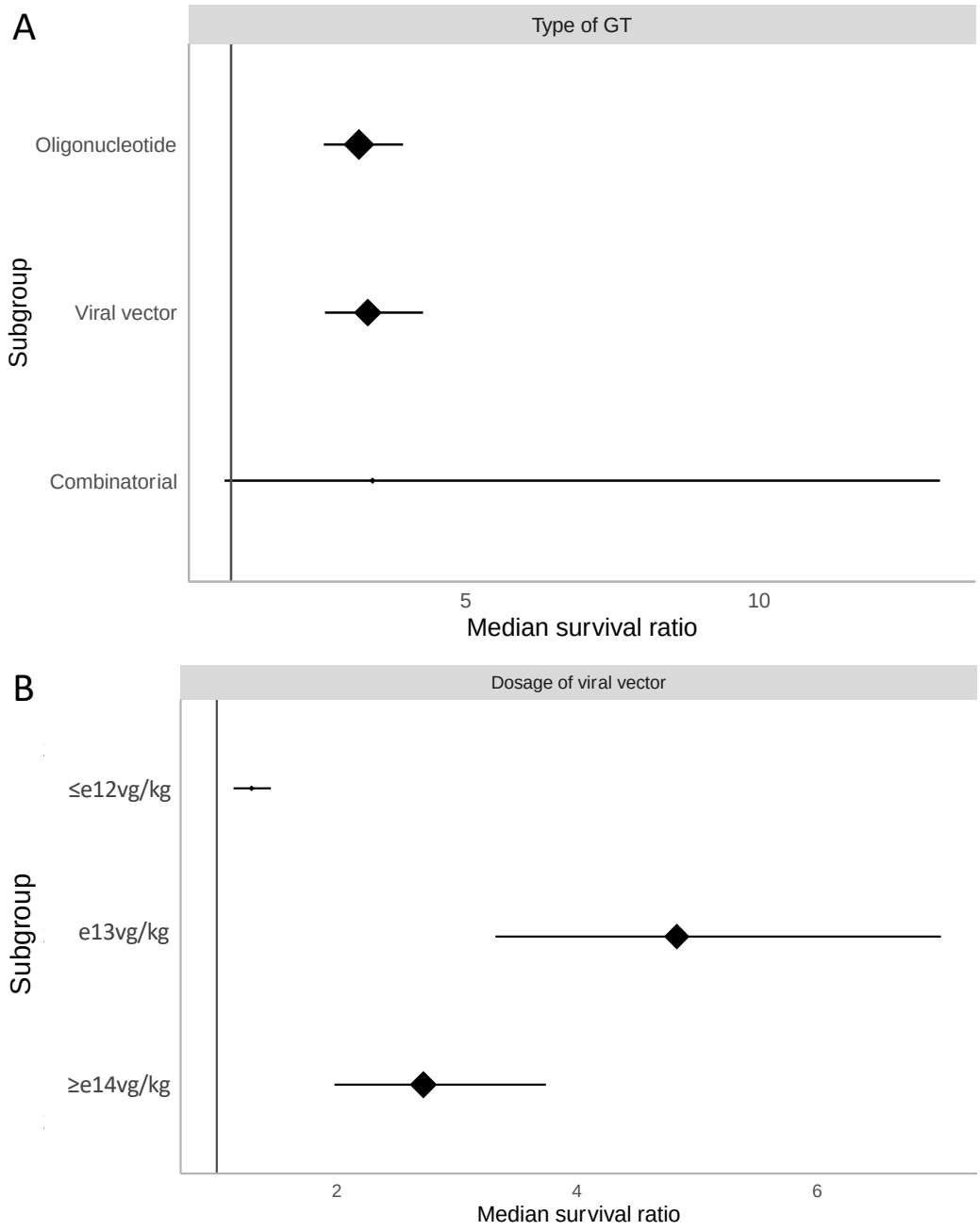


***Figure 3.3 Stratification by type of genetic therapy and dosage of viral vector.***

*Both (A) type of gene therapy and (B) dosage of viral vector accounted for significant heterogeneity in median survival ratio (MSR P<0.0073). (B) Sub-strata were defined as viral vector dosage of ≤e12vg/kg, e13vg/kg and ≥e14vg/kg. (A,B) Plots represent mean ± 95% confidence intervals with the size of diamonds representing the number of comparisons within each stratum. The vertical line at MSR = 1 represents a neutral treatment effect. Grey rectangles represent global 95% confidence intervals.*

#### 3.4.1.2 Therapeutic target

Since SMA is a monogenic disease, augmentation of SMN protein production has been the preferred genetic therapy strategy, however SMN-dependent, SMN-independent and SMN-plus strategies have been reported in the literature, with differing improvements in median survival ($\chi^2$ = 363.02, df = 2; P < 0.0073). Augmentation of SMN protein, whether this be through replacement of the *SMN1* gene, or manipulation of *SMN2* splicing, provided the largest survival benefit here and was used in 86% of comparisons included (MSR: 3.65, 95% CI 3.08-4.34; n = 134; Figure 3.4A). A smaller number of comparisons addressed non-SMN targets: UBA1, Plastin3, PTEN, IGF1, CT1, Stathmin, Stasimon, Myostatin and Synaptotagmin13. These led to a more modest increase in survival (MSR: 1.30, 95% CI 1.15-1.47; n = 17; Figure 3.4A). Furthermore, when combining SMN-dependent and -independent targets into an SMN-plus strategy, the lifespan of animals fell between that of each constituent therapy (MSR: 2.98, 95% CI 1.06-8.36; n = 4; Figure 3.4A). However, only 72 animals were treated in this manner in three publications.

When directly comparing *SMN*-dependent therapeutic targets ($\chi^2$ = 507.97, df = 1; P < 0.0073) it was seen that *SMN1*-targeted therapies produced an MSR of 4.47 (95% CI 3.34-5.97; n = 43; Figure 3.4B) compared to *SMN2*-dependent MSR of 3.36 (95% CI 2.73-4.14; n = 90; Figure 3.4B).

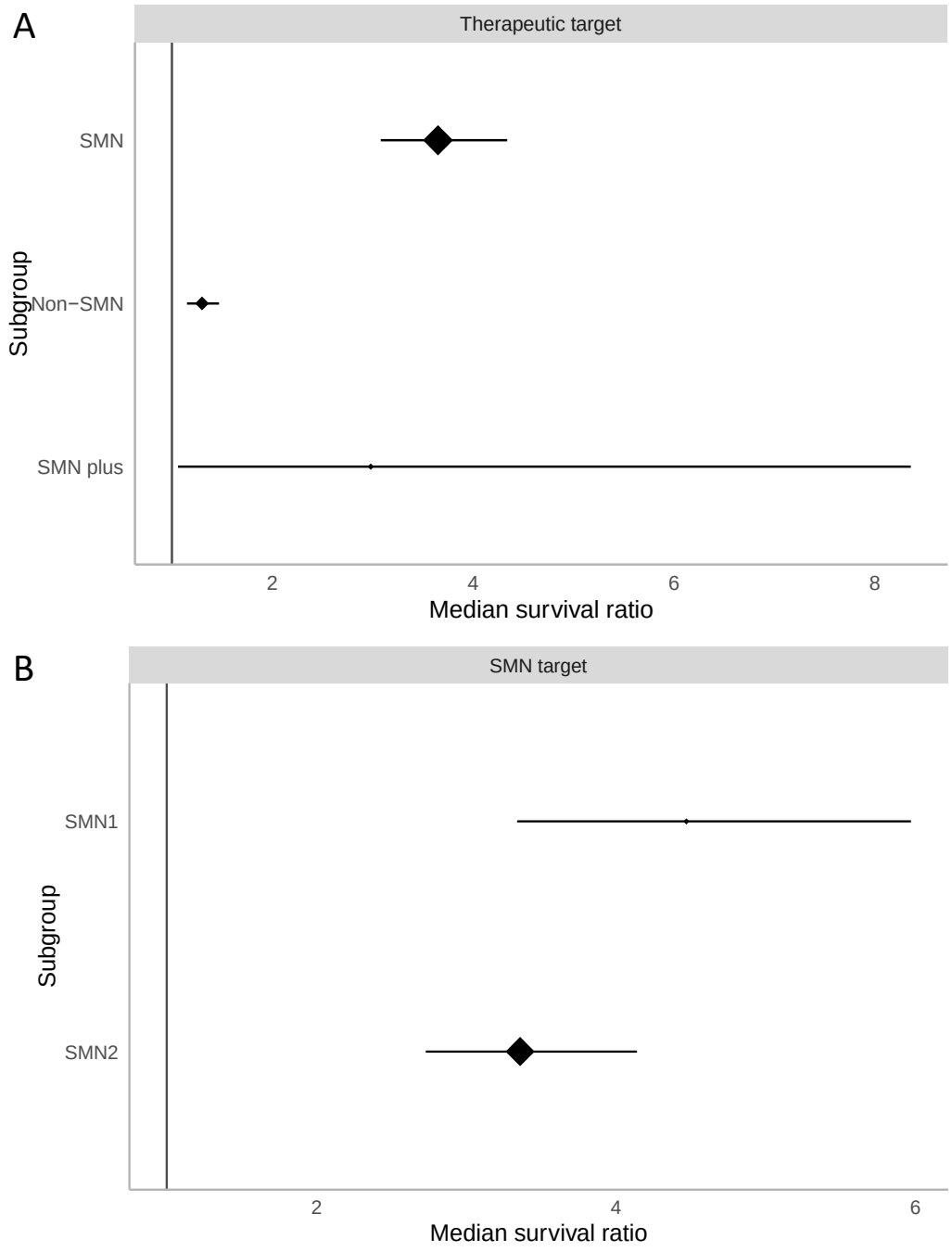


***Figure 3.4 Stratification by therapeutic target.***

*Significant differences in MSR are apparent dependent on (A) overall therapeutic target (MSR P<0.0073) and between (B)* SMN1- *and* SMN2*-dependent therapies (MSR P<0.0073). Plot represents mean ± 95% confidence intervals with the size of diamonds representing the number of comparisons within each stratum. The vertical line at MSR = 1 represents a neutral treatment effect. Grey rectangle represents global 95% confidence intervals.*

### 3.4.2 Mouse model

Although the search employed in this review aimed to retrieve studies from any SMA rodent species, every publication used a mouse model. Most commonly, the SMNΔ7 model was used, followed by the severe Taiwanese model. Other mouse models were also used but in lower frequencies, so have been grouped into one category here. These other models included Smn2B/- (n = 5), type II/III Burgheron (n = 2), hemi-hybrid (n = 1), Burghes' severe (n = 8), SMNRT (n = 1), moderate type II (*Smn*$^{+/-}$ *SMN2* SMNΔ7, n = 1), neuronal *Smn* deletion (NSE-Cre+ *Smn*$^{F7/F7}$, n = 1). Improvements in median survival differed between mouse model sub-strata ($\chi^2$ = 471.05, df = 2; P<0.0073).

Taiwanese mice provide the most severe phenotype within the pure groupings in this review, on average surviving up to 15 days untreated (Hsieh-Li et al., 2000). When genetic therapy was administered to Taiwanese mice a more than six-fold improvement in median survival was found (MSR: 5.49, 95% CI 3.83-7.87; n = 41; Figure 3.5). SMNΔ7 mice survive approximately 15-22 days (Le et al., 2005) without therapeutic intervention, so are useful when a slightly longer lifespan may reveal more subtle phenotypic benefits of a therapy. SMNΔ7 mice showed a 3.4-fold increase in survival (MSR: 2.92, 95% CI 2.45-3.49; n = 96; Figure 3.5). Less frequently used mice models showed a more modest increase in survival (MSR: 1.65, 95% CI 1.28-2.12; n = 18; Figure 3.5).

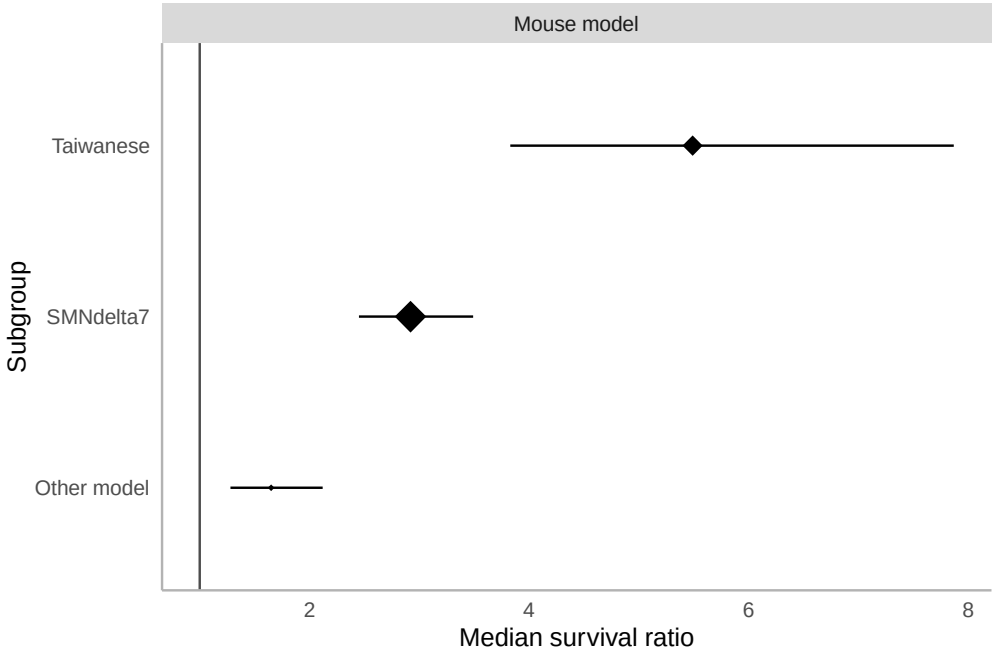


***Figure 3.5 Stratification by SMA mouse model.***

*Significant differences were found between mouse models (MSR P<0.0073). Plots show mean ± 95% confidence intervals with the size of diamonds representing the number of comparisons within each stratum. The vertical line at MSR = 1 represents a neutral treatment effect. Grey rectangle represents global 95% confidence intervals.*

### 3.4.3 Route of administration

Both local (intracranial, intrathecal and intramuscular) and systemic (intravascular, intraperitoneal and subcutaneous) routes of administration were reported in the literature, but significant differences in efficacy were observed between these routes ($\chi^2$ = 422.34, df = 5; P<0.0073). Despite recent advances regarding the systemic nature of SMA, the proportion of comparisons employing systemic or multiple routes of administration has remained relatively stable (Figure 3.6A).

CNS delivery of therapeutics by either intracranial or intrathecal injection was the most commonly used route of administration and was associated with an almost three-fold increase in survival (MSR: 2.70, 95% CI 2.22-3.27; n = 77; Figure 3.6B). Local, intramuscular delivery more than doubled the lifespan of treated mice (MSR: 2.05, 95% CI 1.03-4.07; n = 6; Figure 3.6B), highlighting the importance of treating the muscular pathology of SMA. Regarding systemic routes, both intravascular (MSR: 2.79, 95% CI 1.82-4.28; n = 22; Figure 3.6B) and intraperitoneal (MSR: 2.71,

95% CI 1.30-5.63; n = 10; Figure 3.6B) delivery were associated with similar survival rates as CNS and intramuscular delivery. Subcutaneous delivery was the third systemic route addressed, providing the largest median survival ratio (MSR: 5.75, 95% CI 3.33-9.92; n = 18; Figure 3.6B). Finally, 14% of comparisons investigated used multiple routes of administration within their study. In most cases, these comparisons used intracranial injection in combination with a second route. This led to a 5.32-fold increase in survival (95% CI 3.60-7.84; n = 22; Figure 3.6B).

### 3.4.4 Time of administration

SMA in its most severe form is a childhood disease with onset *in utero*. Therefore, early intervention is thought to be key to halting disease progression or providing phenotypic benefit before irreversible pathology occurs (Robbins et al., 2014). Here, the time of genetic therapy administration greatly impacted the resulting efficacy ($\chi^2$ = 284.93, df = 3; P < 0.0073). The need for early intervention is highlighted here with approximately half of comparisons administering genetic therapy on the day of birth. Intervention on P1 leads to a 3.12-fold increased lifespan (95% CI 2.49-3.90; n = 83; Figure 3.6C). Slightly later intervention within the P2-P5 window provided similar results (MSR: 2.98, 95% CI 2.16-4.12; n = 24; Figure 3.6C). Administration later than P6 provided a much lesser, yet still significant benefit (MSR: 1.37, 95% CI 1.03-1.82; n = 6; Fig. 6C). Finally, repeated administrations provide the largest increase in survival time seen (MSR: 4.08, 95% CI 2.92-5.69; n = 39; Figure 3.6C).

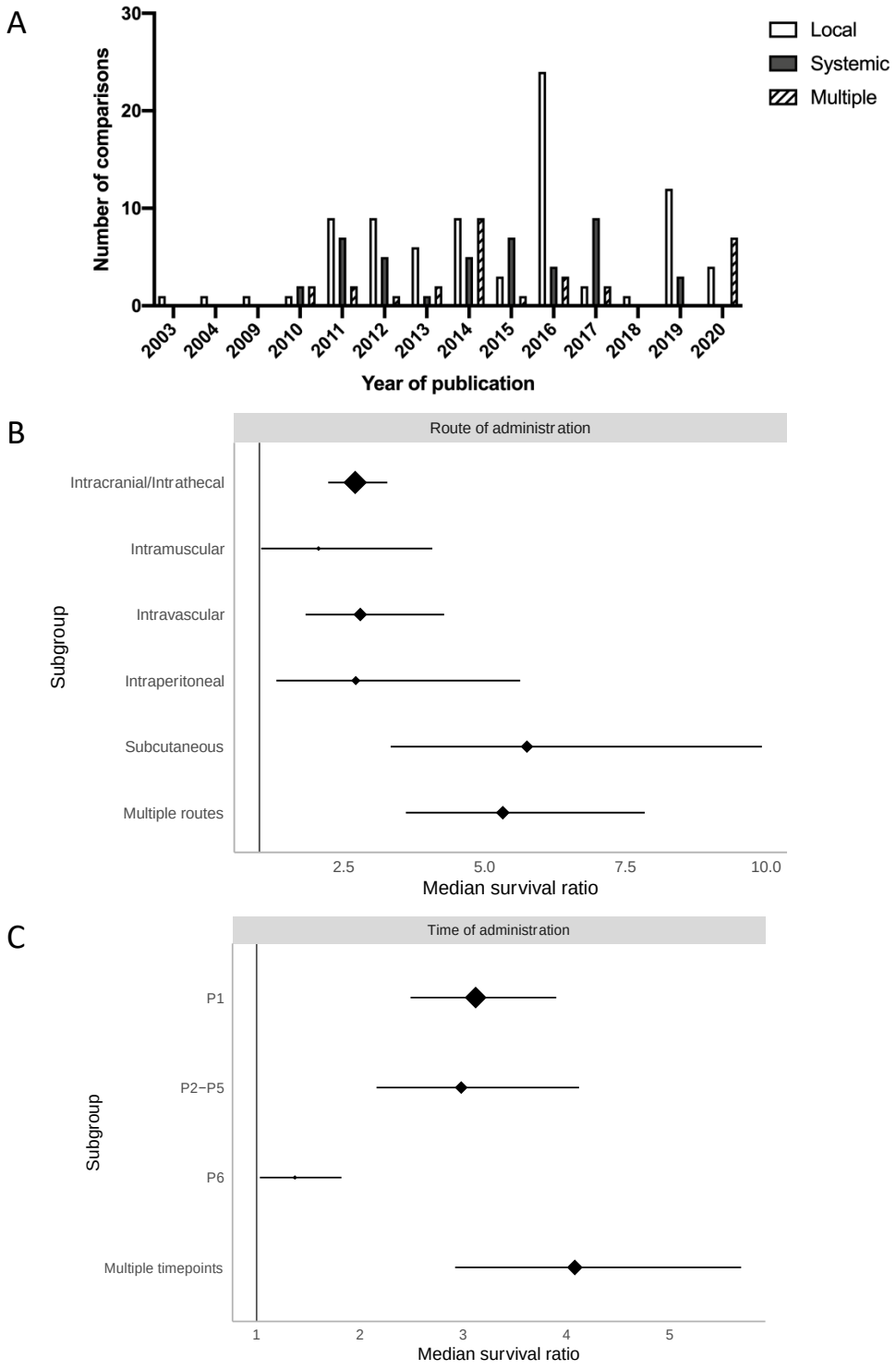


***Figure 3.6 Stratification by route and time of administration of gene therapy.***

*(A) Stratification by year of publication and delivery route shows that local administration remained an often used strategy, despite increasing knowledge of SMA as a systemic disease. (B,C) Forest plots demonstrating significant differences in survival data within both route and time of administration strata (MSR P<0.0073). Plots represent mean ± 95% confidence intervals with the size of diamonds representing the number of comparisons within each stratum. The vertical line at MSR = 1 in B and C represents a neutral treatment effect. Grey rectangles represent global 95% confidence intervals.*

## 3.5 Publication bias

Publication bias in meta-analyses can occur due to unintentional exclusion of missing data, potentially causing misinformed conclusions to be drawn. Evidence of publication bias can be sought using funnel plots, Egger's regression and trim and fill analyses (Figure 3.7). While there was no obvious asymmetry to the funnel plot, only a small relative number of comparisons reported an effect size <1 (n = 7; Figure 3.7A). On Egger's regression a positive intercept was found (Figure 3.7B), suggesting the presence of an excess of small, imprecise comparisons overstating efficacy in this analysis. Trim and fill analysis did not suggest the presence of any 'missing' publications. However, Trim and fill analysis has been suggested as a relatively insensitive technique and can be an inadequate method of correcting for publication bias (Simonsohn et al., 2014).

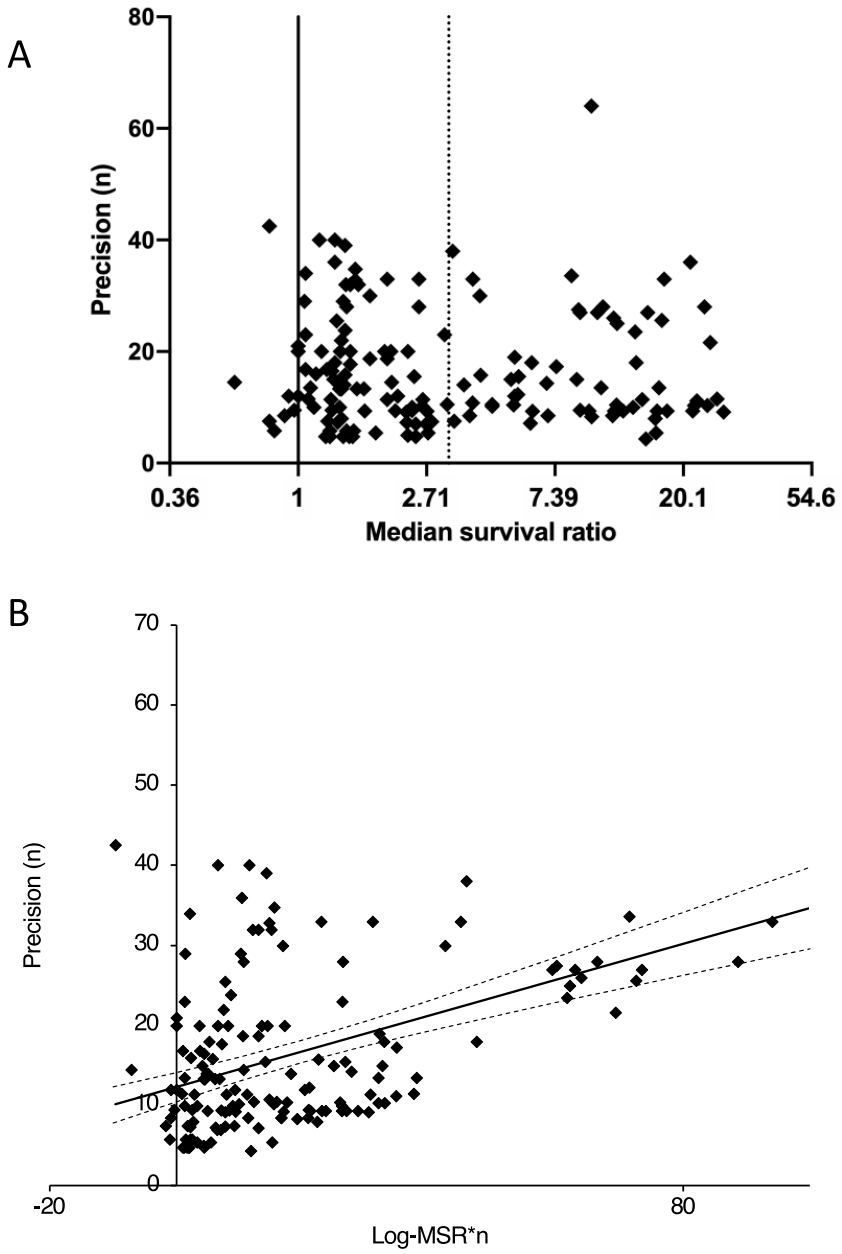


***Figure 3.7 Publication bias in included publications.***

*(A) Funnel plot showing untransformed median survival against study precision (number of animals), representing no obvious asymmetry. The solid line at X=1 represents a neutral treatment effect, whilst the dotted line at X=3.23 represents the global median survival ratio of all comparisons. Data are plotted on a natural logarithmic X axis. (B) Egger's regression revealed positive intercept suggesting imprecise studies showed overstated efficacy. Dotted lines represent 95% confidence intervals.*

## 3.6 Translation of pre-clinical data to clinical trials

One aim of this systematic review and meta-analysis was to assess how predictive pre-clinical studies can be when translated to clinical trials. Therefore, here n = 6 clinical trials have been reviewed; n = 5 of which were assessing Spinraza efficacy (Chiriboga et al., 2016, Darras et al., 2019, Finkel et al., 2016, Finkel et al., 2017, Mercuri et al., 2018) and n = 1 assessing Zolgensma (Mendell et al., 2017). Table 2 details data presented in these studies. Unfortunately, meta-analytic techniques could not be applied to these data for two reasons: (1) no consistent outcomes were reported in all six trials, highlighting the need for consistent outcome reporting across clinical trials, to allow for direct comparison of data; and (2) only two out of six studies included control groups (Finkel et al., 2017, Mercuri et al., 2018), meaning statistical methods could not be employed.

Overall, 255 affected individuals were treated and 83 control individuals were included across the 6 studies. Only two out of six studies included control groups, (ENDEAR (Finkel et al., 2017) and CHERISH (Mercuri et al., 2018)). 16 deaths were reported in treatment vs 39 deaths in control groups. Serious adverse events were reported in all studies except NCT01780246/NCT01494701 (Chiriboga et al., 2016). In the studies that reported HFMSE (Hammersmith Functional Motor Scale Expanded) scores, treated patients showed increases in score including some patients showing increases by ≥3 points which is said to be clinically meaningful. HINE-2 (Hammersmith Infant Neurological Examination section 2) and CHOP-INTEND (Children's Hospital of Philadelphia Infant Test of Neuromuscular Disorders) scores also increased following treatment. Half of the studies reported motor milestones in treated patients compared to control groups, all showing improved responses in treatment groups.

| Gene therapy | Spinraza | | | | | Zolgensma |
|---|---|---|---|---|---|---|
| Study | Chiriboga et al, 2016 | Finkel et al, 2016 | Finkel et al, 2017 | Mercuri et al, 2018 | Darras et al, 2019 | Mendell et al, 2017 |
| | Phase 1 | Phase 2 | Phase 3 | Phase 3 | Phase 1/2 | Phase 1 |
| | NCT01780246 | NCT01839656 | ENDEAR | CHERISH | NCT01703988 | NCT02122952 |
| | NCT01494701 | | NCT02193074 | NCT02292537 | NCT02052791 | |
| Participants | n = 28 | n = 20 | Treatment n = 80 | Treatment n = 84 | n = 28 | n = 15 |
| | | | Control n = 41 | Control n = 42 | | |
| | Type 2 or 3 SMA | Type 1 SMA | Type 1 SMA | SMA onset after 6 months of age | Type 2 or 3 SMA | Type 1 SMA |
| Cohorts | 1, 3, 6 and 9mg | 6 and 12mg | 12mg | 12mg | 3, 6, 9 and 12mg | $6.7x10^{13}$vg/kg |
| | | | | | | $2.0x10^{14}$vg/kg |
| Untreated control group | No | No; compared to natural history cohort n = 23 | Yes | Yes | No | No; compared to natural history cohort |
| Deaths | 0/28 | 3/20 | Treatment = 13/80 | 0/126 | 0/28 | 0/15 |
| | | | Control = 16/41 | | | |
| Serious adverse events | Treatment = 0/28 | Treatment = 16/20 | Treatment = 61/80 | Treatment = 14/84 | Treatment = 5/28 | Treatment = 13/15 |
| | | | Control = 39/41 | Control = 12/42 | | |
| HFMSE increase by ³3 pts | 1, 3 and 6mg = 0% | N/A | N/A | Treatment = 57% | Type 2 = 82% and 78% | N/A |
| | 9mg = 75% | | | Control = 26% | Type 3 = 19% and 36% | |
| HFMSE score | 9mg = increase of 5.8 points | N/A | N/A | Treatment = increase of 4.9 points | Type 2 = 10.8 | N/A |
| | | | | | Type 3 = 1.8 point increase | |
| HINE-2 score | N/A | 6mg = 25% | Treatment = 28% | N/A | N/A | N/A |
| | | 12mg = 100% | Control = 5% | | | |
| CHOP-INTEND score | N/A | 12mg = 15.2 point increase | Treatment = 71% | N/A | N/A | $6.7x10^{13}$vg/kg = 7.7 point increase |
| | | Natural history = 1.27 point decline | Control = 3% increase ³4 points | | | $2.0x10^{14}$vg/kg = 24.6 point increase |
| Motor milestone response | N/A | Treatment = 65% | Treatment = 51% | Treatment = 20% | N/A | Treatment = 92% |
| | | | Control = 0% | Control = 6% | | Natural history = 0% |

***Table 3.2 Characteristics of clinical trials using Spinraza and Zolgensma.***

*Six clinical trials were qualitatively analysed here; five employing Spinraza and one employing Zolgensma. Details of patients, treatment regimens, and reported outcomes are shown here. Outcome measures reported at set follow up time points: Chiriboga et al. (2016): 9-14 months, Finkel et al. (2016): up to 32 months, Finkel et al. (2017): day 394, Mercuri et al. (2018): 15 months, Darras et al. (2019): days 253 and 1050, respectively, Mendell et al. (2017): 24 months. HFMSE, HINE-2 and CHOP-INTEND scores represent change from baseline. Finkel et al. (2016) define motor milestone response as "improvement of two or more levels per motor milestone category in at least one category". Finkel et al. (2017) define motor milestone response as "improvement in at least one HINE-2 motor milestone with more categories with improvement than worsening". Mercuri et al. (2018) define motor milestone response as achievement of "≥1 new World Health Organisation motor milestone". HFMSE = Hammersmith Functional Motor Scale Expanded. HINE-2 = Hammersmith Infant Neurological Examination section 2. CHOP-INTEND = Children's Hospital of Philadelphia Infant Test of Neuromuscular Disorders, N/A = not reported in publication.*

## 3.7 Discussion

In this meta-analysis of 51 publications, containing data from 2,573 animals, it was found that, overall, genetic therapies led to approximately a three-fold increase in median survival. Stratified meta-analysis suggested a significant impact of type of therapy, mouse models, time and route of administration on perceived treatment effect. To my knowledge, this is the first quantitative meta-analysis of published literature of genetic therapy for SMA. Two other systematic reviews (van der Bent et al., 2018, Qomi et al., 2019) were found, but neither analysed survival benefits. Van der Bent and colleagues (2018) assessed ASO use in heritable neurodegenerative or neuromuscular disorders, including SMA, however, the only data quantitatively analysed pertained to Duchenne Muscular Dystrophy. Qomi and colleagues (2019) systematically describe the development of multiple SMA therapeutic advances at both pre-clinical and clinical level.

With two genetic therapy agents approved for the treatment of SMA patients, a major question concerns the predictive value of pre-clinical studies of oligonucleotide-based approaches that led to Spinraza and viral vector-based approaches that led to Zolgensma. The mechanism and efficacy of Spinraza have been extensively reviewed elsewhere (see refs. (Singh et al., 2017b, Singh et al., 2015a, Douglas and Wood, 2013, Porensky and Burghes, 2013)). A recent, succinct review (Pattali et al., 2019) of pre-clinical AAV9 vector gene therapy for SMA highlights multiple animal models, including large animals and non-human primates.

A significant improvement of median survival was observed with the use of both oligonucleotide- and viral vector-based approaches, with very similar resulting MSRs (3.33 and 3.18, respectively) in the pre-clinical studies analysed in this manuscript. A recent paper (Dabbous et al., 2019) compared the Zolgensma NCT02122952 (Mendell et al., 2017) and Spinraza ENDEAR NCT02193074 (Finkel et al., 2017) clinical trials and found that patients treated with Zolgensma had a 20% higher probability of prevented death, than patients treated with Spinraza (risk ratio 1.2, 95% CI 1.1-1.3). At the last follow up visit in each trial, 100% of Zolgensma patients were alive, whereas only 84% of Spinraza patients were (Dabbous et al., 2019). However, several limitations of this comparative study should be noted (Sandrock and Farwell, 2019). Trial design (including aspects such as multi- versus

single-centre design) and baseline characteristics of treated patients (including age at first dose, mean disease duration and mean motor function score) were not adjusted for in the number needed to treat analysis conducted in this study and therefore potentially confound any conclusions drawn. Baseline characteristics show a more severe, older patient population in the ENDEAR trial, perhaps explaining the apparent lower efficacy concluded by Dabbous and colleagues (Dabbous et al., 2019). It should also be stated that the authors of this comparative study were Avexis employees, potentially highlighting a source of bias.

With regards to an oligonucleotide plus viral vector combinatorial approach, the efficacy of combinatorial treatment here in fact led to the most pronounced survival benefit, but data are minimal as only two publications (Kaifer et al., 2017, Zhou et al., 2020) attempted this. Within the clinical setting, three patients from the Zolgensma NCT02122952 (Mendell et al., 2017) clinical trial are now said to be also being treated with Spinraza, but data from these patients are not available at the time of writing.

Mendell et al (2017) presented data from two cohorts of Zolgensma treatment in their clinical trial; one low dose of $6.7x10^{13}$vg/kg and one high dose of $2.0x10^{14}$vg/kg. Their rationale for using these two dosages was that in selected pre-clinical models, the low dose doubled survival, but the high dose led to a 250 day survival compared to 15 day control survival (Foust et al., 2009, Foust et al., 2010, Valori et al., 2010, Dominguez et al., 2011). In contrast, in the preclinical data (which entailed a broader selection of paradigms), a lower dose (e13vg/kg; n = 30) was in fact associated with greater efficacy than higher (≥e14vg/kg; n = 34) viral vector dosage. However, there were some differences in experimental design so this finding may be influenced by unaccounted confounders. Respectively, e13 and ≥e14vg/kg dosage strata showed differences in use of mouse model (83% vs 73.5%: SMNΔ7 mice), route of delivery (43% vs 58%: ICV) and transgene (10% vs 5.9%: codon-optimised *SMN1*). Raw median survival ranges of treated SMA animals also differ between the two strata (e13vg/kg: 7.9-346 days; ≥e14vg/kg: 9-250 days) in favour of the e13vg/kg dosage. Biologically, it may be possible that transgene saturation had occurred in the higher dose. Potentially, if SMN protein was already produced at supraphysiological levels at e13vg/kg, as suggested within Passini et al (2014, 2010), Benkhelifa-Ziyyat et al (2013), and Dominguez et al (2011), increasing viral vector dosage beyond this rodent models may not lead to a further increase in survival and perhaps be even less efficacious. It has also

recently been shown that supraphysiological levels of SMN leads to a late-onset gain of toxic function phenotype caused by disrupted snRNP biogenesis and neuroinflammatory-linked transcriptome changes (Van Alstyne, 2020).

Pre-clinical assessment of therapeutic efficacy can be heavily influenced by the disease model in which the therapy is applied. For SMA, many mouse models exist with varying phenotypes ranging from severe to more mild phenotypes mimicking type II or III SMA. Although SMA mouse models are the most commonly used, models from other species are also available. Increasingly, more non-mouse studies are appearing in the literature using zebrafish (Powis et al., 2016, Hao et al., 2011, Hao et al., 2013), cats (Duque et al., 2009), pigs (Duque et al., 2015) and non-human primates (NHPs) (Foust et al., 2010, Meyer et al., 2015). However, these were not included in this review in order to appreciate the effects of study design and quality more reliably.

Here, greater survival benefits were observed when genetic therapy was given to Taiwanese mice than in treated SMNΔ7 mice. Furthermore, bimodal survival curves were reported in at least three comparisons assessing AAV-treated SMNΔ7 mice, perhaps suggesting there is a population of animals whose phenotype cannot be ameliorated by AAV vector-mediated therapeutics. In these publications, the first group of animals died before approximately 1 month of age (17-27 days (Passini et al., 2010), 25-35 days (Glascock et al., 2012b) and 27-32 days (Dominguez et al., 2011)). The four seminal papers (Foust et al., 2010, Valori et al., 2010, Passini et al., 2010, Dominguez et al., 2011) first describing AAV_*SMN*-mediated increase in survival all used SMNΔ7 mice. These papers cited the choice of SMNΔ7 mice due to the robust phenotype including an approximate two-week lifespan, loss of motor neurons, skeletal muscle atrophy and progressive body weight decline. The SMNΔ7 model had also widely been used in previous pharmacological efficacy studies due to this phenotype (Valori et al., 2010).

It is possible that the mix of different SMA severities within the collated group of less frequently used mouse models contributed to the lower survival benefit seen. For example, Burghes' severe mice survive 4-6 days on average, whilst type II/III models may survive into adulthood. No attempt to delineate a severe and a mild group from these other models was made to avoid inflicting bias when categorising less frequently-used models.

The manner in which a therapy is delivered is important to both patients and clinicians. Spinraza is delivered through an intrathecal injection, whilst Zolgensma is intravenously administered. Lumbar puncture in young children, such as those under the age of 6 months with type I SMA, especially those with severely distorted spines, can be distressing and has associated risks not seen with other modes of delivery. Mercuri et al (2018) observed 9% of adverse events were associated with lumbar puncture 24 hours post Spinraza delivery, rising to 15% at 168 hours and these were at least 5% higher than in the sham lumbar puncture control group. Intrathecal drug delivery, in bypassing the blood-brain barrier, provides good CNS penetrance. SMN protein levels augmented by Spinraza are restored in anterior horn cells, but all tissues outside of the CNS are unaffected. In turn this may prolong survival of SMA patients by preventing motor neuron degeneration and its consequences, but hitherto masked peripheral organ damage may become increasingly prevalent in the clinical phenotype, presenting yet unknown burdens. Because of this issue, systemic gene delivery has been a point of interest within recent SMA research.

The definition of a therapeutic window in which administration of a therapeutic agent provides clinical benefit is important, particularly in a disease like severe SMA whose genesis is *in utero*. Studies have aimed to define this window (Robbins et al., 2014). For some time, it has been thought that the pre-clinical therapeutic window for SMA exists from the day of birth to approximately three days afterwards. However recently, the application of an AAV9_*SMN* therapy for SMA has been delivered *in utero* for the first time with results indicating a significant increase in survival compared to untreated animals (Rashnonejad et al., 2019), highlighting the potential of fetal genetic therapy for SMA too. Here, similar efficacies can be seen when genetic therapy was administered on the day of birth, or between P2 and P5 (MSR: 3.12 and 2.98, respectively). Pre-symptomatic delivery of treatment may prevent development of the SMA phenotype and the irreversible damage that accompanies this, perhaps due to the deficiency being corrected during the period of neuromuscular junction maturation (Farrar et al., 2017). Later delivery, on or after P6, causes a dramatic decrease in efficacy (MSR: 1.37), consistent with current knowledge that symptom onset begins at approximately this time, such as reduction in body weight from P6 onwards in SMN$\Delta$7 mice (Valori et al., 2010). Administering repeated doses of genetic therapy increased MSR further compared to the leading single time point (P1). Of the comparisons that administered genetic therapy at

multiple time points, 55% of these used an oligonucleotide approach. This is consistent with the delivery of Spinraza in the clinic, where intrathecal injections are given every four months during the stable dosing phase, in contrast to a single dose of Zolgensma.

Monogenic diseases such as SMA are prime candidates for gene replacement therapies, thus it is not surprising that 86% of comparisons reviewed here used an *SMN*-dependent approach and these were associated with the greatest survival improvements. It is also reasonable that replacement of the missing *SMN1* gene would provide more benefit than augmentation of SMN protein produced by targeting *SMN2*, as was identified via a 1.3-fold difference between MSRs (4.47 and 3.36, respectively). Nevertheless, the contributions of disease modifiers are increasingly being linked with the alteration of SMA phenotypes. *Plastin3* and *NCALD* are protective modifiers of SMA in humans, although further modifiers have been found in animals (Janzen et al., 2018). When studying the interactome of SMN and SMA disease modifiers, non-SMN proteins have been discovered as potential therapeutic targets. Non-SMN targets have been reviewed excellently elsewhere (Bowerman et al., 2017, Groen et al., 2018). Within this meta-analysis 17 comparisons targeted non-SMN proteins with a 44% increase in survival, albeit lower than SMN-dependent survival.

Further evidence for the use of non-SMN targets to treat SMA is available from non-genetic therapy clinical trials formerly evaluating Olesoxime (now discontinued) and currently assessing Reldesemtiv and SRK-015. These drugs aim to combat oxidative stress in mitochondria, muscle fatigue and improve muscle strength, respectively. With regards to addressing both SMN and non-SMN targets, also known as a SMN plus strategy, it is possible to use ASOs alone (Shababi et al., 2011), viral vectors alone or both (Kaifer et al., 2017), to express or modify each target. Here, these approaches led to an MSR of 2.98, higher than that of non-SMN-dependent strategies. Many further publications were found during the literature search using SMN plus strategies, but were ineligible to be included as they modified the non-SMN target via germline transgenesis, instead of gene therapy delivered *in vivo*. Two example studies showed promising results with transgenic animals (*Smn*$^{-/-}$ *SMN2*$^{tg/0}$ *Chp1*$^{vac/wt}$) plus *SMN2* targeting ASOs (Janzen et al., 2018) as well as transgenic animals (*Smn*$^{-/-}$ *SMN2 KLF15* Mtg) plus viral vectors (Walter et al., 2018).

Limitations of meta-analytic statistics are, of course, present. Risk of bias was prevalent in a random sample of publications describing *in vivo* research (Macleod et al., 2015); coupled with a proclivity for the “file drawer problem”, selective publication of positive results, published treatment efficacies are generally inflated. As conventional meta-analytic techniques could not be used with median survival data, an estimate of standard error was made using sample sizes, weights and inter-study variance so that a random effects model could be implemented (Hirst et al., 2013, Vesterinen et al., 2014). While not as precise as the gold-standard hazard ratio model used in clinical meta-analyses, we believe this model approach to be valid in the context of the limitations in the data. Despite testing the same dataset multiple times, the risk of type 1 errors was managed by using Bonferroni correction.

A significant limitation in this meta-analysis is the application of a univariate model, which does not allow for assessment of how variables interact. Given the varied study designs seen in small animal literature, covariance is generally an issue in preclinical meta-analyses. An example from the data presented here highlights this: all but three comparisons administering genetic therapy via subcutaneous delivery used Taiwanese mice as the chosen model. Both of these two sub-strata showed very high MSRs. With a univariate approach it is impossible to determine which of these factors is influential. Multivariate meta-analysis techniques have been described in preclinical literature (Zwetsloot et al., 2016, Jue et al., 2017), but their adoption with median survival data has not yet been fully validated. On this basis, it is strongly suggested that these results should be interpreted with caution and considered hypothesis-generating only: resulting questions should be investigated through the conduction of high-quality prospective studies.

## 3.8 Conclusions

Genetic therapy is proving to be a promising therapeutic strategy for SMA. This systematic review and meta-analysis has shown that genetic therapies can significantly prolong survival, but that experimental design has a fundamental influence on perceived study outcome. Furthermore, pre-clinical results appear to correlate with clinical experience of Spinraza and Zolgensma. However, pre-clinical data are typically at high risk of bias and single paradigms have not reliably predicted translational efficacy. These conclusions should be borne in mind when

conducting pre-clinical studies of other candidate SMA treatments and small animal research in general.

# 4 Characterisation of vectors expressing *Co-hSMN1* in cell lines

## 4.1 Introduction

### 4.1.1 Analysis of SMA therapeutic strategies *in vitro*

As discussed in section 1.3.1, *in vitro* analysis of basal SMN protein and how this could be augmented in SMN-deficient cells, whether these be transient knockdowns or chronic deficiencies from SMA patients, has been studied extensively. Three main strategies have been used within the literature to increase SMN protein levels; (1) gene addition to replace the missing *SMN1* gene, (2) modulation of *SMN2* splicing to promote exon 7 inclusion and (3) the use of histone deacetylase inhibitors to facilitate transcription of *SMN2*. The use of each of these strategies will be briefly summarised here with select examples.

SMA is a monogenic disease where *SMN1* is missing, meaning this disease is a prime candidate for gene addition therapy. DiDonato et al. (2003) first attempted replacement of the missing *SMN1* gene through expression of the same gene via an adenoviral vector in primary SMA fibroblasts. The authors found that functional SMN protein was increased and gems were restored to a number equal to, or greater than, wild type cells (DiDonato et al., 2003). Introduction of the *SMN1* gene via genome editing expression cassettes has also proven promising. Using a homologous recombination-mediated approach, a *SMN1* cDNA sequence flanked by homology arms located upstream and downstream of the endogenous *SMN1* exon 1 locus, transfected into severe SMA type I fibroblasts (Rashnonejad et al., 2016) resulted in similar outcomes to adenoviral gene replacement. Genome editing at loci other than the endogenous *SMN1* locus has also been tried. Expressing *SMN1* at the ribosomal DNA locus in mesenchymal stem cells has also resulted restoration of SMN levels and gem numbers (Feng et al., 2018). Finally, the gene addition strategies described here often result in SMN levels equal to, or greater than, that of wild type cells, so it was necessary to consider if supraphysiological levels of SMN could in fact be detrimental. This was, however, not found to be the case in an adenoviral over-expression study (2-fold normal SMN at MOI 100 and 10-fold SMN at MOI 1000) where SMN still localised correctly with binding partners in gems and Cajal bodies and no transcriptional dysfunction was seen. The only

deficit that was found was slight reduction in growth rate in transduced fibroblasts (Goulet et al., 2013).

The second strategy involves the modulation of *SMN2* splicing. Normally, only about 10% *FL-SMN* transcripts are produced from this gene due to degradation of transcripts lacking exon 7. The exclusion of exon 7 is mediated by an intronic splice sequence that negative splicing factors bind to, causing splicing machinery to pass over exon 7, not including it in the mature mRNA transcript (Talbot and Tizzano, 2017). Therefore, strategies were identified to promote the inclusion of exon 7, and thus increase amounts of full length SMN translated. ASOs like Spinraza bind to, and prevent recognition of, the intronic splicing sequence within exon 7, causing it to be included in transcripts. Bifunctional RNA oligonucleotides can also be used. These contain an exon 7 targeting domain and another domain that recruits splicing factors, causing the recognition and inclusion of exon 7. These have been used successfully to increase SMN protein and gem number (Baughan et al., 2006), with some increases in protein up to 4.6-fold which was sustained for one month (Owen et al., 2011). Targeting of specific proteins involved in splicing machinery (hnRNP M (Cho et al., 2014)), or RNA molecules involved in histone pre-mRNA processing (U7 snRNA (Geib and Hertel, 2009)) has also shown promise by promoting exon 7 inclusion and increases in resulting SMN protein. Finally, *in vitro* development of Branaplam and Risdiplam was conducted prior the clinical trials mentioned in section 1.1.4.3. Branaplam (formerly known as LM1070 or NVS-SM1) could increase promote exon 7 inclusion leading to increases in SMN protein as assayed by ELISA in mouse myoblasts and SMA patient fibroblasts (Palacino et al., 2015). Risdiplam was shown to target *SMN2* splicing with high selectivity, resulting a 1.5-fold increase in SMN protein when only 29nM of the compound was applied *in vitro* (Ratni et al., 2018).

The final strategy to augment SMN protein uses histone deacetylase inhibitors (HDACis) to enhance *SMN2* promoter activity. These work by increasing the acetylation of histones, particularly at the N terminus, causing a relaxation of chromatin structure, increasing accessibility of target gene sequences to transcriptional machinery (Also-Rallo et al., 2011). Examples of HDACis that are commonly used for SMA include valproic acid, phenylbutyrate and trichostatin A. However, HDACis are not gene therapy agents and thus are not wholly relevant to this thesis, but have been included here briefly for completeness. For an excellent review of HDACi use in SMA, please see Mohseni et al. (2013).

### 4.1.2 Codon optimisation of the *SMN1* transgene

Two different types of vector (IDLVs and AAV9) were used in this project to compare the efficacy of transduction, their respective abilities to induce SMN over-expression and the extent of functional rescue.

The vectors used in this project all express the transgene *Co-hSMN1*, a codon-optimised version of the human *SMN1* gene that was developed in a previous PhD within the Yáñez-Muñoz laboratory (Ali Mohammadi Nafchi, 2017). Codon-optimisation is a strategy that has shown promise when increasing protein translation (Deml et al., 2001, Hamdan et al., 2002, Gustafsson et al., 2004). Mature mRNA transcripts are translated into proteins when ribosomes and associated transfer RNAs form a chain of amino acids based on the DNA codon sequence. Codon-optimisation uses the degenerate nature of DNA nucleotide triplets encoding the same amino acid, by biasing the codon used to one that is preferentially selected by the human pool of transfer RNAs (Waldman et al., 2010).

Previously in this laboratory, *Co-hSMN1*-expressing lentiviral vectors have led to increased SMN intensity when measured by immunofluorescence in primary rat motor neurons and an increase in functional SMN, measured by the number of gems in SMA type I fibroblasts, when compared to wild-type *SMN1* expressing vectors (Ali Mohammadi Nafchi, 2017). Others have also found similar results when using codon-optimised versions of the *SMN1* gene. When SMA type I fibroblasts were transduced with lentiviral vectors expressing either the wild-type or codon-optimised *SMN1* sequences, a two-fold difference in SMN protein was seen between the two, favouring the codon-optimised sequence (Valori et al., 2010).

Although developed in a previous project, the sequence of the *Co-hSMN1* transgene has not yet been reported. The codon-optimised sequence with a comparison to wild type *SMN1* can be found in Figure 4.1.

***Figure 4.1 Alignment of wild type and codon-optimised cDNA sequences of* SMN1*.***

*A codon-optimised* SMN1 *sequence (bottom sequence), known as* Co-hSMN1*, was developed in a previous PhD project (Ali Mohammadi Nafchi, 2017) using GENEART's Gene Optimizer software, compared to the wild type* SMN1 *ORF (top sequence). The* Co-hSMN1 *transgene has been cloned into three lentiviral vector backbones and one AAV vector backbone, all of which are used in this project. Asterisks represent changed nucleotides.*

### 4.1.3 Vector constructs

The *Co-hSMN1* transgene is transcriptionally controlled by one of four promoters within this project. IDLVs contain cytomegalovirus immediate early (CMV), human synapsin (hSYN) or human phosphoglycerate kinase (hPGK) promoters whilst the AAV9 vector used the synthetic CAG promoter, also called chicken β-actin (CBA) by some groups, for example in the Zolgensma construct. Finally, the *Co-hSMN1* transgene is coupled to mWPRE, an RNA element that acts post-transcriptionally to improve transgene expression by stabilising the poly-A tail and promoting nuclear export (Zufferey et al., 1999). Maps of the four existing *Co-hSMN1* transfer plasmids used to make the IDLVs in this project can be seen in Figure 4.2.

The CMV immediate early promoter has become commonly used in expression vectors because of stable, long-term expression it induces (Thomsen et al., 1984, Foecking and Hofstetter, 1986). The ubiquitous hPGK promoter is of use when targeting cells where CMV may be methylated, such as stem cells (Meilinger et al., 2009). Work by a previous MSc student in the Yáñez-Muñoz laboratory has shown it to be promising when driving *Co-hSMN1* expression in lentiviral vectors used to transduce CHO cells (Hayler, 2017). The neuron-specific hSYN promoter can be used to add transcriptional targeting to lentiviral vectors so the transgene is only expressed in neurons, including vulnerable MNs.

The synthetic CAG promoter is a hybrid containing the immediate early enhancer element from the CMV promoter bound to the promoter of the chicken β-actin (CBA) gene. It is important to note that different versions of the CAG promoter exist within the literature and not all contain the same construct assembly (Fitzsimons and During, 2005). As well as the combined CMV immediate early and CBA promoters, it is also possible to clone in the CBA first exon, intron and enhancer, as well as the splice acceptor of the rabbit β-globin gene (Miyazaki et al., 1989), or introns from other viruses such as the minute virus of mice (MVM) (Gray and Samulski, 2011). The CAG promoter used in this project contains a hybrid intron from CBA and rabbit β-globin genes. Adding these elements improves transgene expression, but limits transgene coding capacity; an important consideration when using AAVs, especially scAAVs. Despite the addition of extra elements to improve efficacy, it is known that the CMV promoter is stronger than CAG, but CAG does not become silenced over long periods of CNS expression (Gray et al., 2011).

IDLVs that express *eGFP* were used as reporter systems to assess transduction efficacy. IDLVs contained *eGFP* coupled to WPRE, under the control of the CMV promoter whereas AAV plasmids contained the CAG promoter and *eGFP* transgene, but no WPRE due to size restrictions. Transfer plasmids expressing *eGFP* with the lentiviral backbone and AAV backbone can be seen in Figure 4.3.

#### 4.1.3.1 Comparison to published constructs

The original construct used for lentiviral expression of *SMN1* (Azzouz et al., 2004) consisted of an Equine Infectious Anaemia virus expressing *SMN1* under the control of a CMV promoter, coupled to a WPRE element with self-inactivating LTRs. This construct is very similar to that of the CMV-controlled vector used in this study (Figure 4.2A), except the use of wild type *SMN1* sequence in the published study and the mutated version of the WPRE used here.

The construct present in Zolgensma, first developed by the Kaspar laboratory (Foust et al., 2010), consists of a AAV2 backbone, Rep2Cap9 sequence to encode the AAV9 serotype, with self-complementary ITRs. The *SMN1* gene is transcriptionally controlled by the CAG/CBA promoter, but it has not been published whether this promoter contains any additional intronic or exonic elements. In contrast, the CAG promoter used in this project contains a hybrid intron from CBA and rabbit β-globin genes (Burger et al., 2005).

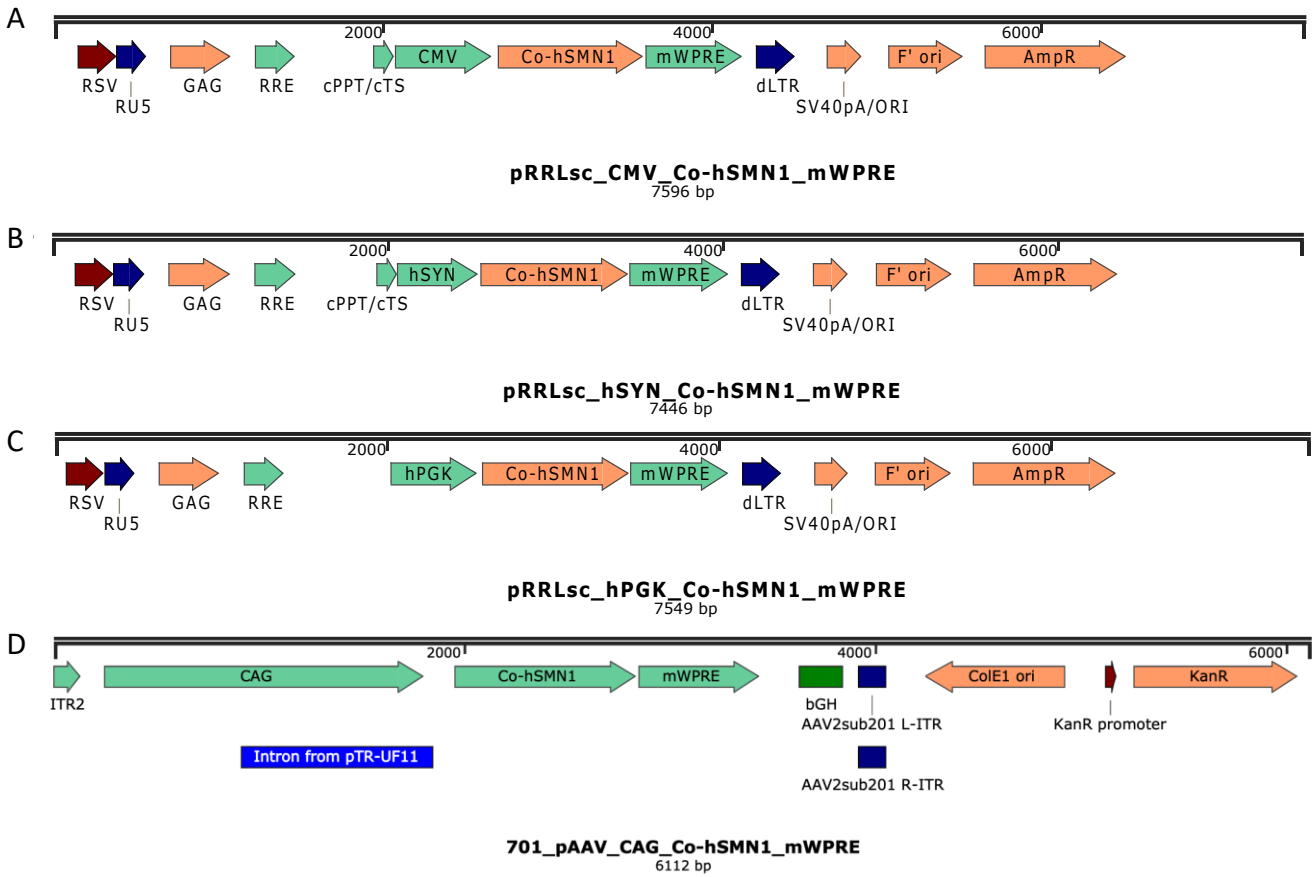


***Figure 4.2 Maps displaying features of the four transfer plasmids encoding* Co-hSMN1.**

*The constructs used in transfer plasmids to produce (A-C) lentiviral or (D) AAV vectors are shown. Each plasmid encodes the* Co-hSMN1 *transgene flanked upstream by a promoter (CMV, hSYN, hPGK or CAG) and downstream by mWPRE, a post-transcriptional element that improves transgene expression. Other features such as lentiviral backbone elements, such as (RSV, GAG, RRE), antibiotic resistance genes (ampicillin or kanamycin) and LTR or ITRs are also shown.*

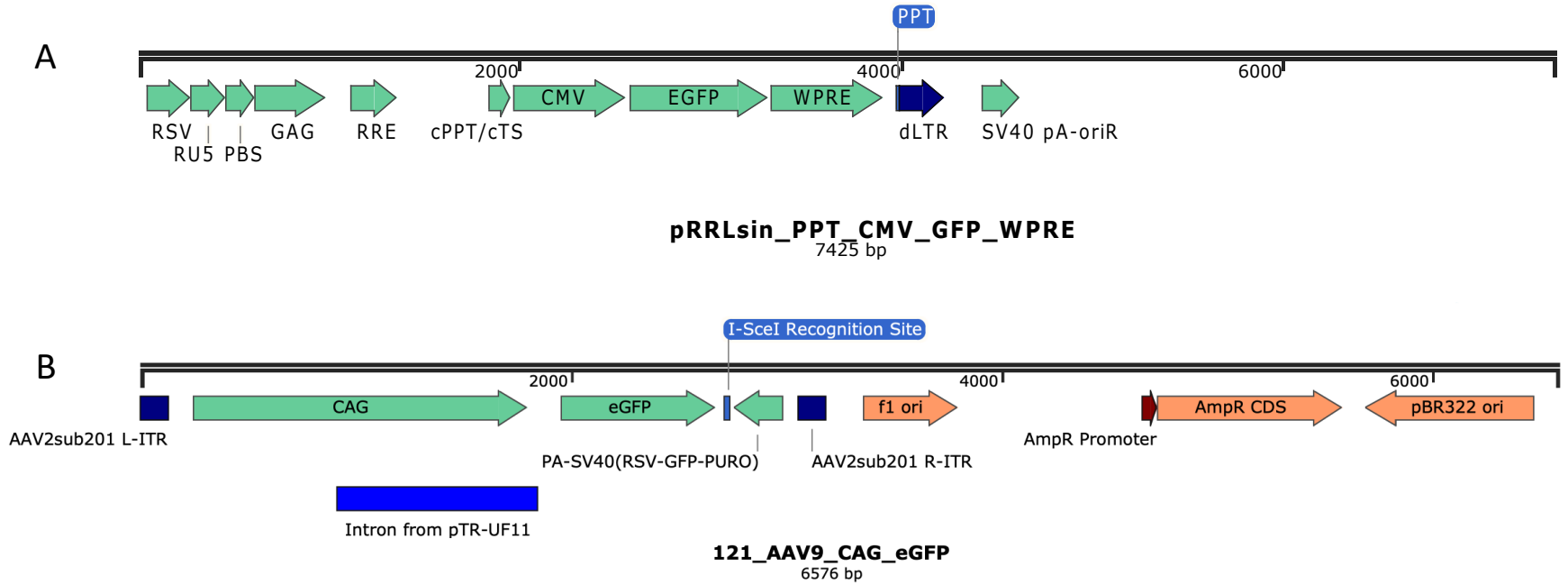


***Figure 4.3 Maps displaying features of* eGFP *transfer plasmids.***

*The constructs used in transfer plasmids to produce (A) lentiviral or (B) AAV vectors are shown. Each plasmid encodes the* eGFP *transgene flanked upstream by a promoter (CMV or CAG and hybrid intron). Downstream of* eGFP *in the lentiviral plasmid only is WPRE, a post-transcriptional element that improves transgene expression. Other features such as lentiviral backbone elements, such as (RSV, GAG, RRE), antibiotic resistance genes (ampicillin for both plasmids) and LTR or ITRs are also shown.*

## 4.2 Aims

In this chapter I aimed to produce lentiviral vectors expressing *Co-hSMN1* and control *eGFP* cassettes and then test these in cell lines and primary patient tissues. Specifically, my objectives were:

(A) Produce lentiviral vectors of sufficient titres.

(B) Determine transduction efficacies of IDLVs and AAV9s expressing *eGFP* in a variety of cell lines.

(C) Over-express SMN protein in cell lines and primary SMA type I patient fibroblasts, quantifying increase in protein directly and with a functional assay detecting gems.

(D) Compare and contrast IDLV_*Co-hSMN1* and AAV9_*Co-hSMN1* vectors.

## 4.3 Production of lentiviral vectors

Lentiviral vectors expressing *eGFP* under the control of CMV promoter or *Co-hSMN1* under transcriptional control of CMV, hSYN or hPGK promoters were constructed using the calcium phosphate plasmid transfection method described. Both integration-proficient and -deficient vectors were produced successfully. qPCR and flow cytometry (given the presence of a fluorescent marker) were used to titrate vectors produced to give a measure of vector potency (Table 4.1). Two batches of CMV_*eGFP* lentiviral vectors were produced on two separate occasions. All subsequent *eGFP* vectors and those not expressing a fluorescent gene were solely analysed by qPCR. Titres calculated using qPCR were used to calculate all experimental MOIs. As well as producing new vector stocks, IDLVs produced by previous lab members were used in some experiments. The characteristics of these vectors are shown in Table 4.2.

| Vector | Transfer plasmid | Integration proficiency | Flow cytometry titre (TU/ml) | qPCR titre (vg/ml) |
|---|---|---|---|---|
| CMV_*eGFP*_WPRE | pRY_396 | IPLV | $2.1x10^9$ | $2.9x10^9$ |
| CMV_*eGFP*_WPRE | pRY_396 | IDLV | $6.9x10^9$ | $2.6x10^9$ |
| CMV_*eGFP*_WPRE | pRY_396 | IDLV | N/A | $1.6x10^{10}$ |
| CMV_*Co-hSMN1*_mWPRE | pRY_543 | IDLV | N/A | $2.6x10^9$ |
| hSYN_*Co-hSMN1*_mWPRE | pRY_544 | IDLV | N/A | $3.4x10^9$ |
| hPGK_*Co-hSMN1*_mWPRE | pRY_552 | IDLV | N/A | $2.2x10^9$ |

***Table 4.1 Summary of titres of lentiviral vectors produced during this project.***

*IDLVs expressing eGFP were produced on multiple occasions so separate titres were determined for each batch. IPLV = integration proficient lentiviral vector, IDLV = integration deficient lentiviral vector, TU = transducing units, vg = vector genomes, N/A = vector not titrated using flow cytometry.*

| Vector | Transfer plasmid | Integration proficiency | qPCR titre (vg/ml) | Producer |
|---|---|---|---|---|
| CMV_*eGFP* | pRY_396 | IDLV | $4.8x10^9$ | Neda Ali Mohammadi Nafchi |
| CMV_*Co-hSMN1* | pRY_543 | IDLV | $5.7x10^9$ | Neda Ali Mohammadi Nafchi |
| hSYN_*Co-hSMN1* | pRY_544 | IDLV | $2.7x10^{10}$ | Neda Ali Mohammadi Nafchi |
| CMV_*Co-hSMN1* | pRY_543 | IDLV | $5.3x10^{10}$ | Daniel Hayler |
| hSYN_*Co-hSMN1* | pRY_544 | IDLV | $2.1x10^{10}$ | Daniel Hayler |
| hPGK_*Co-hSMN1* | pRY_552 | IDLV | $3.6x10^{10}$ | Daniel Hayler |

***Table 4.2: Lentiviral vectors produced by previous lab members that were used in this project.***

## 4.4 Production of AAV9 vectors

Two AAV9 vectors were commercially produced by Atlantic Gene Therapies. These vectors were designed to have equivalent expression cassettes to the lentiviral vectors used in this project. Therefore, a single stranded conformation expressing either *eGFP* alone or *Co-hSMN1* coupled to mWPRE under transcriptional control of the CAG promoter was designed. To achieve this goal 100µg of the pRY_543 IDLV_CMV_*Co-hSMN1* plasmid was sent with instructions to release a 1483bp fragment containing both *Co-hSMN1* and mWPRE by digestion with *Age*I and *Acc*65I or *Kpn*I. From this, AAV9 vectors were produced and titrated by Atlantic Gene Therapies using qPCR against viral ITRs (inverse terminal repeats) and resulted in the following titres; *eGFP* = $3.8x10^{13}$ vg/ml; *Co-hSMN1* = $2.2x10^{13}$ vg/ml.

## 4.5 Determining the transduction efficacies of IDLV and AAV9 vectors

Prior to testing and optimisation of vectors in iPSC MNs, the ability of the vectors to transduce other cell lines with high efficacy was confirmed using a range of MOIs (multiplicity of infection; the number of vector particles available to each cell).

HEK293T/17 and two undifferentiated neuroblastoma cell lines: murine Neuro2a and human SH-SY5Y cells were transduced with IDLVs expressing *eGFP*. All cell types showed high IDLV_*eGFP* transduction efficacy measured by fluorescent microscopy (Figure 4.4A) and flow cytometry in an MOI-dependent manner. When very high MOIs (>200) were used to get a measure of peak fluorescence, up to 98% of cells were GFP-positive. When lower, more routinely used MOIs (10-150) were tested a linear increase in GFP-positive cells was present (range 27-89%; Figure 4.4B,C).

CHO cells were chosen to determine the efficacy of AAV9_CAG_*eGFP* transduction due to previous experience in the laboratory with other AAVs. For efficient gene expression from AAVs a much higher MOIs is required than is used with lentiviral vectors. A time course of *eGFP* expression was obtained using fluorescent microscopy 24, 48 and 72 hours post-transduction when CHO cells were transduced with the highest tested MOI (Figure 4.4D). However, at MOIs of $1x10^5$ and $1x10^6$ an average of only 2.1% ($P=0.0038$) and 18.8% ($P<0.0001$) GFP-positive

cells, respectively, were seen after flow cytometry compared to mock-treated cells (Figure 4.4E).

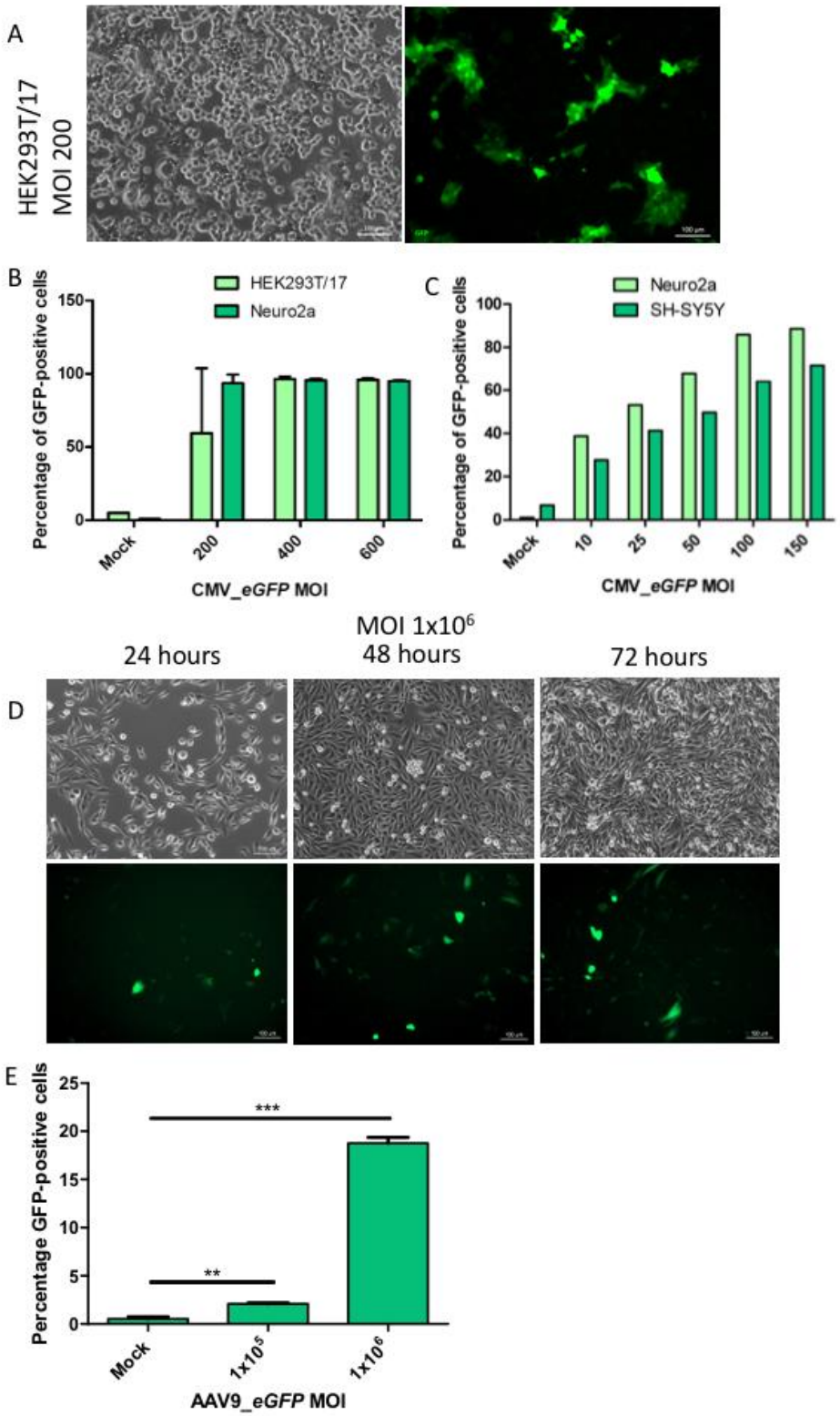


***Figure 4.4 Transduction of cell lines with vectors expressing eGFP.***

*All cells were transduced for 72 hours then assessed by fluorescent microscopy and flow cytometry. (A) Visual representation of HEK293T/17 cells showing bright GFP*

*fluorescence following IDLV_CMV_*eGFP *transduction at MOI 200. (B) Very high MOIs were first tested to prove that nearly all cells can be transduced when in the presence of high concentrations of IDLV_CMV_*eGFP*. (C) Lower more feasible MOIs are to be used in actual experiments so a dose-response assay was used to determine optimal MOIs to use in the future. (D) Time course of eGFP expression after transduction with AAV9_CAG_*eGFP *at MOI 1x10$^6$. (E) Transduction of CHO cells with an AAV9 vector encoding an equivalent cassette requires much higher MOIs to achieve lower transduction efficacy than IDLVs (MOI 1x10$^5$ P=0.0038, 1x10$^6$ P<0.0001). One-way ANOVA with Dunnett's post-hoc test was used to calculate statistical significance. MOI = multiplicity of infection.*

## 4.6 Optimising endogenous gem detection

SMN forms a multiprotein complex with five other proteins known as gemins and these complexes are located in nuclear gems; SMA patients show fewer gems due to SMN deficiency. Therefore, detection of gems is an endpoint that can be used to test the functionality of *SMN* expressed by the vectors. The immunofluorescence procedure used to detect these gems was optimized to detect the best possible gem signal. Undifferentiated Neuro2a cells were cultured for 96 hours (the length of time used to seed and transduce cells) without vector transduction to allow visualisation of endogenous protein levels following immunostaining. As Gemin2 is a protein located solely in nuclear gems, rather than SMN which is expressed within multiple cellular compartments, this is the preferred target for immunostaining as this should lead to clearer images with easily quantifiable gems.

However, issues arose when the Gemin2-stained samples were not as clear as desired, showing cytoplasmic as well as nuclear staining with high background signal (Figure 4.5A,B). Potential solutions to this problem have been identified and some tested by altering aspects of the immunofluorescence staining protocol. These include increasing primary antibody incubation time whilst also increasing the dilution factor, using a more concentrated blocking solution, changing secondary antibody from Alexa Fluor 488 to 555, reducing fixation time and combining permeabilisation and blocking steps in the protocol to reduce cells lifting from the plate (Figure 4.5C-F). These alterations have produced slightly clearer images, but unfortunately still not eliminating problems altogether. The use of a primary antibody against SMN protein was also tested showing cytoplasmic signal as well but gem signal was stronger. Further potential solutions that were not tested include using a different fixative, for example using methanol instead of paraformaldehyde (PFA) or using a different serum in the blocking solution, for example fetal horse serum.

The decision was made to test the immunofluorescence protocol in a second neuroblastoma cell line (SH-SY5Y) to assess if the problems arising could be cell-specific rather than protocol-specific. In both SH-SY5Y and Neuro2a cells Gemin2-stained samples showed fewer gems with less intense signal strengths than SMN-stained samples. However again, immunostained SH-SY5Y cells proved difficult to focus upon with background signal in many areas (Figure 4.5G,H), suggesting that this may not be a cell-specific issue. In conclusion, the following protocol was used for the remainder of experiments; 1:400 anti-SMN diluted in 1% BSA in 0.1% PBST with an overnight incubation for 4ºC, followed by 1:1000 anti-mouse Alexa Fluor 555 diluted in 1% BSA in 0.1% PBST incubated for 1 hour at room temperature.

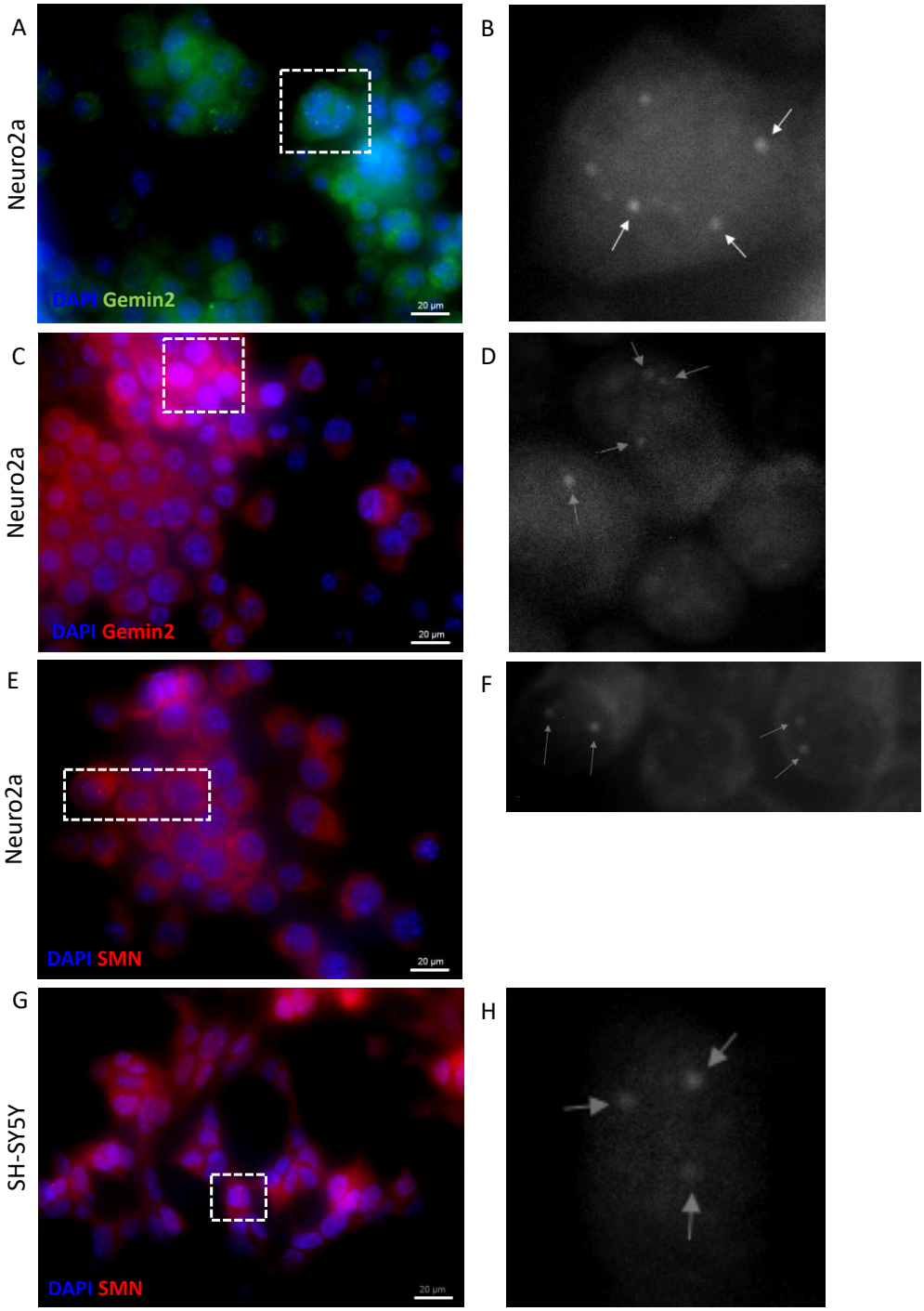


***Figure 4.5 Immunostaining against endogenous protein levels of Gemin2 and SMN in two cell lines at different stages optimisation.***

*Gemin2-stained samples consistently show fewer gems with lower intensity than SMN-stained samples in both SH-SY5Y and Neuro2a cell lines. Cells were plated at the same density in 24 well plates and allowed to grow for 96 hours before fixing and immunostaining protocols were applied. Scale bar = 20µm. (A) 1 hour primary antibody incubation (anti-Gemin2; 1:200 dilution), Alexa Fluor 488 secondary antibody (1:1000 dilution), (B) inset images showing gems more closely. (C-H) Overnight primary antibody incubation (either anti-Gemin2 or anti-SMN; 1:400), Alexa Fluor 555 (1:1000), with insets showing gem visibility.*

## 4.7 Quantitative assessment of IDLV_*Co-hSMN1* functionality

An assessment was attempted to quantitate any increase in gem number after transduction with *Co-hSMN1* vectors under control of CMV, hSYN and hPGK promoters in Neuro2a and SH-SY5Y cells, despite the difficulties described surrounding gem detection following immunostaining. Following on from the dose-response seen in Figure 4.6C, as well as evidence showing that SMN can be increased by transduction with IDLVs expressing SMN at MOIs of 30, 60 and 100 (Ali Mohammadi Nafchi, 2017), MOIs between 25 and 100 were chosen for continued use in this chapter as these were able to transduce cells with between 50-90% efficacy, as well as no detrimental effects on cell viability seen. 100 nuclei were randomly selected from each vector treatment then the number of gems within those 100 nuclei were subsequently counted. Triplicates were obtained for each condition immunostained with anti-Gemin2 and anti-SMN.

Neuro2a cells showed higher numbers of gems present when cells were transduced with an MOI of 75 rather than 25, as expected (Figure 4.6B,D). When comparing transduced and mock treated cells, no significant difference was seen in the number of gems present, except for cells transduced with CMV_*Co-hSMN1* immunostained against SMN (Figure 4.6B; MOI 25 $P=0.0017$, D; MOI 75 $P<0.0001$). Fluorescent images (Figure 4.6A,C) show similar immunostaining problems as seen before which caused gem counting to become difficult, thus meaning that gem numbers in samples with particularly high background and low gem signal may be over- or under-represented, calling significance of results into question.

SH-SY5Y cells showed similar results where, again, CMV_*Co-hSMN1* transduced (MOI 75) cells stained against SMN were the only samples to show significantly increased numbers of gems compared to mock (Figure 4.6F; $P<0.0001$). Immunostained images (Figure 4.6E) also show background signal but clear gems were visible. More gems were seen in samples transduced with MOI 75 rather than 25 when cells were transduced with CMV- and hSYN-controlled vectors but not with hPGK-controlled vectors.

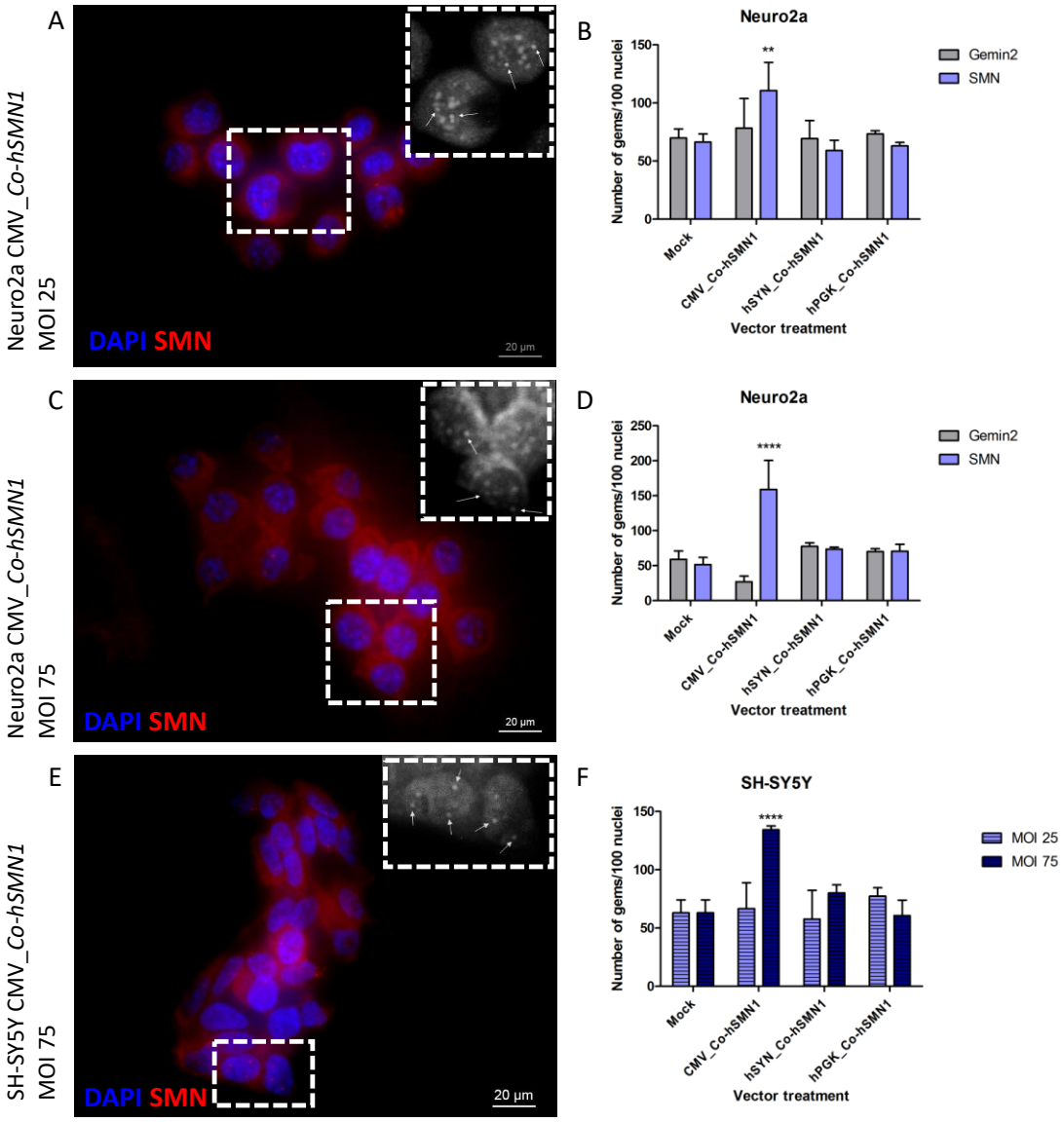


***Figure 4.6 Quantitative assessment of vector functionality.***

*Undifferentiated Neuro2a and SH-SY5Y cells were transduced for 72 hours with Co-hSMN1 vectors under the control of CMV, hSYN or hPGK promoters to quantitate any increase in SMN expression. Any increase would be detected by increased numbers of nuclear gems. (A,C,E) Fluorescent images of CMV_*Co-hSMN1 *transduced cells at MOI 25 and 75 following fixation and immunostaining against SMN protein. Scale bar = 20µm. (B,D) CMV_Co-hSMN1 anti-SMN Neuro2a cells showed significantly increased gems compared to mock samples (B; MOI 25 P=0.0017, D; MOI 75 P<0.0001), but all other samples were non-significantly different. However, images with high background signal made counting gems difficult. Clearer images would allow easier counting and may provide evidence for an increase in gem number. (F) Again, only CMV_*Co-hSMN1 *SH-SY5Y cells at MOI 75 showed a significant increase in gem number (P<0.0001). Two-way ANOVA with Dunnett's post-hoc test was used to compare treated to mock.*

## 4.8 *eGFP* expression in differentiated neuronal-like cells

Following confirmation of high transduction efficacy and an increased number of gems in undifferentiatied cells of a neuronal lineage, Neuro2a and SH-SY5Y cells were then differentiated to become neuron-like by replacement of proliferation medium (DMEM+Glutamax, 10% FBS, 1% Penicillin/Streptomycin) with differentiation medium (DM; DMEM+Glutamax, 1% FBS, 1X Non-essential amino acids , 0.7M $NaCO_3$, 20μM retinoic acid). Serum starvation and addition of retinoic acid promotes a neuronal phenotype. $NaCO_3$ in Neuro2a DM counteracts acidic conditions produced by these cells, but is not necessary for SH-SY5Y cells which do not produce this acidity. The aim of this experiment was to compare transduction efficacies in a neuronal-like population of easy to grow cells, but separate progress was made to establish an iPSC-derived neuronal model (presented in chapter 5).

Neuro2a and SH-SY5Y cells were cultured for 6 days in DM before transduction with CMV_*eGFP* vectors at MOIs of 25 and 75. The majority of cells showed a neuronal-like morphology with long dendritic projections, however some remained in a rounded morphology similar to that of undifferentiated cells. When assessed by fluorescent microscopy and flow cytometric analysis a very low proportion of Neuro2a cells exhibited eGFP expression (Figure 4.7A,B). A peak of 9% eGFP-positive differentiated cells when transduced with an MOI of 75 (Figure 4.7E) is far below than the value for undifferentiated cells at an MOI of 10 (38.7% eGFP-positive; Figure 4.7D; also Figure 4.4C). We can see that transduction was successful in some cells (Figure 4.7), however these cells that express *eGFP* appear to have a rounded, flattened morphology with no evidence of dendritic projections, suggesting these were not differentiated. This provides evidence that the protocol was successful and it is something about the differentiated cells specifically that causes transduction to fail. It is possible that differentiated cells may require a higher MOI to detect *eGFP* expression than undifferentiated cells.

In contrast, SH-SY5Y cells did not show the same lack of *eGFP* expression following transduction. GFP-positive values for differentiated cells were lower than those for undifferentiated cells at equivalent MOIs (MOI 25 30.2% vs 41.3% respectively; Figure 4.7D,E), but not to the same extent as Neuro2a cells. It is interesting to note the comparison between cell types at undifferentiated and

differentiated stages. When undifferentiated, Neuro2a cells display more GFP-positive cells than SH-SY5Y cells (Figure 4.7D) under the same conditions, yet once differentiated, this pattern is reversed with SH-SY5Y cells showing increased numbers of GFP-positive cells (Figure 4.7E).

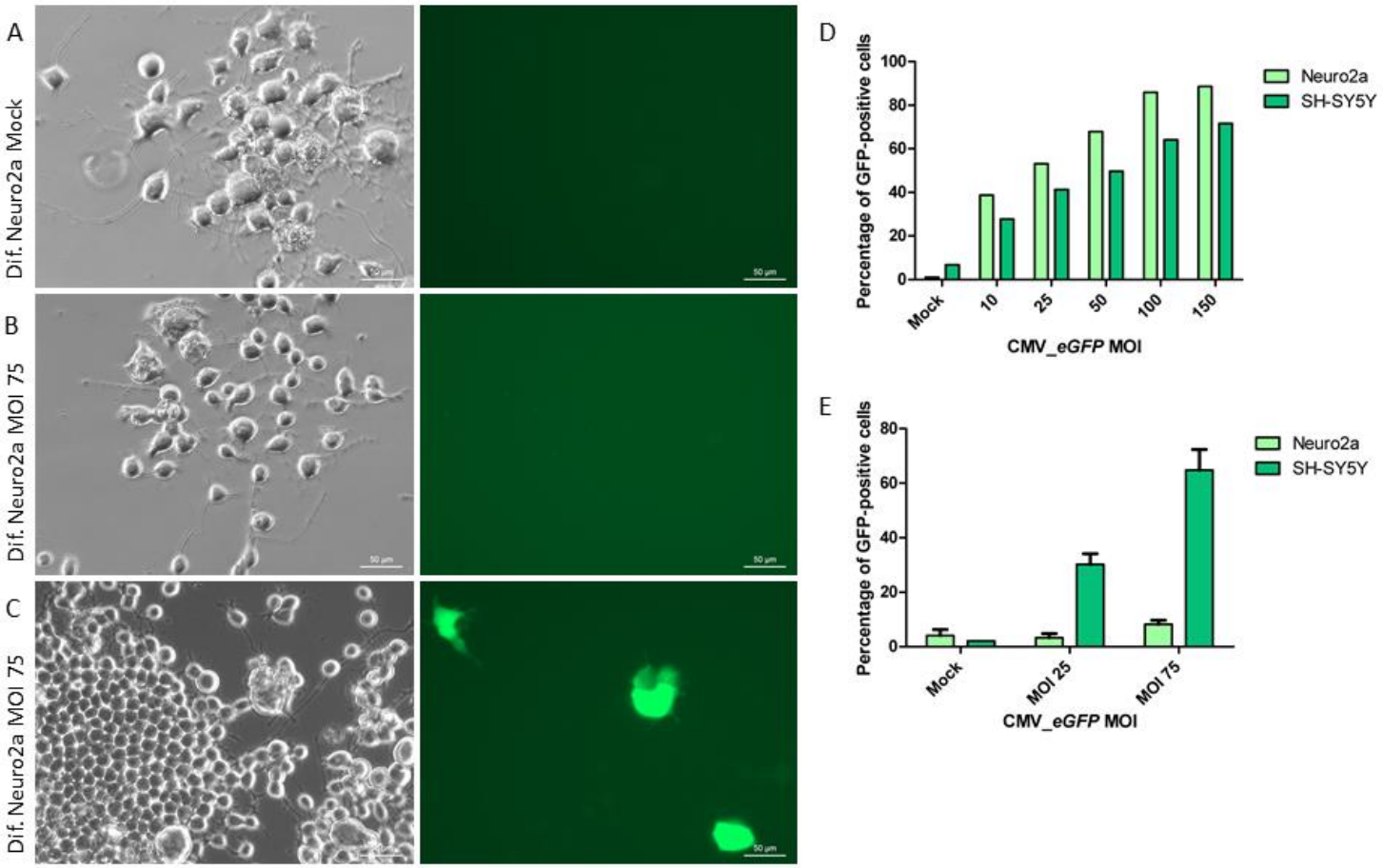


***Figure 4.7 Differentiated Neuro2a and SH-SY5Y cells show lower transduction efficacy than undifferentiated cells.***

*(A-C) Neuro2a cells were transduced with IDLV_CMV_*eGFP *for 72 hours following 6 days of differentiation then imaged using phase contrast and fluorescent microscopy. (B) and (C) show the same conditions but represent two different fields of view, highlighting differences in* eGFP *expression in cells of different morphology. Undifferentiated Neuro2a cells (D) at the lowest MOI show 38.7% GFP-positive cells whereas differentiated cells (E) with the highest tested MOI of 75 do not exceed 9% GFP-positive cells. Replicates were not obtained when undifferentiated cells were tested. SH_SY5Y cells show far higher* eGFP *expression, similar to levels seen in undifferentiated cells.*

## 4.9 Rescue in primary patient cells following IDLV transduction

In the previous sections, I have shown that increases in gem detection were observed in Neuro2a and SH-SY5Y cells after IDLV_CMV_*Co-hSMN1* transduction when immunostained with an anti-SMN antibody. In a previous PhD project (Ali Mohammadi Nafchi, 2017), primary type I SMA fibroblasts were also observed to have significant increases in gem number, consistent with data presented here. To gain an understanding of total SMN increases following transduction, in addition to positive data regarding increases in gem number, an alternative approach employed immunofluorescence to assess cytoplasmic and nuclear staining, as well as quantitative western blot for whole cell analysis.

Firstly, a comparative experiment was undertaken in both wild type and SMA type I fibroblasts assessing the efficacy by which these cells express *eGFP* following IDLV transduction. SMA type I fibroblasts show a maximum of 21% GFP-positive cells at an MOI of 150, compared to 72% in wild type cells (Figure 4.8A). To try to increase the efficacy of transduction, polybrene was added to media at the time of transduction. At 2µg/ml polybrene maximum efficacy increased to 74.6% and at 4µg/ml this was further increased to 98.1%, a value higher than wild type efficacy (Figure 4.8A).

SMN immunofluorescence was employed in wild type and SMA type I fibroblasts following IDLV transduction with 2µg/ml polybrene. Here, there was clear increase in cytoplasmic SMN signal (Figure 4.8B,C). Confirmation of a significant difference between wild type and SMA type I fibroblast SMN protein levels was seen by western blot (Figure 4.8D, $P<0.0001$). Transduction of SMA type I fibroblasts (2µg/ml polybrene) with IDLVs encoding *Co-hSMN1* under transcriptional control of CMV, hSYN and hPGK promoters shows significant protein over-expression (Figure 4.8D) at all tested MOIs compared to mock treated SMA type I fibroblasts when assessed by western blot (SMA mock vs CMV both MOIs $P<0.0001$, vs hSYN MOI 75 $P=0.0386$, MOI 100 $P=0.0243$, vs hPGK both MOIs $P<0.0001$). CMV- and hPGK-controlled vectors also produced significantly higher SMN protein levels than in wild type cells (Figure 4.8D; WT mock vs CMV both MOIs $P<0.0001$, hPGK MOI 75 $P=0.0005$, MOI 100 $P<0.0001$).

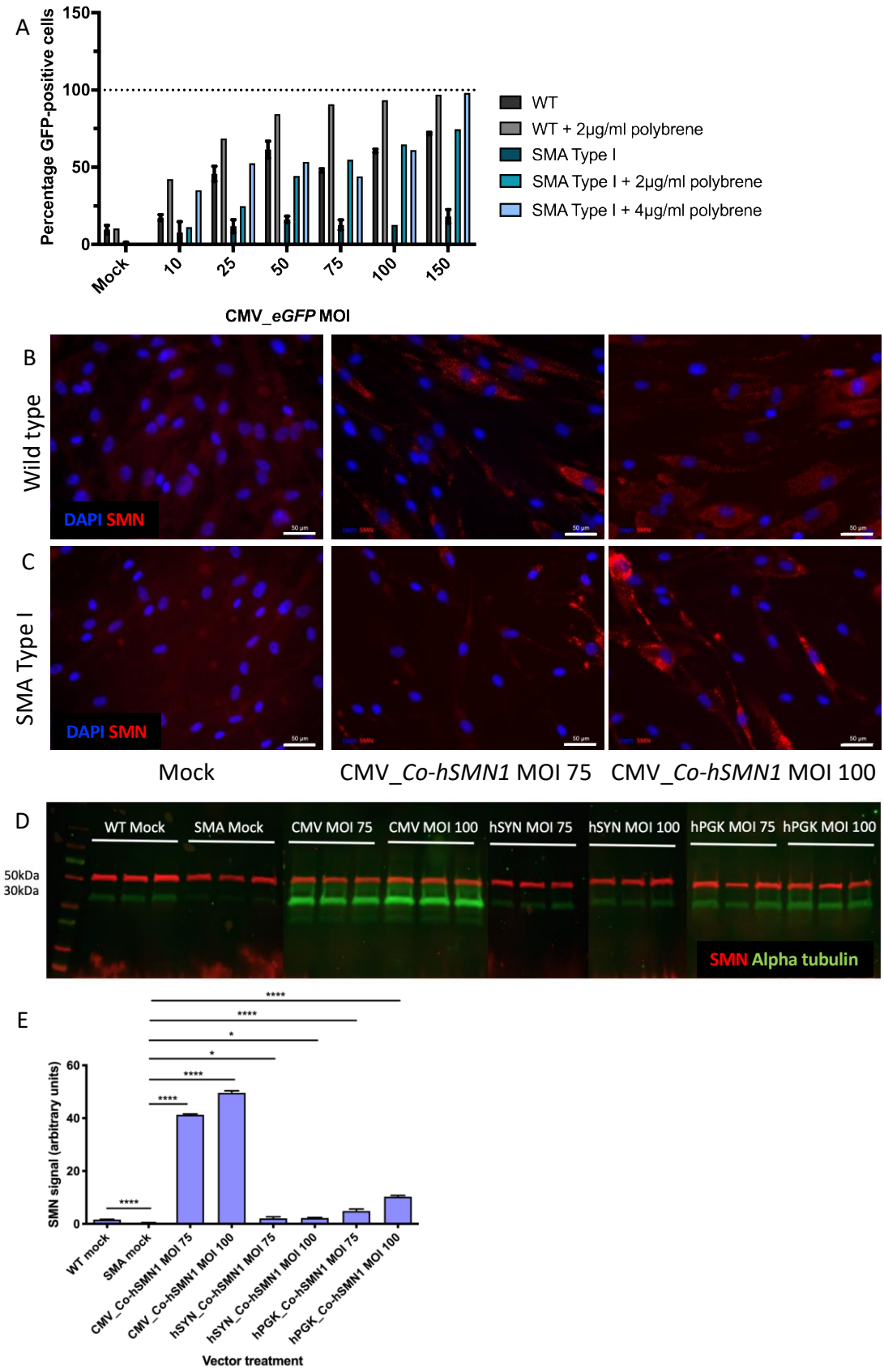


***Figure 4.8 Transduction of SMA type I patient fibroblasts.***

*(A) Efficacy (measured as percentage of GFP-positive cells by flow cytometry) was compared in wild type and SMA type I fibroblasts with and without polybrene (2µg/ml). Replicates were not obtained for all samples. (B,C) Wild type and SMA type I fibroblasts transduced with IDLV_CMV_*Co-hSMN1 *in the presence of 2µg/ml*

*polybrene at MOIs 75 and 100, then immunostained against SMN. Scale bar = 50µm. (D) Western blot using lysates from SMA type I fibroblasts transduced in the same manner as in (B,C) and wild type untransduced fibroblasts. (E) All SMA type I fibroblasts transduced produced significant increases in SMN protein level (SMA mock vs CMV both MOIs P<0.0001, vs hSYN MOI 75 P=0.0386, MOI 100 P=0.0243, vs hPGK both MOIs P<0.0001). One-way ANOVA with Dunnett's multiple comparison post-test was used to assess statistical significance. Comparing wild type and SMA mock only confirms a significant difference in SMN protein (unpaired, two-tailed t-test, P<0.0001).*

## 4.10 AAV9 vector-mediated *Co-hSMN1* expression

### 4.10.1 Transduction and transfection of AAV9_CAG_*Co-hSMN1* in CHO cells

The IDLVs tested in neuronal cell lines and primary patient fibroblasts were then compared with a commercially produced AAV9 vector in CHO cells to assess any differences in their ability to induce SMN over-expression. CHO cells were transduced with AAV9_CAG_*Co-hSMN1* at MOIs of $1x10^4$, $1x10^5$ and $1x10^6$, however no significant increase in SMN protein levels was detected by western blot (Figure 4.9A,C; Mock vs MOI $1x10^4$ P=0.2328, vs $1x10^5$ P=0.8544, vs $1x10^6$ P=0.2889) without even evidence of a trend of increased SMN in transduced samples. As stated in section 4.5, the efficacy of transduction with AAV9_CAG_*eGFP* in CHO cells was low here also (Figure 4.9B; also Figure 4.4E; MOI $1x10^5$ 2.1%, $1x10^6$ 18.8%) so this perhaps accounts for no evidence of over-expression. The low percentage of cells that were transduced could have indeed had higher levels of SMN protein, but this may have been masked by the majority of untransduced cells, leading to no detection by western blot.

Given the low expression levels detected from Atlantic Gene Therapies AAV vectors, I confirmed the presence of the main plasmid elements in the relevant transfer plasmids. To confirm presence of the *Co-hSMN1* transgene, CAG promoter, mWPRE and bGH (bovine growth hormone) polyA elements, sequence alignments and restriction digests were performed. Sequence files for the two transfer plasmids used to make the vectors (pRY_586 for *eGFP* and pRY_587 for *Co-hSMN1*) were analysed on SnapGene along with the plasmids from which the desired elements were taken. Of importance, when pRY_587 and pRY_543 (the transfer plasmid contained with CMV_*Co-hSMN1* IDLVs) were aligned an 882bp fragment encoding *Co-hSMN1* was found in both plasmids and a 590bp fragment from pRY_543 and 588bp fragment from pRY_587 were found encoding the mWPRE (11bp after the end of *Co-hSMN1*). Sequence alignments also

revealed the presence of the CAG promoter and bGH polyA transcriptional terminator in the AAV9 plasmids.

Appropriate restriction enzymes were chosen during sequence analysis to digest DNA of the pRY_586 *eGFP* and pRY_587 *Co-hSMN1* plasmids. Plasmid DNA was obtained by streaking bacterial glycerol stocks on LB agar plates containing either ampicillin or kanamycin, growing mini-cultures then extracting DNA using the QIAprep Spin Miniprep kit. Single and combination digests were performed using *Apa*I*, SphI*, *Eco*NI, *Eco*RI, *Sac*II, *Xba*I and *Nco*I in appropriate buffers and temperatures. pRY_587 digests showed all expected bands when imaged (Figure 4.9D shows a representative gel) corresponding to the presence of all desired elements within the DNA. Therefore, this proves that the lack of SMN over-expression after transduction with these vectors was not due to missing expression cassette elements.

As the pRY_587 plasmid contained all the desired elements, it was decided to confirm SMN over-expression following transfection of this plasmid into CHO cells. This would allow confirmation that the expression cassette is viable and the lack of SMN protein level increase was due to an issue with the vector configuration. In order to obtain sterile plasmid DNA at sufficient concentrations for transfection, two maxi-cultures were set up from the same pRY_587 mini-cultures used for restriction digests then DNA was extracted. These were digested again to confirm retention of the expected pattern, then used for transfection experiments.

Concurrently with preparing DNA, other elements of the transfection protocol were optimised. The density at which to seed CHO cells was determined so that at the time of transfection they were 70-90% confluent. This density was found to be $0.5x10^5$ cells in 24 well plates and $2.5x10^5$ cells in 6 well plates which both are equivalent to $0.26x10^5$ cells/$cm^2$. Next, the ratio of DNA to Lipofectamine 2000 transfection reagent was investigated; as the concentration of Lipofectamine 2000 increased the percentage of GFP-positive cells, but at the expense of cell viability. It was decided that a ratio of 2:1 DNA:Lipofectamine 2000 would be used as this gave 80% live cells and approximately 20% GFP-positive cells. Increasing the Lipofectamine 2000 concentration further did not significantly increase transfection efficiency, but did lead to a 20% drop in cell viability.

With these optimal transfection conditions, a control lentiviral *eGFP* plasmid (pRY_396), a lentiviral *Co-hSMN1* plasmid (pRY_543) and the AAV9_CAG_*Co-hSMN1* (pRY_587) plasmid were transfected into CHO cells. *eGFP*-transfected cells

were analysed by flow cytometry (Figure 4.9E) and it was seen that only those cells in the presence of DNA-lipid complexes produced any GFP-positive cells ($P<0.0001$), however, despite original estimates of 20% transduction efficacy only 3% of GFP-positive cells were seen here. A potential explanation for this would be that cells were over-confluent when harvested, even though seeded at the optimal density, so the plasmid could have been diluted out during cell divisions.

Regardless of low transfection efficacy, the cells transfected with either *Co-hSMN1* plasmid showed evidence of significantly increased SMN protein levels by western blot (Figure 4.9F). It is visible that the AAV9 plasmid (pRY_587 $P=0.0022$) produced lower over-expression than the lentiviral plasmid (pRY_543 $P=0.0002$). From these data, we can see that the expression cassette contained with the AAV_CAG_*Co-hSMN1* is functional and the lack of over-expression originally seen is likely due to the vector itself.

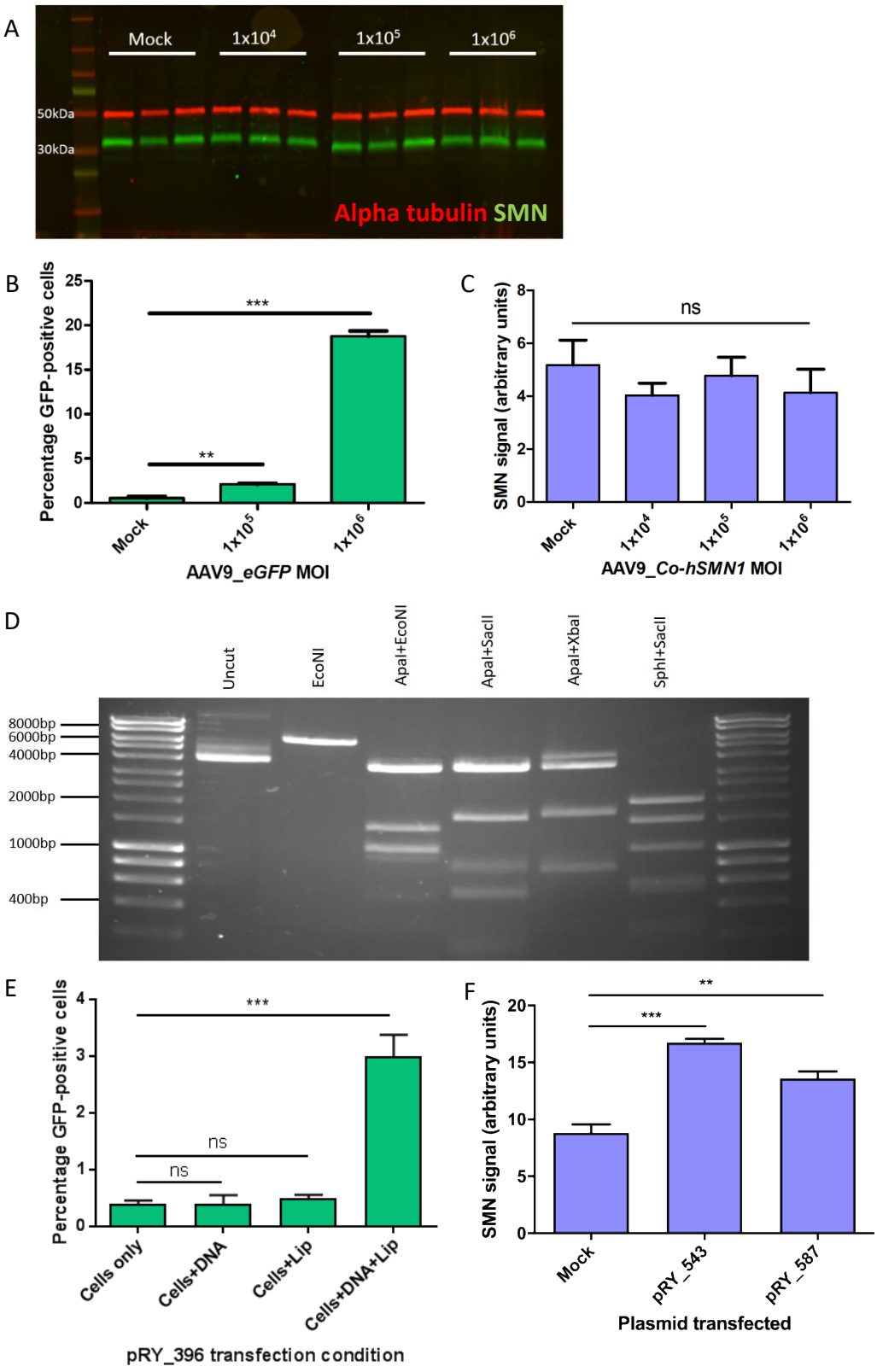


***Figure 4.9 Transduction and transfection of AAV9 vectors encoding* eGFP *or* Co-hSMN1 *in CHO cells.***

*(A) Western blot image showing samples transduced with AAV9_CAG_*Co-hSMN1 *at three MOIs, red = alpha tubulin (~50kDa), green = SMN (~38kDa). (B) Transduction efficacy of AAV9_CAG_*eGFP *in CHO cells (Mock vs MOI 1x10$^4$ P=0.2328, vs 1x10$^5$ P=0.8544, vs 1x10$^6$ P=0.2889). The same data were presented in Figure 4.4E. (C) Quantification of western blot image shown in (A) showing no significant increases in*

*SMN protein. (D) Representative restriction digest of AAV9_CAG_*Co-hSMN1 *plasmid DNA that confirmed the presence of* Co-hSMN1 *transgene, CAG promoter and mWPRE. (E) Transfection efficacy 48 hours after incubation with a control lentiviral* eGFP *plasmid (pRY_396) with 2:1 DNA:Lipofectamine 2000 ratio, (Cells only vs Cells+DNA P>0.9999, vs Cells+Lipofectamine P=0.9727, Cells+DNA+Lipofectamine P<0.0001. (F) Quantification of a western blot using samples from CHO cells transfected with AAV9_CAG_*Co-hSMN1 *(pRY_587; P=0.0022) and IDLV_CMV_*Co-hSMN1 *(pRY_543; P=0.0002) plasmid DNA in parallel with cell transfected in (E). SMN signal was normalised to alpha tubulin. One-way ANOVAs with Dunnett's post-hoc test were used to analyse all statistical significances. mWPRE = mutated woodchuck hepatitis virus RNA element.*

### 4.10.2 Transduction of SMA type I patient fibroblasts with AAV9_CAG_*Co-hSMN1*

To provide data showing the use of AAV9_CAG_*Co-hSMN1* in a relevant cell population, primary type I SMA patient fibroblasts were transduced with these vectors, again in the presence of 4µg/ml polybrene, for 5 hours before serum-free vector-containing media was replaced with full serum media. 4µg/ml polybrene concentration was chosen here to maximise potential for SMN expression increase as a result of transduction.

Firstly, transduction of these cells with AAV9_CAG_*eGFP* provided a maximum of 7% eGFP-positive cells at MOI $1x10^6$ in the presence of 4µg/ml polybrene (Figure 4.10A). Those samples transduced without polybrene had significantly lower numbers of eGFP-positive cells than in the presence of polybrene, assessed by flow cytometry at the two MOIs tested ($1x10^5$ 0.47% vs 0.9% P>0.05, $1x10^6$ 2.3% vs 6.7% P>0.0001). These values are far below even the lowest IDLV MOI used to transduce SMA type I fibroblasts (MOI 10 35.3% eGFP-positive cells; Figure 4.8A).

AAV9_CAG_*Co-hSMN1* transduction, using the same experimental procedures, showed no significant increase in SMN protein expression by western blot (Figure 4.10B,C). A small trend might be inferred from these data, but this was not significantly different from mock transduced cells (P=0.2627).

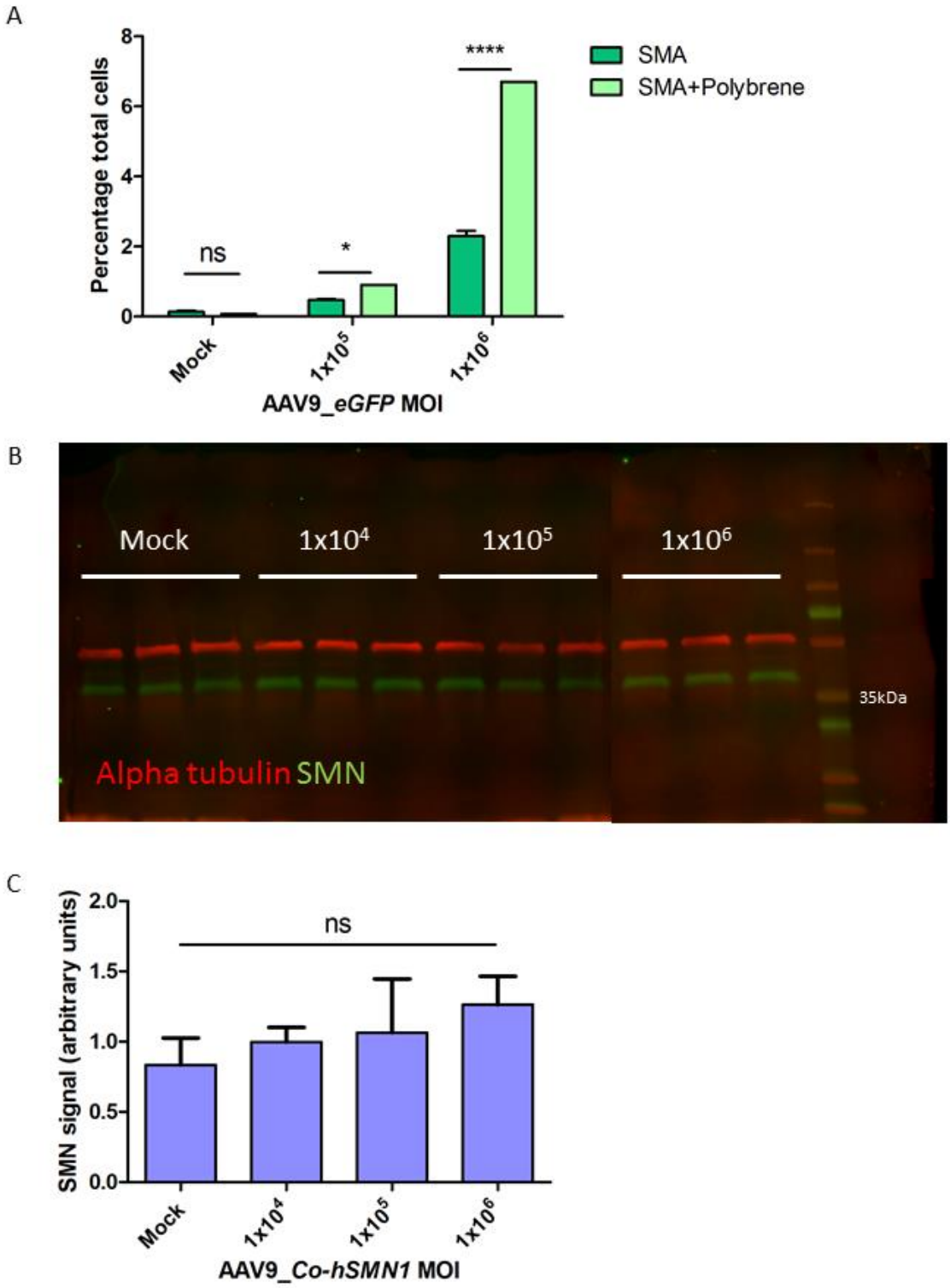


***Figure 4.10 SMA type I patient fibroblasts transduced using AAV9 vectors expressing* eGFP *or* Co-hSMN1.**

*(A) SMA fibroblasts were transduced with AAV9_*eGFP *at two MOIs with or without 4µg/ml polybrene. 72 hours later cells were harvested and subjected to FACS. Significance compared to mock using two-way ANOVA and Bonferroni multiple comparisons test. (B) Western blot scan and (C) quantification of SMA fibroblasts transduced with AAV9_*Co-hSMN1 *in the presence of 4µg/ml polybrene at three MOIs. Two-way ANOVA with Bonferroni multiple comparison, significance compared to mock, P=0.2627.*

### 4.10.3 Transduction following cell cycle arrest in CHO cells

Proliferating cells gradually lose vector load (if the vector is in a non-integrative configuration), causing dilution of the transgene following division. To limit this, transduction of growth arrested cells is advantageous and can reveal increases in transgene protein expression that may have been missed in a proliferating population.

To this end, CHO cells were growth arrested by replacing normal proliferation medium (DMEM+Glutamax, 10% FBS, 1% Penicillin/Streptomycin, 0.02g/l L-proline) with medium containing no methionine and with reduced serum content (Methionine-free DMEM+Glutamax, 2% FBS, 1% Penicillin/Streptomycin, 0.02g/l L-proline). Growth arrest medium was changed every other day for 5 days before analysis of DNA content was performed using DAPI staining (1µg/ml) and flow cytometry. Figure 4.11A shows representative plots from both proliferating and growth arrested populations of cells. There is a shift towards G0/G1 phase with a smaller shoulder in S phase and peak in G2/M. From these histograms we can see some cells still within the S and G2/M phases of the cell cycle, representing incomplete cell cycle arrest. DAPI fluorescence was measured here by flow cytometry, however, due to data being acquired on the log scale instead of linear, accurate DNA content measurements within each cell cycle stage could not be obtained using software such as FloJo. Nevertheless, as the main goal of this experiment was to minimise vector dilution, the shift between populations was deemed sufficient to proceed with transductions.

Both proliferating and growth arrested cells were seeded in triplicate with equal numbers of cells on day 0. The following day, each population of cells were transduced with AAV9 vectors expressing either *eGFP* or *Co-hSMN1* at MOIs $1x10^4$-$1x10^6$. When eGFP-positive cells were analysed by flow cytometry, growth arrested populations appeared to have approximately double the number of fluorescent cells than proliferating populations (Figure 4.11B; $1x10^5$ 2.3% vs 0.7% $P<0.05$, $1x10^6$ 9.27% vs 3.8% $P<0.0001$). It is worth noting the difference in eGFP-positive cells in proliferating populations between the values shown here and those presented earlier in the chapter in section 4.10.1 and Figure 4.4B. Here, a maximum of 3.8% fluorescent cells were seen at $1x10^6$, but previously this value was higher at 19.4%. Both values show low transduction efficacy but are quite different from one another. Despite the same number of cells seeded, the same volume of vector added and the same time courses, the differences in efficacy could have arisen due to different length of culture before experiments were ran. Cells in the later experiments would have been cultured for approximately 1 week longer due to the need for growth arresting a second population

for use in the same experiment. Therefore, comparisons should only be drawn between cells in the same section and figure.

Despite the low transduction efficacy in both growth arrested and proliferating populations of CHO cells, transduction with AAV9_CAG_*Co-hSMN1* was continued. Upon protein extraction, it was found that the concentration of proteins within the lysates from growth arrested samples was very low (0.07-0.21µg/µl) compared to that from proliferating samples (0.7-1.69µg/µl). Due to this issue, only 2µg of protein was loaded onto western blots instead of the usual 8µg, but still one mock replicate and two $1x10^4$ replicates from growth arrested populations could not reach the required 2µg so were not loaded at all. Despite the same 2µg protein being loaded for proliferating and arrest samples, the western blot scan (Figure 4.11C) shows far brighter bands in proliferating samples.

Nevertheless, quantification was attempted and results are shown in Figure 4.11D-F (the same data are used in D and E-F but are compared in two separate manners). Relative to alpha tubulin signal, the SMN signal in growth arrested samples was significantly higher than in proliferating samples (Figure 4.11D; Mock $P<0.01$, $1x10^4$ $P<0.05$, $1x10^5$ $P<0.0001$, $1x10^6$ $P<0.0001$). This suggests that in cells exited from the cell cycle, either entry to the cell was facilitated, transgene expression was more efficient or more vector was retained within the cell following transduction. When comparing the growth arrested or proliferating cell populations separately from one another, we see a significant ($P<0.01$) increase in SMN signal at $1x10^5$ and $1x10^6$ MOI AAV9_CAG_*Co-hSMN1* in arrested cells only (Figure 4.11E). Proliferating cells show a non-significant ($P>0.05$) difference across all tested MOIs (Figure 4.11F).

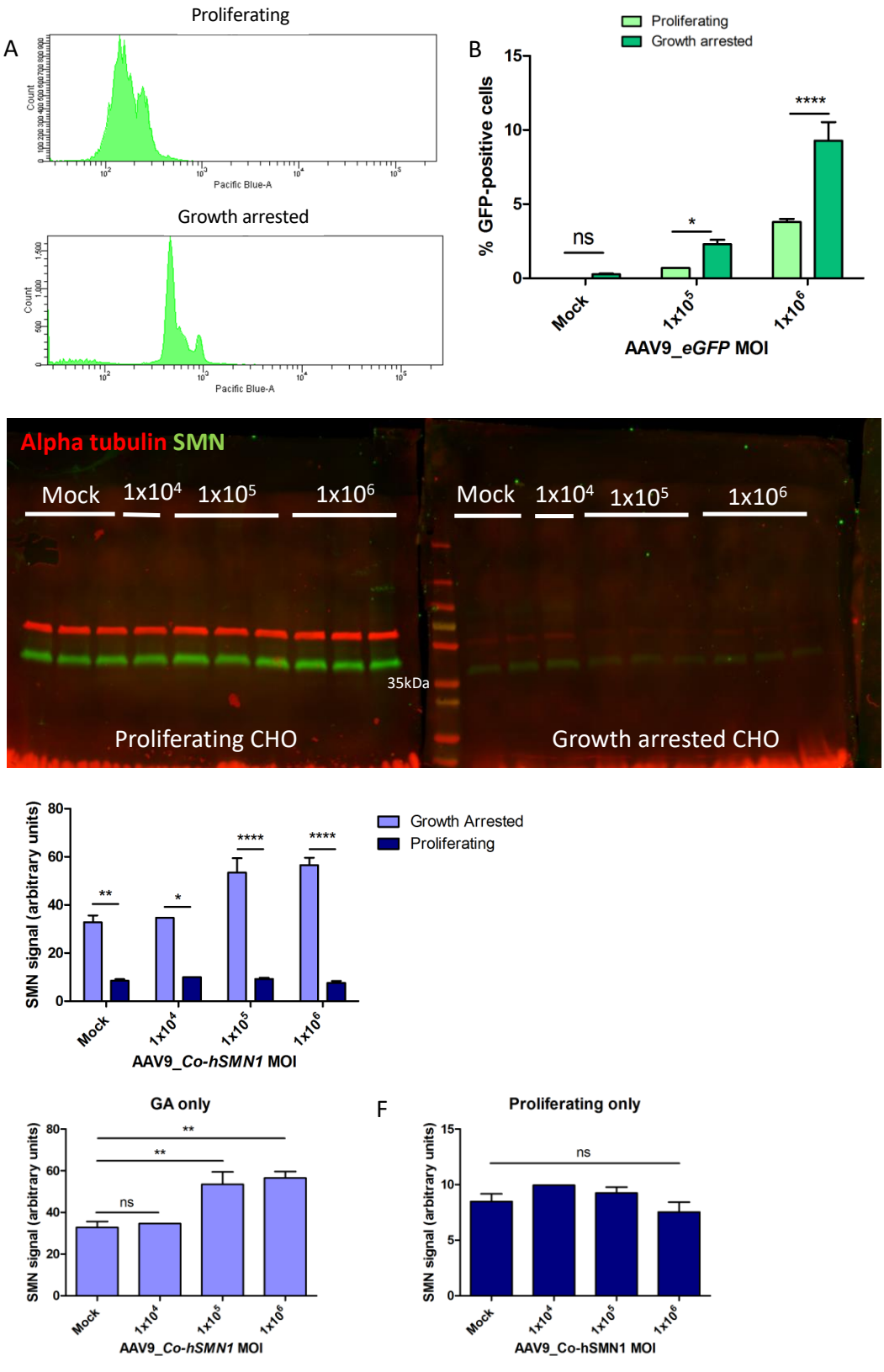
A
Proliferating
Count
Pacific Blue-A
Growth arrested
Count
Pacific Blue-A
B
Proliferating
Growth arrested
% GFP-positive cells
ns
*
****
Mock
1x10^5
1x10^6
AAV9_eGFP MOI
C
Alpha tubulin SMN
Mock
1x10^4
1x10^5
1x10^6
Mock
1x10^4
1x10^5
1x10^6
35kDa
Proliferating CHO
Growth arrested CHO
D
Growth Arrested
Proliferating
SMN signal (arbitrary units)
**
*
****
****
Mock
1x10^4
1x10^5
1x10^6
AAV9_Co-hSMN1 MOI
E
GA only
SMN signal (arbitrary units)
**
**
ns
Mock
1x10^4
1x10^5
1x10^6
AAV9_Co-hSMN1 MOI
F
Proliferating only
SMN signal (arbitrary units)
ns
Mock
1x10^4
1x10^5
1x10^6
AAV9_Co-hSMN1 MOI

***Figure 4.11 AAV9 transduction efficacy and SMN protein expression in both growth arrested and proliferating CHO cells.***

*(A) Cell cycle analysis of PFA fixed cells from both proliferating and growth arrested population to confirm arrested DNA content. (B) Following confirmed arrest, both cell populations were transduced with AAV9_*eGFP *at two MOIs then subjected to FACS. Significance compared to mock using two-way ANOVA and Bonferroni multiple comparisons test. Mock P>0.05, 1x10$^5$ P<0.05, 1x10$^6$ P<0.0001. (C) Western blot with 2µg protein loaded (instead of usually 8µg due to low protein concentrations) and (D-F) quantification of SMN expression following transduction with AAV9_*Co-hSMN1*. Note bands are much weaker from growth arrested protein lysates due to very low protein concentration, but quantification was still possible. Also note, only one sample for 1x10$^4$ MOI was loaded as the other two replicate samples had too low protein concentration to even load 2µg. (D) A two-way ANOVA and Bonferroni multiple comparisons test were used to compare significance of SMN signal between growth arrested and proliferating populations under each treatment condition. Mock P<0.01, 1x10$^4$ P<0.05, 1x10$^5$ P<0.0001, 1x10$^6$ P<0.0001. (E,F) Using the same data as that presented in (D), a comparison of SMN signal between treatment conditions was performed using a one-way ANOVA. (E) Growth arrested (GA) samples, mock compared to: 1x10$^4$ P>0.05, 1x10$^5$ P<0.01, 1x10$^6$ P<0.01. (F) Proliferating samples, mock compared to: 1x10$^4$ P>0.05, 1x10$^5$ P>0.05, 1x10$^6$ P>0.05.*

### 4.10.4 Detection of *Co-hSMN1* in HeLa cells by RT-PCR

In an alternate attempt to compare expression from IDLVs and AAV9 vectors, HeLa cells were transduced with either IDLV_CMV_*Co-hSMN1* (MOI 75) or AAV9_CAG_*Co-hSMN1* (MOI 1x10$^6$) and RNA was harvested at 72 hours post-transduction. From this, cDNA was synthesised and an RT-PCR differentiating between endogenous *SMN* and transgene *Co-hSMN1* transcripts was ran. Full primer details can be found in Table 2.10. *Co-hSMN1* transcript (856bp) was detected in both IDLV and AAV9 vector transduced cells, but not in untransduced samples (Figure 4.12A). Endogenous SMN transcript (552bp) was detected in all samples. When quantified and normalised to endogenous SMN, more *Co-hSMN1* transcript was present in IDLV- than AAV9-transduced samples (p=0.0127; Figure 4.12B), consistent with increased SMN protein in pRY_543 (IDLV_CMV_*Co-hSMN1* transfer plasmid) compared to pRY_587 (AAV9_CAG_*Co-hSMN1* transfer plasmid) transfections (section 4.10.1).

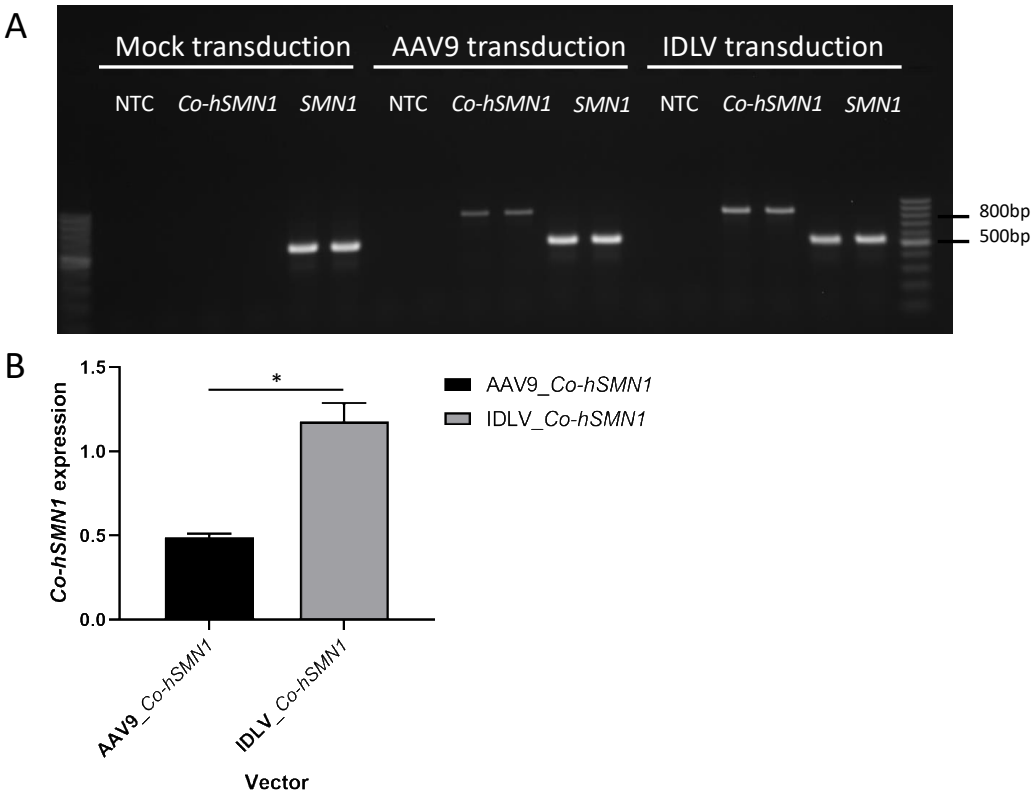


***Figure 4.12 Transgene-specific RT-PCR.***

*HeLa cells were transduced with either IDLV_CMV_*Co-hSMN1 *(MOI 75) or AAV9_CAG_*Co-hSMN1 *(MOI 1x10$^6$) and processed downstream to reveal presence of the* Co-hSMN1 *transcript in both IDLV- and AAV9-transduced cells (A), with IDLV-transduced cells exhibiting higher levels of expression following agarose gel quantification with ImageJ (B; P=0.0127 unpaired t-test).*

## 4.11 Discussion

Within this chapter, I have provided evidence of high transduction efficacy from IDLVs, resulting in increases in SMN protein in a variety of cell types and evaluated by different assays. Comparisons have also been drawn between the efficacy of IDLVs and AAV9 vectors, with IDLVs generally proving more promising.

SMN-gemin complexes provide essential functions during the biogenesis of snRNPs for RNA metabolism and splicing. Hence, assessing the ability of transduced cells to form gems provides an endpoint to showing that the SMN expressed by the IDLVs is functional, can bind to its partners and could complete its necessary housekeeping roles. In both neuroblastoma cell lines tested for gem increase post-transduction, only one of the three vectors tested provided a significant increase in gem number. This was controlled with the CMV promoter, the strongest of the three promoters tested. Theoretically, each of the three promoters should be active within the two neuroblastoma cell lines tested as CMV and hPGK are constitutive and hSYN is

neuronal specific. It has been reported that CMV is often able to induce strongest transgene expression within comparisons of multiple mammalian promoters. Systematic, comparative analyses of mammalian promoters has revealed that CMV leads to high levels of GFP expression (both GFP intensity and percentage GFP-positive cells) but variability between cell lines is also present. Within two such analyses, CMV was found to induce the highest GFP expression out of six promoters (Damdindorj et al., 2014), but this can also be highly variable (low GFP fluorescence in MRC5 and MSC cells, but very high in HT1080 and HEK293T cell lines (Qin et al., 2010)). This reflects the pattern observed here with CMV inducing strongest SMN expression, detected by a significant increase in gem number in these samples only.

Moreover, an increased number of gems could only be detected when samples were immunostained against SMN rather than Gemin2, reflecting the same findings of the optimisation period. Several cells within each sample showed no gems and occasionally these cells appeared to be actively undergoing mitosis at the time of fixation. Both of these features have been reported before (Liu and Dreyfuss, 1996). Approximately 10% of cells will show no gems, whilst those undergoing mitosis, or have recently divided, only show diffuse cytosolic staining of SMN. Following addition of a viral vector to culture medium, there is a period of time encompassing viral entry of cells, transgene transcription and translation of the fully formed protein. Hence, the 72 hour period before any analyses are conducted may be sufficient time for SMN protein to increase, however, there may be further period of time before complete formation of SMN-gemin complexes. This may explain why gems can be detected more readily with SMN antibody than Gemin2. It is possible, given a longer incubation time, the increased SMN protein could increase Gemin2 protein through transcriptional regulation, given that SMN itself (Lorson and Androphy, 1998) and Gemin5 (another gemin protein within the macromolecule complex) (Workman et al., 2015) are both capable of directly binding mRNA. Transcriptional and translational control of Gemin2 has been proposed before (Wang and Dreyfuss, 2001), as well as the notion of SMN and Gemin2 associations stabilising the SMN-gemin complexes (Ogawa et al., 2007).

It has been shown that the IDLVs tested in this chapter can successfully rescue SMN protein levels in SMA type I patient fibroblasts. This was shown visibly with immunofluorescence against protein with clear increases in cytoplasmic signal similar to that published (Valori et al., 2010) and also with direct quantification of protein levels by western blot. IDLVs expressing *Co-hSMN1* under all three transcriptional controls (CMV, hSYN, hPGK) were able to significantly increase SMN compared to mock-treated cells, whilst CMV and hPGK vector transduction also led to full SMN rescue

above wild type SMN levels. It is interesting to note that increases in SMN protein were induced by all three transcriptionally controlled vectors, but increases in gem number were only seen in IDLV_CMV_*Co-hSMN1* transduced neuroblastoma cell lines. Nevertheless, this rescue in patient cells represents an important translational step in pre-clinical development of any therapy and directly leads on to the use of iPSCs derived from SMA type I patient fibroblasts, as well as the differentiation of these into iPSC MNs, the primarily affected cell type in SMA.

As stated previously, the use of differentiated, neuronal-like Neuro2a and SH-SY5Y cells was a proof of concept experiment to determine if transduction efficacy differed between undifferentiated and differentiated cells. This information could then be used to inform decisions (such as necessary MOI or length of transduction) made later when an iPSC MN model was established. It is unclear at this time why IDLVs expressing *eGFP* were unable to transduce Neuro2a cells post-differentiation. There is evidence in the literature that lentiviral transduction of Neuro2a cells is difficult (Holehonnur et al., 2015) and is not commonly tested, perhaps due to the problems encountered in this study. A possible cause may be that the VSV-G protein receptors may be down-regulated in murine neuronal-like cells, causing viral entry into the differentiated Neuro2a cell to be blocked. It is now known that VSV-G binds to the low density lipoprotein (LDL) receptor (LDLR) (Finkelshtein et al., 2013) (see (Nikolic et al., 2018) for crystal structures of VSV-G bound to LDLR). Binding of VSV-G to LDLR (and other secondary proteins such as phosphatidylserine and Gp96) permits viral entry to cells via clathrin-mediated endocytosis. Evidence suggests that LDLR is expressed in Neuro2a cells while cultured in proliferation media (Fan et al., 2001), but there is no literature suggesting if it is still expressed following differentiation. Certain cells such as T, B and haematopoietic stem cells are unamenable to efficient gene transfer with VSV-G pseudotyped vectors due to low LDLR expression (Amirache et al., 2014). The transduction efficacy of natural killer cells has been shown to increase following rosuvastatin treatment by increasing LDLR expression on these cells (Gong et al., 2020). Thus, it is possible that differentiated Neuro2a cells pose similar barriers to efficient lentiviral transduction.

It may be possible to transduce Neuro2a cells in their undifferentiated state and subsequently differentiate these transduced cells into neurons to see if transgene expression is still detectable. As the vectors used are IDLVs where the viral genome is retained in episomal circles not inserted into the host genetic sequence, viral DNA will be diluted during cell divisions, however as differentiation proceeds cell division should slow, perhaps allowing sufficient viral DNA to be present post-differentiation.

When comparing the vectors tested in this study, it is clear to see that IDLVs are more efficient than AAVs *in vitro*. Initial transduction efficacies show maximal transduction efficacy of 18.8% at MOI $1x10^6$ for AAV9 vectors, whereas IDLVs can achieve 4.7-fold higher transduction with an MOI 6000-fold lower. The results here present different findings for AAV9 vectors and IDLVs regarding the optimal expression cassette configuration for over-expression. SMN over-expression was seen from the AAV9_CAG_*Co-hSMN1* vector only in CHO cells that had exited from the cell cycle, not proliferating CHO cells or primary SMA type I fibroblasts. However, the transfer plasmid used to make this vector is capable of significantly increasing SMN protein levels upon transfection. This contrasts to lentiviral results showing significant SMN over-expression upon transfection of plasmid DNA, but this is enhanced greatly when in its vector configuration.

One potential explanation for this may rely on the serotype of AAV used. Differential increases in SMN protein resulting from lipofectamine transfection of plasmid DNA should only be caused by those elements contained within the transfer plasmid, such as the CMV vs CAG promoters. In contrast, viral vector transduction relies on entry to cells of interest mediated by receptor interactions. The IDLVs in this project were all pseudotyped with VSV-G meaning that entry to most, if not all, cell types was possible. The AAV used here had the serotype 9 with specific tropisms such as skeletal (Tarantal et al., 2017) and cardiac muscle (Pacak et al., 2006), as well as the CNS (Foust et al., 2009). The cell types transduced here, ovarian and skin, do not fall within these favoured tropisms. Extensive effort was put into cloning the CAG promoter from the AAV9 vector transfer plasmid, into a lentiviral vector backbone to obtain IDLV_CAG_*Co-hSMN1* as a means to investigate the above issues, however, this was not possible and thus data were not presented in this thesis.

It is also necessary though to reflect on the sensitivity of the western blots used to detect any increase in SMN protein expression. Western blots were run with total protein lysates from a large population of cells. Therefore, if a low proportion of these cells were actually transduced, any increases in SMN protein expression may not be detected if the vast majority express normal levels. This is supported by the appearance of a significant number of eGFP-positive cells after AAV9_CAG_*eGFP* transduction and analysis by flow cytometry (a method of detection at the single-cell level), but this significance not carrying over to significant SMN increases. Inefficient entry of AAV9 vectors, but not lipofected plasmid DNA, into cells, combined with proliferating cells' continually decreasing vector load may explain why using an assay

such as western blot to detect protein expression increasing by a minimal amount may not be entirely suitable here. Therefore, a transgene specific RT-PCR was tested here and this was able to detect more subtle changes. This assay was indeed able to detect increased *Co-hSMN1* transgene transcripts in IDLV-transduced samples compared to AAV9-transduced samples, consistent with increased SMN protein following IDLV, but not AAV9, plasmid lipofection. Together, these results demonstrate that a variety of assays should be used to detect true changes in transgene expression, assessing if consistent outcomes are seen in all assays attempted.

## 4.12 Conclusions

In summary, within this chapter I have shown that IDLVs are able to transduce cell lines with high efficiency, leading to significant increases in SMN protein in three cell lines and primary SMA type I fibroblasts. In contrast, AAV9 vectors expressing the same cassette cannot increase SMN protein unless cells have exited the cell cycle. These results are important because they highlight the promise of IDLV-based therapeutics for SMA, increasing the number of viral vectors that may be able to treat this disease. IDLVs have not been studied outside of this laboratory for SMA and thus the results shown in this chapter are novel. The promising results found in this chapter could then be translated to a more clinically relevant iPSC-derived MN model of SMA type I.

# 5 Establishment of an iPSC-derived motor neuron model of SMA

## 5.1 Introduction

### 5.1.1 Embryogenesis of MNs

When developing a differentiation protocol from pluripotent cells, it is important to understand how the target cell is naturally derived *in vivo*; thus understanding the embryogenesis of the central nervous system is important before modelling MN differentiation from iPSCs. Three important physiological stages of MN genesis (neuralisation, caudalisation and ventralisation) are tightly regulated *in vivo* and are key to translation into an *in vitro* differentiation protocol.

The embryogenesis of the central nervous system begins with the specification of neuroectoderm and its folding to form the neural tube. This process is known as neuralisation and is chiefly regulated by bone morphogenetic protein (BMP). The neural tube is subjected to patterning via the actions of different signaling molecules and morphogens present along its rostrocaudal and dorsovental axes. Morphogens induce the activation of intracellular pathways leading to transcriptional activation of cell type specific genes and resulting cellular differentiation (Faravelli et al., 2014).

Caudalisation, the second physiological stage, defines distinct differences between the anterior (rostral) regions of the neural tube that will later form the brain, and the posterior (caudal) regions that will form the spinal cord. The combinatorial action of Wnt and FGF signaling maintains neural progenitor cells in a proliferative state with a caudal identity. This is maintained until secretion of retinoic acid (RA) from nearby somites reaches these cells, inhibiting FGF and thus releasing cells from their progenitor state. RA acts as a neuralising agent exerting its effects through suppression of Nodal signaling (Engberg et al., 2010) and regulation of pro-neural factors such as Neurogenin2 (Kam et al., 2012).

Caudal cells then become sensitive to dorsoventral cues such as sonic hedgehog (SHH) signaling (Ulloa and Briscoe, 2007) in the final specification stage known as ventralisation. SHH signaling is extremely important when patterning early neural tissue and specifying neuronal identity (Jacob and Briscoe, 2003). An antagonistic

relationship exists between BMP secreted dorsally and SHH secreted from the ventral most point, the floorplate, close to the region of MN birth. This antagonistic signaling specifies distinct regions along the dorsoventral axis of the neural tube. Expression of specific transcription factors delineates boundaries between each region (Jacob and Briscoe, 2003), such as the SHH-induced expression of OLIG2 and Nkx2.2 in ventral cells destined to become MNs.

### 5.1.2 iPSCs as model systems

As stated previously (section 1.3.1.2), iPSCs are somatic cell-derived pluripotent cells that have been reprogrammed to indefinitely self-renew, whilst also retaining the ability to differentiate into somatic cell types of the three germ layers. Since their advent in 2006 (Takahashi and Yamanaka, 2006) iPSCs have been extensively used in both their pluripotent and differentiated states. Disease modelling is perhaps the most relevant application of iPSCs in this project, as this can be used to give insight into disease phenotypes in live human cells, a feat that cannot be achieved in animal models and post-mortem analysis (Dolmetsch and Geschwind, 2011). iPSCs derived from an individual patient with a genetic disease will capture the disease genome, meaning these cells can be used to model cellular and molecular pathophysiological features, specifically affected in that patient.

Human neurons are a cell type with innate inaccessibility, precluding their isolation for *in vitro* studies of molecular pathogenesis or therapeutic testing (Frattini et al., 2015). This leads to a lack of proper models of neurological diseases, perhaps contributing to the large disparity between the number of effective therapies for neurological diseases, yet their huge impact on public health (Frattini et al., 2015). *In vivo* models, both rodent and large animals, will remain important for disease visualisation and long term progression of macro phenotypes such as survival. However, it has been shown that some therapeutic strategies proving promising in animal models did not translate well in clinical trials (Dragunow, 2008). Pre-clinical models of neurological disease sometimes have gross differences in the genetics of disease in question (for example the lack of the *SMN2* gene in species other than humans, or differences within the development or structure of the CNS compared to humans (Dolmetsch and Geschwind, 2011). Post-mortem analysis of human CNS tissue reveals the terminal phenotype, but does not allow insights into disease manifestations occurring at initial stages of disease onset, a particular problem in early onset neurological disorders (Dolmetsch and Geschwind, 2011). The advent of iPSC disease modelling has potential to resolve these issues.

### 5.1.3 iPSC models of SMA

Ebert and colleagues provided early evidence that the derivation of SMA iPSC MNs was possible (Ebert et al., 2009) using a differentiation protocol including RA, SHH, cAMP, ascorbic acid and glial- and brain-derived neurotrophic factors (GDNF/BDNF). These compounds were chosen specifically to mimic signaling pathways present in early embryogenesis during neural induction and patterning, as described in section 5.1.1. Various differentiation protocols exist in the literature, but most display a common theme using RA and SHH, agonists, or derivatives of these, to neuralise, caudalise and ventralise iPSCs – the three physiological stages of MN embryogenesis stated earlier. This is then supplemented with other compounds such as Chir99021 (Wnt agonist), DMH1/Compound C (BMP inhibitors), DAPT (Notch inhibitors) and many others.

Many groups have now been able to differentiate iPSCs into MNs (Ebert et al., 2009, Chang et al., 2011, Corti et al., 2012, Du et al., 2015, Yoshida et al., 2015, Fuller et al., 2016, Powis et al., 2016, Bhinge et al., 2017, Yi et al., 2018), the cell type primarily affected in SMA. Proof of principle that differentiation of these cells can be achieved at high efficiency, whilst still retaining features such as reduced *SMN* mRNA has been published (Du et al., 2015). Morphologically, SMA iPSC MNs exhibit shorter axons with small growth cones and do not form functional NMJs in co-cultures (Corti et al., 2012); all hallmarks of SMA *in vivo*. Downstream analysis of SMA iPSC MNs show deficits in protein levels other than SMN. Fuller et al. (2016) reported decreased expression of UBA1, UCHL1 (two enzymes involved in ubiquitin homeostasis) and Gemin2.

## 5.2 Aims

In this chapter I aimed to establish and characterise a model of SMA using iPSCs differentiated to MNs. Specifically, my objectives were:

(A) Characterisation of SMA type I iPSC lines.
(B) Optimisation of a published protocol for the differentiation of iPSC derived MNs.
(C) Characterisation of resulting MNs.

Wherever possible within this chapter, experiments were aimed to be performed with three wild type and three SMA iPSC lines, where appropriate, to improve validity of results. However, it was not always possible to differentiate all at the same time with

similar success rates. Therefore, some experiments were performed with less than six lines.

## 5.3 Key characteristics of the wild type and SMA type I iPSC lines

### 5.3.1 Wild type and SMA type I iPSC lines used here

Six iPSC lines were used in this project; three wild type (4603, 19-9-7T, AD3-CL1) and three SMA type I (CS13iSMAI-nxx, SMA-19 and CS32iSMAI-nxx). Here, CS13iSMAI-nxx and CS32iSMAI-nxx are referred to as SMA-13 and SMA-32, respectively, for brevity and consistency. Detailed information regarding parent cell line, genotype, reprogramming methods, where known, can be found in Table 5.1. The three SMA type I iPSC lines used here have been used in studies by other laboratories in published literature (SMA-19: (Chang et al., 2011), SMA-13: (Du et al., 2015, Yoshida et al., 2015, Ebert et al., 2009, Lai et al., 2017), SMA-32: (Du et al., 2015, Yoshida et al., 2015, Fuller et al., 2016)).

The SMA type I iPSC lines used here were derived from three independent infants that had homozygous deletions of exons 7 and 8 within *SMN1*, leading to no SMN protein production from this gene. As *SMN2* copy number is the most important disease modifier in SMA patients, it is important to know how many copies of this gene each infant, and their respective iPSCs, possessed. SMA-13 and SMA-19 both harbor three copies of *SMN2*, whereas SMA-32 contains only two *SMN2* copies. It is important to note that type I SMA patients usually only have two copies of *SMN2*, so SMA-13 and SMA-19 are abnormal in this regard. Recently, due to the discovery of three *SMN2* copies in SMA-13 (Stabley et al., 2015), this iPSC line, and its fibroblast parent cell line GM03813 (Coriell), have been re-classified as SMA type II. Despite this re-classification, several colleagues are continuing to use this iPSC line in their projects. The donor of SMA-13 died at 23 months of age and exhibited several symptoms of SMA type I including hypotonia, abnormal muscle biopsy and absent deep tendon reflexes. A personal communication with Allison Ebert (whose laboratory developed the first SMA iPSCs; (Ebert et al., 2009)) revealed a lack of differences between SMA-13 and other SMA type I iPSC lines she possesses (Patitucci and Ebert, 2016) with the important conclusion that SMA-13 has a particularly severe molecular signature.

| iPSC line | Diagnosis | Donor age/gender | Parent cell line (if known) | *SMN* genes (SMA lines only) | Reprogramming method (if known) | Source |
|---|---|---|---|---|---|---|
| AD3-CL1 | Wild type | M | Unknown | N/A | Donor cells transduced with Sendai virus | Transferred by Majlinda Lako, Newcastle University |
| 19-9-7T | Wild type | M | Unknown | N/A | Foreskin fibroblasts reprogrammed vector free with EBNA-1/oriP episome | WiCell |
| 4603 | Wild type | Adult, M | GM04603 Coriell | N/A | Fibroblasts transduced with recombinant Moloney Murine Leukemia viral vectors (OCT4, SOX2, KFL4 AND c-MYC) | Reprogrammed by Gaby Boza-Moran at iStem |
| SMA-19 | SMA type I | 2 years, M | GM09677 Coriell | *SMN1*: Homozygous deletion exons 7-8 *SMN2*: 3 copies | Eye lens fibroblasts transduced with recombinant Moloney Murine Leukemia viral vectors (OCT4, SOX2, KFL4 AND c-MYC) | Transferred by Majlinda Lako, Newcastle University |
| CS32iSMAI-nxx (referred to here as SMA-32) | SMA type I | 7 months, M | GM00232 Coriell | *SMN1*: Homozygous deletion exons 7-8 *SMN2*: 2 copies | Episomal plasmid | Purchased from Cedars-Sinai |
| CS13iSMAI-nxx (referred to here as SMA-13) | SMA type I | 3 years, M | GM03813 Coriell | *SMN1*: Homozygous deletion exons 7-8 *SMN2*: 3 copies | Episomal plasmid | Purchased from Cedars-Sinai |

***Table 5.1: Detailed information, where known, regarding the six iPSC lines used in this project.***

*Details of the iPSC line, donor cell information including diagnosis, age, gender and genotype, and their reprogramming method are shown here. Some debate regarding the re-classification of GM03813 fibroblasts and their derived SMA-13 iPSCs has arisen due to the three copies of SMN2 present, however symptoms of SMA type I disease and a particularly severe molecular phenotype act as evidence that these cells are still relevant models for this project.*

### 5.3.2 Determining *SMN* gene and protein expression in undifferentiated iPSCs

Firstly, confirmation of SMN transcript and protein down-regulation in SMA type I iPSC lines (SMA-32, SMA-19 and SMA-13) was sought in comparison to wild type iPSC lines (AD3-CL1, 19-9-7T and 4603). To do this, an RT-PCR and western blot were used.

For analysis of *SMN1* and *SMN2* transcripts, RNA was extracted from all lines and cDNA was synthesised from this. An RT-PCR amplifying exons 6-8 of the *SMN* genes was used to produce two products corresponding to *FL-SMN* (504bp) and *SMNΔ7* (450bp). Two control genes (GAPDH; 184bp and β-actin; 295bp) were also amplified. Figure 5.1A displays two bands amplified from each line at expected sizes. Control gene amplification was consistent across all iPSC lines (Figure 5.1B). *SMN* bands were gel extracted together and then subjected to restriction digestion with *Dde*I at 37°C for 2 hours. Digested products were electrophoresed on a second gel to separate *FL-SMN1* (504bp), *FL-SMN2* (382+122bp) and *SMN2Δ7* (328+122bp) transcripts (Figure 5.1C). The transcript pattern was as expected with wild type lines showing four bands whereas SMA lines lacked the 504bp *FL-SMN1* transcript.

A western blot was used to confirm a reduction in SMN protein consistent with the lack of *FL-SMN1* transcript in SMA type I iPSC lines. When using iPSC and MN protein extracts for western blots, it was advised by colleagues in University of Edinburgh to use total protein as a normalisation control, rather than a more commonly used housekeeping protein. This is due to housekeeping proteins often being differentially expressed in models of neurodegeneration. For example, β-actin expression decreases by 19% in spinal cord samples from Taiwanese mice, compared to wild type (Eaton et al., 2013). As expected, wild type lines show more SMN than SMA type I lines (Figure 5.1D,E). No replicates were used here so no statistics could be performed to assess the significance of the SMN difference. Following differentiation of these iPSCs to MNs, confirmation of the same SMN reduction was obtained (see section 5.5.3).

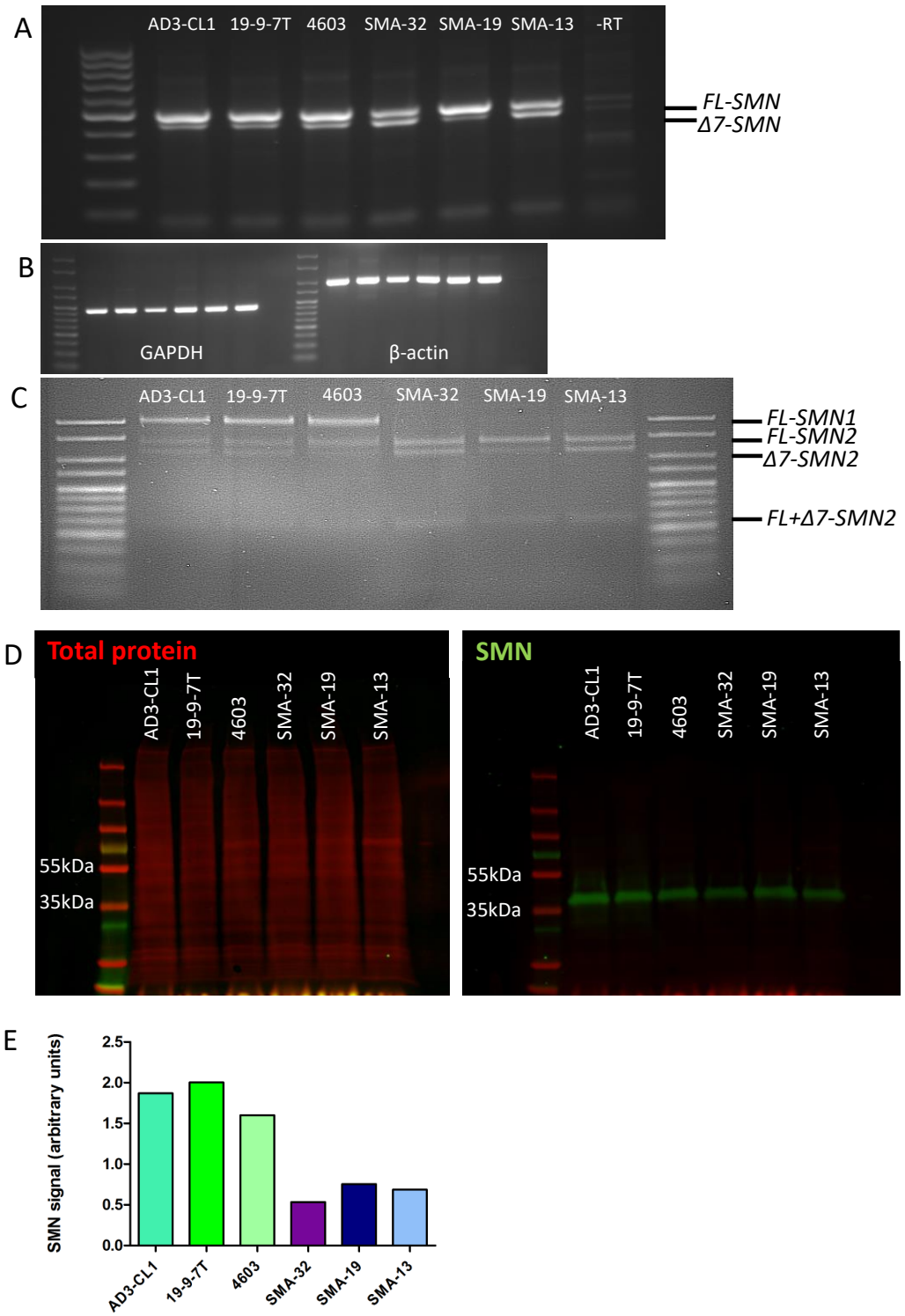


***Figure 5.1 Determining* SMN *transcript origin and protein expression in all six iPSC lines.***

*(A-C) An RT-PCR was performed using primers to amplify a region between exons 6-8 of the* SMN *genes in all iPSC lines. -RT = minus reverse transcriptase control reaction. (A) Full length* SMN *(*FL-SMN*) products were expected to be 504bp, whilst those amplified from* SMNΔ7 *transcripts should be 450bp. (B) Two control genes (*GAPDH*: 184bp and* β-actin*: 295bp) were also amplified and were expected to show consistent bands across all lines. The same lane order is present in all gels.*

*(C) The two bands seen at 504 and 450bp in (A) were excised and amplicons extracted. PCR amplicons were digested with* DdeI *for 2 hours before running digested products on a second gel. Transcripts from the* SMN1 *gene do not possess a* DdeI *restriction site and were expected to give 504bp products. Transcripts from* SMN2 *do contain a diagnostic* DdeI *restriction site, so* FL-SMN2 *504bp amplicon is cleaved to give 382 and 122bp fragments, whilst* SMN2Δ7 *450bp amplicon when cleaved gives 328 and 122bp fragments. (D) Protein lysates from undifferentiated iPSCs were extracted and run on a western blot to determine how SMN protein expression varies between lines. Normalisation of SMN signal to that of total protein reveals lower SMN protein in SMA iPSC lines, as expected. Replicate samples were not used so no statistical significance can be calculated here.*

### 5.3.3 Assessment of pluripotency markers in undifferentiated iPSCs

Before experiments differentiating iPSCs could take place, it was important to determine if the iPSCs were in fact pluripotent. To do this, flow cytometric assessment of the expression of markers of pluripotency was used. Three markers were tested here; TRA-181, SSEA1 and SSEA3. These are cell surface antigens that are commonly used to characterise the pluripotency of embryonic stem cells and iPSCs (Brimble et al., 2007).

Initially, a pilot experiment was completed to determine optimal antibody concentration for each marker using $5x10^5$ undifferentiated AD3-CL1 iPSCs per sample. Starting antibody dilutions were obtained from a previous PhD thesis in this laboratory (Boza-Moran, 2012). This dilution, along with 0.5- and 1.5-fold this amount, was used to identify the optimal dilution. Table 5.2 contains details from this experiment.

| **Antibody** | **Fluorophore** | **Volume of antibody per $5x10^5$ cells (µl)** |
|---|---|---|
| Mouse/human anti-SSEA1 | PE-Cy7 | 0.315<br>0.63<br>0.945 |
| Human anti-SSEA3 | Alexa Fluor 647 | 2.5<br>5<br>7.5 |
| Human anti-TRA-181 | PE | 5<br>10<br>15 |

***Table 5.2 Optimisation of antibody staining for flow cytometric analysis of pluripotency markers in AD3-CL1 iPSCs.***

*Initial dilutions of antibodies were those used by Boza-Moran (2012) in a previous PhD project, shown as the middle figure for each antibody. 0.5- and 1.5-fold these volumes were used for optimisation purposes.*

No signal was obtained from SSEA1-stained iPSCs at all antibody concentrations tested in Table 5.2. A further test using 10x higher concentration also revealed 0% SSEA1-positive cells, therefore this antibody was not used in the remainder of experiments. Examination of literature suggested that although the SSEA1 epitope is expressed in early mouse embryos and highly undifferentiated murine ESCs and iPSCs, it may not in fact be expressed in human equivalents (Draper et al., 2002, Inada et al., 2019), instead only being expressed in subsets of adult stem cells such as neuronal stem cells (Pruszak et al., 2009).

The highest concentrations of SSEA3 and TRA-181 antibodies were identified as optimal concentrations for further analysis. Following this, all six iPSC lines were subjected to both single and dual staining for SSEA3 and TRA-181 using optimised protocols. Populations of cells in lower, left quadrants of dot plots represent autofluorescent cells (Figure 5.2 and Figure 5.3). Variability in the number of SSEA3 and TRA-181 positive cells was observed between all lines (Figure 5.2 and Figure 5.3). Generally, a lower percentage of single-stained cells expressed TRA-181 than SSEA3, despite TRA-181 antibody being used at a higher concentration. Dual stained populations revealed some cells co-expressed both SSEA3 and TRA-181, but again variability was present between lines (Figure 5.2 and Figure 5.3). Although expression was non-significantly different between iPSC lines in all cases (TRA-181: P=0.2366, SSEA3: P=0.9705, TRA-181 and SSEA3 P=0.0748; Figure 5.4), it appears that SMA lines exhibited much lower levels of TRA-181 expression, visible in single-stained population as well as a lower percentage of TRA-181 and SSEA3 double-positive cells. Nevertheless, together these results suggest that the iPSCs used in this project expressed markers of pluripotency and therefore were suitable for use in differentiation experiments.

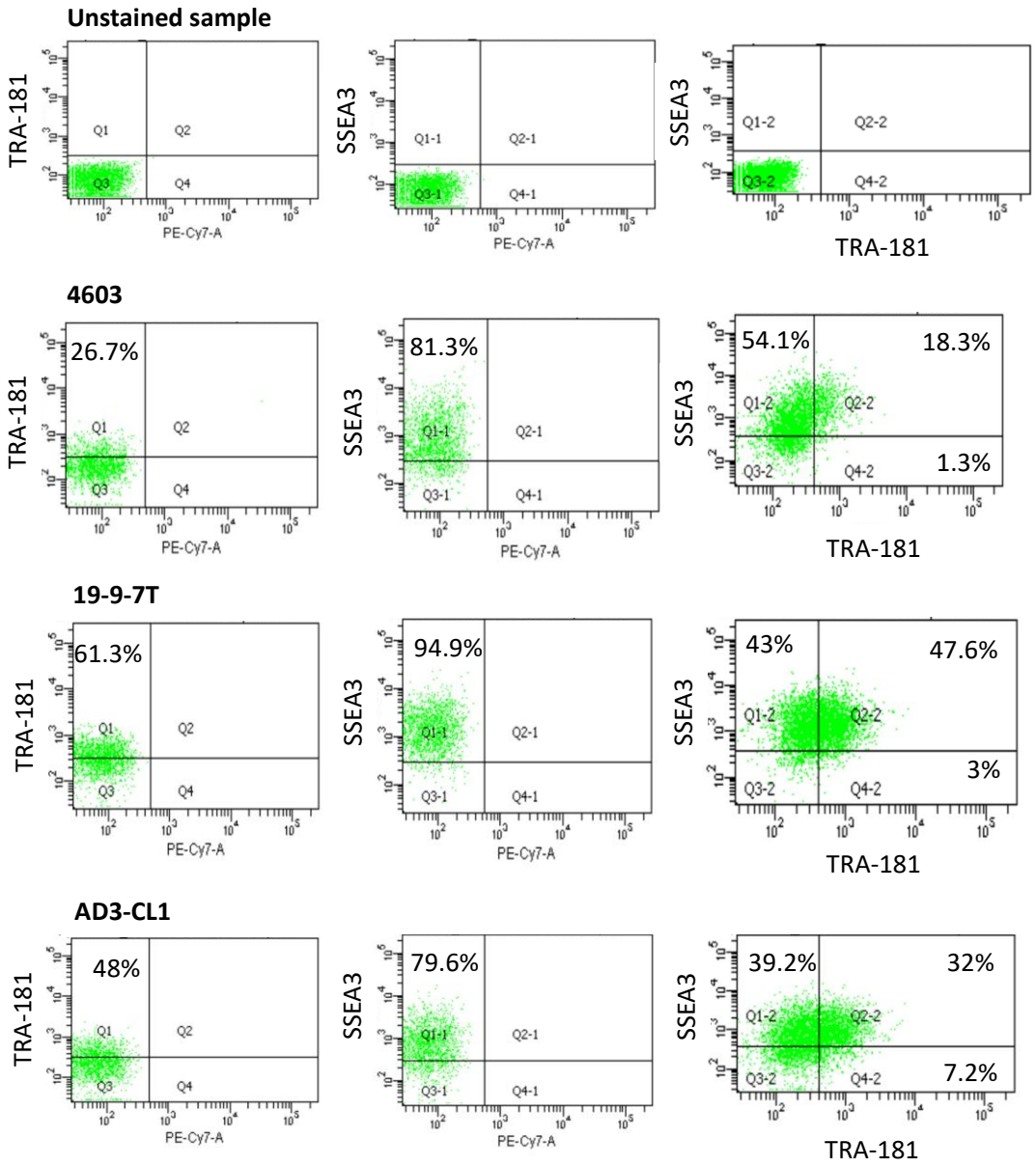


***Figure 5.2 Assessment of pluripotency markers TRA-181 and SSEA3 in wild type iPSC lines.***

*Three wild type iPSC lines (4603, 19-9-7T and AD3-CL1) were immunostained against two markers of pluripotency; TRA-181 and SSEA3 before expression of these cell surface markers was measured by flow cytometry. Percentages are representative values from one technical replicate. The TRA-181 antibody used here was conjugated to the fluorophore PE, so was measured using the PE-A bandpass filter on the blue/green laser. The SSEA3 antibody used here was conjugated to the fluorophore Alexa Fluor 647, so was measured using the APC-A bandpass filter on the red laser. Single stained samples (the first two graphs in each row) were measured against a fluorophore filter that should not produce any signal (i.e. PE-Cy7-A). Quadrant 3, 3-1 and 3-2 represent autofluorescent cells as represented in the unstained control plots.*

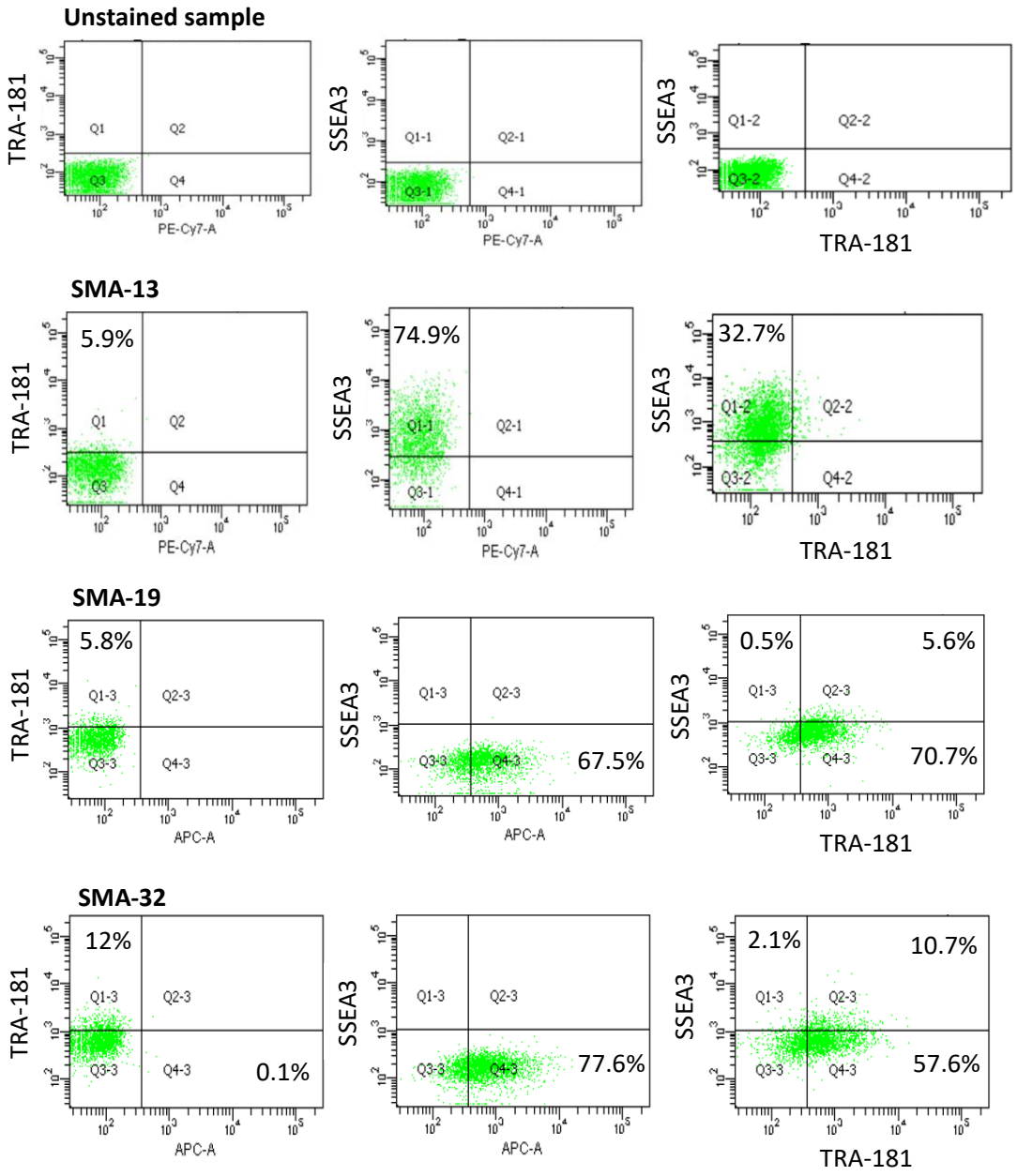


***Figure 5.3 Assessment of pluripotency markers TRA-181 and SSEA3 in SMA type I iPSC lines.***

*Three SMA type I iPSC lines (SMA-13, SMA-19 and SMA-32) were immunostained against two markers of pluripotency; TRA-181 and SSEA3 before expression of these cell surface markers was measured by flow cytometry. Percentages are representative values from one technical replicate. The TRA-181 antibody used here was conjugated to the fluorophore PE, so was measured using the PE-A bandpass filter on the blue/green laser. The SSEA3 antibody used here was conjugated to the fluorophore Alexa Fluor 647, so was measured using the APC-A bandpass filter on the red laser. Single stained samples (the first two graphs in each row) were measured against a fluorophore filter that should not produce any signal (i.e. PE-Cy7-A). Quadrant 3, 3-1 and 3-2 represent autofluorescent cells as represented in the unstained control plots.*

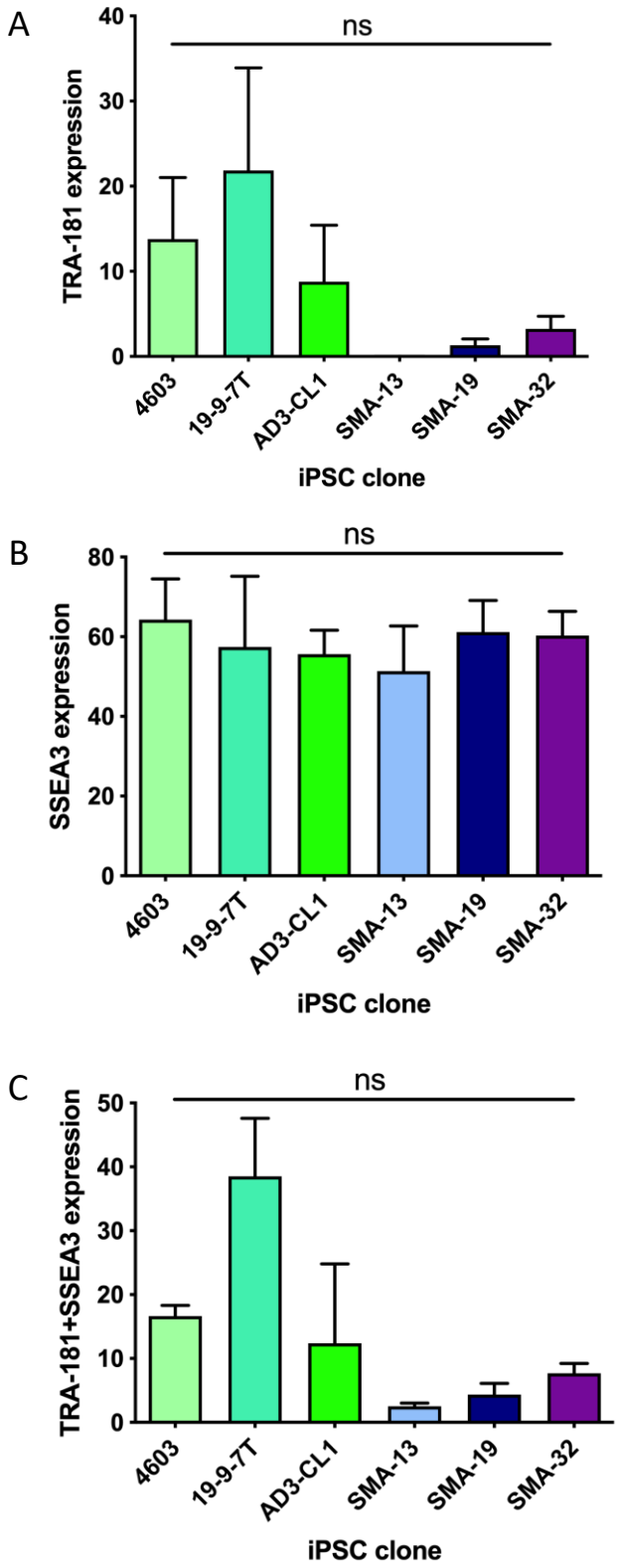


***Figure 5.4 Quantification of pluripotency marker expression in all six iPSC lines.***

*TRA-181, SSEA3 and dual TRA-181 and SSEA3 expression was extracted from flow cytometry data and analysed using One-way ANOVAs. Expression was non-significantly different in all cases. (A) TRA-181: P=0.2366, (B) SSEA3: P=0.9705, (C) TRA-181 and SSEA3 P=0.0748.*

### 5.3.4 Assessment of genomic stability in undifferentiated iPSCs

Traditionally following reprogramming from fibroblasts, or another parent cell line, to iPSCs, these cells are subject to quality checks. These typically involve morphological analysis to ensure a similar morphology to ESCs, as well as the expression of pluripotency markers, testing the ability of iPSCs to differentiate into cells of the three germ layers and the possession of a normal karyotype (Takahashi et al., 2007). Karyotyping following reprogramming is normally performed using G-banding, a complex technique that involves the partial digestion of chromosomes, staining with Giemsa and then identifying any chromosomal abnormalities by assessing the unique banding pattern for each chromosome. However, this assessment of karyotype is typically only conducted once following reprogramming, not after some time in culture.

Human stem cells (both ESCs and iPSCs) acquire recurrent genomic abnormalities following prolonged periods of time in culture (Andrews et al., 2017). It is apparent that specific genomic abnormalities are more frequently found in iPSC cultures than others. These abnormalities may provide a selective advantage via enhanced cell proliferation and survival or reduced spontaneous differentiation. Cells harbouring these could increase in proportion to genetically stable cells (Andrews, 2006). Frequent monitoring of genomic stability would be advisable at set passage intervals and before banking any cells for future use.

A qPCR-based assay was used to determine genomic stability of iPSCs used in this project. This hPSC Genetic Analysis Kit (STEMCELL Technologies) was designed to identify the eight most common karyotypic abnormalities reported elsewhere in ESC and iPSC literature with results previously validated by G-banding and fluorescent *in situ* hybridisation.

Here, this kit was used to analyse five out of the six iPSC lines used within this project. Unfortunately, DNA could not be extracted from the SMA-19 cell line at the time of this assay and to avoid large inter-run variability between lines (as suggested by kit instructions), this line was not analysed. Specific primer-probe mixes to the following regions were used; chromosomes 1q, 8q, 10p, 12p, 17q, 18q, 20q and Xp and chromosome region 4p as a negative control. No evidence of chromosomal abnormalities within the 4p region has been reported, and thus copy number can be normalised to this within the assay. Following internal normalisation

to each lines' own chromosome 4p values, this was further normalised to a confirmed genetically stable control sample provided in the kit, using the ΔΔCt method.

Overall, three out of the five tested lines presented with potential forms of genetic instability (Figure 5.5). Should a cell line contain a copy number of <1.8 or >2.2 (with an associated P value of <0.05 that is drawn from a comparison to all other chromosomal locations), it is considered that there may be an abnormality within this chromosomal region. This assay is able to detect abnormalities in cultures exhibiting genetic mosaicism and it is therefore possible that only a fraction of cells within the culture do contain this abnormality.

19-9-7T and AD3-CL1 were found to be genetically normal at all tested loci (Figure 5.5). The 4603 iPSC line presented with two potential chromosomes of abnormal copy number (Chr20q = 2.85, ChrXp = 0.67) that were only significant when directly compared to each other, not any other loci. However, as the P value for Chr20q was highly non-significant when compared to all other loci, but ChrXp showed varying levels of significance in all comparisons (Figure 5.6), it was deemed more likely the probable deletion of ChrXp was more accurate. A similar case was seen in SMA-13 where the copy number of 3.78 (Figure 5.5) suggested a duplication of Chr20q where varying levels of significance were again seen (Figure 5.6), but none confirmed as being P<0.05, suggesting that potentially there may be an abnormality but this not confirmed. SMA-32 showed two probable amplifications of Chr12p and Chr17q (copy numbers 2.4 and 2.68, respectively; Figure 5.5) with significance in both comparisons (P=0.0183 and P=0.0078, respectively; Figure 5.6). Some comparisons to ChrXp approached significance in SMA-32 (Figure 5.6), but as the copy number was in range (0.86; Figure 5.5), this was deemed to be normal.

The four loci (Chr12p, 17q, 20q and Xp) that were found to be potentially abnormal in these cells, have commonly been found elsewhere in the literature. Studies have found that amplifications (complete chromosome duplications, or sub-chromosomal locations) of chromosomes 12, 17 and 20 have been found in approximately 34% of pluripotent stem cell lines. Amplified loci generally provide selective advantages to those cells containing them. For example, amplification of a centromeric region of the q arm of chromosome 20, specifically the 20q11.21 section, has been identified to encode 25 genes, one of which is Bcl-xL, an anti-apoptotic gene that enhances ESC survival (Avery et al., 2013, Nguyen et al., 2014).

Although, four loci were found to be potentially abnormal across three iPSC lines, it was deemed these were still adequate to work with. These cells were only going to be used *in vitro* for differentiation assays, not transplanted into animals where cells harbouring karyotypic abnormalities would pose tumourigenic risks. To avoid using cells with instabilities, earlier passages could be checked and then confirmed to be genetically normal. However, as early passage cells were not available in this project, the decision was made not to go ahead with this as no transplantation assays were planned.

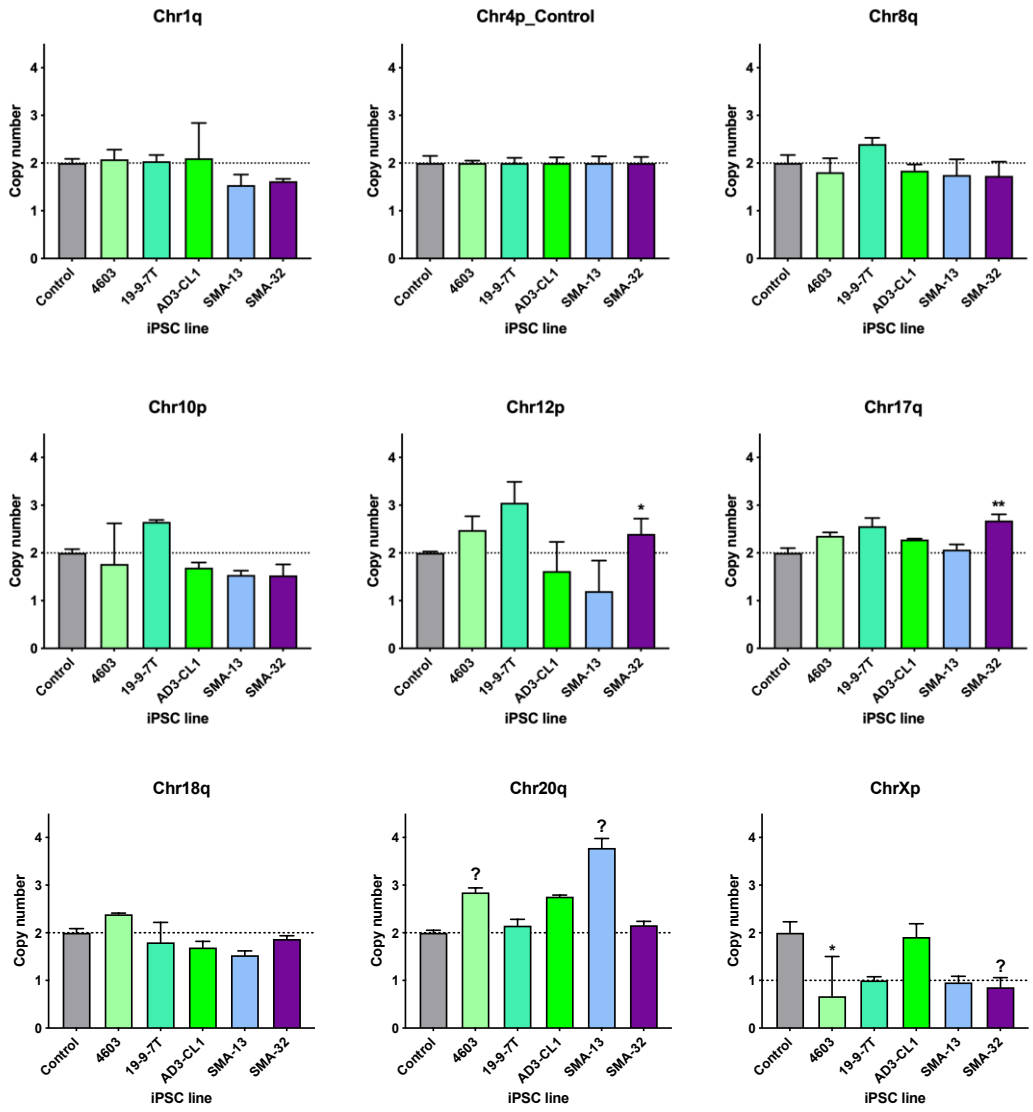


***Figure 5.5 Assessment of chromosomal copy number in five iPSC lines.***

*A qPCR based assay to assess the copy number of chromosomes using the hPSC Genetic Analysis Kit by STEMCELL Technologies was conducted using DNA from five out of six iPSC lines. Confirmed genetically stable control DNA was provided in the kit as a normalisation control. Chr4p also acts as a negative control as this is rarely, if ever, unstable. DNA from SMA-19 was not available at the time of assay and to avoid gross inter-run variability, this assay was not completed in the SMA-19 iPSC line. A copy number of <1.8 or >2.2 with a P value of <0.05 (indicated by *), is a probable indication of an abnormality within the culture. A ? indicates cases where an abnormality is potentially present as the copy number falls outside of the normal range and shows a trend when compared to all other chromosomes. A dotted line is shown at two on the y-axis in all but ChrXp, as this is the expected copy number, ChrXp has an expected copy number of one as all iPSC donors were male. Significance was determined with a one-way ANOVA with Tukey post-test and significance values can be found in Figure 5.6. Error bars represent the standard deviation of raw Ct values before copy number calculations.*

| 4603 | chr1q | chr4p_CTRL | chr8q | chr10p | chr12p | chr17q | chr18q | chr20q | chrXp |
|---|---|---|---|---|---|---|---|---|---|
| chr1q | | | | | | | | | |
| chr4p_CTRL | 0.9999 | | | | | | | | |
| chr8q | 0.9997 | 0.9999 | | | | | | | |
| chr10p | 0.9982 | 0.9998 | 0.9999 | | | | | | |
| chr12p | 0.9965 | 0.9889 | 0.9279 | 0.8317 | | | | | |
| chr17q | 0.9997 | 0.9983 | 0.974 | 0.9243 | 0.9999 | | | | |
| chr18q | 0.9994 | 0.997 | 0.9653 | 0.9048 | 0.9999 | 0.9999 | | | |
| chr20q | 0.8657 | 0.802 | 0.6177 | 0.4315 | 0.9977 | 0.9866 | 0.9909 | | |
| chrXp | 0.2766 | 0.3321 | 0.4992 | 0.4266 | 0.1028 | 0.1395 | 0.1293 | 0.0393 | |

| 19-9-7T | chr1q | chr4p_CTRL | chr8q | chr10p | chr12p | chr17q | chr18q | chr20q | chrXp |
|---|---|---|---|---|---|---|---|---|---|
| chr1q | | | | | | | | | |
| chr4p_CTRL | 0.9999 | | | | | | | | |
| chr8q | 0.999 | 0.998 | | | | | | | |
| chr10p | 0.9751 | 0.9645 | 0.9999 | | | | | | |
| chr12p | 0.7396 | 0.705 | 0.963 | 0.9978 | | | | | |
| chr17q | 0.9892 | 0.9832 | 0.9999 | 0.9999 | 0.9929 | | | | |
| chr18q | 0.9999 | 0.9999 | 0.9739 | 0.8664 | 0.5235 | 0.9137 | | | |
| chr20q | 0.9999 | 0.9999 | 0.9999 | 0.9929 | 0.8315 | 0.9978 | 0.9991 | | |
| chrXp | 0.7224 | 0.7565 | 0.4098 | 0.2549 | 0.1039 | 0.3005 | 0.9029 | 0.6204 | |

| AD3-CL1 | chr1q | chr4p_CTRL | chr8q | chr10p | chr12p | chr17q | chr18q | chr20q | chrXp |
|---|---|---|---|---|---|---|---|---|---|
| chr1q | | | | | | | | | |
| chr4p_CTRL | 0.9999 | | | | | | | | |
| chr8q | 0.9997 | 0.9999 | | | | | | | |
| chr10p | 0.9939 | 0.9991 | 0.9999 | | | | | | |
| chr12p | 0.984 | 0.9965 | 0.9999 | 0.9999 | | | | | |
| chr17q | 0.9999 | 0.9996 | 0.9898 | 0.9456 | 0.9061 | | | | |
| chr18q | 0.9945 | 0.9992 | 0.9999 | 0.9999 | 0.9999 | 0.9488 | | | |
| chr20q | 0.9014 | 0.8151 | 0.6285 | 0.4514 | 0.3779 | 0.9826 | 0.4591 | | |
| chrXp | 0.9999 | 0.9999 | 0.9999 | 0.9999 | 0.9995 | 0.9969 | 0.9999 | 0.7168 | |

| SMA-13 | chr1q | chr4p_CTRL | chr8q | chr10p | chr12p | chr17q | chr18q | chr20q | chrXp |
|---|---|---|---|---|---|---|---|---|---|
| chr1q | | | | | | | | | |
| chr4p_CTRL | 0.999 | | | | | | | | |
| chr8q | 0.9999 | 0.9999 | | | | | | | |
| chr10p | 0.9999 | 0.999 | 0.9999 | | | | | | |
| chr12p | 0.9999 | 0.9662 | 0.9964 | 0.9999 | | | | | |
| chr17q | 0.9974 | 0.9999 | 0.9999 | 0.9974 | 0.9477 | | | | |
| chr18q | 0.9999 | 0.9988 | 0.9999 | 0.9999 | 0.9999 | 0.997 | | | |
| chr20q | 0.1897 | 0.3997 | 0.2703 | 0.1897 | 0.1033 | 0.4425 | 0.1865 | | |
| chrXp | 0.995 | 0.8794 | 0.9684 | 0.995 | 0.9999 | 0.8421 | 0.9955 | 0.0671 | |

| SMA-32 | chr1q | chr4p_CTRL | chr8q | chr10p | chr12p | chr17q | chr18q | chr20q | chrXp |
|---|---|---|---|---|---|---|---|---|---|
| chr1q | | | | | | | | | |
| chr4p_CTRL | 0.9957 | | | | | | | | |
| chr8q | 0.9999 | 0.9976 | | | | | | | |
| chr10p | 0.9986 | 0.9999 | 0.9992 | | | | | | |
| chr12p | 0.799 | 0.9954 | 0.8681 | 0.9886 | | | | | |
| chr17q | 0.5527 | 0.9387 | 0.6692 | 0.9023 | 0.9999 | | | | |
| chr18q | 0.9981 | 0.9999 | 0.999 | 0.9999 | 0.9907 | 0.9124 | | | |
| chr20q | 0.982 | 0.9999 | 0.9898 | 0.9999 | 0.9994 | 0.9772 | 0.9999 | | |
| chrXp | 0.3166 | 0.0852 | 0.4586 | 0.1059 | 0.0183 | 0.0078 | 0.1003 | 0.0587 | |

| | |
|---|---|
| <0.05 | Significant |
| 0.051-0.1 | Approaching significance |
| 0.11-0.2 | Non-significant |
| 0.21-0.5 | Non-significant |
| >0.51 | Highly non-signifcant |

***Figure 5.6 One-way ANOVA pair-wise statistical comparisons for chromosomal copy number.***

*A one-way ANOVA was performed using the copy numbers calculated in Figure 5.5 to assess if the copy number was truly likely to be abnormal. Copy number at each locus was compared to all other loci within each iPSC line. To determine patterns, a heat-map based colour system was implemented to identify chromosomes with multiple levels of significance against multiple other loci.*

## 5.4 Differentiation protocol optimisation

As stated in section 2.2.8, the protocol used to differentiate iPSCs into MNs has been previously published (Maury et al., 2015), however modifications to this protocol were made by colleagues at University of Oxford. The published protocol uses an embryoid body formation method (3D spherical aggregations of pluripotent cells) for iPSC MN differentiation, but this was foregone here, instead only using single cell cultures. A few other modifications were made to the media used, including the replacement of penicillin/streptomycin with antibiotic-antimycotic (Fisher Scientific), the consistent use of Rock Inhibitor was replaced with use for 24 hours only after each passage and the dual SMAD inhibitors SB431542 and LDN193189 were removed from media.

Further to these adaptations made by the team at University of Oxford, I have also optimised this protocol for use in this laboratory (Figure 5.7). The first wild type MNs differentiated showed signs of cell death on the final day of differentiation and were later found to be largely dead by flow cytometry at day 31 (see section 4.3 for these results). To combat this issue, the growth factors used from day 16 of differentiation were altered. Instead of 20ng/ml BDNF and 10ng/ml GDNF in the published protocol (Maury et al., 2015), BDNF, GDNF, CNTF and IGF1 were used in a cocktail all at the concentration of 10ng/ml. CNTF (ciliary neurotrophic factor) is a cytokine critical for the survival of spinal MNs. When expression is lost MN degeneration occurs (Masu et al., 1993) and exogenous CNTF can prevent the progression of degeneration *in vivo* (Sendtner et al., 1992). IGF1 is important when maintaining certain subsets of MNs such as trigeminal MNs (Vicario-Abejón et al., 2004), however it displays general neurotrophic properties of use here.

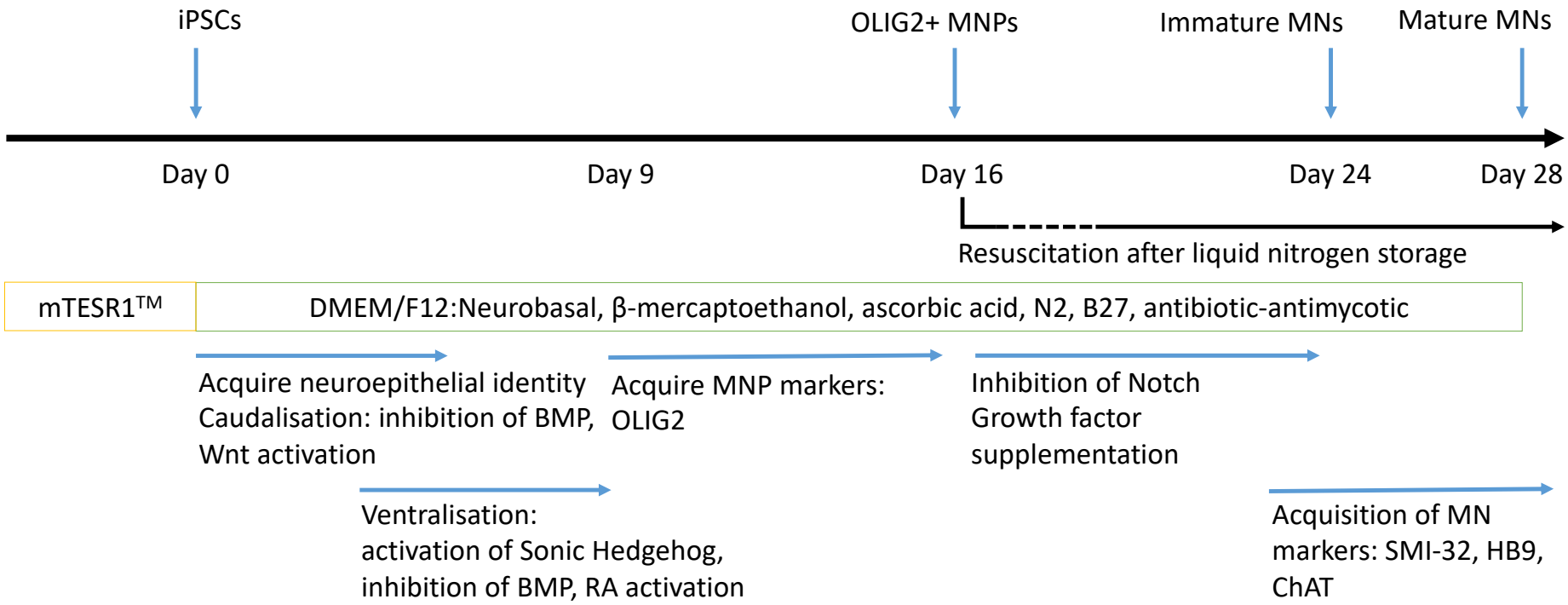


***Figure 5.7 Schematic representing the protocol used to differentiate iPSCs into MNs.***

*The 28-day differentiation protocol acts in a stepwise manner mimicking signaling pathways present in early embryogenesis. The basal media used for culture of cells is shown with mTESR1 being used during expansion stages prior to day 0, then this is switched to a DMEM/F12/Neurobasal based media for the rest of the protocol.*

## 5.5 Characterisation of MNs

All six iPSC lines were differentiated with high efficiency within this project. To characterise all stages of the differentiation process from iPSCs to MNs, the morphology was documented daily from day 0 to 28, immunofluorescence was used to assess the expression of MNP markers from day 9-16 and later immunofluorescence was used again to assess markers of maturity at days 23, 25 and 28. I have also characterised the SMN protein content at different stages of maturity as well as the set-up of assays to measure neurite length and soma size. Within this section I present the characterisation of subsets of iPSC MNs for each assay for the sake of brevity, however data presented in figures was representative of all iPSC MN lines.

It is very important to fully characterise the MNs resulting from the differentiation of iPSCs to ensure the resultant cells recapitulate the features expected from MNs *in vivo* (Faravelli et al., 2014), thus ensuring translatability of results presented here. The number of different starting iPSC lines available, as well as variability between differentiation protocols, are increasing as the iPSC disease modeling field progresses. The inherent variation caused by these two factors highlights the necessity for ongoing characterisation of resultant MNs to ensure they meet required standards (Faravelli et al., 2014) and phenotypes emerging from these experiments are valid. Looking for consistently shared features across a range of experiments using different iPSCs and protocols will tend to give most important, conserved phenotypes (Bhinge et al., 2017).

### 5.5.1 Morphological analysis

Phase contrast images of cellular morphology can be seen in Figure 5.8. At early stages (day 0-9) when iPSCs were acquiring a neuroepithelial identity, cells formed large colonies which then merged together. From day 5, particularly dense, circular areas formed, known as neural rosettes. Cells within rosettes acquire neural stem cell properties and exhibit high proliferative capacity (Faravelli et al., 2014). Between days 5-16 cells continued to grow in a dense monolayer without further gross morphological changes. At day 16, DAPT (a gamma secretase inhibitor) accelerates the transition from progenitor cells to post-mitotic neurons (Maury et al., 2015). This was highlighted by the appearance of axon sprouting 24 hours post-

addition (Figure 5.8). DAPT promotes this transition by inhibiting Notch signaling, thereby delaying the cell cycle transition from G1 to S, committing cells to neurogenesis (Borghese et al., 2010). Cells were only kept in the presence of DAPT for 7 days before this was removed from media. From day 20 onwards the network of connecting axons becomes more complex with increasing numbers of neurites present, then from day 25-28 migration of the cell somas to form clusters can be seen (Figure 5.8).

Measurements of neurite length and soma size were taken in a subset of MN lines to demonstrate the validity of differentiation protocols. The average length of wild type 4603 iPSC-derived MN neurites (measured with ImageJ plugin NeuriteTracer) was between 280-400µm and soma size was between 20-60µm for 4603, AD3-CL1 and SMA-19 MNs, both of which values fall within the expected range seen in *in vivo* studies.

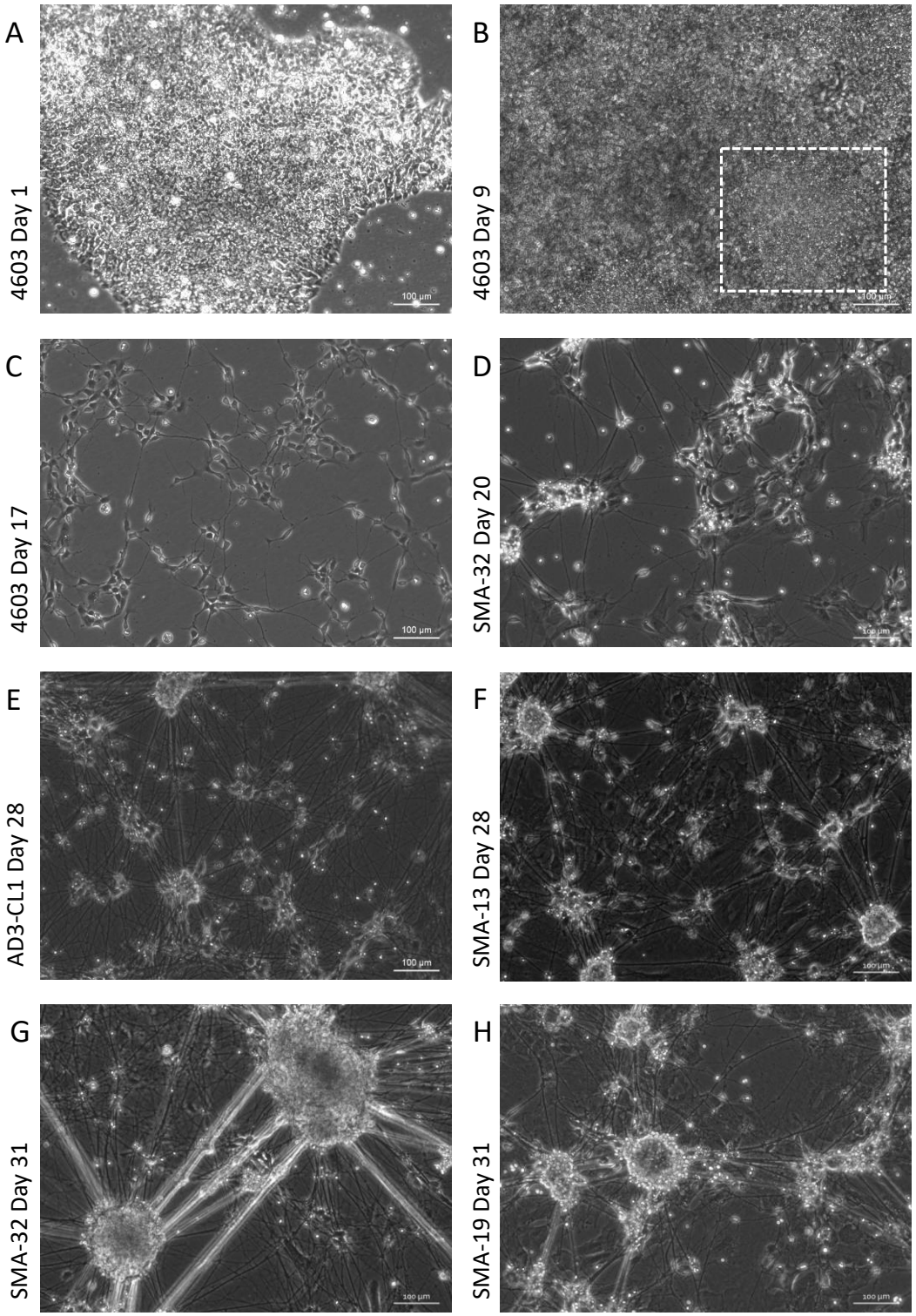


***Figure 5.8 Phase contrast images of iPSC MNs throughout the differentiation protocol.***

*Wild type 4603 colonies on day 1 (A) where colonies are tightly packed and (B) day 9 with some evidence of neural rosette formation (highlighted in bottom right corner). (C) Day 17 iPSC MNPs 24 hours following DAPT addition to initiate axon sprouting. (D) SMA-32 MNs at day 20 with more extensive connections. (E) Mature AD3-CL1 and (F) SMA-13 MNs with interconnecting axonal network and large clusters cell bodies. (G) SMA-32 and (H) SMA-19 mature MNs after the end of differentiation protocol.*

### 5.5.2 Expression of relevant markers

Neural rosettes were dissociated at day 9 to prevent over-confluency and to encourage cells to gain OLIG2-positivity. OLIG2 is a basic helix-loop-helix transcription factor whose role is critical in MN development, demonstrated by the knockout leading to complete absence of spinal MNs (Li et al., 2011a). During days 9-16 MNPs grew quickly, often requiring a further passage half-way through this period to encourage monolayers of cells. Immunofluorescence was used here to assess the increase in OLIG2-positive cells from day 9-16 (Figure 5.9). Immunostaining for these cells was problematic at times due to different lines dividing at different rates, despite a consistent seeding density, hence some samples were more confluent than others, so high background signal was present in these images (Figure 5.9A). Different lines tested have acquired OLIG2-positivity at different rates, however, at day 13 approximately 50% of cells were positive and this increased to >90% at day 16.

To assess whether or not the MNs produced were in fact mature or not at the end of the differentiation protocol, immunofluorescence against a range of a neuronal and MN-specific proteins was undertaken in a subset of MN lines. SMI-32 is a component of neurofilament heavy chains that is expressed as an early marker of MN maturity from day 23 onwards (Figure 5.10). βIII-tubulin, a pan-neuronal marker, was used to stain axons, often counterstained with SMI-32 to show overlapping expression of these markers (Figure 5.10). HB9 is a homeobox MN-specific transcription factor which is shown in Figure 5.10, where expression can be seen colocalising with DAPI staining in the nucleus. MNs are cholinergic neurons as opposed to dopaminergic or glutamatergic, meaning they use choline as the primary neurotransmitter. Choline acetyltransferase (ChAT) is responsible for recycling the neurotransmitter choline. This was used as a specific marker to show the MNs produced have the machinery for functional neurotransmission. Figure 5.10 shows strong ChAT expression in somas of MNs at day 25, also with expression in axons, however, the signal is less intense. I would expect the axonal signal to increase in strength at later time points, however due to technical issues during fixation and immunostaining of day 28 MNs this was not possible to test.

Immunofluorescence of mature MNs has proven very difficult throughout this project. Images presented within this chapter are the result of rare successes where MNs were not removed from the coverslip during the immunofluorescence protocol.

Fixation of mature MNs without complete removal of cells from the glass coverslip has proven challenging, despite several protocols and colleague's recommendations being trialed. Fixation was completed using 4% PFA in all cases, yet differences in temperature and time of fixation were tested. iPSC-MN fixation protocols recommended to me included dipping coverslips once very briefly in pre-warmed PBS and PFA, whereas another suggested ice-cold PBS and PFA incubation for 20 minutes. Generally, the brief, dipping method was found to be more successful. Nevertheless, the same protocol could be implemented to stain MNs from the same iPSC line in different differentiation rounds, yet show variability in attachment capabilities. It was also found that simultaneous fixation of multiple lines led to successful attachment in samples of one line, but not the other. Together, these two observations suggest the quality of MNs produced by each line, in each separate round of differentiation, caused some variability in success rates.

Due to the technical difficulties described here, it was difficult to obtain accurate measure of SMI-32, HB9 and ChAT expression across all six iPSC-MN lines as this required high quality images, whereas images from some lines were of too low quality to quantify. However, approximately 77.3% SMI-32-, 61.4% HB9- and 90.1% ChAT-positive MNs were obtained in samples from 4603 and AD3-CL1 MNs and values between these lines were consistent. These values are comparable to those presented in literature, with some values even exceeding those published. Previously, HB9 has been found to be expressed in approximately half of iPSC-derived MNs, often with HB9 expression alternating with that of Islet1 (another transcription factor expressed in MNs) (Amoroso et al., 2013), thus the expression pattern here with approximately 60% HB9-positive MNs is comparable to, or slightly exceeding that of published values.

Although SMI-32 and ChAT expression was also detected in multiple rounds of MN differentiation throughout this project, their expression was also detected in one specific round of differentiation of AD3-CL1 and SMA-32 MNs that did not complete the protocol successfully. These MNs appeared to differentiate well to MNs leading up to day 17, but axons had degraded by day 21 when immunostained (Figure 5.11). Nevertheless, evidence of markers of maturity was still apparent at this stage.

Together, I have shown that of the two wild type and one SMA line from which images of a sufficient quality were available, these all expressed the expected MN-specific markers. As all lines differentiated with similar efficacy and phase contrast

images (Figure 5.8) revealed the similar morphology between lines, it is probable that expression of maturity markers would be very similar across all lines as well.

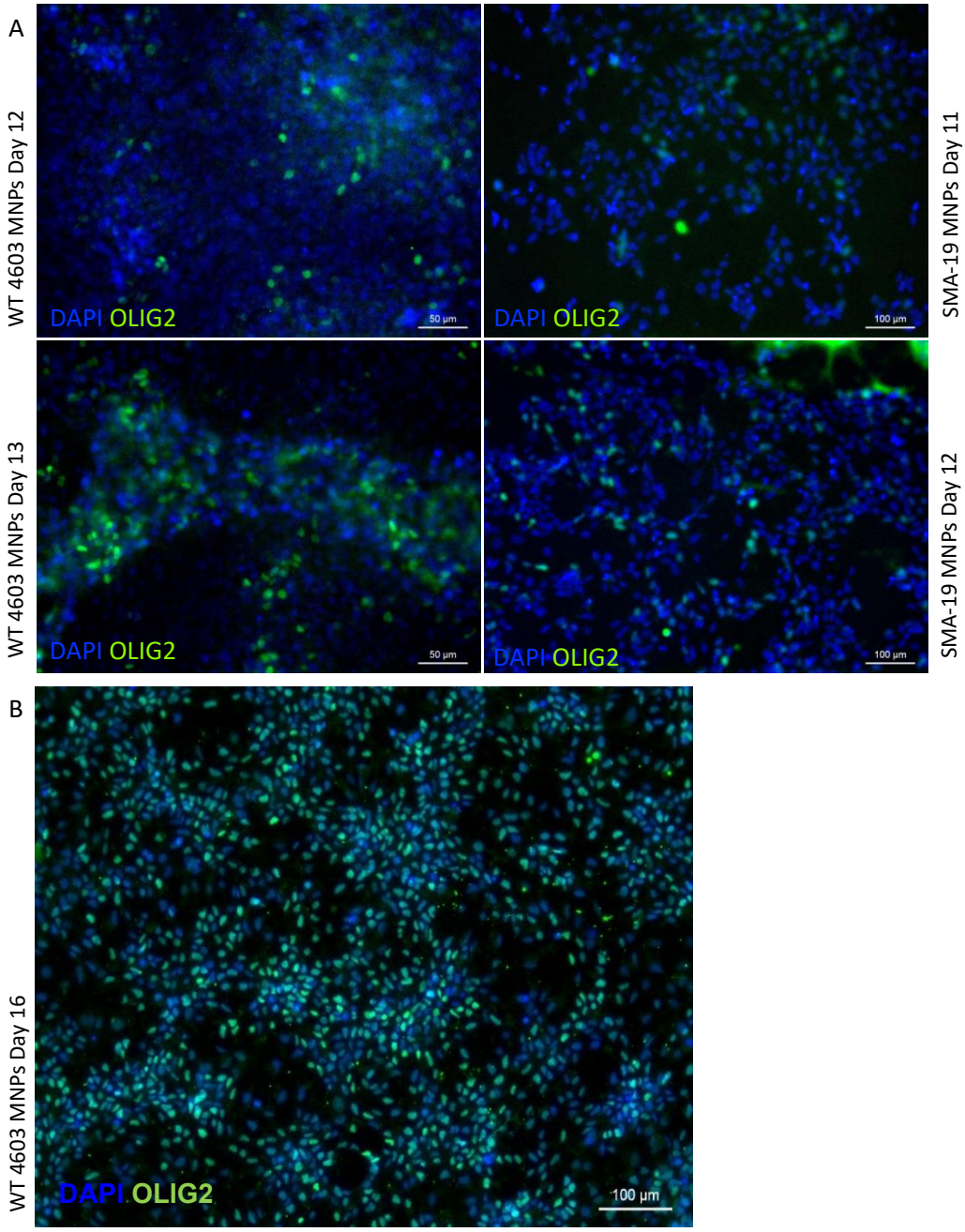


***Figure 5.9 OLIG2 expression in MN progenitors at early stages of differentiation.***

*(A) Wild type (4603) and SMA type I (SMA-19) MN progenitors (MNPs) were immunostained with an anti-OLIG2 antibody to detect the acquisition of OLIG2 expression at several time points leading up to the mid-point of the differentiation protocol. (B) As images shown in (A) are a little blurry, a higher quality image was provided by Neda Ali Mohammadi Nafchi of wild type (4603) MNPs at day 16. This image was acquired during optimisation of the differentiation protocol in a collaboration between myself and Neda and is used here with her permission.*

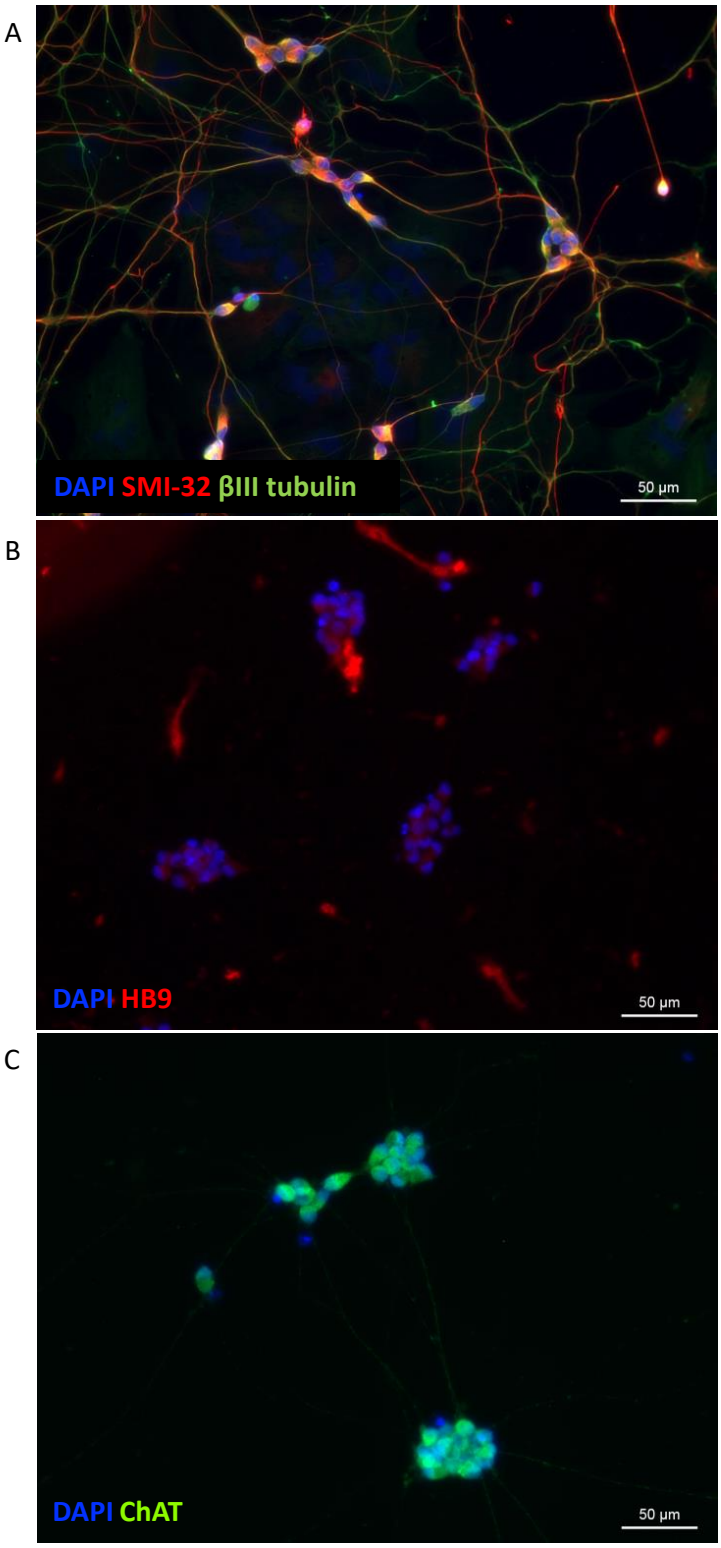


***Figure 5.10 iPSC MNs express markers indicative of maturity.***

*MNs derived from (A) 4603 wild type iPSC line stained against SMI-32 (red) and β III tubulin (green) on day 23 of differentiation protocol. Wild type AD3-CL1 iPSC-derived MNs stained against (B) HB9 and (C) ChAT on day 25 of differentiation protocol, all counterstained with DAPI.*

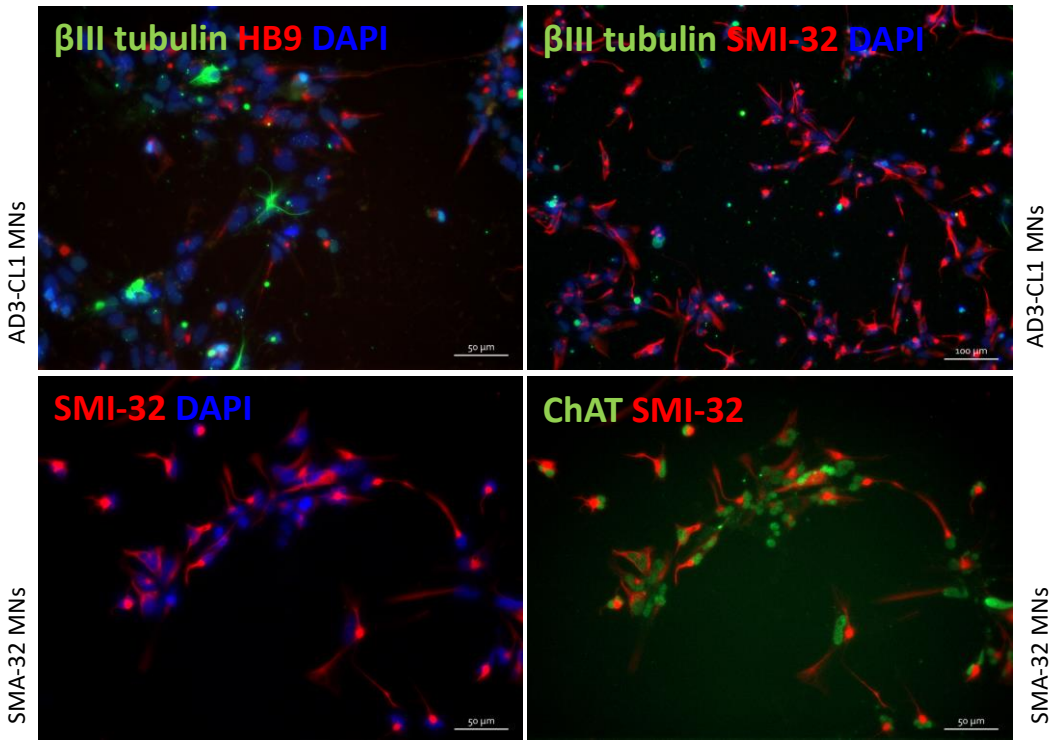


***Figure 5.11 Expression of maturity markers present in iPSC MNs that failed to fully differentiate.***

*Expression of MN markers HB9, SMI-32 and ChAT can still be seen in cells that begun acquiring an MN identity, but failed to fully differentiate or began to degrade towards the end of the differentiation protocol. Images of wild type AD3-CL1 and SMA type I (SMA-32) immature MNs taken at day 21 of differentiation.*

### 5.5.3 Confirmation of SMN gene expression and protein reduction in SMA type I MNs

To confirm that data from undifferentiated iPSCs (section 5.3.2) still held true once differentiation to MNs was completed, the same assays to determine the origin of SMN transcripts and the level of SMN protein were completed again using MN extracts.

The origin of *FL-SMN* and *SMNΔ7* transcripts was completed using the same protocol as in section 5.3.2. The expected pattern of products was seen in all lines except 19-9-7T (Figure 5.12A), but this was likely due to the low RNA concentration that only allowed 1µg cDNA to be synthesised, unlike 2µg in other lines. This sample was discarded from further analyses. All other lines showed two bands at approximately 500bp and 450bp (Figure 5.12A), corresponding to *FL-SMN* and *SMNΔ7* transcripts, respectively. Following digestion of products with *Dde*I, the same results were found in MN extracts as in iPSCs. The two wild type lines showed a strong *FL-SMN1* band (504bp), whilst the three SMA lines did not (Figure 5.12C). Two close bands representing the larger fragments of *FL-SMN2* (382bp) and *SMN2Δ7* (328bp) digested by *Dde*I, were present in all samples, whilst fainter bands were seen at lower molecular weight, representing the 122bp smaller digest product of *FL-SMN2* and *SMN2Δ7* (Figure 5.12C).

Wild type (4603, AD3-CL1 and 19-9-7T) MN lysates contained significantly more SMN protein than SMA type I (SMA-13, SMA-19 and SMA-32) MN lysates, showing an 18-fold difference ($P<0.0001$; Figure 5.13). There was no significant differences within the wild type lines or SMA type I lines, the only difference being observed between wild type and SMA lines (Figure 5.13).

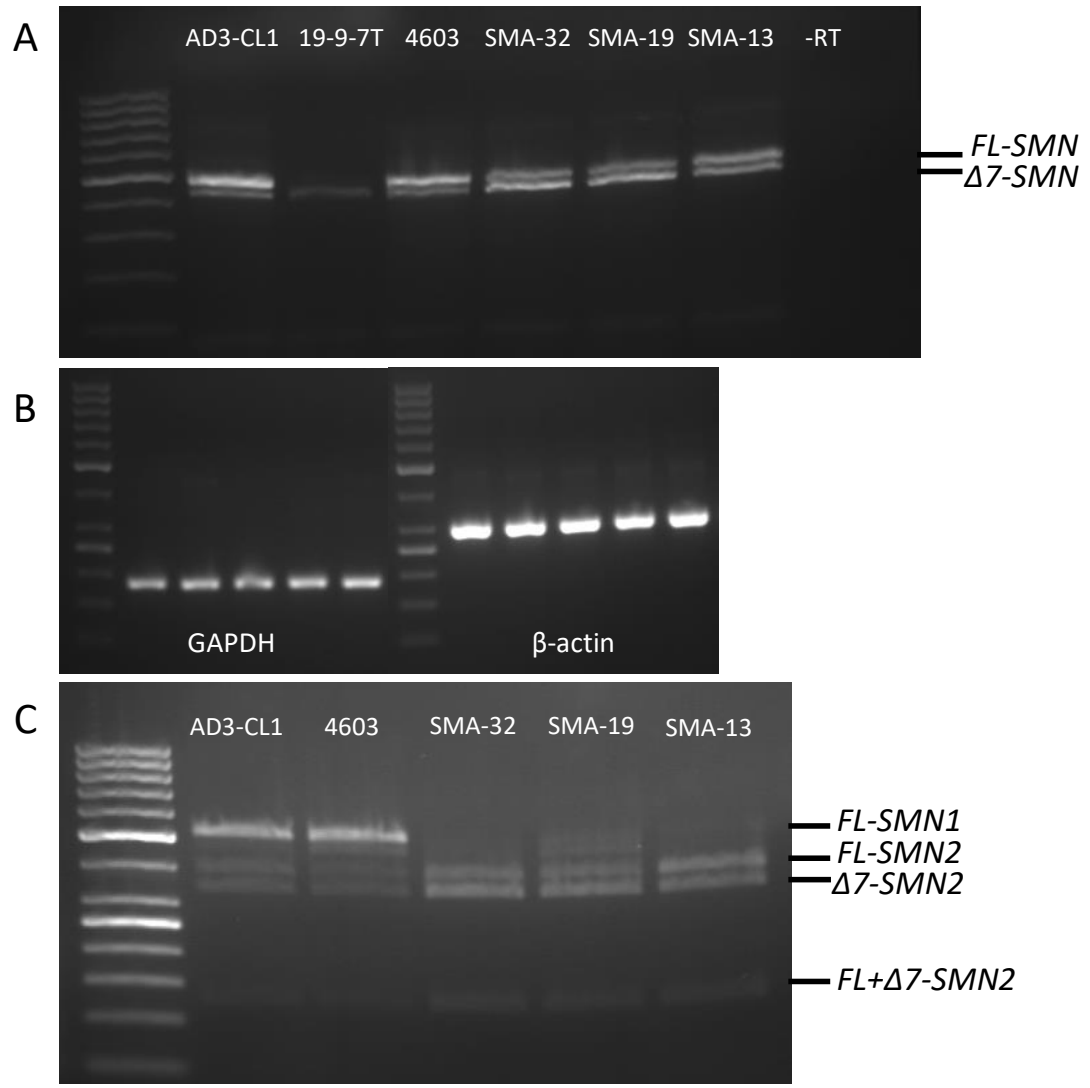


***Figure 5.12 Determining SMN transcript origin in iPSC-derived MNs.***

*An RT-PCR was performed using primers to amplify a region between exons 6-8 of the* SMN *genes in iPSC-derived MNs. -RT = minus reverse transcriptase control reaction. (A) Full length* SMN *(*FL-SMN*) products were expected to be 504bp, whilst those amplified from* SMNΔ7 *transcripts should be 450bp. 19-9-7T sample RNA was of low concentration and only 1µg of cDNA could be synthesised, unlike 2µg for all other lines. This meant poor amplification of the SMN targets were seen. The 19-9-7T sample was not included in the further analysis shown in parts (B and C). (B) Two control genes (*GAPDH*: 184bp and* β-actin*: 295bp) were also amplified and were expected to show consistent bands across all lines. The same lane order is present in all gels. (C) The two bands seen at 504 and 450bp in (A) were excised and amplicons extracted. PCR amplicons were digested with* DdeI *for 2 hours before running digested products on a second gel. Transcripts from the SMN1 gene do not possess a* DdeI *restriction site and were expected to give 504bp products. Transcripts from* SMN2 *do contain a diagnostic* DdeI *restriction site, so cleavage of* FL-SMN2 *504bp amplicon is cleaved to give 382 and 122bp fragments, whilst* SMN2Δ7 *450bp amplicon (from initial PCR amplification) when cleaved gives 328 and 122bp fragments.*

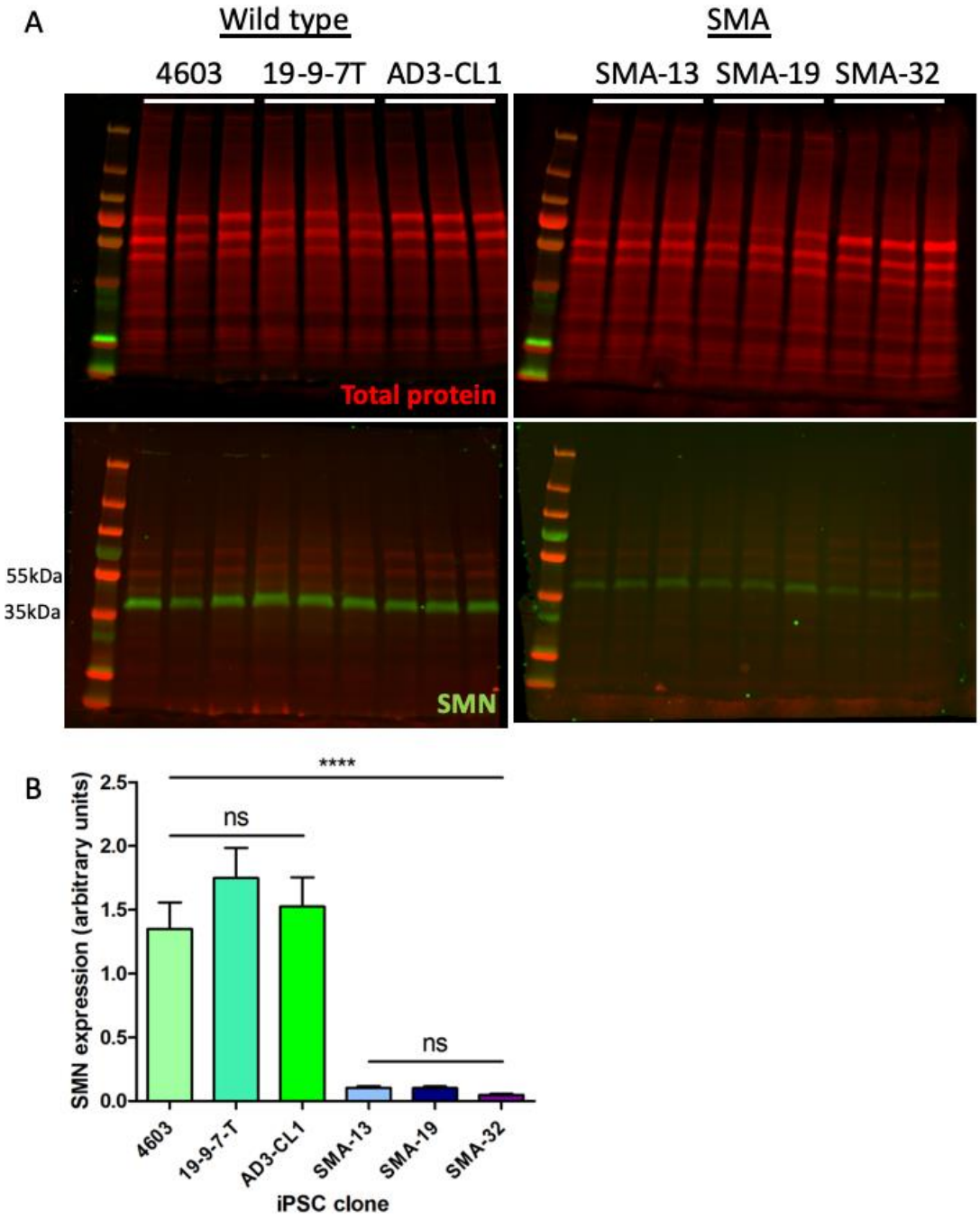


***Figure 5.13 SMN protein expression in wild type and SMA type I mature MNs.***

*SMA type I MNs show 18-fold (P<0.0001) less SMN protein than wild type MNs at day 31 of differentiation. Total protein was used as a loading control to minimize normalization bias if disease specific changes in standard loading control targets had occurred. One-way ANOVA with Bonferroni multiple comparisons post-test.*

### 5.5.4 SMN protein variation in immature and mature MNs

Despite the need for SMN protein increasing during development and the early post-natal period within the CNS (Figure 1.5) (Bowerman et al., 2017), it has been previously reported that SMN may in fact decrease during the differentiation of iPSCs to MNs (Boza-Moran, 2012). However, SMN protein was only assessed at distinct stages of differentiation such as neural rosettes, neurospheres and MNs, with broad windows of time between stages. Here, I sought to confirm if SMN levels varied within a small window of time in which MNs go from immaturity to maturity at the end of differentiation protocol, as this was not assessed in the previous study. It was hypothesised that the level of SMN protein may become critical at this stage, just before MNs begin degenerating postnatally.

Protein lysates were extracted from three SMA type I lines and one wild type line (19-9-7T) at days 23, 28 and 31 of differentiation. Day 23 was chosen as immature MNs have developed the morphology expected and begin to express markers such as SMI-32 and ChAT (see section 5.5.2). Day 28 represents the end of the differentiation protocol where MNs should have reached full maturity, whilst day 31 represents the maintenance stage of mature MNs. Blots can be seen in Figure 5.14. A repeated blot using protein lysates collected on day 28 for 19-9-7T, SMA-13 and SMA-32 was re-ran to obviate technical issues present; results from this successful blot (scan not shown) were used in quantitation (Figure 5.15). Consistently with results seen in sections 5.3.2 and 5.5.3, SMN protein expression was higher in wild type 19-9-7T MNs than SMA MNs at all three time points (Figure 5.15). Similar SMN expression was seen in all three of the SMA lines at each time point (Figure 5.15). When comparing the SMN expression within each of the four lines at all time points, non-significant differences were seen (Figure 5.15), suggesting that no SMN protein decay is seen within this small window.

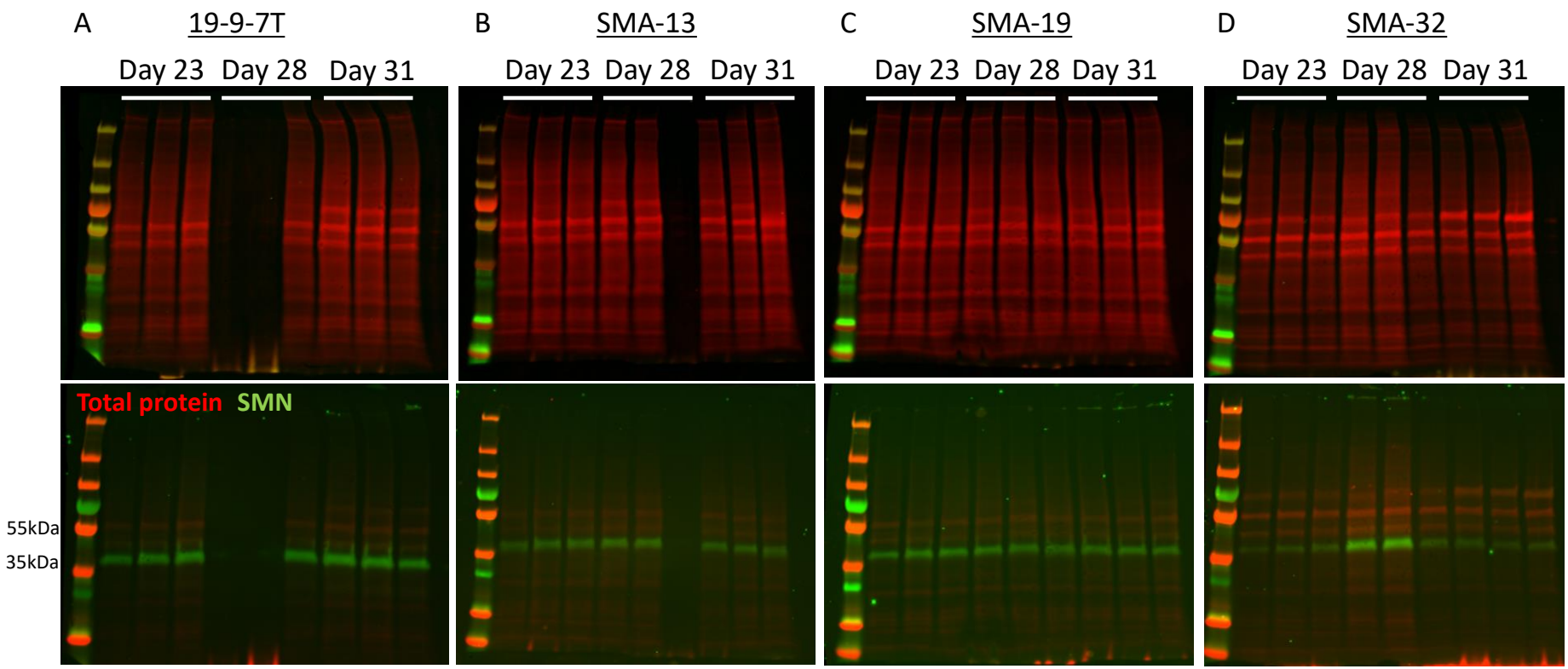


***Figure 5.14 Assessment of SMN expression at immature, mature and mature maintenance stages of differentiation.***

*SMN protein was assessed at each of three stages; immature MNs (day 23), newly mature MNs (day 28) and MNs undergoing maintenance (day 31). Total protein was used as a loading control to minimize normalisation bias if disease specific changes in standard loading control targets had occurred. Blots were quantified and are presented in Figure 5.15.*

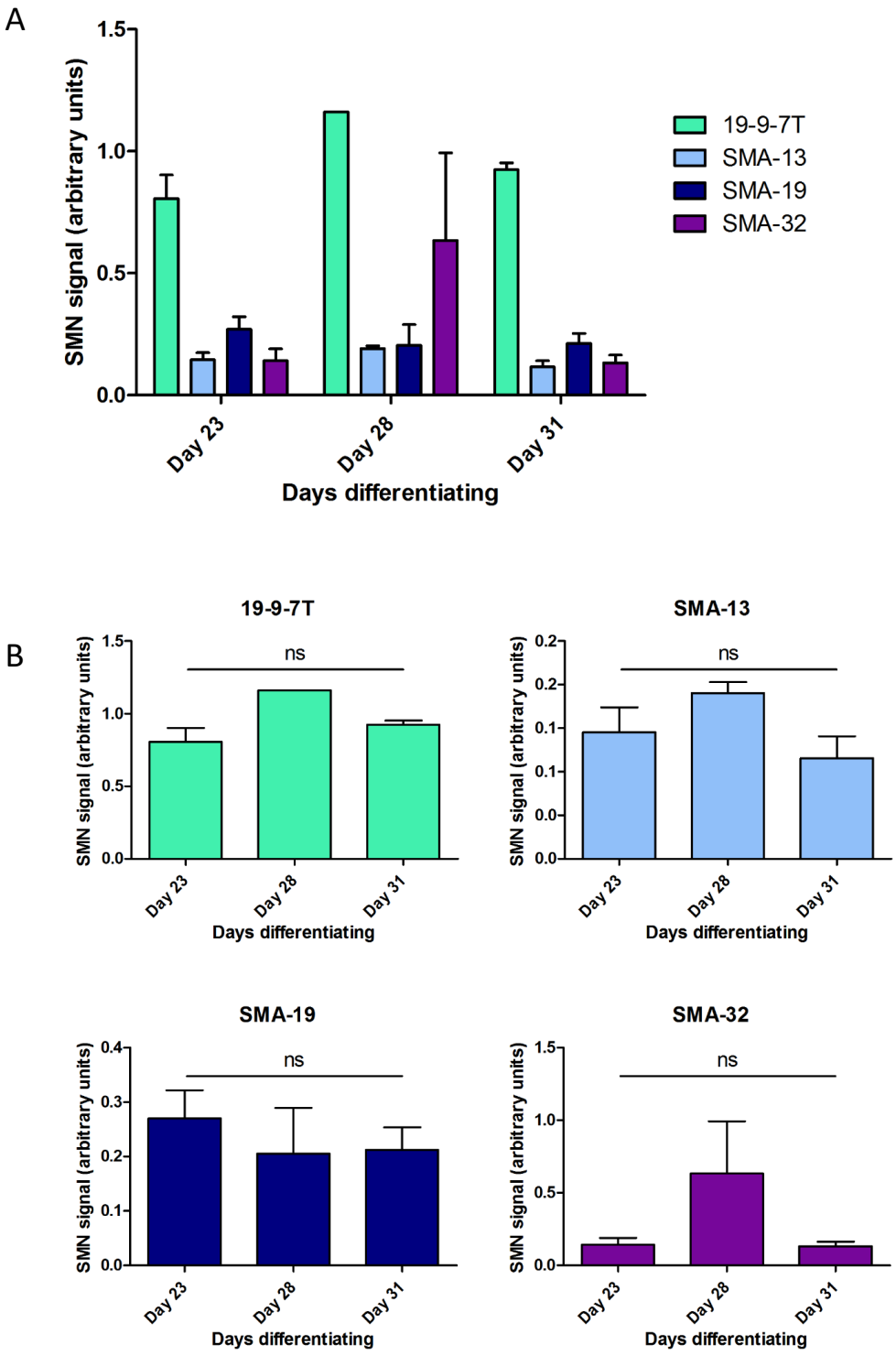


***Figure 5.15 Quantification of SMN expression at three time points indicating different stages of MN maturity.***

*Normalisation of SMN expression to total protein was used to determine SMN expression from western blots (see Figure 5.14 for blots). Two-way ANOVA with Bonferroni multiple comparisons post-test was used to assess significance (all P>0.05).*

## 5.6 Discussion

Although the recognition of SMA as a systemic disease is increasing, it is still vitally important that therapies developed can fundamentally improve MN phenotype. Therefore, it is necessary to have robust models of human SMA MNs that can be used for understanding the progression of SMA phenotype in these vulnerable cells and testing new therapeutic agents for toxicity and efficacy. Here, I have identified and optimised a protocol (Maury et al., 2015) to differentiate iPSCs into MNs within 28 days that can produce MNs, recapitulating hallmarks of SMA MNs *in vivo*. The characterisation of the model described in this chapter is a necessary precursor to the attempted rescue of SMA hallmarks and phenotypes described in the following chapters.

Efficiency of MN differentiation from iPSCs has been a challenge; early studies showed approximately 10% MNs positive for markers such as SMI-32 and ChAT (Ebert et al., 2009). However, increases in efficiency have been achieved through the addition of compounds like DAPT (55% increase) (Maury et al., 2015), a gamma secretase inhibitor that suppresses Notch signaling, in turn inducing the expression of proneural genes (Maury et al., 2015). Homogeneous populations (~95%) of OLIG2-positive MN progenitors (MNPs) reported by Du et al. (2015) and the addition of Compound E increased efficiency to 91% ChAT+, electrophysiologically active SMA MNs. Here, a high efficiency of MNPs (>90%) was seen at day 16, translating to high proportions of SMI-32-positive and ChAT-positive MNs in a further 12 days. This represents a similar, or improved differentiation efficiency compared to published literature. Furthermore, it was possible to differentiate all six iPSC lines with similar efficiency confirming that SMA genetics do not predispose against efficient MN generation.

*SMN* gene and protein expression here in both iPSCs and MNs was found to be comparable to levels found in the literature. The RT-PCR used here to assess the origin of *SMN* transcripts provided the same results as in a previous PhD thesis in this laboratory (Boza-Moran, 2012). A lack of FL-*SMN1* transcripts by RT-PCR was shown here with results very similar to that of a published paper where SMA iPSCs too showed a complete lack of FL-*SMN1* and approximately 67% reduction in total *FL-SMN* transcripts in SMA type I iPSCs (Ebert et al., 2009). Similarly, SMN protein

expression in both undifferentiated iPSCs and mature MNs showed significant differences between wild type and SMA type I cells similar to that presented in Powis et al. (2016) and Fuller et al. (2016).

Furthermore, SMA iPSC MNs show other hallmarks such as reduced cell survival represented by reductions in cell number over time (Yoshida et al., 2015), also with deficient neurite outgrowth (Chang et al., 2011) and reduced cell soma area (Ebert et al., 2009), compared to wild type MNs. In the literature, it has also been observed that continuing neurogenesis can occur in long-term cultures of iPSC derived neurons (8-10 weeks of differentiation), however, the numbers of MNs specifically declines in SMA, but not wild type cultures. In the literature this was represented by declining ratios of SMI-32-positive MNs to total βIII-tubulin positive neurons (Sareen et al., 2012), with similar phenotypes seen in other MN diseases such as ALS (Bhinge et al., 2017), but this was not studied within this thesis.

iPSC MNs differentiated *in vitro* have been described as fetal-like (Sances et al., 2016, Barral and Kurian, 2016), in part due to aging characteristics of fibroblast donor cells being reset upon reprogramming to iPSCs. This is highlighted by the disappearance of abnormal nuclear morphology, DNA damage (as measured by γH2AX foci) and mitochondrial reactive oxygen species upon reprogramming fibroblasts from an aging donor (82 years old) to iPSCs (Miller et al., 2013). Differentiated neurons may correspond to those present in first trimester, human fetuses (Vera and Studer, 2015), with mRNA expression profiles suggesting despite extended post-differentiation culture, iPSC MNs may lack full neuronal maturity. This aspect of iPSC MN culture may provide a unique environment to test therapeutics on immature cells, like those developing in SMA fetuses during the period of increasing need for SMN protein (Figure 1.5) (Bowerman et al., 2017). Therefore, analysis of SMN protein content in SMA iPSC MNs is necessary to determine if these cells could be a good model for infantile diseases such as severe SMA. Here, SMN protein was analysed at three time points reflecting immature, newly mature and mature MNs in the maintenance phase of differentiation, however no difference in SMN protein was seen across the phases which spanned a time period of nine days. This suggests that SMN protein levels are stable within this small window.

NMJs have been reported to show pathogenesis in SMA mouse models (Murray et al., 2008) and patients (Swoboda et al., 2005), suggesting a lack of SMN protein

impacts the connections between MNs and muscles. In this chapter, I have shown that the MNs derived from iPSCs using the differentiation protocol here passed visual inspections of morphology and mature MN marker expression, but no proof that these cells were functional was obtained. A co-culture assay was designed between iPSC-derived MNs and myotubes differentiated from mouse C2C12 cells, however this assay was not implemented in this thesis due to time constraints, but has been included within this discussion as a future avenue of investigation.

Co-cultures of myotubes and MNs to produce NMJs has been achieved in the literature (Boza-Moran, 2012, Yoshida et al., 2015, Abd Al Samid et al., 2018), however a critical barrier to the replication of these protocols is the necessity to dissociate late stage, differentiating MNs. These dissociated MNs were then seeded onto differentiated myotubes, co-cultured for a few days and NMJs analysed. However, these studies primarily used different MN differentiation protocols utilising embryoid bodies and neurospheres; spherical 3D, suspension structures that easily can be transferred between cultures. The adherence-based protocol used in this thesis to differentiate MNs does not allow dissociation of cells past day 16; 12 days before mature MNs appear. Differentiated myotubes from C2C12 cells tend to only survive approximately 7 days once mature, thus creating a problematic time difference.

The basic co-culture model designed would involve the differentiation of C2C12 cells into myotubes then seeding day 16 MNPs onto these, establishing if C2C12 myotubes could survive the further 12 days required for post-mitotic MN generation. Optimisation of C2C12 differentiation media to allow for efficient fusion of myotubes and most importantly survival of both myotubes and MNs would be necessary. It would also be noted if myotubes could survive for the whole 12 days necessary for mature MN differentiation, or if only part of this time period could be achieved. If only partly, the potential for NMJs to form with immature MNs at earlier stages would also be assessed.

An alternative to C2C12-myotubes, would be the possibility of differentiating the muscle cells from iPSCs. Colleagues at iStem have successfully differentiated wild type and Facioscapulohumeral Muscular Dystrophy (FSHD) iPSCs using a three-stage protocol to myogenic progenitors, myoblasts and finally myotubes (Caron et al., 2016). Proof of concept experiments showing iPSC-derived contractile muscle cells could be co-cultured successfully with MNs, leading to the formation of NMJs,

would be possible if a similar protocol was applied to this project. Both myotubes and MNs could be differentiated with from a syngenic background from the same starting iPSCs. Distinct combinations of wild type and SMA myotubes and motor neurons could have been examined and the importance of SMN levels within each cellular compartment underpinned.

An enriched media similar to the one used in (Guo et al., 2010) could also be tested. This paper showed NMJs formed between human spinal cord stem cells differentiated to MNs and primary rat skeletal myocyte cultures. Optimisation of media reagents included the addition of G5 supplement to significantly enhance myocyte proliferation, removal of neurotrophic growth factors gradually as these prevent synaptogenesis and the addition of cholesterol, estrogen and creatine to promote synaptogenesis (Guo et al., 2010). Myotubes and MNs should exist in a symbiotic environment, respectively secreting neurotrophic factors by myotubes to support MN survival and attract neurite outgrowth and the secretion of neuregulin and agrin by MNs to increase acetylcholine receptor (AChR) synthesis, stabilise and refine synapses (Guo et al., 2010).

Once a co-culture system has been established two assays would be used to characterise any resultant NMJs as well as the ability for MNs to innervate myotubes. All assays would first be conducted using wild type MNs as proof of concept before moving onto SMA MNs that may fail to produce functional NMJs as expected due to the lack of SMN. Immunofluorescence would be employed to stain for markers of mature MNs and myotubes, as well as NMJs. Specifically, myosin heavy chain, SMI-32, Glutamate receptor 1 (Glut1) and α-bungarotoxin would be used to mark each cell type as well as clusters of AChRs, a representative feature of NMJs. Both aneural and amuscular controls would also be used.

Secondly, to assess functional innervation of myotubes by MNs, the Glut-Curare contractile assay described in (Guo et al., 2010) would be used. Although MNs are described as cholinergic due to their release of acetylcholine (ACh) onto muscle targets, MNs can receive excitatory input via the neurotransmitter glutamate *in vivo* from interneurons or sensory neurons, or *in vitro* from the exogenous application of glutamate or its agonists. Exogenous application of glutamate to MNs is an established procedure (Rekling et al., 2000) used to depolarise MNs and to electrophysiologically record their action potentials. If functional NMJ formation has occurred, the addition of glutamate should enable MN depolarisation, release of

ACh onto myotubes, causing their contraction. It should be possible to arrest contractions by administering a specific nAChR-blocking compound called curare (Guo et al., 2010). The use of this assay revealed significantly increased contractile frequency after addition of glutamate mediated specifically by MNs, which when followed by curare addition led to complete attenuation of myotube contractions within two minutes (Guo et al., 2010).

## 5.7 Conclusions

In conclusion, in this chapter I have identified and optimised a protocol used to differentiate human iPSCs from three wild type and three SMA type I patients into MNs that appear to recapitulate *in vivo* features. MNs express markers such as SMI-32 and ChAT that indicate MN maturity, whilst SMA lines specifically also retain characteristics such as a lack of *FL-SMN1* transcripts and significantly reduced SMN protein. The design of a co-culture based functional assay was explored as an avenue of future investigation for this work. Following on from the successful implementation SMA iPSC MN differentiation and characterisation, experimental evidence of SMN over-expression and its effects are explored in subsequent chapters.

# 6 Characterisation of Co-hSMN1 vectors in iPSC-derived motor neurons

## 6.1 Introduction

It is currently unclear if the two licensed SMA therapies could effectively treat all the symptoms of SMA in the long term, primarily because the majority of patients treated with these agents are still children, although some treatment of adults is just beginning. Time will tell if the SMA phenotype has been well managed or if it has shifted in its clinical presentation. The field is moving towards “combinatorial therapy” in an attempt to prepare for this and as a means to increase the treatment options available to all SMA patient populations. Individual treatments may preferentially correct particular hallmarks of SMA, but if these are combined there is a greater chance of systemic improvement in the disease phenotype.

The use of IDLVs provides one such option, particularly in an environment where clinical use of gene therapy is becoming more widely considered and accepted. The work here describing iPSC testing of IDLVs will be the first work testing these vectors in human cells relevant to the primary pathophysiology of SMA. This increases translatability between pre-clinical and clinical work and is an important step in the progress towards human trials. The high quality IDLVs developed may provide advantages over other viral vectors, such as strong and focal expression with highly diminished risk of insertional mutagenesis. The IDLVs to be developed in this project may be used as a stand-alone therapeutic approach, or more likely as one aspect of a combinatorial therapy.

### 6.1.1 MN pathology in SMA

It was long thought that MNs were the sole pathological target of SMA, but this idea is becoming increasingly challenged as pathology is discovered in other tissues (see Hamilton and Gillingwater (2013) for an excellent review). Nevertheless, it is still clear that MNs are particularly vulnerable along the spectrum of affected tissues (Sleigh et al., 2011) and should be targeted by therapeutic strategies.

SMA MN loss occurs in a predictable pattern with particular sub-populations of MNs lost at early or late stages of disease progression and some that are more

vulnerable than others. For example, MNs that innervate abdominal core muscles, as well as proximal upper and lower limbs degenerate early compared to distal limb innervating-MNs, in which loss occurs later (Deymeer et al., 2008), or cranial MNs that are spared completely (Kubota et al., 2000, Bowerman et al., 2018). Transcriptional differences have been highlighted in differentially vulnerable populations of MNs in SMA patients and mouse models, as well as comparison to equivalent healthy populations of MNs (Bowerman et al., 2018). These analyses have revealed commonalities between SMA and ALS (both diseases in which MN degeneration is a hallmark pathology), such as increased IGF-2 expression in sub-populations in MNs correlating with high levels of axon sprouting and a resistance to degeneration (Hedlund et al., 2010, Murray et al., 2015). Further transcriptional analysis aims to elucidate molecular mechanisms that will help to understand why MNs are so vulnerable in SMA, but also to reveal potential neurodegenerative and neuroprotective pathways (Kline et al., 2017) that could be targeted by therapeutic interventions.

### 6.1.2 Increasing SMN levels in MNs as a therapeutic strategy

In the previous chapter I presented the optimisation of a differentiation protocol used to obtain mature iPSC-derived MNs that recapitulated expected phenotypes of SMA. In this chapter, I will build upon this by assessing the effect of IDLV transduction of these MNs to induce expression of *Co-hSMN1*.

SMN levels in iPSC MNs have been increased by a number of interventions; for an excellent summary please see Frattini et al. (2015). The small molecules valproic acid and tobramycin were respectively able to increase SMN protein levels by 2- and 3-fold (Ebert et al., 2009). Valproic acid acts as a histone deacetylase inhibitor acting upon the promoter upstream of *SMN2* to increase activity (Kernochan et al., 2005). Tobramycin is an aminoglycoside that halts the recognition of a stop codon present in exon 8 of *SMN2*, forming a more stable *SMN∆7* isoform (Wolstencroft et al., 2005). Genome editing of SMA iPSCs has also been reported to increase *SMN* expression following genetic correction of *SMN2* exon 7 (Zhou et al., Corti et al., 2012), improving the phenotype of MNs differentiated from these. Transplantation of gene edited iPSC-derived MNs has shown promise as a cell therapy strategy also (Corti et al., 2012). RNA therapeutics including antisense morpholinos and small nuclear RNAs have shown promise targeting *SMN2* splicing, increasing the

proportion of full length transcripts and SMN protein (Nizzardo et al., 2015). No attempt so far has been made to use SMA iPSC MNs as a model for LV delivery, therefore this will be addressed in this project.

## 6.2 Aims

In this chapter I aimed to use both IDLV and AAV9 vectors expressing a *Co-hSMN1* cassette to induce increased SMN expression. Specifically, my objectives were:

(A) Assess the efficacy by which vectors transduce mature MNs.
(B) Induce over-expression of SMN protein in mature MNs.
(C) Compare and contrast IDLV_*Co-hSMN1* and AAV9_*Co-hSMN1* vectors.
(D) Compare the effect of CMV, hSYN and hPGK transcriptional controls on the levels of SMN expression.
(E) Assess any downstream rescue of Gemin2.

Wherever possible within this chapter, experiments were aimed to be performed with three wild type and three SMA type I iPSC lines, where appropriate, to improve validity of results. This also avoids bias inflicted by differing genetic backgrounds or modulators of severity that may contribute to clonal variation (Barral and Kurian, 2016). However, it was not always possible to differentiate all at the same time with similar success rates, whilst also considering the cost and time-consuming nature of this work. Therefore, some experiments were performed with less than six lines.

## 6.3 Transduction efficacy

The same experiments performed in section 4.5 assessing the transduction efficacy of cell lines were repeated here with MNs. Analysis of transduction efficacy with IDLV_CMV_*eGFP* shows that MNs derived from two wild type iPSC MN lines (4603 and AD3-CL1) show minimum 23% GFP-positive cells at MOI of 25, increasing to maximum 63% at MOI 75 (Figure 6.1C). These encouraging results provided proof of principle that IDLVs can successfully transduce iPSC MNs. Transduction efficacy with AAV9_CAG_*eGFP* was also assessed in SMA-19 iPSC-derived MNs. Similar to the values reported in section 3.3.2 when transducing CHO cells, AAV9 transduction resulted in 1.7% ($P=0.2162$) and 17% ($P<0.0001$) transduction at MOIs $1x10^5$ and $1x10^6$, respectively (Figure 6.1D).

During these experiments it was noted that large proportions of the MNs appeared to be dead according to flow cytometry forward vs side scatter plots (Figure 6.1B). An average of 32.9% cells appeared to be viable at day 31. This was deemed unlikely to be due to vector presence as both mock-treated and transduced samples showed very similar plots (Figure 6.1B). It was likely that cell death or the generation of cellular debris occurred during the preparation for flow cytometry. Sample preparation for flow cytometry involved the removal of MNs from their adherent environment and thorough dissociation. This likely caused axon shearing and break-up of the MN clusters, presenting as debris in flow cytometry forward vs side scatter plots.

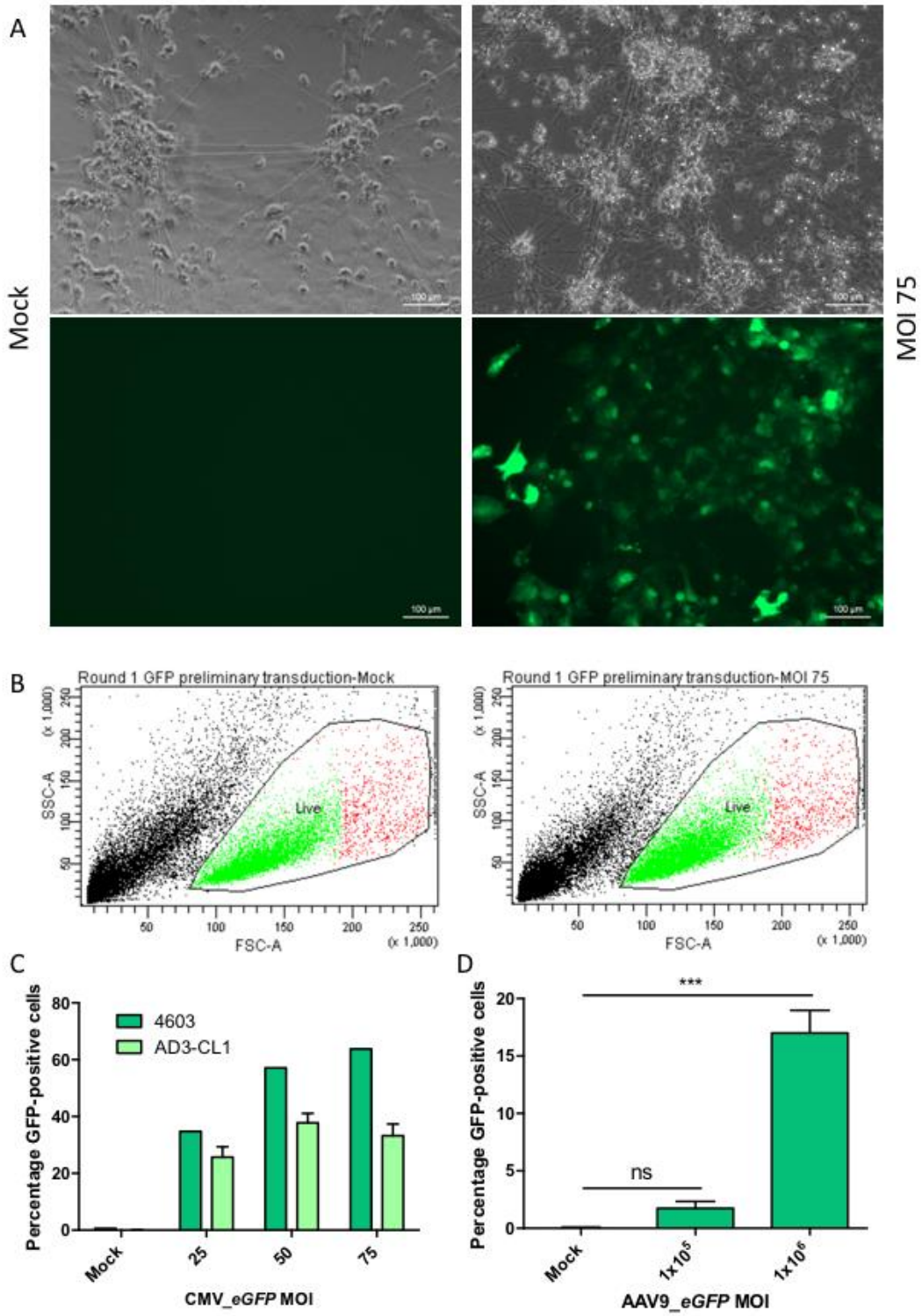


***Figure 6.1 Transduction of mature MNs with IDLVs and AAV9 vectors encoding* eGFP*.***

*(A) Fluorescent microscopy of mock-treated and MOI 75 IDLV_CMV_*eGFP *transduced MNs analysed at day 31. (B) Representative forward vs side scatter flow cytometry plots showing similar proportions of cell death in both mock-treated and transduced samples. (C) Wild type 4603 and AD3-CL1 MNs show clonal variability in transduction efficacy (range 23%-63% GFP-positive cells). (D) SMA-19 MNs transduced with AAV9_CAG_*eGFP *show much lower percentages of GFP-positive*

*cells (MOI 1x105 P=0.2162, 1x106 P<0.0001). One-way ANOVA with Dunnett's post-hoc test.*

## 6.4 *Co-hSMN1* expression in iPSC MNs following transduction

Two independent pilot experiments were conducted in SMA-19 and SMA-32 iPSC MNs where mature cells were transduced with IDLV_CMV_*Co-hSMN1* to determine if over-expression of SMN was possible in the most vulnerable SMA cell type. IDLV_CMV_*Co-hSMN1* was used as the IDLV of choice, rather than hSYN or hPGK controlled vectors as CMV produced the largest increases in SMN expression in cell line and primary culture testing. Comparisons between different transcriptional controls in MNs has been undertaken and results are presented in section 6.4.2.

Results of this pilot experiment show that compared to mock-treated cells, those transduced with IDLV_CMV_*Co-hSMN1* at MOI 75 show significantly upregulated SMN protein in lysates. SMA-19 MNs showed more than 23-fold higher SMN levels than untransduced counterparts (P=0.0080; Figure 6.2B shows representative blot), whereas this difference was more pronounced in SMA-32 MNs with 66-fold higher SMN protein (P<0.001). Strong SMN signal was also verified by immunofluorescence in SMA-19 transduced MNs (Figure 6.2A) that without transduction show little or no SMN fluorescence.

Positive results from pilot data provided the basis for more extensive testing of IDLV_CMV_*Co-hSMN1* in MNs to assess if this SMN increase was robust in all three SMA type I MN lines. Simultaneous differentiation, transduction and harvesting of SMA-13, SMA-19 and SMA-32 MNs was undertaken to reduce variability. This experiment also led to increases in SMN protein in all transduced samples compared to untreated counterparts (SMA-13: 14.5-fold, P=0.001; SMA-19: 79.8-fold, P=0.0046; SMA-32: 42.8-fold, P=0.0032; bottom red stars in Figure 6.2C). Comparison of SMN protein in lysates from wild type MNs to transduced SMA MNs was also undertaken, revealing supraphysiological SMN protein in two lines (2.1-fold, P>0.05; SMA-19: 12.5-fold, P<0.0001; SMA-32: 3.6-fold, P<0.05; top black stars in Figure 6.2C).

It should be noted that variation between SMN protein fold differences is present within the same line in independent rounds of differentiation and transduction, however the significance of these increases is common across all experiments. The

most comparable results are available when all MNs were simultaneously differentiated, transduced and harvested, as in the later experiments represented in Figure 6.2C. It is, however, interesting to note that SMA-32 MNs showed the largest fold difference between mock and treated cells in pilot experiments, but that SMA-19 showed the largest fold difference in later experiments, reversing the pattern seen earlier.

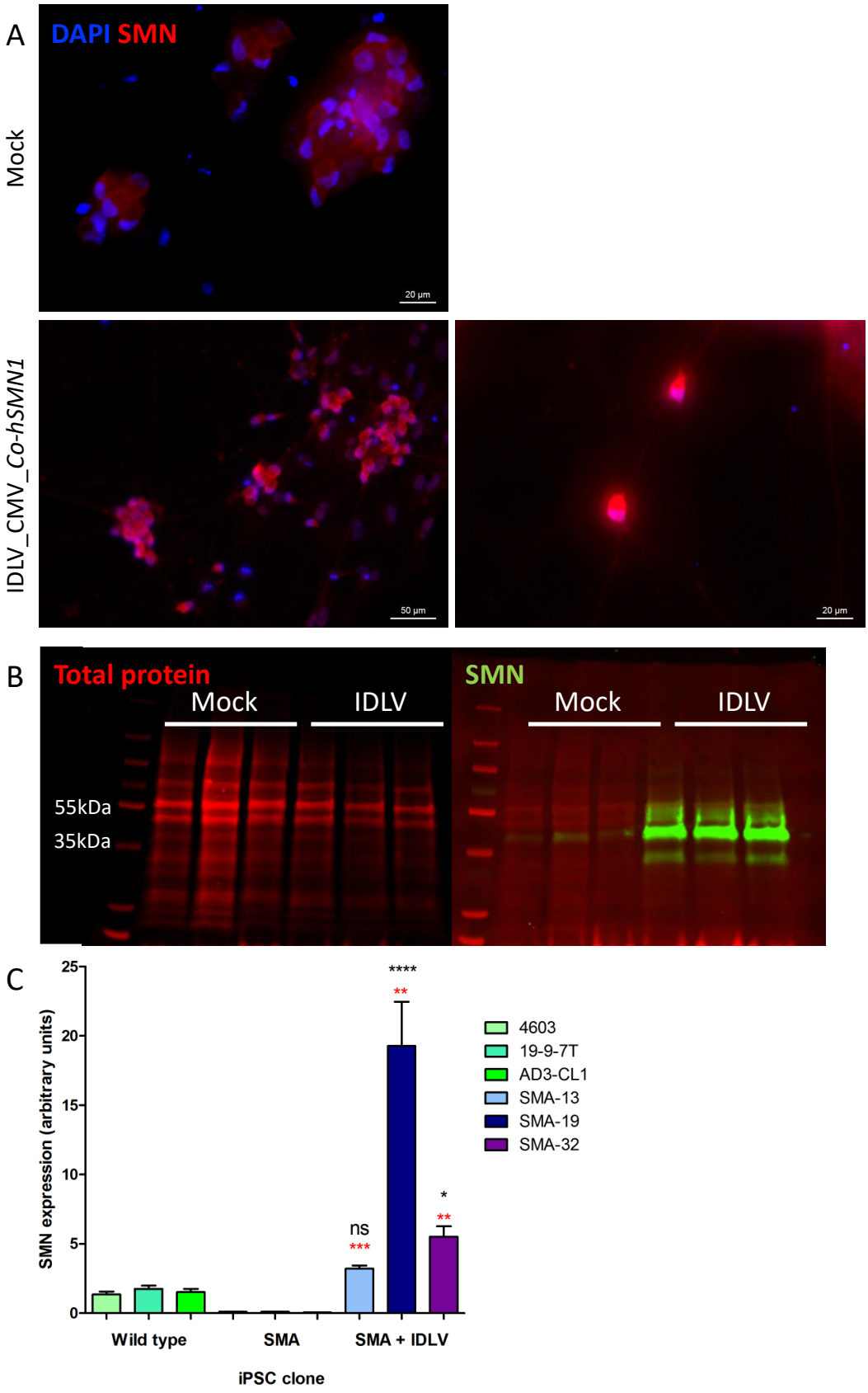


***Figure 6.2 Transduction of SMA type I MNs with IDLV_CMV_Co-hSMN1.***

*(A) Representative images of SMA-19 MNs transduced with IDLV_CMV_*Co-hSMN1 *at MOI 75 upon reaching maturity and immunostained for SMN protein expression. (B) Representative western blot of SMA-19 MNs with and without transduction. (C)*

*Quantification of western blots from all three SMA type I MN lines with IDLV_CMV_*Co-hSMN1 *at MOI 75 transduction. All three SMA MN lines showed significantly increased SMN protein following transduction (SMA-13: 14.5-fold, P=0.001; SMA-19: 79.8-fold, P=0.0046; SMA-32: 42.8-fold, P=0.0032) assessed by statistical comparison between mock and transduced samples of the specific SMA line (one-tailed t-test with Welch's correction; lower stars in red font). SMA-19 and SMA-32 MNs revealed higher SMN protein than WT samples (12.5-fold, P<0.0001 and 3.6-fold, P<0.05, respectively), but transduced SMA-13 MNs did not (2.1-fold, p>0.05). This is represented by the top stars (black font) showing statistical comparison between combined wild-type SMN protein and that SMA line (assessed by one-way ANOVA with Bonferroni multiple comparison post-test).*

### 6.4.1 Comparison of AAV9_*Co-hSMN1* and IDLV_*Co-hSMN1*

In sections 6.4 it was observed that IDLV transduction led to increases in SMN protein above that of mock treated cells and indeed transduced SMA MNs exhibit supraphysiological SMN protein compared to wild type cells.

Previously, in section 4.10 and sections therein, I showed that AAV9_CAG_*Co-hSMN1* cannot induce SMN over-expression in CHO cells or SMA type I fibroblasts, unless cells have exited from the cell cycle. Here, I aimed to confirm if this was the case in SMA-32 MNs in a pilot experiment. A 1.9-fold increase in SMN protein was observed following AAV9 transduction, but IDLV transduction significantly increased SMN protein by 66-fold (P>0.001). When comparing IDLV_CMV_*Co-hSMN1* and AAV9_CAG_*Co-hSMN1* transduction to mock transduced samples, the latter do not provide significant over-expression (P=0.3219; Figure 6.3), suggesting that IDLVs may be more preferable than more commonly used vectors like AAVs when transducing MNs.

As preliminary data showed ineffective SMN expression, it was decided that no further experiments would be completed using AAV9_*Co-hSMN1* or AAV9_CAG_*GFP*.

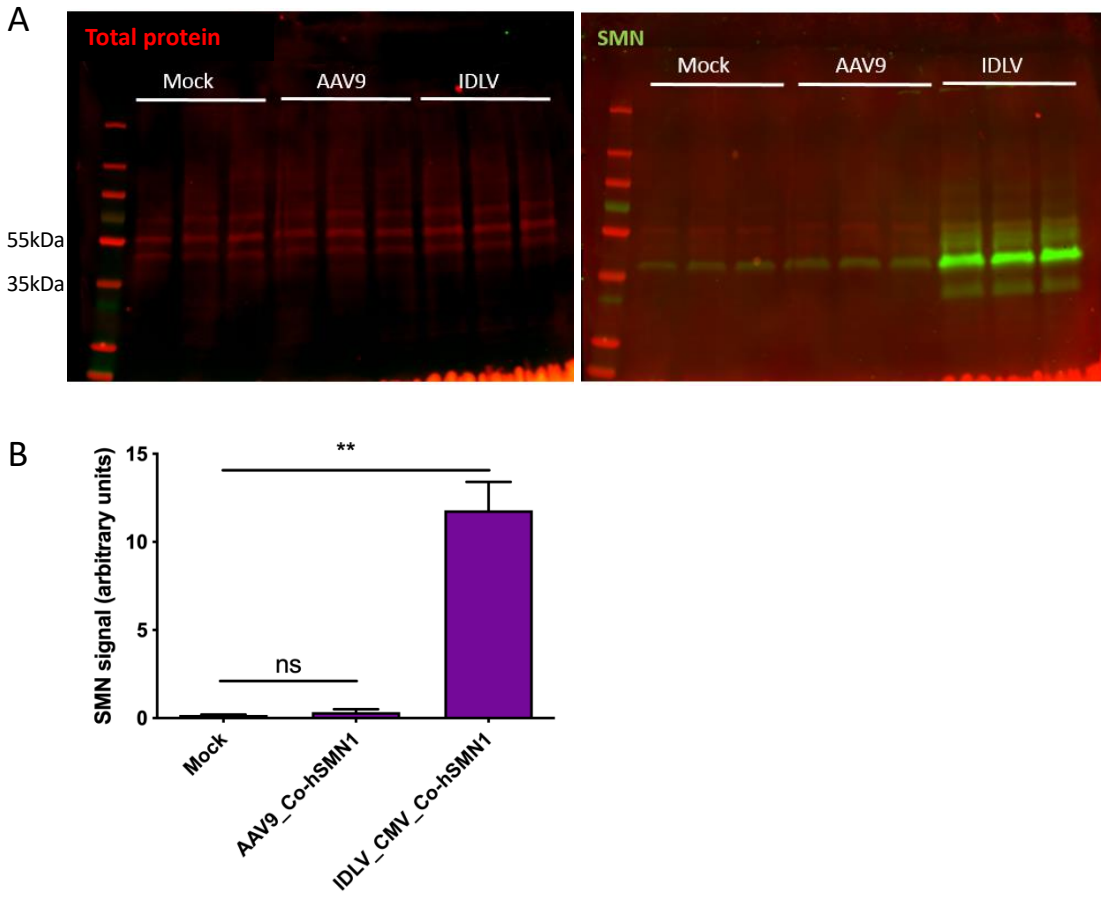


***Figure 6.3 Protein analysis of SMA-32 MNs following transduction with IDLVs or AAV9s encoding* Co-hSMN1.**

*(A) SMA-32 MNs transduced with either AAV9_CAG_*Co-hSMN1 *at MOI 1x10$^5$ or IDLV_CMV_*Co-hSMN1 *at MOI 75. (B) Quantification of (A) showing 1.9-fold increase in SMN following AAV9 transduction, but IDLV transduction significantly increased SMN protein by 66-fold (P>0.001). Significance assessed by one-way ANONA with Dunnett's multiple comparison test.*

### 6.4.2 Transcriptional regulation of *Co-hSMN1* expression from IDLVs

An initial experiment was performed in wild type AD3-CL1 MNs to assess any differences in SMN protein expression following IDLV_*Co-hSMN1* transduction where three different promoters were used to drive transgenic expression. Here, as expected, we see IDLV_CMV_*Co-hSMN1* vectors led to significant increases in SMN of 4.36-fold (P=0.0350; Figure 6.4) whereas, hSYN_*Co-hSMN1* and hPGK_*Co-hSMN1* vectors led to 2.97- and 2.87-fold increases in SMN protein compared to mock treated cells, however, these were not significant (P=0.2580 and P=0.3998, respectively). In part, this result reflects the pattern observed when SMA fibroblasts were transduced with vectors transcriptionally regulated by the three different promoters. In both experiments, CMV controlled vectors outperformed hSYN and hPGK controlled vectors. A difference, however, was apparent where hSYN-controlled vectors induced marginally higher SMN protein expression compared to hPGK controlled vectors in MNs, although this was non-significant. This data may be reflective of the neuronal-specific nature of the hSYN promoter.

Further to the initial pilot experiment in wild type AD3-CL1 MNs, this experiment was repeated in three SMA MN lines to determine if the same pattern was recapitulated. As expected IDLV_CMV_*Co-hSMN1* transduction led to significant increase in SMN expression in all three SMA type I MN lines (SMA-13: 14.5-fold, P<0.0001; SMA-19: 79.8-fold, P<0.0001; SMA-32: 42.8-fold, P<0.0001; Figure 6.5 and Figure 6.6). IDLV_hSYN_*Co-hSMN1* only produced a significant increase in SMN protein following transduction of SMA-13 MNs (SMA-13: 3.66-fold, P=0.0182; SMA-19: 9.55-fold, P=0.3441; SMA-32: 5.60-fold, P=0.2514; Figure 6.5 and Figure 6.6). IDLV_hPGK_*Co-hSMN1* transduction led to significant increases in SMN protein following transduction of all SMA MN lines (SMA-13: 6.13-fold, P=0.0004; SMA-19: 13.2-fold, P<0.05; SMA-32: 18.0-fold, P=0.0005; Figure 6.5 and Figure 6.6). Data were statistically analysed using a one-way ANOVA with Dunnett's multiple comparisons post-test.

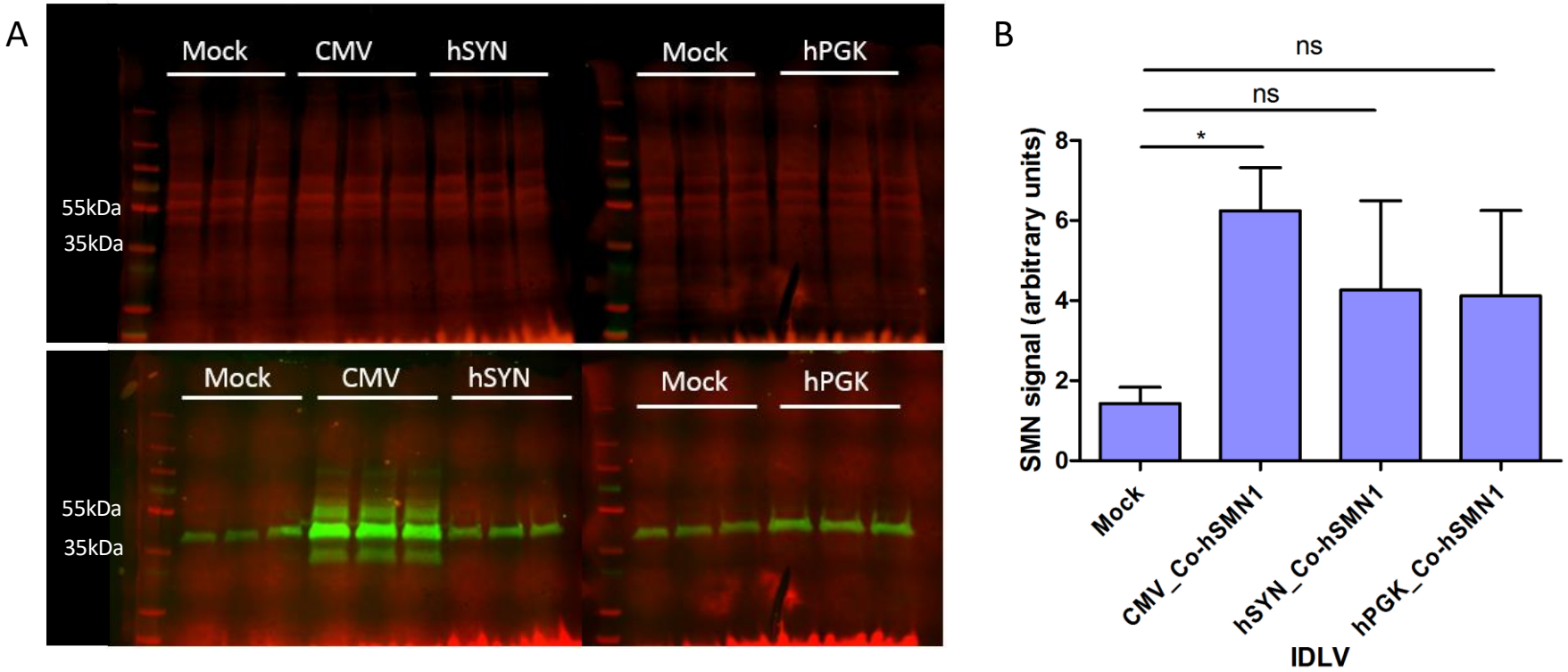


***Figure 6.4 Transduction of wild type AD3-CL1 MNs with IDLVs expressing* Co-hSMN1 *under three transcriptional controls.***

*Wild-type AD3-CL1 iPSC-MNs were transduced with IDLV_*Co-hSMN1 *under transcriptional control of either CMV, hSYN or hPGK at MOI 75 then protein was harvested and analysed after 72 hours. (A) Mock samples were loaded onto both gels to avoid any effects of differing transfer efficiencies; all six lanes were quantified and used in statistics. The first hPGK replicate in (A) was not quantified due to the appearance of a bubble or tear that would interfere with results. (B) A one-way ANOVA with Dunnett's multiple comparison test to compare all transduced samples to the mock control revealed significant increases in SMN protein only by CMV_*Co-hSMN1 *P=0.0350), but not by hSYN- or hPGK-controlled vectors (P=0.2580 and P=0.3998, respectively).*

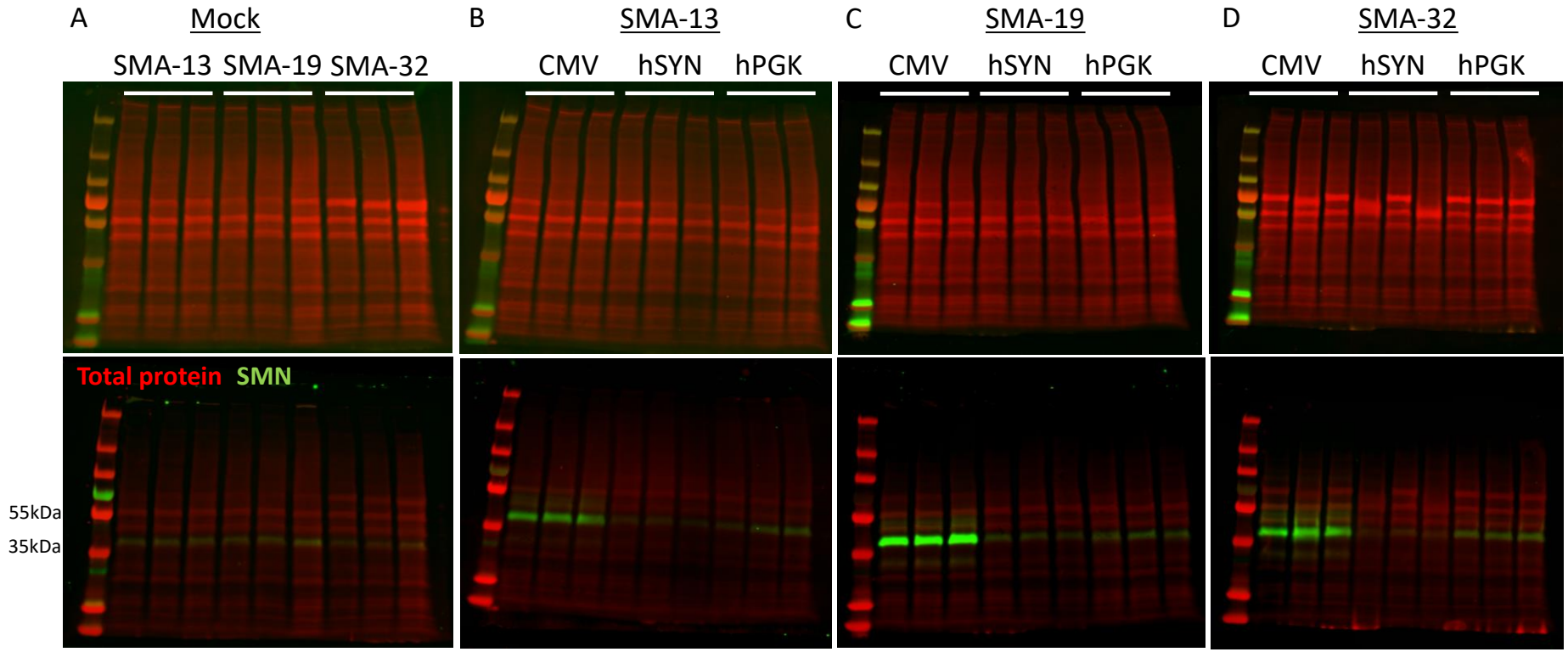


***Figure 6.5 Transcription regulation of* Co-hSMN1 *expression from IDLVs using CMV, hSYN and hPGK promoters in SMA MNs.***

*Three SMA type I MN lines (SMA-13, SMA-19 and SMA-32) were transduced upon reaching maturity (day 28 of differentiation) at MOI 75. Total protein was used as a loading control. Blots were quantified and are presented in Figure 6.6.*

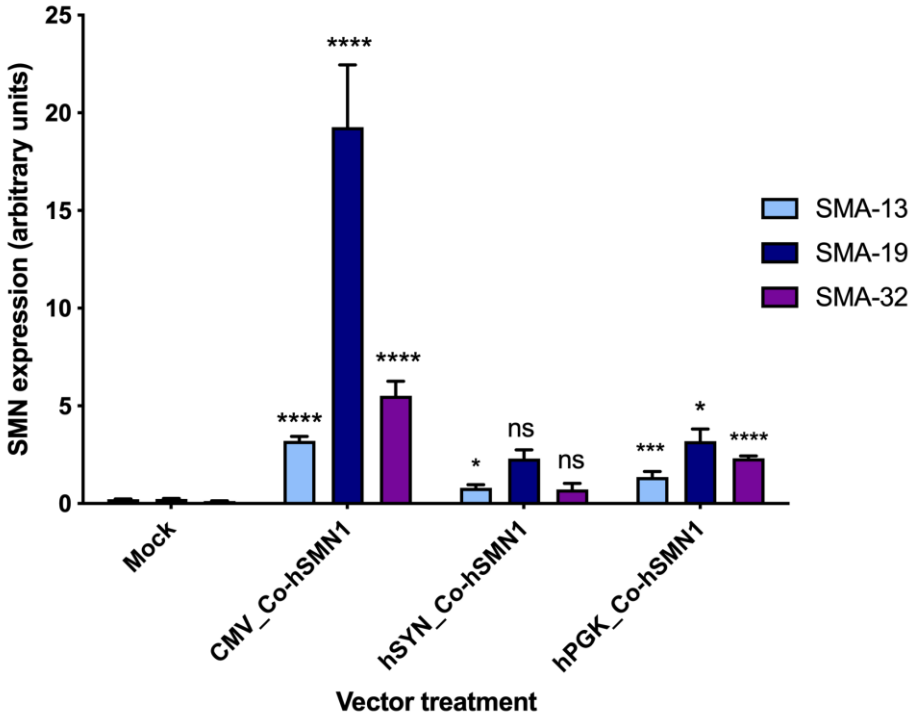


***Figure 6.6 Quantification of SMN expression following transduction of three SMA type I MNs with IDLV_Co-hSMN1 using CMV, hSYN or hPGK promoters.***

*Western blots performed using protein lysates from SMA type I MNs transduced with either IDLV_CMV_*Co-hSMN1*, IDLV_hSYN_Co-hSMN1 or IDLV_hPGK_Co-hSMN1 (see Figure 6.5 for blots) were quantified. One-way ANOVAs were used to assess statistical significance within each MN line. Transduction with IDLV_CMV_*Co-hSMN1 *led to significant increases in SMN protein expression in all three lines (all P<0.0001) compared to mock treated cells. This was not the case for IDLV_hSYN_*Co-hSMN1*, where only SMA-13 IDLV_CMV_*Co-hSMN1 *MNs had significant increases in SMN protein (P=0.0182). SMN levels in IDLV_hPGK_*Co-hSMN1 *transduced cells were significantly increased in all three lines (SMA-13: 6.13-fold, P=0.0004; SMA-19: 13.2-fold, P<0.05; SMA-32: 18.0-fold, P=0.0005).*

## 6.5 Downstream protein analysis in MNs

Reduced expression of Gemin2 has been shown in SMA MNs compared to wild type controls (Fuller et al., 2016), consistent with SMA type I fibroblasts expressing only 36% of control Gemin2 levels (Hao et al., 2007). Other gemin proteins (Gemin3, 4, 6 and 7) also showed similar levels of reduction, except for Gemin5, whose reduction was less pronounced (78%) (Hao et al., 2007). Transient knockdown of chicken SMN via tetracycline-repressible system was shown to cause a proportional decrease in Gemin2 protein (Wang and Dreyfuss, 2001).

### 6.5.1 Gemin2

A pilot experiment performed in SMA-32 MNs was completed to assess if transduction with IDLV_CMV_*Co-hSMN1* would affect Gemin2 protein levels. When assessed by western blotting, it was found that two bands appeared (Figure 6.7A), however, only the lower band was quantified as this was located just below the 35kDa ladder band, more accurately representing the 32kDa protein Gemin2. Preliminary data from this experiment showed that IDLV_CMV_*Co-hSMN1* transduced SMA-32 MNs (MOI 75) had significantly increased Gemin2 protein levels (Figure 6.7B, $P<0.0001$) above mock transduced samples. As this evidence proved that transduction does affect Gemin2 levels, a larger scale experiment was conducted to confirm this.

Basal levels of Gemin2 were assessed in all six iPSC MN lines, as well as levels in SMA-13, SMA-19 and SMA-32 MNs transduced upon reaching maturity with IDLV_CMV_*Co-hSMN1* at MOI 75. Again, only the lower band appearing on western blots was quantified according to the expected size (32kDa) of Gemin2. Non-significant differences were observed between almost all line's basal levels of Gemin2, except when 19-9-7T and SMA-32 specifically were compared which showed a significant difference (Figure 6.8A,B $P=0.0416$). These two lines, respectively, showed the highest and lowest levels of Gemin2 in samples assessed. Upon transduction of SMA type I MNs, levels of Gemin2 were not different to basal levels, in contrast to preliminary data (SMA-13: $P=0.0859$, SMA-19: $P=0.0683$, SMA-32: $P=0.3363$; Figure 6.8C). Specifically, the SMA-32 data here highlight inter-experiment variability; although an increased Gemin2 was seen after transduction in

both the pilot and larger scale experiment, this was only significant in preliminary data.

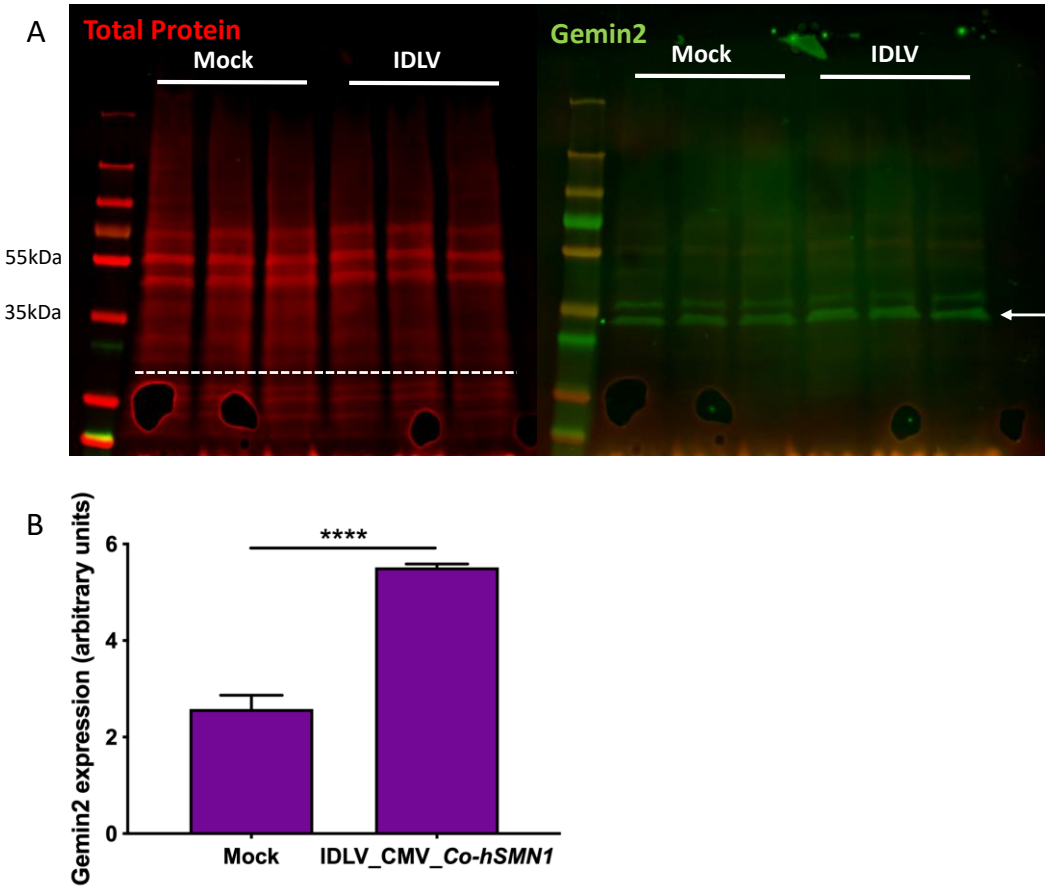


***Figure 6.7 Preliminary data assessing Gemin2 expression in SMA-32 MNs transduced with IDLV_CMV_Co-hSMN1.***

*SMA-32 MNs were transduced with IDLV_CMV_*Co-hSMN1 *at MOI 75 upon reaching maturity at day 28 of differentiation; 72 hours later, cells were lysed for protein extraction. Total protein was used as a loading control but was only quantified above the dotted line in (A) to avoid bubbles. Gemin2 was blotted for and produced two bands, the lower band was quantified as this matched the expected 32kDa size of Gemin2. (B) Transduced samples showed significant increased levels of Gemin2, compared to mock transduced samples (P=0.05). Statistical analysis was performed using an unpaired, one-tailed Mann-Whitney test.*

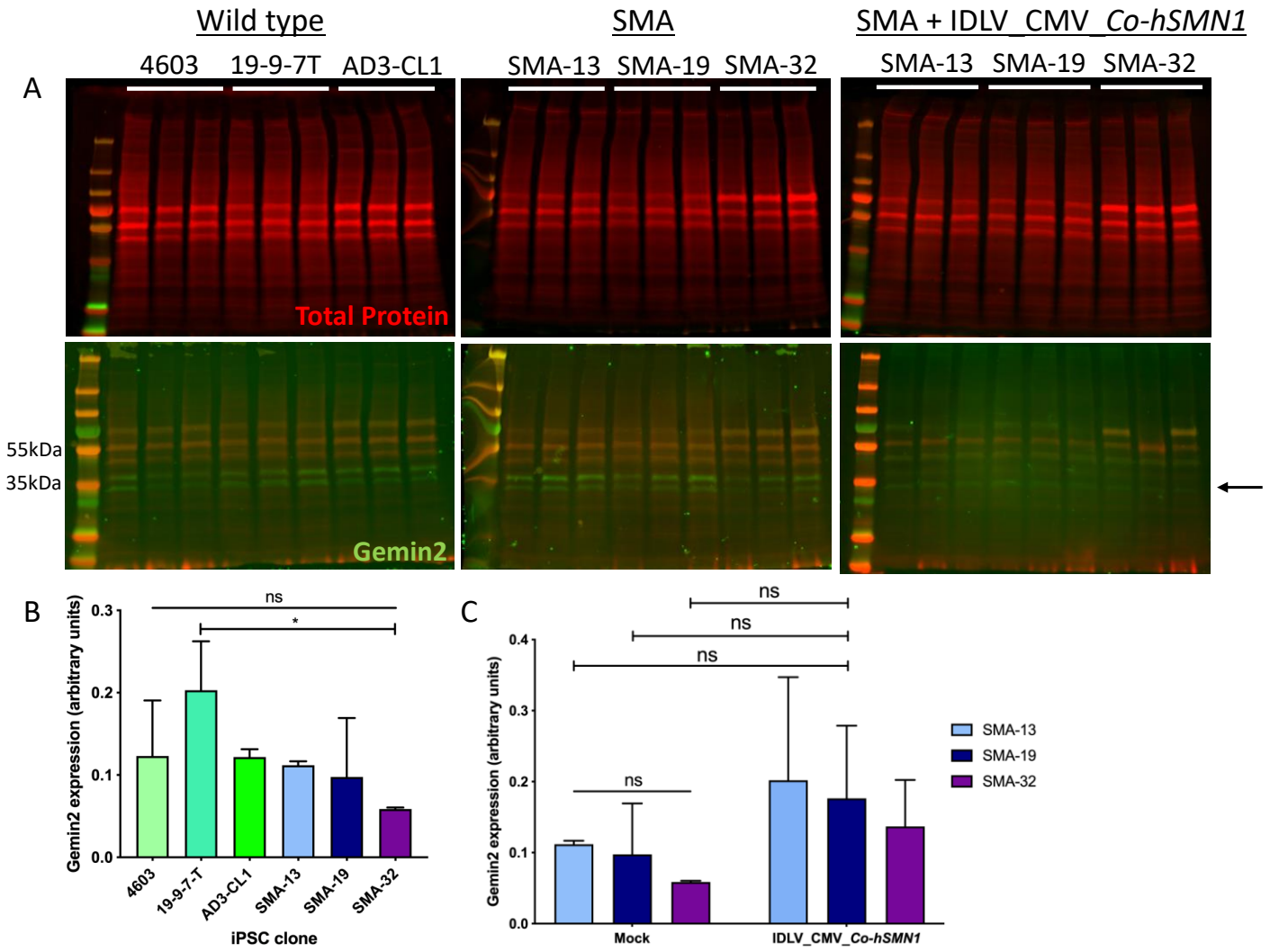


***Figure 6.8 Gemin2 expression in wild type, SMA type I and SMA type I MNs transduced with IDLV_CMV_Co-hSMN1.***

*(A) Protein lysates from wild type and SMA type I MNs were run on western blots alongside samples from SMA type I MNs transduced with IDLV_CMV_*Co-hSMN1 *at MOI 75 as in the previous figure. Total protein was used as a loading control. Gemin2 was blotted for and produced two bands, the lower band was quantified as this matched the expected 32kDa size of Gemin2 (indicated by arrow). (B) Basal levels of Gemin2 expression were assessed in wild type and SMA type I MNs and generally no significant differences were found, except when comparing 19-9-7T and SMA-32 specifically which was just significant (P=0.0416). Statistical analysis was performed using a one-way ANOVA with Bonferroni multiple comparisons. (C) Transduced SMA type I MNs were expected to show increased levels of Gemin2 based on preliminary data from SMA-32 MNs shown in Figure 6.7; but this was not confirmed here as all three SMA lines were found to have non-significant differences between basal and transduced levels of Gemin2 (SMA-13: P=0.0859, SMA-19: P=0.0683, SMA-32: P=0.3363). Statistical analyses was performed using an unpaired, two-tailed t-tests.*

## 6.6 Discussion

Despite many groups having generated and characterised SMA iPSC MNs, little evidence exists in the literature regarding the transduction of these with viral vectors and subsequent use as a therapeutic avenue. The vast majority of SMA gene therapy research has been conducted in mouse models of SMA (see chapter 3). Although, some literature has presented iPSC MN data in papers that also contain *in vivo* correction. This being said, the phenotype or deficiency revealed in iPSC MNs is never normally corrected *in vitro*, instead *in vivo* correction is sought more immediately. Colleagues at University of Edinburgh, in collaboration with iStem in France, have presented data confirming reduced SMN and UBA1 protein expression in MNs and then subsequently the delivery of an AAV9_*UBA1* vector to mice models (Powis et al., 2016). However, this vector was not used to transduce MNs. It is unclear why this *in vitro* work was not carried out as it would have provided translational evidence of UBA1 expression *in vitro* in human tissues and then later *in vivo*, strengthening their argument that *UBA1* is a viable therapeutic target for gene therapy. It is important to test therapeutics in iPSC MNs as well as attempting rescue *in vivo* so that a better understanding of MN biology following treatment can be ascertained. Otherwise, only general assumptions of MN health based on cell number and biodistribution of the transgene within MNs can be sought, whereas improvements in survival or health of an animal as a whole may be due to non-MN related benefits.

Here, evidence that IDLVs expressing *Co-hSMN1* can induce SMN protein increases in three SMA type I MN lines was obtained. These data corroborate

results observed in chapter 4, where transduction with IDLVs expressing *Co-hSMN1* was able to both increase SMN protein in SMA type I fibroblasts (section 4.9) and increase gem number as a functional endpoint in Neuro2a and SH-SY5Y neuroblastoma cells (section 4.7). Further to this, iPSC MN results are similar to those obtained when primary embryonic rat MNs were cultured *in vitro* and transduced with the same vectors (Ali Mohammadi Nafchi, 2017). Results showed significant increases in SMN mean fluorescent intensity in a dose dependent manner (Ali Mohammadi Nafchi, 2017). Taken together, these results provide robust evidence that IDLVs present a viable therapeutic strategy to increase SMN expression *in vitro*; the potential physiological benefits of which will be explored in the following chapter.

When comparing equivalent expression cassettes configured in both IDLV and AAV9 vector forms, no significant increases in SMN protein were seen following transduction by AAV9_CAG_*Co-hSMN1*. This recapitulates earlier evidence in SMA type I fibroblasts that were transduced even in the presence of polybrene to increase transduction efficiency (section 4.9). In this project, significant increases in SMN protein following AAV9 transduction have only been seen in CHO cells that were induced to exit the cell cycle (section 4.10.3) at MOIs of $1x10^5$ or higher. However, MNPs stop proliferating at approximately day 18 of differentiation and mature into quiescent MNs, yet no SMN increase was seen. The poor results here from AAV9_CAG_*Co-hSMN1* are in stark contrast to the successes seen in *in vivo* models of AAV9 gene therapy for SMA. Biodistribution of GFP expression following *in vivo* administration of AAV9 vectors has shown 42% GFP-positive lumbar spinal MNs 10 days post-injection (Foust et al., 2010), whilst other studies have shown higher values up to 66% (Valori et al., 2010). SMN expression has been seen in ChAT-positive cells by immunofluorescence (Foust et al., 2010) with one study reporting 49% MNs in cervical spinal cord sections expressing SMN (Valori et al., 2010). SMN-expressing MNs increase in number in AAV9-treated mice to levels similar to wild type animals (Dominguez et al., 2011), highlighting a survival benefit to MNs specifically following this gene therapy.

Transcriptional control of transgene expression is an important factor to consider when designing gene therapies. In chapter 4 it was shown that CMV-driven *Co-hSMN1* cassettes outperformed those transcriptionally controlled by hSYN or hPGK, but all of which could induce significant increases in SMN expression. Here, data from wild type and three SMA type I MNs revealed a similar pattern with CMV-

controlled vectors consistently providing the highest SMN increases in all lines, whilst hPGK transduced SMA-19 MNs was the only other condition to induce an increase in SMN protein. SMA-19 consistently had the largest fold differences in SMN expression, suggesting that perhaps this line is easier to transduce with IDLVs than SMA-13 or SMA-32. It was interesting to learn that hSYN-controlled vectors could not increase SMN protein expression in any MN line, despite the neuronal specificity of this promoter. The hSYN promoter has been shown to drive strong transgene expression *in vivo* following administration of both lentiviral (Dittgen et al., 2004) or adenoviral (Kugler et al., 2001, Kugler et al., 2003) vectors, but it's use *in vitro* has been less well studied. It remains unclear why increased SMN expression could not be seen here.

In this thesis it has been shown that the number of gems can be restored by IDLV_*Co-hSMN1* transduction as assessed by immunofluorescence when cells where immunostained with an SMN, but not Gemin2, antibody (section 4.7) . In this chapter, it was shown that a similar pattern of data emerges when assedded by western blot. IDLV_*Co-hSMN1* transduction can lead to an increase in SMN protein, similar to the increase in gems detected by SMN immunofluorescence, but neither assay was able to detect an increase in Gemin2. This perhaps suggests that an increase in, and correct localisation of, Gemin2 may require a slightly longer time period before detection by immunofluorescence and western blot following IDLV_*Co-hSMN1* transduction. SMN and Gemin2 are closely interlinked within the cell and together with other SMN-complex members aid in snRNP assembly, promoting interactions between newly transcribed RNA and it's binding partners (Monani, 2005). It has been found that Gemin2 stabilises the SMN complex via self-interaction (Ogawa et al., 2007), Gemin5 is able to bind *SMN* mRNA to transcriptionally regulate expression (Workman et al., 2015) and gemin-bound SMN is more stable than unbound SMN assessed by a pulse-chase assay (Burnett et al., 2009). It is therefore tempting to speculate that if gemin proteins can promote *SMN* expression and stabilisation, that this role could occur vice versa and SMN could indeed post-translationally stabilise the Gemin2 protein, although not confirmed here.

It is interesting to note that data presented here show no difference between overall wild type and SMA type I Gemin2 levels, contradictory to what has been published elsewhere (Hao et al., 2007). However, quantitative mass spectrometry has revealed notable differences in proteomic expression profiles in wild type control

and SMA motor neurons (Fuller et al., 2016), but even this technique was not able to detect differential expression of SMN or gemin proteins between wild type and SMA MNs (Fuller et al., 2016). Only the 30% most abundant proteins can be accurately identified (Hornburg et al., 2014) through this technique and as such, differences in the expression of SMN and gemin proteins (whose complex only constitutes a small fraction of the proteome) may have been below the limit of detection (Fuller et al., 2016).

## 6.7 Conclusions

It is encouraging to notice that the IDLV_*Co-hSMN1* expression data presented in this chapter reflect the data from equivalent experiments in cell lines, providing robust evidence of the promise of these vectors. It has been shown that iPSC-derived MNs are able to be transduced with high efficacy and the presence of viral vectors is tolerated well. Upon IDLV_*Co-hSMN1* transduction, all three SMA lines showed increased SMN protein and analysis of different vector transcriptional controls revealed that CMV-driven vectors were superior, as shown in fibroblasts previously. Finally, an increase in SMN protein expressed by IDLVs, does not turn increase the downstream expression of Gemin2. IDLV_*Co-hSMN1* expression in MNs is vitally important in the development of IDLVs as a potential therapeutic strategy for SMA, it is still necessary to translate this *in vivo* to see if the *in vitro* successes seen here translate to an increase in survival or functional benefits in a SMA mouse model, although this was beyond the scope of this project.

# 7 Phenotypic rescue using IDLV expression of *Co-hSMN1*

## 7.1 Introduction

It is well-established that MNs are particularly vulnerable to a lack of SMN protein, so a goal of gene therapy for SMA has been to increase SMN in these at-risk populations. SMA MNs show phenotypes *in vitro* including reduced soma size, neurite length and growth cone area (Corti et al., 2012), significant declines in cell number over time (Sareen et al., 2012), abnormal nicotinic AChR clustering at NMJs (Yoshida et al., 2015), and evidence of proteomic dysregulation (Fuller et al., 2016) compared to wild type MNs.

In the previous chapters, and elsewhere in the literature, it has been shown that transduction of MNs with an *SMN*-encoding vector can increase the SMN protein levels within vulnerable MNs. However, it is important to understand the consequences of SMN restoration to wild type levels or higher, and what effect this might have on cells that have always been severely deficient in SMN.

### 7.1.1 DNA damage- and apoptosis-related proteins and their involvement in SMA

In this chapter, I have attempted to identify and correct DNA damage and apoptotic phenotypes to elucidate how SMN modulates these. These phenotypes have been less well studied in SMA model systems than those highlighted above and so the molecular links between SMN and DNA damage- and apoptosis-related proteins are less clear. Understanding how SMN interacts with and modulates these pathways is an important step to understanding why SMA MNs degenerate and how this may be prevented by treatment with a *SMN*-encoding vector. Here, three proteins of interest were investigated; ATM (and its phosphorylated form, pATM), γH2AX and cleaved caspase 3. Details of their involvement in SMA and the molecular mechanisms or pathways that link these proteins (Figure 7.1) are provided in the sections below.

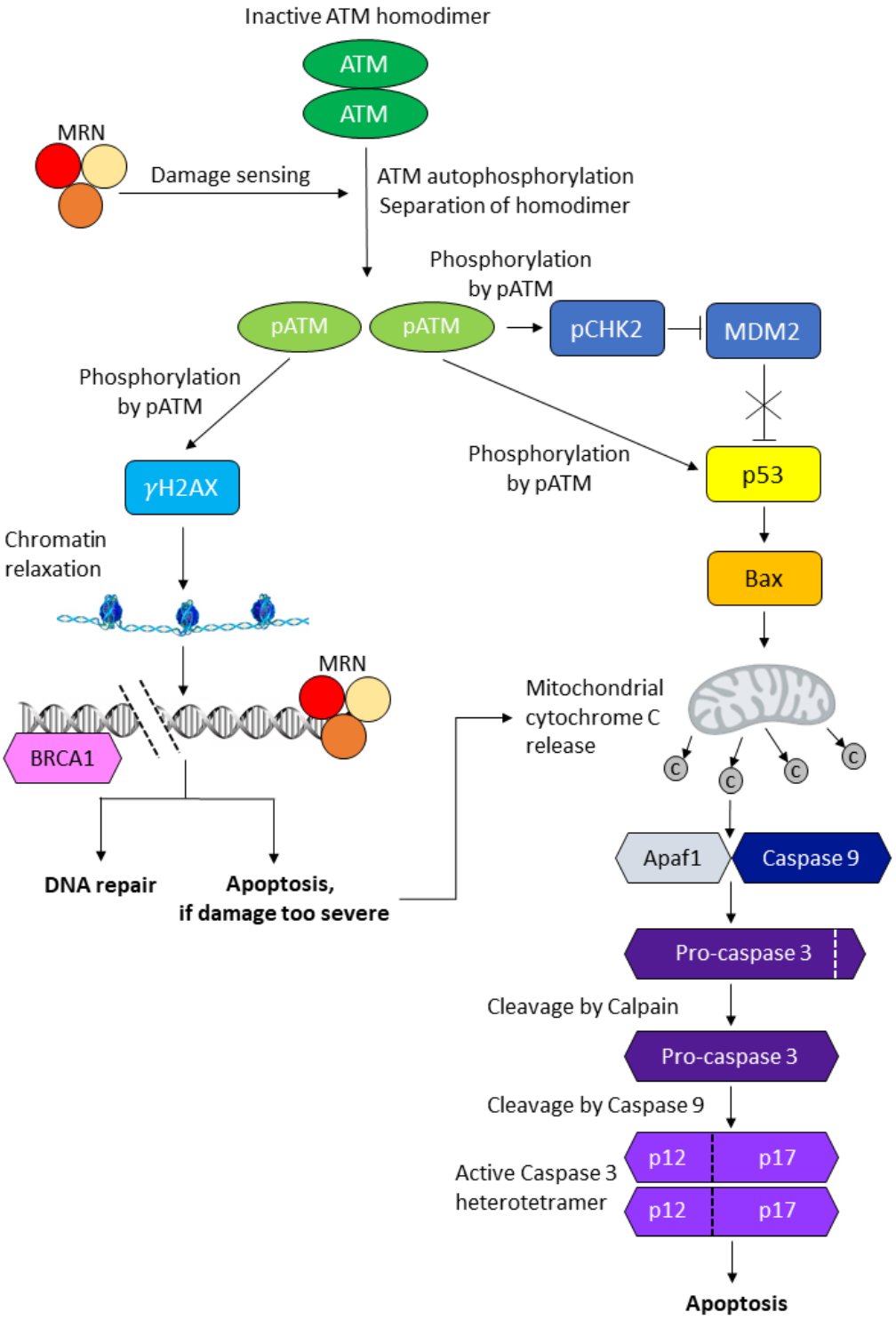


***Figure 7.1 The involvement of ATM, γH2AX and cleaved caspase 3 in DNA damage and apoptotic pathways.***

*In its role as 'chief mobiliser' of the cellular response to damage, ATM is activated (by autophosophorylation at Ser1981 and separation of its homodimer) upon the MRN complex (consisting of the proteins MRE11, Rad50 and NBS1) sensing damage such as DNA double strand breaks (DSBs). pATM then phosphorylates downstream transducer proteins such as H2AX at Ser139 to form γH2AX, p53 at Ser15 or others such as CHK2. γH2AX induces decondensation of chromatin through acetylation of histones surrounding DSBs, again sensed by the MRN*

*complex. Effector proteins such as BRCA1 are then recruited to initiate DNA repair pathways. Should ATM recognize that the cellular damage is too severe, it can transduce a signal to initiate apoptosis by phosphorylating CHK2 to prevent p53 degradation via MDM2, or by phosphorylating p53 itself. The action of p53 then proceeds via activation of Bax and release of cytochrome c from mitochondria. Cytochrome c, Apaf1 and caspase 9 together are known as the apoptosome as they initiate caspase 3 activation. Caspase 3 is activated through calpain-mediated cleavage of the pro-domain then caspase 9 mediated cleavage of the remaining 29kDa protein into p12 and p17 subunits. These subunits aggregate into a heterotetramer representing the cleaved, or active form of caspase 3, executing apoptosis within the cell. Circles represent sensor proteins, ovals represent transducers, boxes represent secondary transducers and hexagons represent effector proteins.*

#### 7.1.1.1 ATM

Ataxia Telangiectasia Mutated (ATM) is a 350kDa protein kinase that is a member of the phosphatidylinositol 3-kinase-like family, also including proteins such as ATR and DNA-PKcs (Blackford and Jackson, 2017). ATM is often called the 'chief mobiliser' of the cellular DNA damage response, most importantly following DNA double strand break (DSB) incidence. ATM acts as a transducer, coordinating the phosphorylation of downstream proteins such as p53, CHK2, and H2AX (discussed in section 7.1.1.3), either leading to DNA repair by effector proteins like BRCA1 or apoptosis via the caspase cascade (discussed in section 0) if the damage is too severe (Figure 7.1).

Reductions in SMN have been shown to causes increases in signaling pathway proteins relating to the DNA damage response (DDR) such as ATM, BRCA1 and particularly p53 which showed very early activation following SMN depletion (Jangi et al., 2017). Upregulation of phosphorylated ATM (pATM) has been seen following acute siRNA knockdown of SMN in HeLa cells and in chronic SMN depleted, SMA type I fibroblasts, but phosphorylation was not induced in post-mitotic SMA spinal cord lysates or primary SMA mouse neurons (Kannan et al., 2018).

pATM and pBRCA1 are proteins involved in homologous recombination (HR)-mediated DNA repair, as well as pATR and pCHK1. pATR and pCHK1 are upregulated in SMA primary neurons and spinal cord lysates, but DNA DSBs still accumulate, suggesting the HR DDR pathway is inactive in SMA post-mitotic tissues (Figure 7.2). DNA-PKcs is the primary protein that transduces non-homologous end joining (NHEJ)-mediated DNA repair, but this has been found to be deficient in SMA fibroblasts, primary neurons and spinal cord (Kannan et al., 2018).

This DNA-PKcs deficiency will render post-mitotic SMA neurons without a working DDR pathway (Figure 7.2). This will lead to genomic instability and markers of DSBs, e.g. γH2AX (as discussed in section 7.1.1.3), as well as the induction of apoptosis by cleaved caspase 3 (section 0). Genomic instability has been proposed as a cause of neurodegeneration in ALS systems where defective ATM-mediated DNA repair signaling is also seen, highlighting conserved mechanisms of MN degeneration across diseases (Walker et al., 2017).

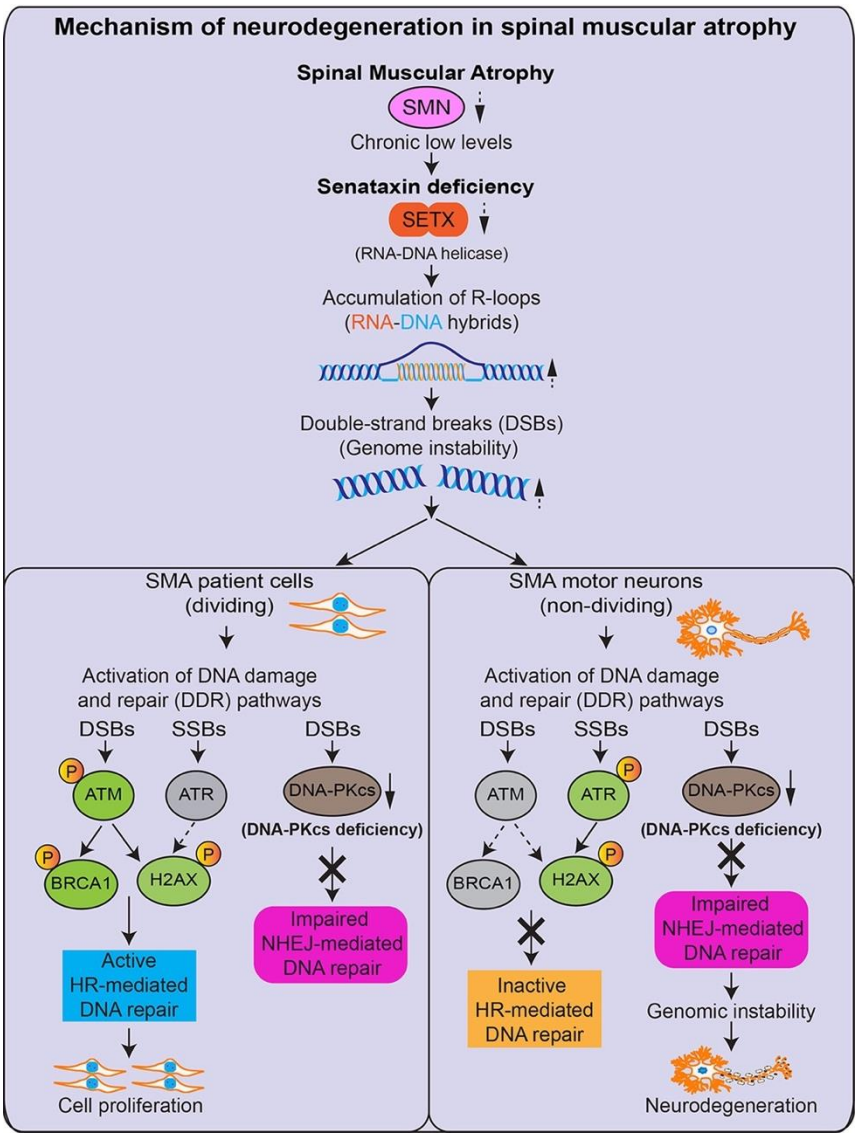


***Figure 7.2 A proposed molecular mechanism to explain how a defective DNA damage response may cause neurodegeneration in SMA cells.***

*A lack of SMN protein may lead to deficiencies of proteins such as Senataxin (SETX; a RNA-DNA helicase) and DNA-PKcs (DNA-dependent protein kinase, catalytic subunit). Genomic instability may be caused by structures such as R loops (three stranded nucleic acid structures consisting of two DNA and one RNA strands), causing DSBs to form. These can be repaired in dividing cells by BRCA1 and γH2AX (pH2AX) in HR coordinated by ATM. Post-mitotic neurons have inactive HR-mediated repair, but cannot repair DSBs by NHEJ either due to the DNA-PKcs deficiency caused by a lack of SMN. The inability to repair DSBs may cause neuronal degeneration. DSB = DNA double strand break, SSB = DNA single strand break, HR = homologous recombination, NHEJ = non-homologous end joining. Figure taken from Kannan et al. (2018).*

#### 7.1.1.2 Cleaved caspase 3

Caspase 3 is known as an executioner caspase of apoptotic cell death (Figure 7.1) (Martin and Green, 1995). The activation of caspase 3 is tightly regulated by the apoptosome consisting of apaf1 and caspase 9; this itself is only activated upon release of cytochrome c from mitochondria (Deveraux et al., 1998). The activation of caspase 3 is initiated by calpain-mediated proteolysis and removal of a 3kDa peptide from the pro-caspase 3 protein. Removal of this silencing pro-domain (Meergans et al., 2000) induces spontaneous proteolysis by caspase 9, separating the remaining 29kDa protein into p12 and p17 subunits (so named due to their respective sizes in kDa) (Han et al., 1997). Active, or cleaved, caspase 3 forms a heterotetramer of two p12 and two p17 subunits that then executes apoptosis. Cleaved caspase 3 may then act in a positive feedback loop by activating caspase 9 (Deveraux et al., 1998), further enhancing the apoptotic cascade.

The viability of NSC-34 neuroblastoma cells has been shown to be reduced by 23% following siRNA knockdown of SMN with 37.4% of cells exhibiting DNA fragmentation, a significant increase compared to control siRNA treated cells (Parker et al., 2008). Caspase 3 activity remained elevated in SMN depleted cells long after an initial spike caused presumably by the transfection of the siRNA itself (Parker et al., 2008). SMA iPSC MN cultures showed more cleaved caspase 3-positive cells than wild type MN cultures, with nuclear condensation seen in a higher percentage of cells too (Sareen et al., 2012).

Figure 7.3 shows the multiple points at which SMN exerts anti-apoptotic properties, something that SMNΔ7 is unable to do (Kerr et al., 2000). SMN has been proposed to interact with anti-apoptotic Bcl-2 to provide dual protein-mediated anti-apoptotic action against Bax-and Fas-mediated apoptosis (Iwahashi et al., 1997), but this binding is contentious (Sareen et al., 2012) as another study found no binding *in vivo* (Coovert et al., 2000). SMN itself blocks calpain-mediated removal of a 3kDa pro-domain to activate pro-caspase 3 (Anderton et al., 2011), reducing caspase 3 activation. Furthermore, SMN-ZPR1 interactions (Gangwani et al., 2001), may reduce caspase 3 cleavage by caspase 9 still. One study has also found that 67% of SMA type I patients also had deletions in the first two coding exons of the *NAIP* gene which lies immediately adjacent to *SMN* (Roy et al., 1995). The NAIP protein directly inhibits caspase 3 and 7 (Maier et al., 2002), so truncating mutations will further increase levels of apoptosis in SMA patients.

Apoptosis is a tightly regulated pathway that is controlled by both intrinsic and extrinsic means and the question of SMN's role in either of these pathways, independently of each other, or interlinked, remains to be answered. Although many of the anti-apoptotic roles of SMN are known and have been described above, it is still unclear how the addition of ectopically expressed SMN may modulate the apoptotic phenotype in SMA. Should ectopic SMN be able to reduce the level of apoptosis in SMA cells, this could prove beneficial for SMA patients by reducing MN loss.

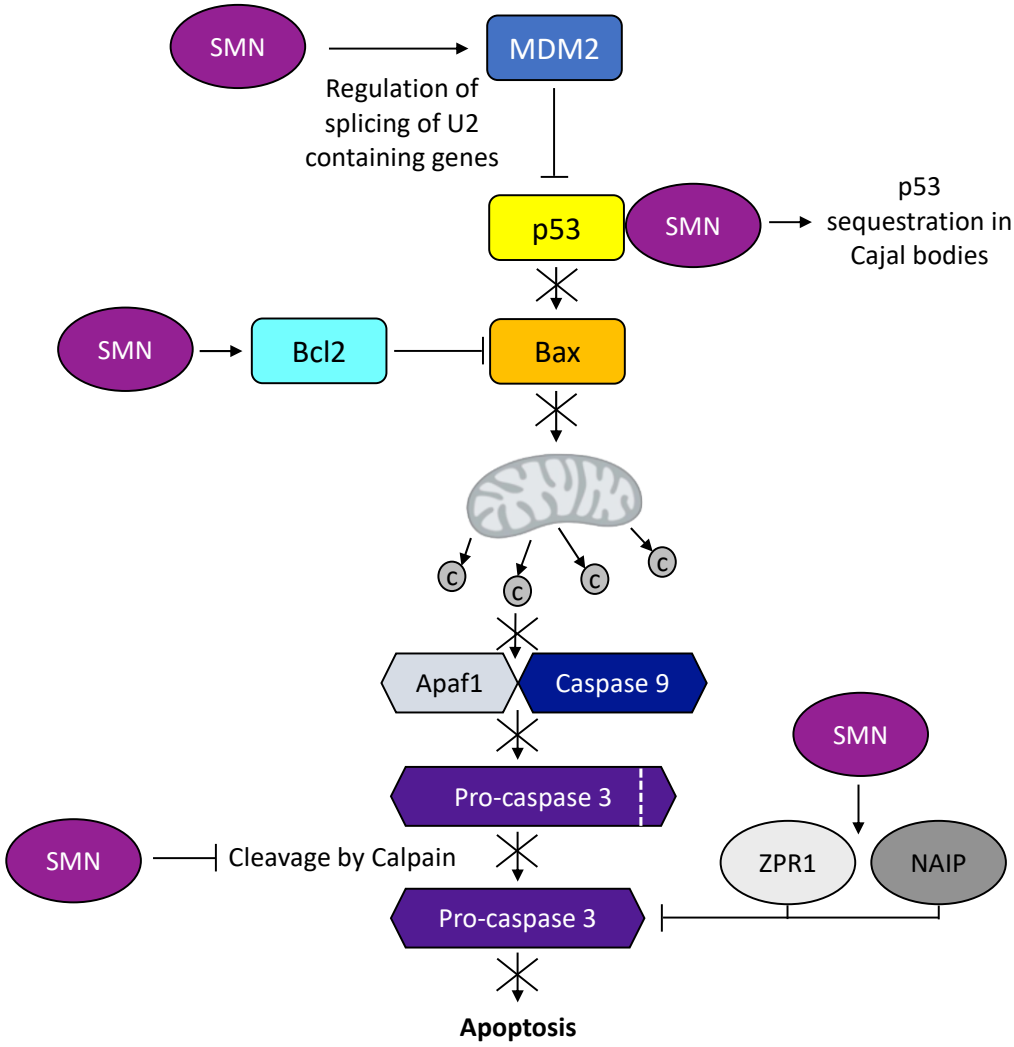


***Figure 7.3 The role of SMN as an anti-apoptotic protein.***

*SMN acts as an anti-apoptotic factor at multiple stages of the apoptotic pathway. Through the action of snRNPs, SMN regulates the splicing of U2-intron-containing genes, such as MDM2. SMN binds to p53 via a domain encoded by exon 2 of the SMN gene, this leads to localisation of the complex within Cajal bodies in the nucleus. p53 can then no longer activate the pro-apoptotic protein Bax. Bax is also inhibited by the action of Bcl2, a protein proposed to interact with SMN. SMN itself inhibits Calpain-mediated cleavage of pro-caspase 3 and then interacts with ZPR1 and NAIP proteins that further inhibit caspase 9-mediated cleavage. Together, these actions tightly regulate apoptosis, preventing unnecessary cell death.*

#### 7.1.1.3 γH2AX

H2AX, a histone protein, was discovered to be phosphorylated on Ser139 following DSBs (Rogakou et al., 1998) resulting in the phosphorylated form (γH2AX) accumulating in nuclear foci within three minutes of exposure to ionizing radiation or laser treatment (Rogakou et al., 1999). The presence of γH2AX at DSBs recruits chromatin modifier complexes that acetylate neighbouring histones and leads to the decondensation of chromatin surrounding the DSB (Figure 7.1). Relaxed chromatin structures sensed by the MRN complex of proteins (MRE11, Rad50 and NBS1) recruit effector proteins such as BRCA1 to initiate DNA repair (Figure 7.1).

In an inducible model of SMA where adult mice (*Smn*$^{-/-}$ with 4 copies of *SMN2*) were administered an ASO that mediated the skipping of exon 7 causing a severe SMA phenotype, γH2AX foci were found in 12.11% of pyramidal neurons within the hippocampus, compared to 0.13% in control animals (Jangi et al., 2017). It was also found that transient short hairpin RNA-mediated knockdown of SMN in both SH-SY5Y neuroblastoma cells and healthy iPSC-derived MNs induced activation of γH2AX signaling (Jangi et al., 2017). γH2AX can be detected in chronic SMA systems as well as those acute SMN knockdowns just described. Immunohistochemistry of muscle sections from the Burghes' severe SMA model has shown strongly γH2AX-positive cells, something not seen in littermate controls (Mutsaers et al., 2011). γH2AX activation has been seen in both fibroblasts and lumbar spinal cord sections from SMA type I patients (Kannan et al., 2018).

The presence of γH2AX in multiple SMN depleted systems suggests an accumulation of DNA damage or dysregulation of DNA damage signaling proteins. It is therefore important to understand how a lack of SMN mediates this, how DNA damage response proteins are interlinked with those controlling apoptosis in SMA models and how these phenotypes might be rescued if SMN was ectopically expressed.

## 7.2 Aims

In this chapter I aimed to validate DNA damage response and apoptotic phenotypes in SMA cells and assess if these could be rescued by transduction. As this work involved the use of previously untested reagents in this laboratory, it was necessary

to first optimise some of the assays described using SMA type I fibroblasts before their attempted implementation in SMA type I MNs. This aimed to reduce resource wastage on harder-to-grow MNs and provide proof of principle that detection of selected phenotypes was successful. Specifically, my objectives were:

(A) Design and implement a flow cytometric assay to assess MN survival with and without transduction.
(B) Optimise assays to detect the expression of ATM, pATM, cleaved caspase 3 and γH2AX.
(C) Compare the expression of the above proteins in SMA type I and wild type fibroblasts.
(D) Assessment of the effect of transduction with IDLV_CMV_*Co-hSMN1* on ATM and pATM expression in both SMA type I fibroblasts and MNs.

## 7.3 MN survival

An overt phenotype has been reported where SMA MNs show survival deficits, compared to wild type cultures, towards the end of iPSC to MN differentiation protocols (Sareen et al., 2012). The numbers of SMI-32- and ChAT-positive MNs decline over time. This has also been seen in other MN diseases such as ALS (Bhinge et al., 2017). Therefore, a flow cytometry-based assessment of MN survival was implemented here to assess if this phenotype was recapitulated. This assay was also designed to measure survival of MNs with and without transduction to assess the effects of ectopic SMN.

### 7.3.1 Assay optimisation

Deficits in MN survival have been proposed to be caused by apoptosis, rather than a lack of MN genesis in cultures, or any other means of cell death. CellEvent™ Caspase-3/7 Green Detection Reagent is a visualisation tool that can be used to detect cells undergoing apoptosis by either fluorescent microscopy or flow cytometry. It has been shown to detect an increased population of apoptotic cells in ALS mutant MN cultures, compared to wild type (Bhinge et al., 2017).

Fluorescent microscopy of mature SMA-19 MNs showed some apoptotic nuclei (green staining overlaying DAPI staining) within large clusters of MN soma (Figure 7.4B). Yet, due to the nature of these cells growing in large networks (Figure 7.4A),

it was difficult to visualise many individual cells so a quantitative measure of apoptosis could not be drawn. Repetition of this experiment using MNs seeded at lower density, like that used for immunofluorescence analysis, would have been optimal, but due to time constraints this was not completed. To improve single cell analysis, this assay was translated to a flow cytometric protocol using MNs stained with propidium iodide (PI) or CellEvent™ Caspase-3/7 Green Detection Reagent.

Here, MNs were treated with 0.1% Virkon for 5 minutes prior to staining to act as a positive control for cell death. Virkon was used as a substance to insult MNs leading to immediate cell death, rather than the use of another compound (such as hydrogen peroxide or bleomycin used later in this chapter) with long incubation times for ease of flow cytometry set up. Single-stained samples were used as controls to set up the flow cytometry experiment (Figure 7.4C-E) and to measure the values for dead cells (stained with PI) or apoptotic cells (stained with CellEvent™). Unstained cells showed the expected population of autofluorescent cells to the left of the histograms (Figure 7.4C), with no detectable signal within gates for PE-A (to detect PI) and FITC-A (to detect CellEvent™) channels. PI only stained samples revealed a large population of dead cells in PE-A (Figure 7.4D, left) whilst also showing a peak with a small shoulder in the FITC-A channel gate (Figure 7.4D, right) suggesting some bleed through of PI signal detected in the wrong channel. CellEvent™ stained samples showed an apoptotic peak in the FITC-A channel (Figure 7.4E, right) only with no detection in PE-A channel.

When assessing SMA-19 MNs stained with PI or CellEvent™ Caspase-3/7 Green Detection Reagent in dot plots with both PE-A and FITC-A channels displayed simultaneously, we see diagonal line-shaped populations of cells for those stained with PI (Figure 7.5A) representing the signal being detected in both channels. This bleed through could not be omitted using compensation techniques. CellEvent™ only stained, insulted (0.1% Virkon) samples showed a clustering of points at the bottom of the dot plot (Figure 7.5A), but untreated samples still showed a diagonal line-shaped population again (Figure 7.5A). Dual-stained, untreated samples showed a different population shape, but unfortunately analysis of the dual-stained insulted sample was not possible for technical reasons. Overall, it was unclear what this data were representing so a different cell type was used simultaneously to assess if difficulties were cell type specific.

Primary splenocytes are particularly amenable to FACS analysis (owing to their small, round morphology which leads to easily definable populations) so these were isolated from a C57BL10 mouse by Dr Shan Herath then cultured for 2 days before being subjected to flow cytometry with help from Shan. 0.1% Virkon insulted, PI stained samples reveal a dense population of cells towards the top of the PE-A axis that is not present in the untreated sample (Figure 7.5B; circled in red), highlighting that 0.1% Virkon is able to induce cell death as expected. Insulted, CellEvent™ stained cells show an increase in density of the population towards the right of the FITC-A axis (Figure 7.5B; circled in red). Dual-stained samples show a denser population of cells towards the centre of the plot, representing dead, or dying cells (Figure 7.5B; circled in red).

Taken together, it is possible to say that the staining techniques and the flow cytometry protocols used were able to detect dead and dying populations of cells in this positive control experiment using primary splenocytes. As these were identical protocols used to that in MNs, with all flow cytometry represented in Figure 7.5 conducted simultaneously, it is possible to conclude that using these protocols for MNs specifically posed a challenge.

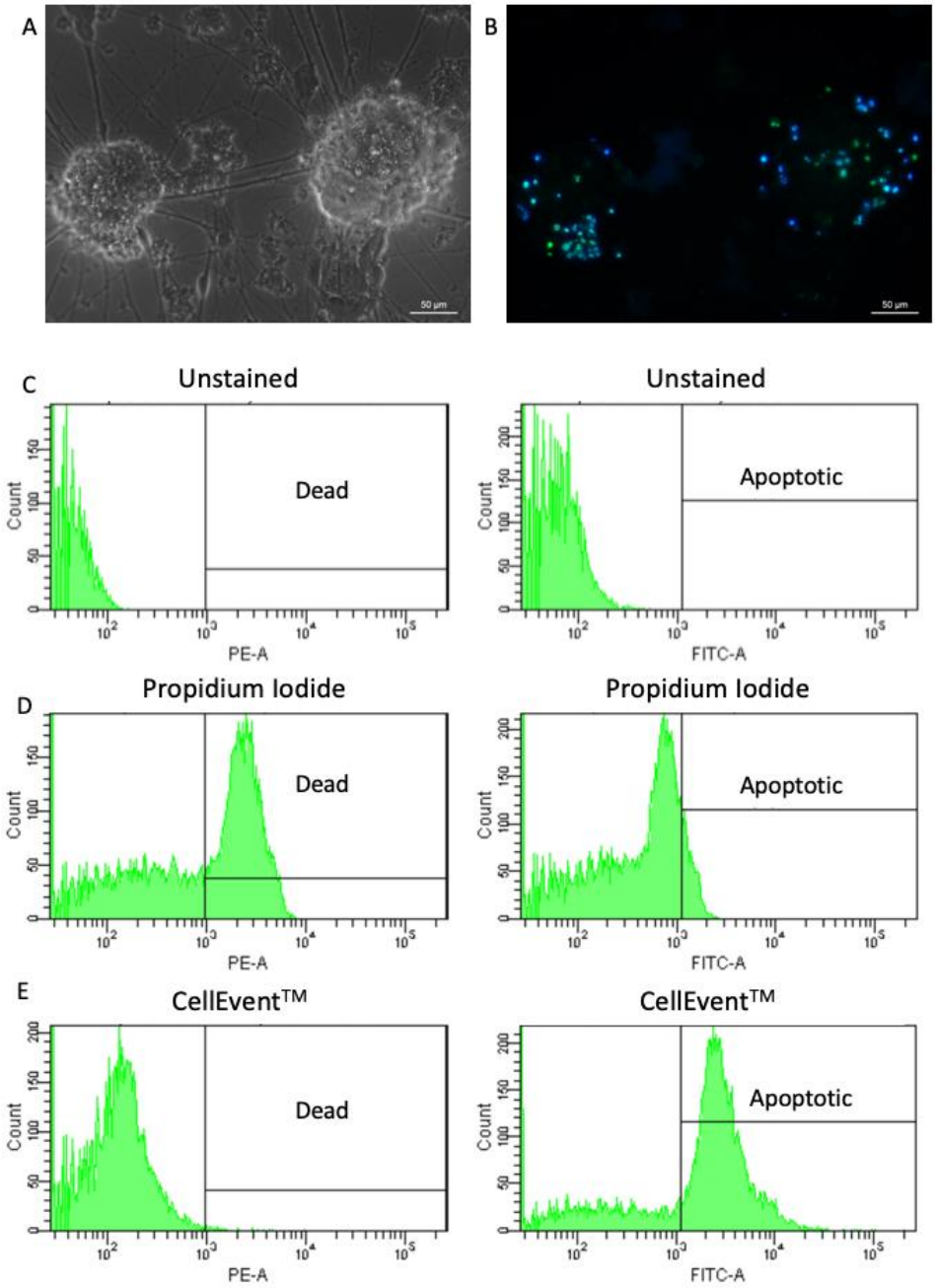


***Figure 7.4 Detection of cleaved caspase 3/7 activity in MNs.***

*(A) Phase contrast and (B) fluorescent images of mature SMA-19 MNs at day 32 of differentiation. (B) SMA-19 MNs were stained with CellEvent™ Caspase-3/7 Green Detection Reagent in PBS with 5% FBS at a 2µM final concentration, then counterstained with DAPI. (C-E) SMA-19 MNs treated with 0.1% Virkon to induce cell death for a positive control was used. Histograms showing cell populations: (C) unstained, untreated cells or cells stained with either (D) 20µg/ml propidium iodide or (E) 5µM CellEvent™ Caspase-3/7 Green Detection Reagent. Left histograms show signal in the PE-A channel and right histograms show signal in FITC-A channel.*

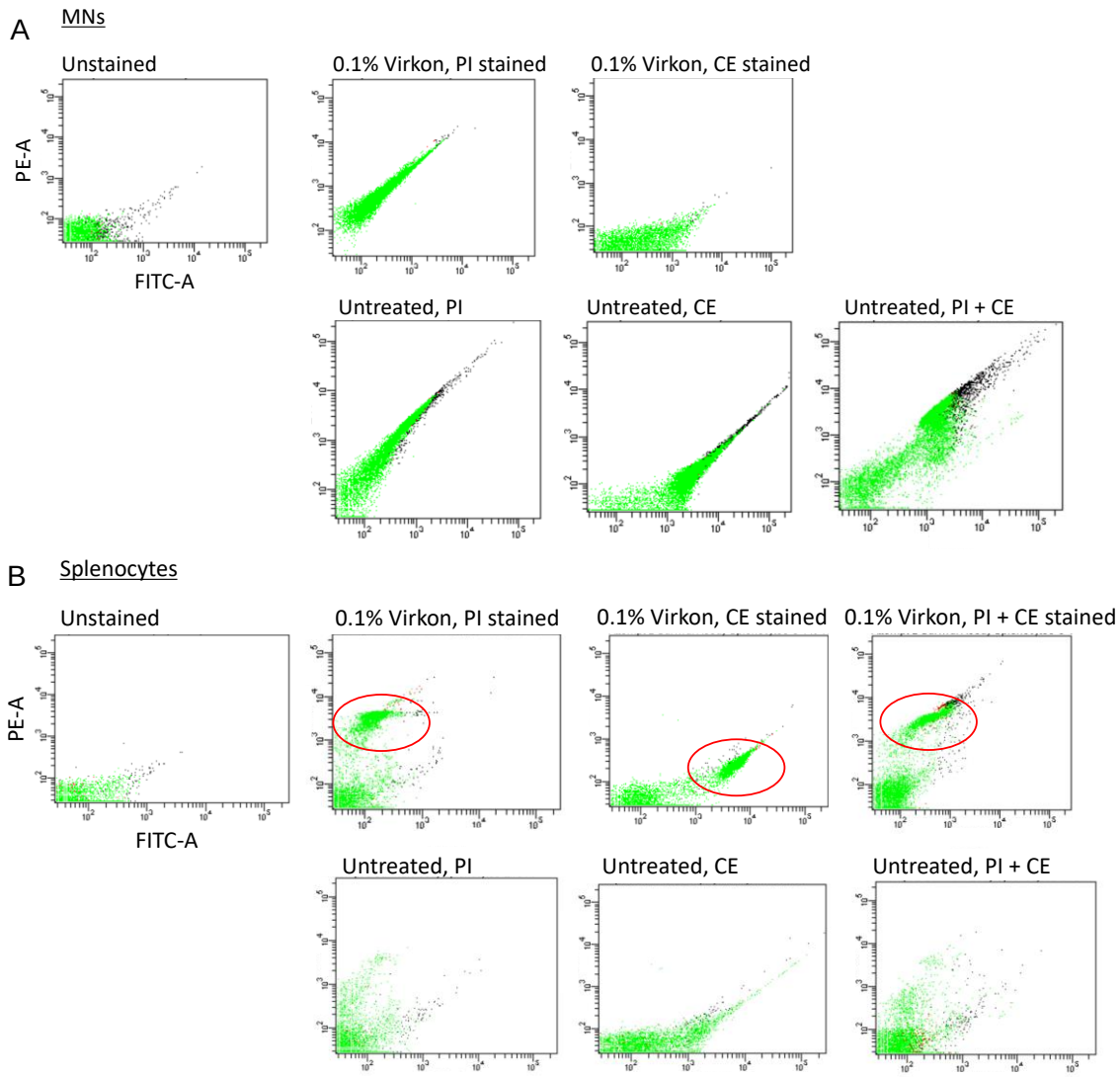


***Figure 7.5 Optimisation of Propidium Iodide and CellEvent™ Caspase-3/7 Green Detection Reagent staining in SMA-19 iPSC MNs and primary splenocytes.***

*(A) Mature SMA-19 MNs at day 28 of differentiation were either left untreated or insulted with 0.1% Virkon for 5 minutes before being stained with 20µg/ml propidium iodide or 5µM CellEvent™ Caspase-3/7 Green Detection Reagent. Unclear results were seen. (B) Primary splenocytes cultured for 2 days following isolation from a C57BL10 mouse were used for assay set up using FACS amenable cells. Red circles indicate populations of interest. Propidium iodide signal is detected in the PE-A channel (y axis), whilst CellEvent™ is detected in FITC-A (x axis).*

### 7.3.2 Effect of early and late IDLV_CMV_*Co-hSMN1* transduction of MNs on their survival

The assessment of MN survival both with and without transduction is important to study if ectopically expressed SMN can rescue declining SMA MN numbers. As an alternative to the use of PI for dead cell staining, the use of SYTOX™ AADvanced™ Dead Cell Stain was proposed as this live/dead stain has been proven to multiplex with CellEvent™ Caspase-3/7 Green Detection Reagent successfully (Thermo Fisher, 2020). Despite the challenges faced when optimising this assay, a pilot experiment was performed nevertheless to attempt to assess the effect of transduction on survival in SMA-32 MNs.

Firstly, a trend showing reducing SMN protein levels between immature stages of differentiation (day 23) and maturity (day 28) was found (Figure 7.6A-C) and that transduction of either early or late stage MNs with IDLV_CMV_*Co-hSMN1* could increase SMN protein significantly (Figure 7.6D; day 23: 15.6-fold (P=0.0051) and day 28: 29.1-fold (P=0.0493)). SMN protein levels did not differ (P=0.5169) at day 32 between those transduced at early or late stages of differentiation (Figure 7.6E) suggesting that, at least in this pilot experiment, the time of transduction does not impact resulting SMN expression.

These transduced MNs were concurrently analysed by flow cytometry for their survival. Baseline levels of dead and dying cells were analysed in mock transduced SMA-32 MNs at day 32 of differentiation and compared to MNs transduced at either day 23 or day 28 and harvested again at day 32. SYTOX™ AADvanced™ Dead Cell Stain was used to avoid signal from dead cells bleeding into the FITC-A channel for CellEvent™ Caspase-3/7 Green Detection Reagent signal detection. Figure 7.7 shows the results of this pilot experiment. Large amounts of debris can be seen in Figure 7.7A representing either dead cells, debris such as sheared axons or other cellular matter, perhaps reiterating that MNs are not a suitable cell type for flow cytometric analysis. Nevertheless, quadrant, dot plot analysis with PerCP-Cy5.5-A SYTOX™ and FITC-A CellEvent™ channels revealed the expected autofluorescent population of cells in the bottom left of plots (Figure 7.7B; left plot, Q3) whilst single stained CellEvent™ samples showed movement of the cell populations into apoptotic quadrants (Figure 7.7B; middle plot, Q2 and Q4) and SYTOX™ single stained samples showed a dense dead population (Figure 7.7B;

right plot, Q1). The small apoptotic cell population is expected due to natural levels of cell death in any population, corroborating the evidence of green nuclei seen in SMA-19 MNs (Figure 7.4B) by fluorescent microscopy. Cell death could also be induced by the harvesting procedure for this analysis; removing adherent cells from their culture dish with thorough resuspension is likely to cause damage to cells particularly fragile cells like MNs.

Dual-stained mock transduced, baseline samples (Figure 7.7C, left plot) shows both apoptotic (Q2) and dead populations (Q1) and this appears to be very similar in samples transduced at day 23 (Figure 7.7C, middle plot), suggesting no decrease in cell death despite significant increases in SMN protein levels. Unfortunately, day 28 transduced samples could not be dual-stained with both SYTOX™ and CellEvent™ stains due to reagent supplies, but evidence of large cell death can still be seen in the SYTOX™ PerCP-Cy5.5-A channel, again corroborating data from day 23 with no reduction in cell death following transduction. When replicates were quantified, very little difference between mock and transduced samples was evident (Figure 7.7D).

In summary, assay optimisation was challenging and data obtained from flow cytometry experiments employing CellEvent™ Caspase-3/7 Green Detection Reagent showed little difference between the survival of transduced and untransduced cells. However, due to the technical challenges encountered, findings from these experiments can be deemed inconclusive. Time constraints did not allow for further implementation of this assay in non-MN cell types that could be transduced, for example fibroblasts. Therefore, this assay was discarded for the remainder of this project.

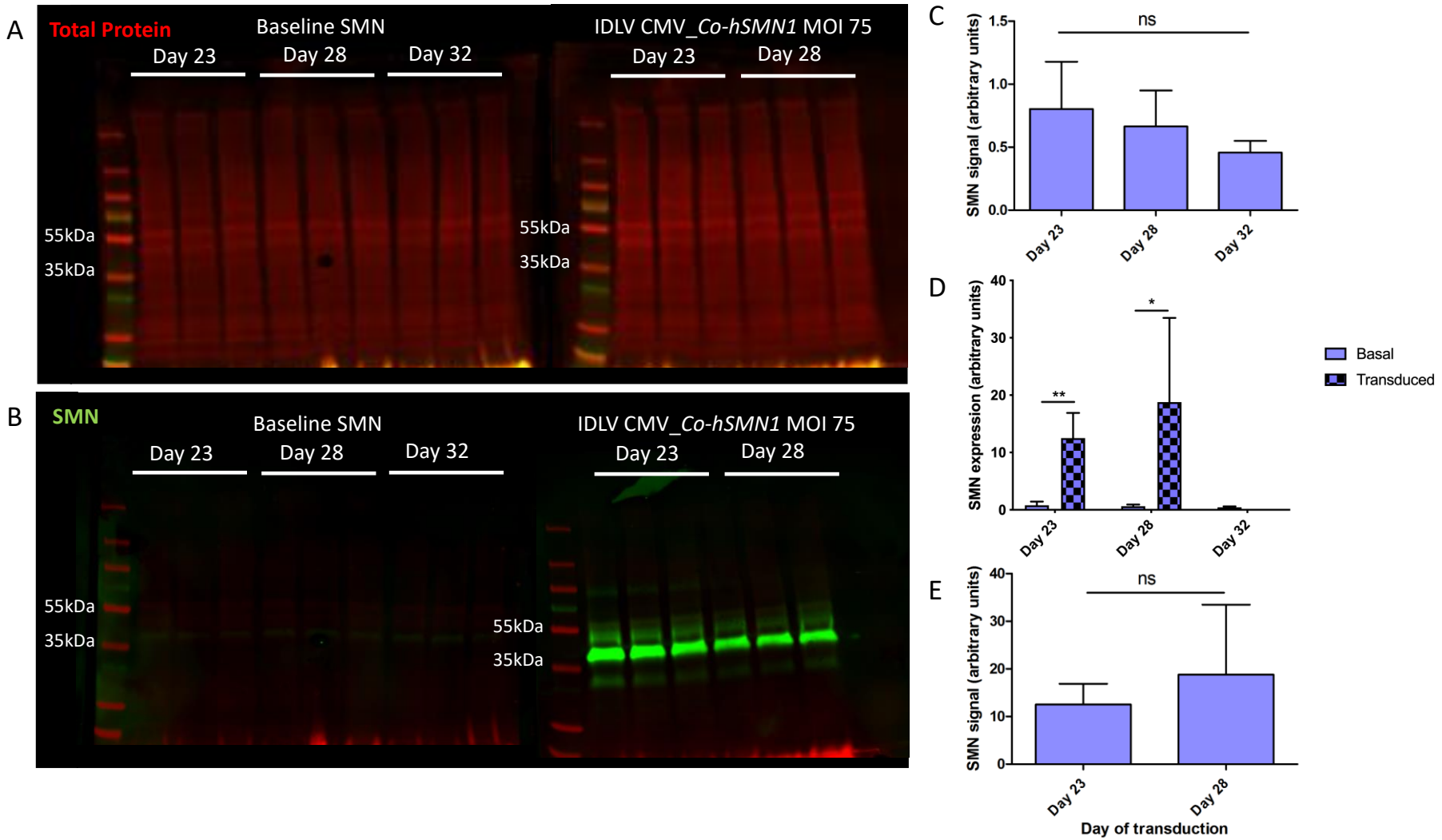


***Figure 7.6 Transduction of immature and mature SMA-32 MNs with IDLV_CMV_Co-hSMN1.***

*(A,B) Protein was extracted from untreated SMA-32 MNs at three time points corresponding to different stages of MN maturity (left hand blots). Day 23; immature, day 28; mature, day 32; mature plus transduction incubation. Protein was also extracted (at day 32) from SMA-32 MNs that had been transduced with IDLV_CMV_*Co-hSMN1 *at MOI 75 at either day 23 or day 28. (C) Quantification revealed a trend for SMN decreases during the maturation period, but this was non-significant (P=0.6715, one-way ANOVA). (D) Transduction at either day 23 or 28 increases SMN protein by 15.6-fold (P=0.0051) and 29.1-fold (P=0.0493) compared to basal SMN at the time of transduction, respectively (unpaired, one-tailed t-test). (E) However, extent of SMN expression measured at day 32 following immature or mature transduction are not significantly different from one another (P=0.5169, unpaired, two-tailed t-test).*

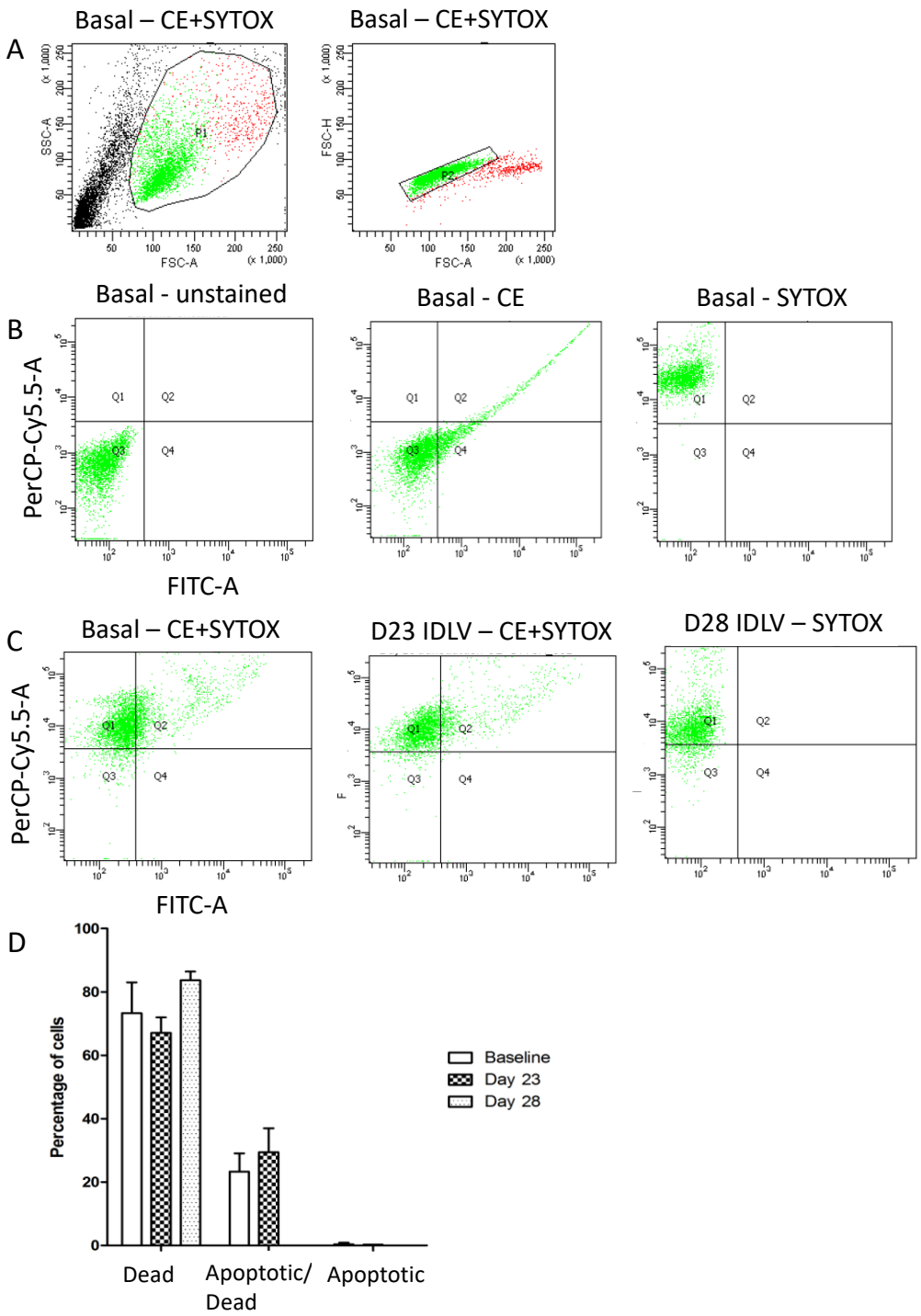


***Figure 7.7 Attempted analysis of cell death and cleaved caspase 3/7 activity in SMA-32 MNs transduced at day 23 or day 28.***

*SMA-32 cells analysed at day 32 of differentiated unstained or stained with 1µM SYTOX™ AADvanced™ Dead Cell Stain or 1µM CellEvent™ Caspase-3/7 Green Detection Reagent. (A) Large amounts of debris (black dots) can be seen in forward vs side scatter dot plots. (B) Baseline = mock transduced SMA-32 MNs analysed at day 32 of differentiation. (C) Day 23 and day 28 = SMA-32 MNs transduced at day 23 or day 28, respectively, then analysed at day 32 of differentiation. SYTOX™ AADvanced™ Dead Cell Stain signal is detected in the PerCP-Cy5.5-A channel, whilst CellEvent™ is detected in FITC-A. Q1 = dead cells, Q2 = apoptotic/dead cells, Q4 = apoptotic, Q3 = autofluorescent cells.*

## 7.4 Assessing DNA damage response and apoptotic marker expression

As no appropriate data were gathered from the above flow cytometry assay employing CellEvent™ Caspase-3/7 Green Detection Reagent, a different approach was designed to assess apoptosis and DNA damage markers. This molecular analysis is described below.

### 7.4.1 Cleaved caspase 3 and γH2AX

#### 7.4.1.1 Optimisation of detection methods

The detection of both γH2AX and cleaved caspase 3 was first sought using immunofluorescence. Primary antibody concentration titrations were performed if necessary, based on recommended concentrations from product literature or from colleagues. 5, 10 and 25µg/ml rabbit anti-cleaved caspase 3 were tested as product literature suggested a range of 10-20µg/ml for immunohistochemistry. Here, it was found that the highest concentration showed diffuse signal throughout the nuclei, without distinct localisation of the protein (Figure 7.8A, left). 10µg/ml began to reveal more distinct foci (Figure 7.8A, middle), but the lowest concentration was chosen for further analyses as the pattern of expression was clear (Figure 7.8A, right).

Optimisation of γH2AX immunostaining involved titrating secondary antibody concentration. The primary antibody concentration was provided by a colleague at University of Sheffield. Using 1µg/ml mouse anti-γH2AX and 2µg/ml goat anti-mouse Alexa Fluor 488 revealed high background signal with no detectable nuclear foci (Figure 7.8B, left). Both increasing primary (2µg/ml) and lowering secondary (1µg/ml) antibody concentrations were tested with differing secondary antibody fluorophores (Figure 7.8B). The optimal combination was determined as 1µg/ml each antibody, with an Alexa Fluor 488 secondary conjugate. These two optimised protocols were deemed suitable for use detecting any potential changes in γH2AX and cleaved caspase 3 expression following transduction of fibroblasts.

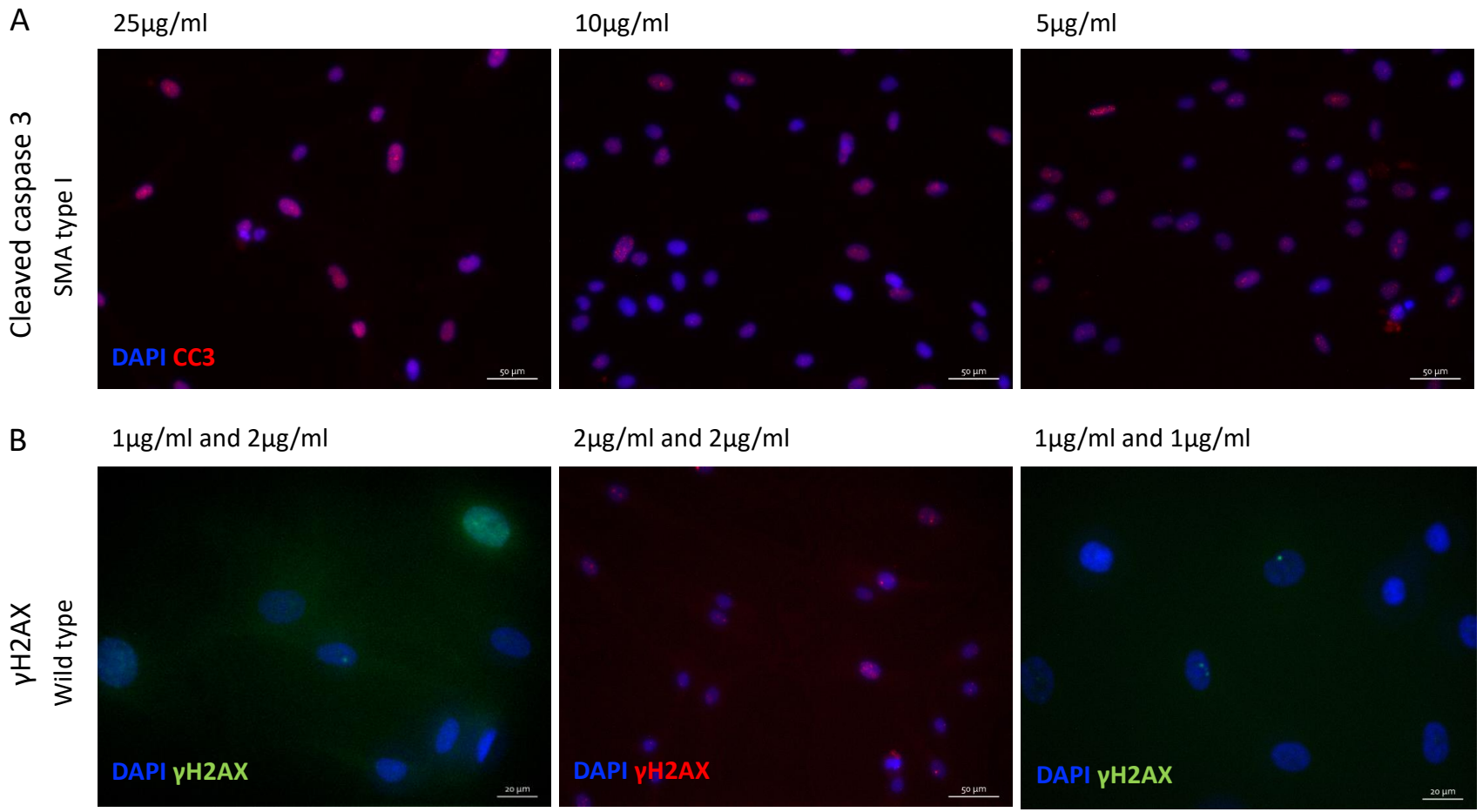


***Figure 7.8 Optimisation of cleaved caspase 3 and H2AX immunofluorescence detection.***

*(A) Three cleaved caspase 3 primary antibody concentrations were trialled in SMA type I fibroblasts, with 5µg/ml providing optimal results. (B) Different combinations of anti-γH2AX primary and secondary antibody concentrations and fluorophores were tested, with 1µg/ml of each antibody, with the secondary antibody Alexa Fluor 488 conjugated, was optimal. Scale bars = 50µm in all, but (B) left and right).*

Technical challenges of using immunofluorescence in MNs were a concern (as stated in section 5.5.2), so optimisation of an alternative detection method by western blot was also attempted, despite this not necessarily being the gold standard method of DNA damage protein detection. A standard western blot protocol was employed to detect both γH2AX and cleaved caspase 3 in samples from wild type, SMA type I fibroblasts and SMA type I fibroblasts treated with 200μM hydrogen peroxide. No signal from either γH2AX or cleaved caspase 3 at 17kDa was seen (Figure 7.9) despite alpha tubulin loading control bands and SMN bands seen very clearly. The 10kDa protein standard was still visible on the membrane precluding the suggestion that these small molecular weight proteins simply ran off the gel.

Three further attempts to detect γH2AX by modification of the western blot protocol were trialed, but without success. γH2AX was chosen as the target for further optimisation based on colleague's advice and successful western blots in the literature. Pharmacological treatment of both wild type and SMA type I fibroblasts with bleomycin served as a positive control for the induction of γH2AX expression. Bleomycin is a DNA damage inducing agent that has previously been shown to induce transient γH2AX signal (Scarpato et al., 2013, Di Tomaso et al., 2014, Mavuluri et al., 2016) that is detectable 1-3 hours following treatment. 10μg/ml and 5μg/ml recommended concentrations of bleomycin were applied to fibroblasts for either 2 hours or 4 hours before cells were lysed and extracts used for western blots.

Firstly, the same standard protocol was applied as in (Figure 7.9) but this time using bleomycin treated samples. Again, no clear γH2AX bands were observed, despite good alpha tubulin signal and the presence of the 10kDa protein standard (Figure 7.10A). Secondly, the same samples were run again but with slight modifications to the western blot protocol. An increased amount of protein was loaded onto the gel (13μg rather than 8μg), nitrocellulose membrane with a smaller pore size (0.2μm rather than 0.45μm) membrane was used and a commercial blocking buffer was employed (Odyssey Intercept® (TBS) instead of 5% BSA in TBS). These modifications were aimed at increasing any γH2AX that may simply have been too faint to see before. However, these modifications were not successful (Figure 7.10B). Finally, a more radical change in protocol was employed by reducing the voltage at which the gel electrophoresis was conducted (100V vs 200V), elongation

of transfer time at a low voltage (15V overnight vs 100V for 2 hours) and the use of a 0.2µm PVDF membrane. Again, no γH2AX was able to be detected (Figure 7.10C).

Although every care was taken to produce a positive control for this assay, it is known that bleomycin is a very unstable compound and it is possible that the pharmacological induction itself was potentially not optimal causing very little, if any, γH2AX to be present in the cells to detect. Therefore, this was assessed by immunofluorescence of wild type fibroblasts treated with the same bleomycin compound at 10µg/ml for a period of two hours. Immunofluorescence images (Figure 7.10E) showed a clear increase in γH2AX signal. Cleaved caspase 3 was also assessed in bleomycin treated fibroblasts and was also found to be increased too (Figure 7.10E). The increase in signal was not quantitated in either case as this was just deemed a confirmatory experiment.

It was unclear why none of these steps provided any improvement of γH2AX detection by western blot. It was difficult to ascertain what aspect of the western blot protocol may not have been optimal as no signal was ever detected, rather than being able to tweak blocking conditions, for example, to improve intensity of a faint, but present band. Finally, it is possible that simply not enough protein lysate was loaded onto gels so proteins in low abundance may not be detected, but due to low concentrations of protein within lysates, the maximum (13µg) was indeed loaded here. Taken together, the challenges uncovered here resulted in the decision not to further attempt western blotting as a method of detection. This decision posed no problem for experimental work using fibroblasts, however, due to the technical challenges involving immunofluorescence in MNs, it would unfortunately no longer be possible to detect γH2AX and cleaved caspase 3 in MNs.

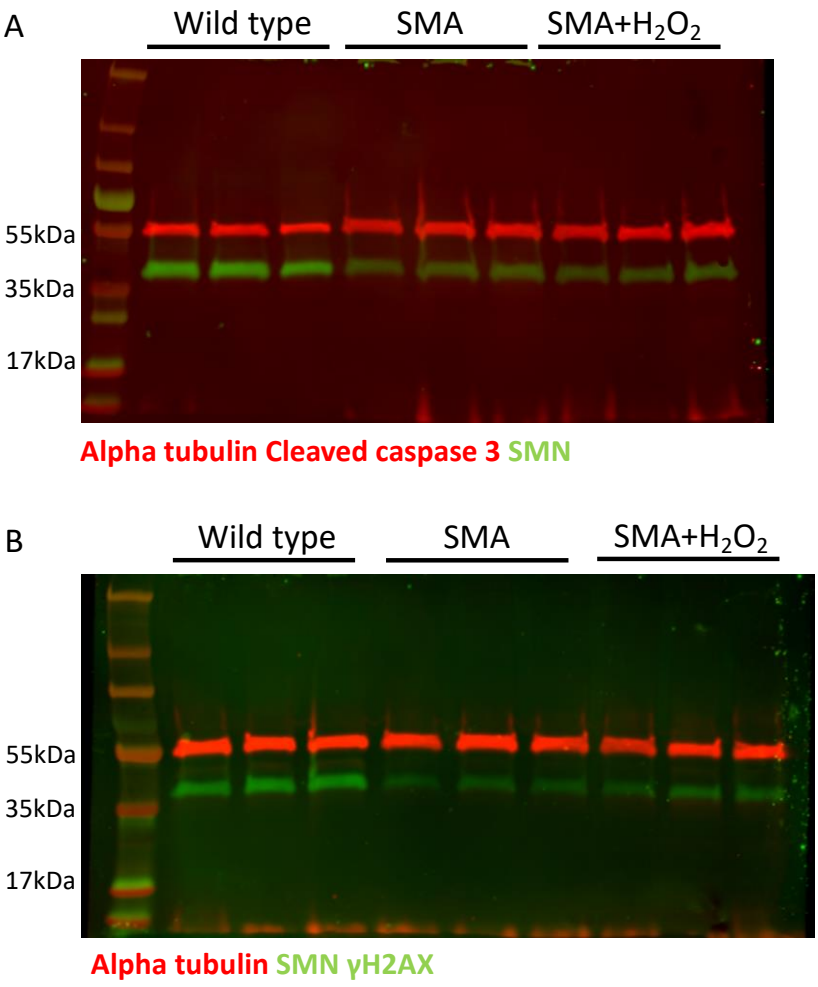


***Figure 7.9 Detection of cleaved caspase 3 and γH2AX in wild type, SMA type I fibroblasts and SMA type I fibroblasts treated with hydrogen peroxide.***

*Lysates from wild type, SMA type I fibroblasts and SMA cells treated with 200μM hydrogen peroxide for 2 hours were western blotted in an attempt to detect (A) cleaved caspase 3 and (B) γH2AX. Both proteins of interest are an approximate size of 17kDa. Alpha tubulin acted as a housekeeping protein and SMN was a positive control showing differences between genotypes. No cleaved caspase 3 or γH2AX bands could be seen on these blots.*

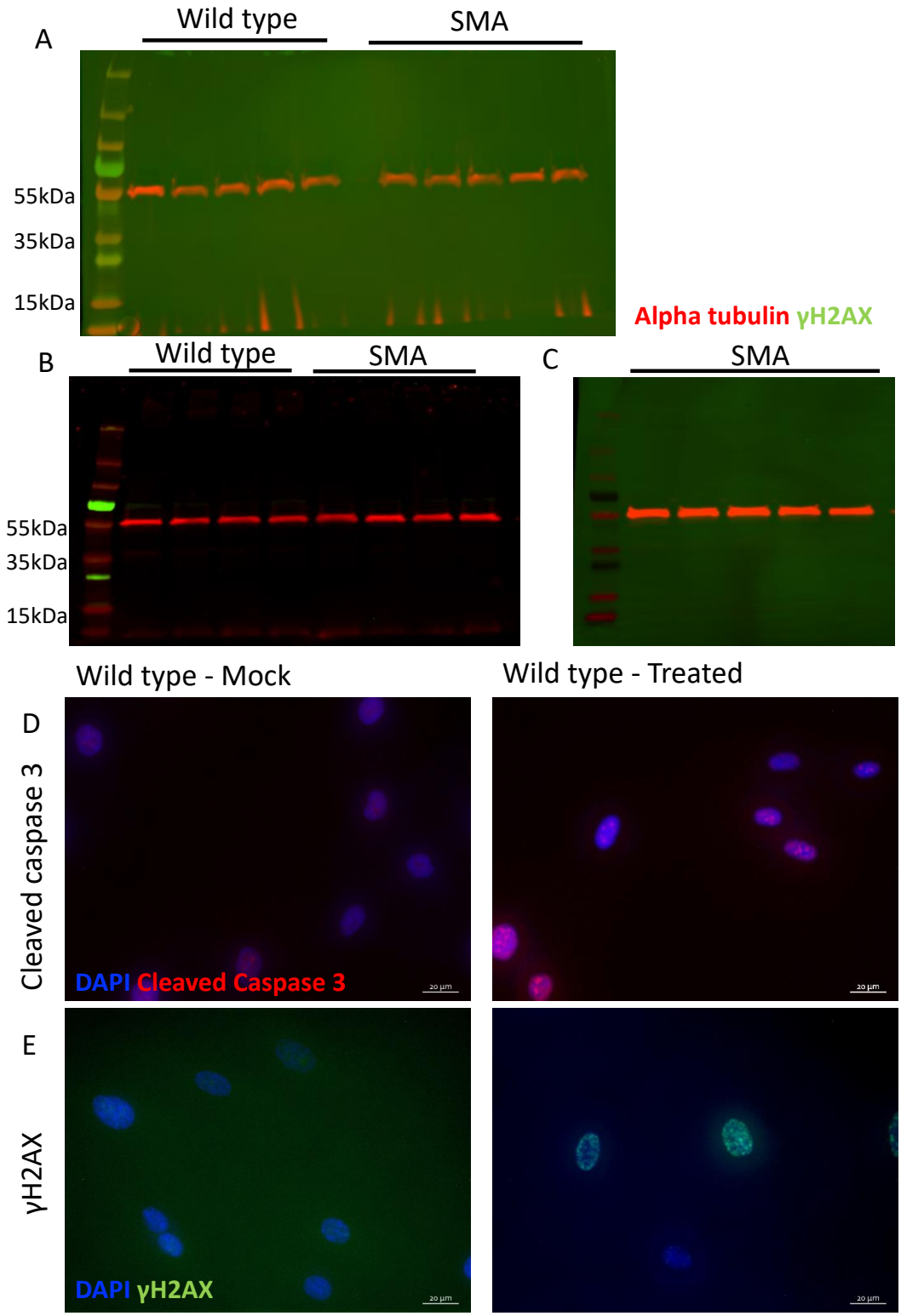


***Figure 7.10 Further attempts to detect γH2AX in bleomycin-treated wild type and SMA type I fibroblasts.***

*(A) Each genotype of cells was treated with bleomycin as follows; from left to right, Mock, 5µg/ml for 2 hours, 10µg/ml for 2 hours, 5µg/ml for 4 hours, 10µg/ml for 4 hours. Western blot conditions: run 200V 30 minutes, transfer 100V 1 hour with 0.45µM nitrocellulose, blocking 5% BSA in 0.1% TBS. (B) The same samples as in (A) were ran again using different western blotting conditions: run 200V 30 minutes,*

*transfer 100V 1 hour 0.2µM with nitrocellulose, blocking Odyssey Intercept® (TBS). One sample per genotype was not able to be loaded due to insufficient protein concentration (Wild type 5µg/ml for 4 hours and SMA type I 10µg/ml for 4 hours). (C) SMA type I fibroblasts samples only were run with the following conditions: run 100V 30 minutes, transfer 15V overnight with 0.2µM PVDF, blocking 5% BSA in 0.1% TBS. Concentrations of bleomycin were the same as in (A). (D,E) Bleomycin treatment (10µg/ml for 2 hours) was applied to wild type fibroblasts to indicate if the compound was capable of increasing γH2AX and cleaved caspase 3 signal and thus proving lysates from these cells would be a valid positive control for western blot optimisation.*

#### 7.4.1.2 Expression of cleaved caspase 3 and γH2AX in wild type and SMA fibroblasts

Using optimal immunofluorescence conditions, any differences between wild type and SMA type I fibroblast expression of cleaved caspase 3 and γH2AX was analysed to determine if apoptotic or DNA damage phenotypes were indeed present.

More diffuse cleaved caspase 3 signal was seen in wild type nuclei (Figure 7.11A, left), whereas SMA nuclei revealed a more punctate signal pattern (Figure 7.11A, right). Expression was scored from 0 being no signal, to 4 being strong signal (examples of nuclei assigned scores 1-4 can be seen in Figure 7.12A), and a value for each score as a percentage of the total cells was calculated. Wild type cells showed similar values across all scores (range 17.54-24.56%; Figure 7.12B), suggesting there are varying levels of apoptosis, but all are approximately, equally likely. SMA type I fibroblasts exhibited a trend for increasing percentages of cells with stronger cleaved caspase signal (increasing from 1.34% to 36.16%; Figure 7.12B). Significant differences were observed between wild type and SMA type I cleaved caspase 3 expression levels at scores 0-2, but not at 3 or 4.

γH2AX immunostaining was able to reveal distinct foci in the nuclei of both cell genotypes, but foci were more frequently found in SMA cells (Figure 7.11B). The number of individual foci per cell and the percentage of foci-positive cells were calculated and showed that SMA type I cells exhibited higher values for both conditions (P=0.0057 and P=0.0069, respectively; Figure 7.12C).

Taken together, these data reveal that SMA type I fibroblasts exhibit hallmark signs of DNA double strand breaks and undergo apoptosis in more cells, and with stronger cleaved caspase 3 signal, than wild type cells.

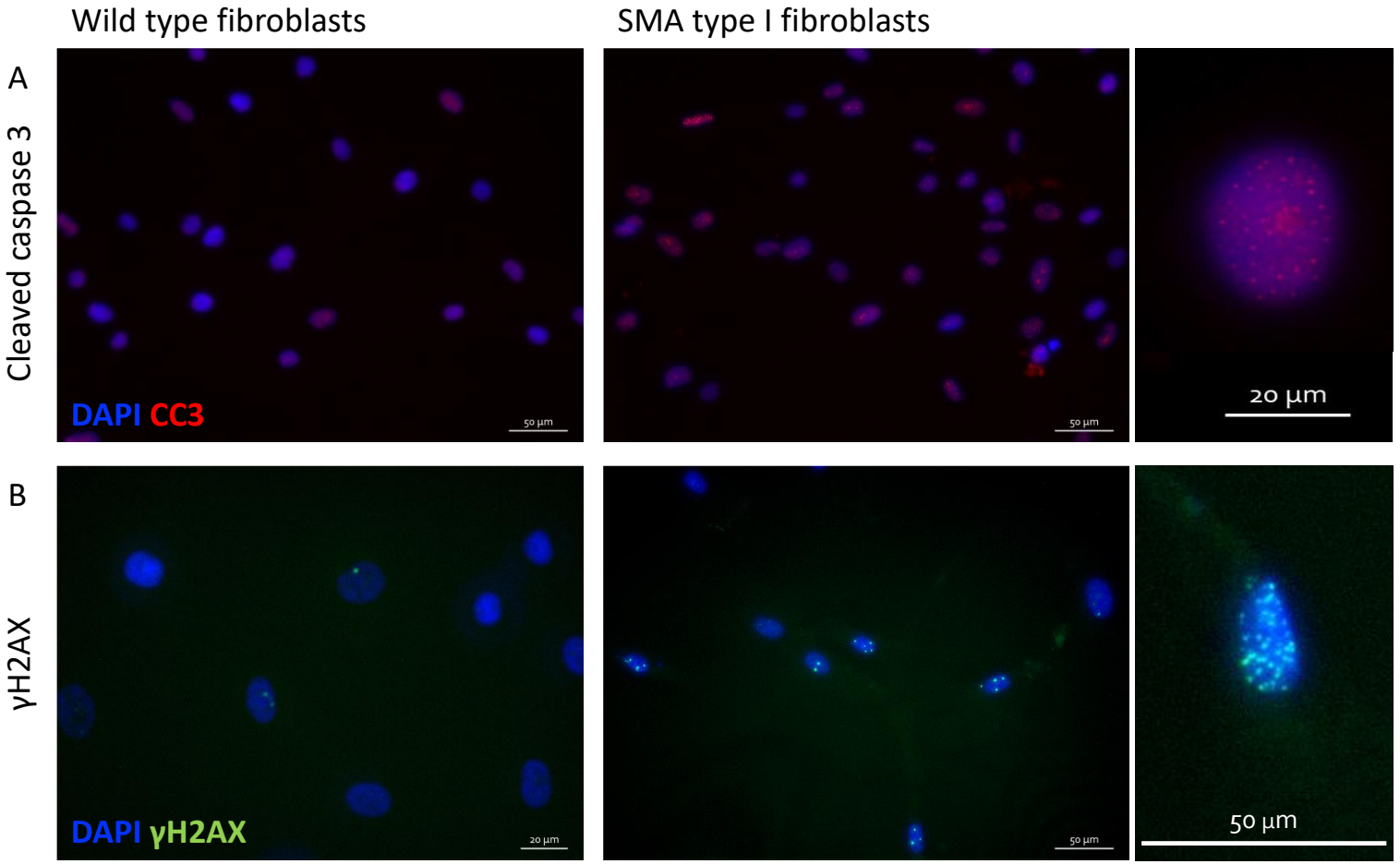


***Figure 7.11 Visualisation of cleaved caspase 3 and γH2AX expression in wild type and SMA type I fibroblasts.***

*Untreated wild type and SMA type I fibroblasts were immunostained for two target proteins (A) cleaved caspase 3 and (B) γH2AX. A view of two separate SMA type I fibroblasts at increased magnification shows nuclear staining more clearly.*

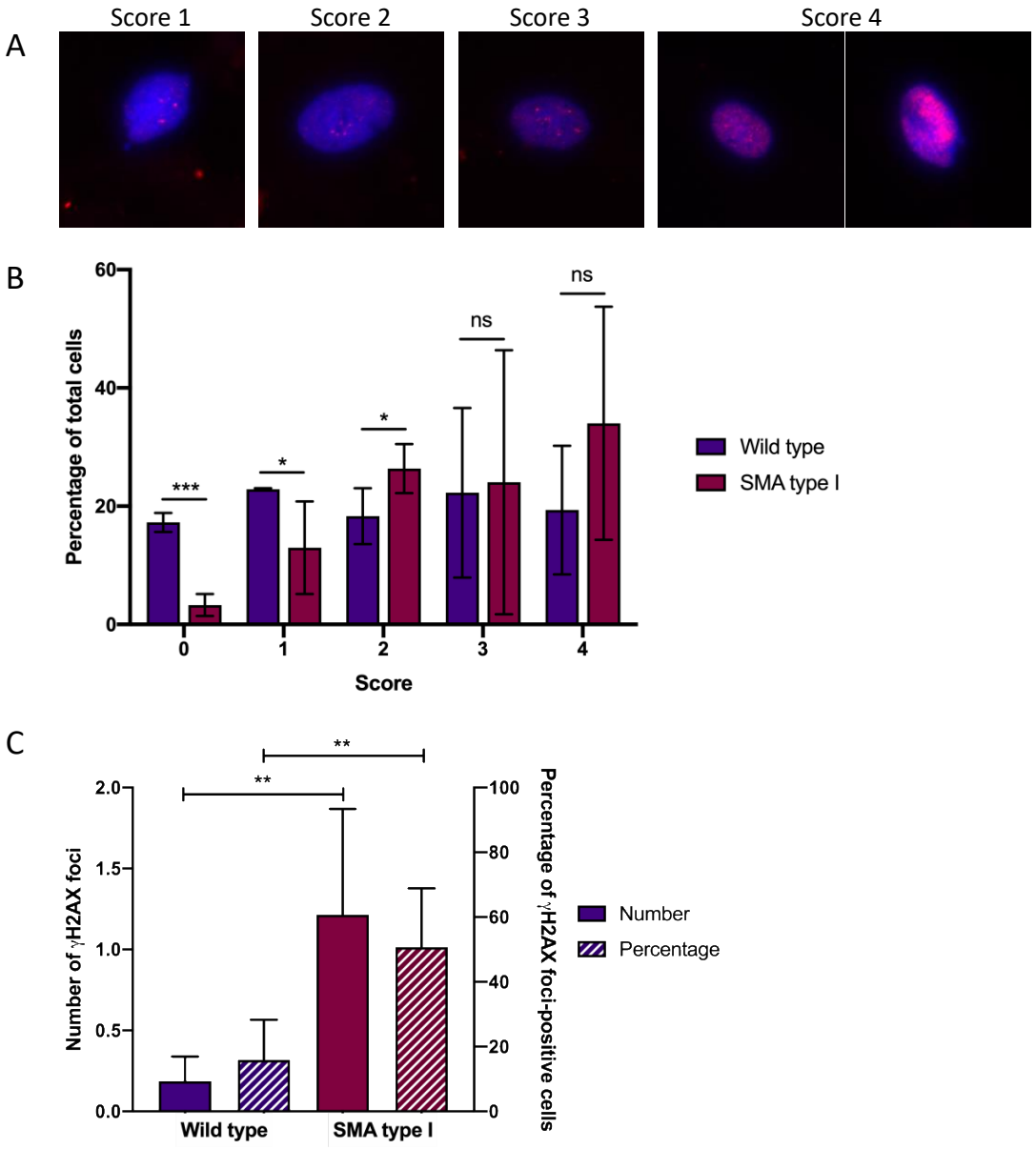


***Figure 7.12 Expression of cleaved caspase 3 and γH2AX in wild type and SMA type I fibroblasts.***

*Fibroblasts were immunostained against cleaved caspase 3 and γH2AX before expression was quantified. (A) As it was difficult to count individual foci in cleaved caspase 3 stained samples, a scoring system was designed to delineate levels of expression: 0 = no signal, 1 = less than 5 foci, 2 = more than 5 foci, 3 = light, diffuse staining, 4 = strong, diffuse staining throughout whole nucleus, or very strong expression in a concentrated area. Examples of nuclei representative of scores 1-4 are shown, an example of score 0 is not shown as no signal is self-explanatory. (B) Values for each cleaved caspase 3 score as a percentage of total cells in each replicate were calculated and an unpaired, one-tailed t-test between wild type and SMA (average 19 and 37 cells per replicate, respectively), at each score was conducted (0: P=0.0006, 1: P=0.0472, 2: P=0.0451, 3: P=0.4565, 4: P=0.1613). (C) A count of individual γH2AX foci per cell (left axis) as well as the number of cells positive for any number of foci (right axis) were recorded (wild type n=31 cells, SMA n=65 cells). Unpaired, one-tailed t-tests were conducted for each condition: number of foci P=0.0057, percentage of foci-positive cells P=0.0027.*

#### 7.4.1.3 The effect of transduction on cleaved caspase 3 and γH2AX in SMA type I fibroblasts

Following on from the conclusion that SMA cells show increased levels of DNA damage and apoptosis and evidence in the literature suggestive of SMN's anti-apoptotic effect, it was hypothesised that transduction of cells with IDLV_CMV_*Co-hSMN1* may improve this phenotype.

SMA type I fibroblasts were transduced at MOI 75 with IDLV_CMV_*Co-hSMN1*. Following immunostaining against cleaved caspase 3, the same scoring system as above was implemented. Similarly to the basal cleaved caspase 3 levels seen when comparing to wild type, large proportions of the mock transduced cell population here showed either light, diffuse or strong, diffuse signal (35.5% and 38.3%, respectively; Figure 7.14A,B). Transduced samples appeared to show a similar pattern as mock transduced with all comparisons non-significant (Figure 7.14B). However, large amounts of variation were seen in both mock and transduced samples. Within transduced samples, some images showed large differences in cleaved caspase 3 signal in adjacent cells (Figure 7.13A), with some exhibiting strong signal of the highest score, whilst adjacent cells showed two levels of scoring lower. This may suggest that either, cells in the population are undergoing apoptosis at different rates, or maybe that some individual cells are rescued, but not enough to be detected by overall statistics.

Both the number of γH2AX foci per cell and the proportion of γH2AX foci-positive cells were significantly different between mock and transduced cells, with fibroblasts transduced with IDLV_CMV_*Co-hSMN1* exhibiting signs of increased DNA damage ($P=0.0134$ and $P=0.0068$, respectively; Figure 7.13 and Figure 7.14).

Taken together, in contrast to the stated hypothesis, here it was observed that transduction of SMA type I fibroblasts with IDLV_CMV_*Co-hSMN1* led to no apparent decrease in cleaved caspase 3 signal, and actually increased the percentage of γH2AX foci-positive cells.

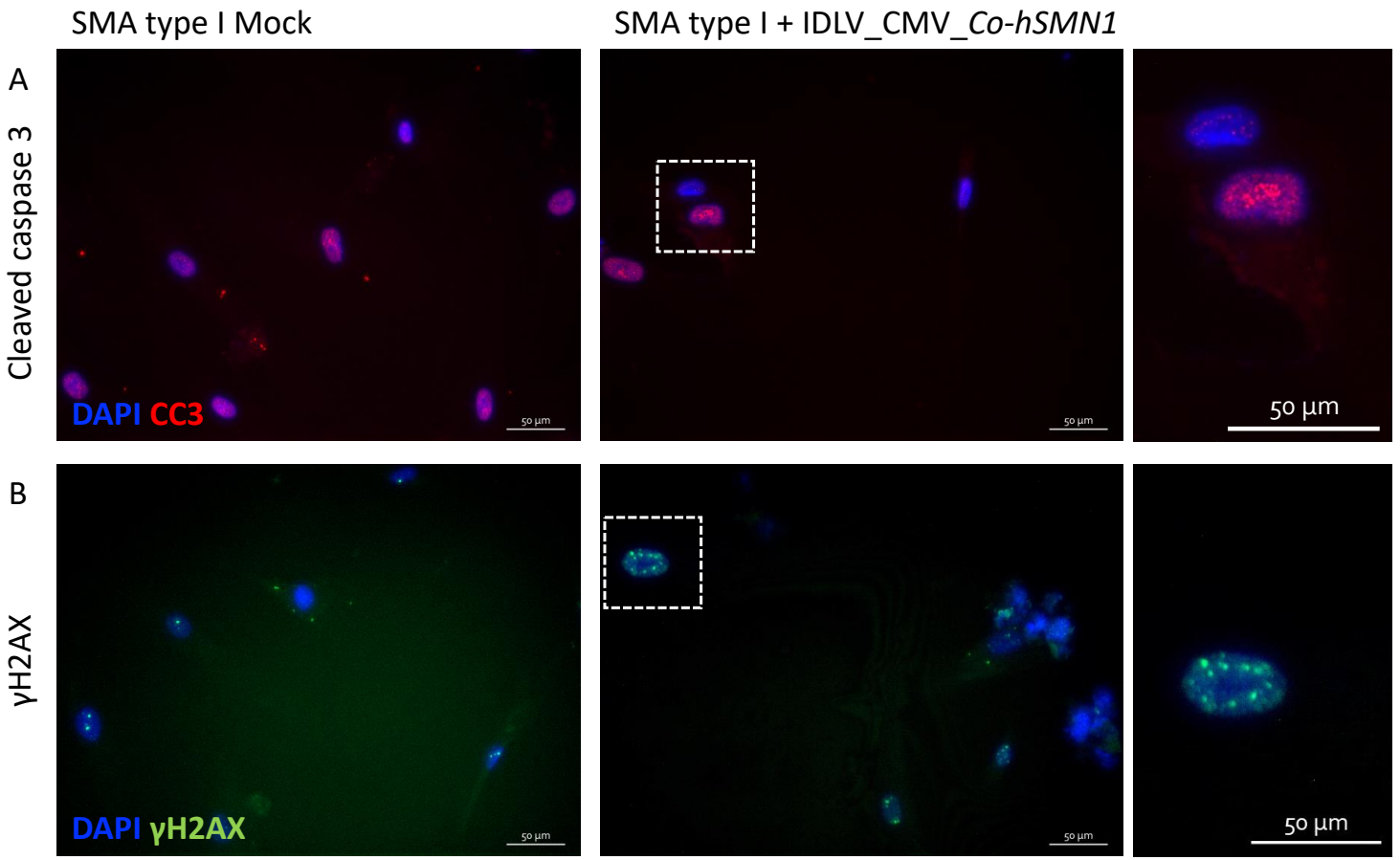


***Figure 7.13 The effect of IDLV_CMV_Co-hSMN1 transduction on cleaved caspase 3 and γH2AX expression in SMA type I fibroblasts.***

*SMA type I fibroblasts were immunostained for two target proteins (A) cleaved caspase 3 and (B) γH2AX following transduction with IDLV_CMV_*Co-hSMN1 *at MOI 75. A view of transduced cells of interest at increased size shows nuclear staining more clearly.*

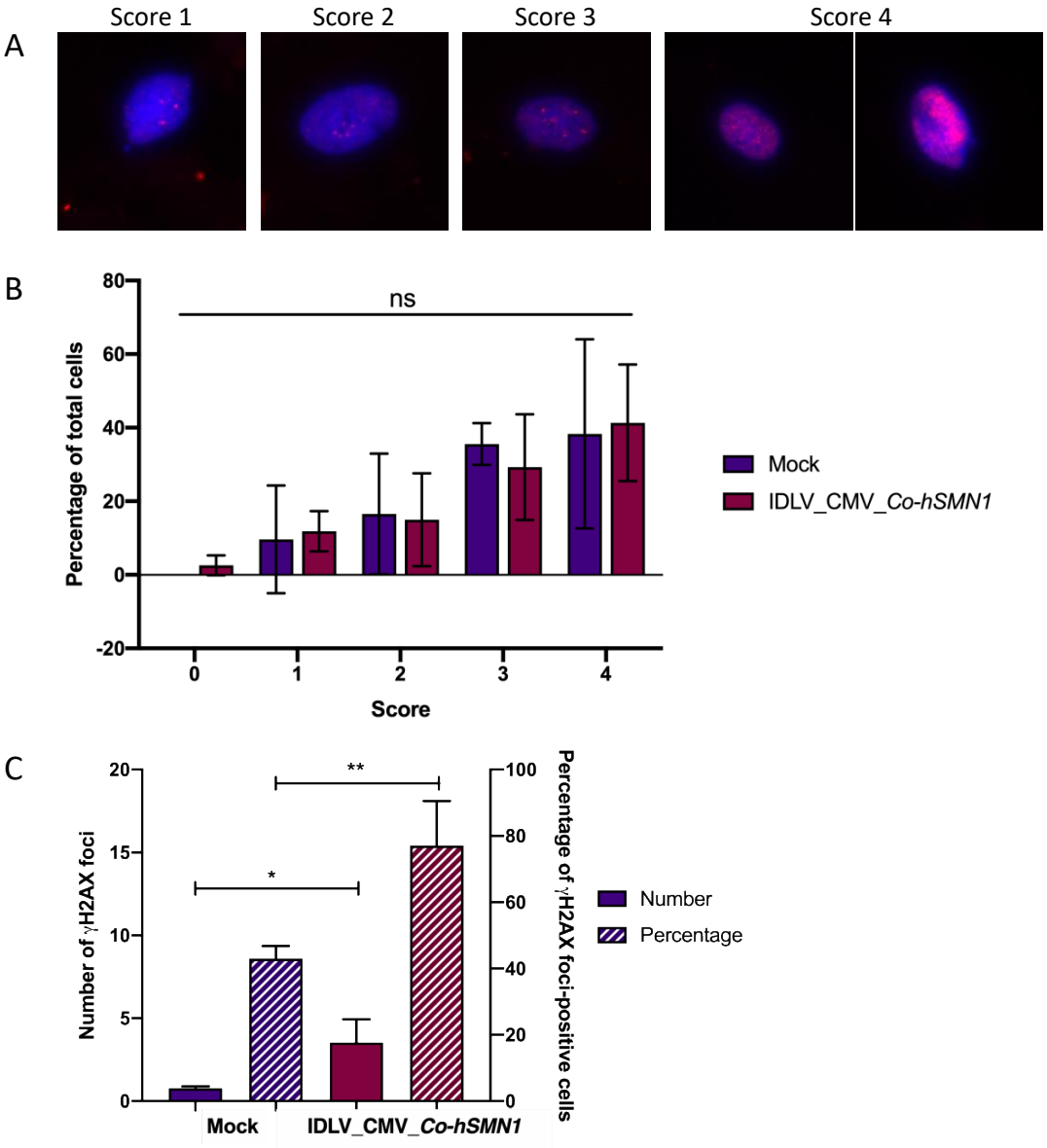


***Figure 7.14 Quantification of cleaved caspase 3 and γH2AX expression following SMA type I fibroblast transduction with IDLV_CMV_Co-hSMN1.***

*(A) Cleaved caspase 3 was assessed by the same scoring system as used previously (0 = no signal, 1 = less than 5 foci, 2 = more than 5 foci, 3 = light, diffuse staining, 4 = strong, diffuse staining throughout whole nucleus, or very strong expression in a concentrated area). Examples of nuclei representative of scores 1-4 are shown, an example of score 0 is not shown as no signal is self-explanatory. (B) The percentage of total cells exhibiting each score was calculated, but large variation is seen in both mock and transduced samples. At least 30 cells per replicate were scored for each condition (total n=107 mock transduced cells, n=115 transduced cells). Significance was assessed at each score by unpaired, two-tailed t-tests (0: P=0.1751, 1: P=0.8194, 2: P=0.9031, 3: P=0.5228, 4: P=0.8709). (C) A count of individual γH2AX foci per cell (left axis) as well as the number of cells positive for any number of foci (right axis) were recorded. At least 25 cells per replicate were scored for each condition (total n=205 mock transduced cells, n=80 transduced cells). Unpaired, one-tailed t-tests were conducted for each condition: number of foci P=0.0134, percentage of foci-positive cells P=0.0068.*

### 7.4.2 ATM and phosphorylated ATM

#### 7.4.2.1 SMA type I fibroblasts

No difference between ATM expression in wild type and SMA type I fibroblasts was detected (Figure 7.15A,B), yet a trend for increased pATM was seen in SMA type I lysates (Figure 7.15C,E). pATM expression could be further increased following treatment of cells with hydrogen peroxide. 700µM hydrogen peroxide for 30 minutes led to a slight increase, but 200µM hydrogen peroxide for 2 hours increased pATM significantly above background levels (Figure 7.15C,E, wild type vs SMA+$H_2O_2$ $P<0.01$, SMA vs SMA+$H_2O_2$ $P<0.05$). 200µM hydrogen peroxide treatment was then used as a positive control for increased pATM expression.

As SMA type I fibroblasts seem to show a trend for increased pATM compared to wild type cells, it was hypothesised that the restoration of SMN protein levels through IDLV_CMV_*Co-hSMN1* transduction, may too restore pATM levels nearer to that of wild type cells. Transduction with an IDLV expressing *eGFP* for 72 hours increased pATM above mock transduced levels ($P=0.0160$; Figure 7.16C), whereas IDLV_CMV_*Co-hSMN1* transduced samples showed a non-significant increase in pATM compared to mock ($P=0.4983$; Figure 7.16C). It appears that the act of transduction causes an increase in pATM, but this can be downregulated when the transgene expressed is *Co-hSMN1.*

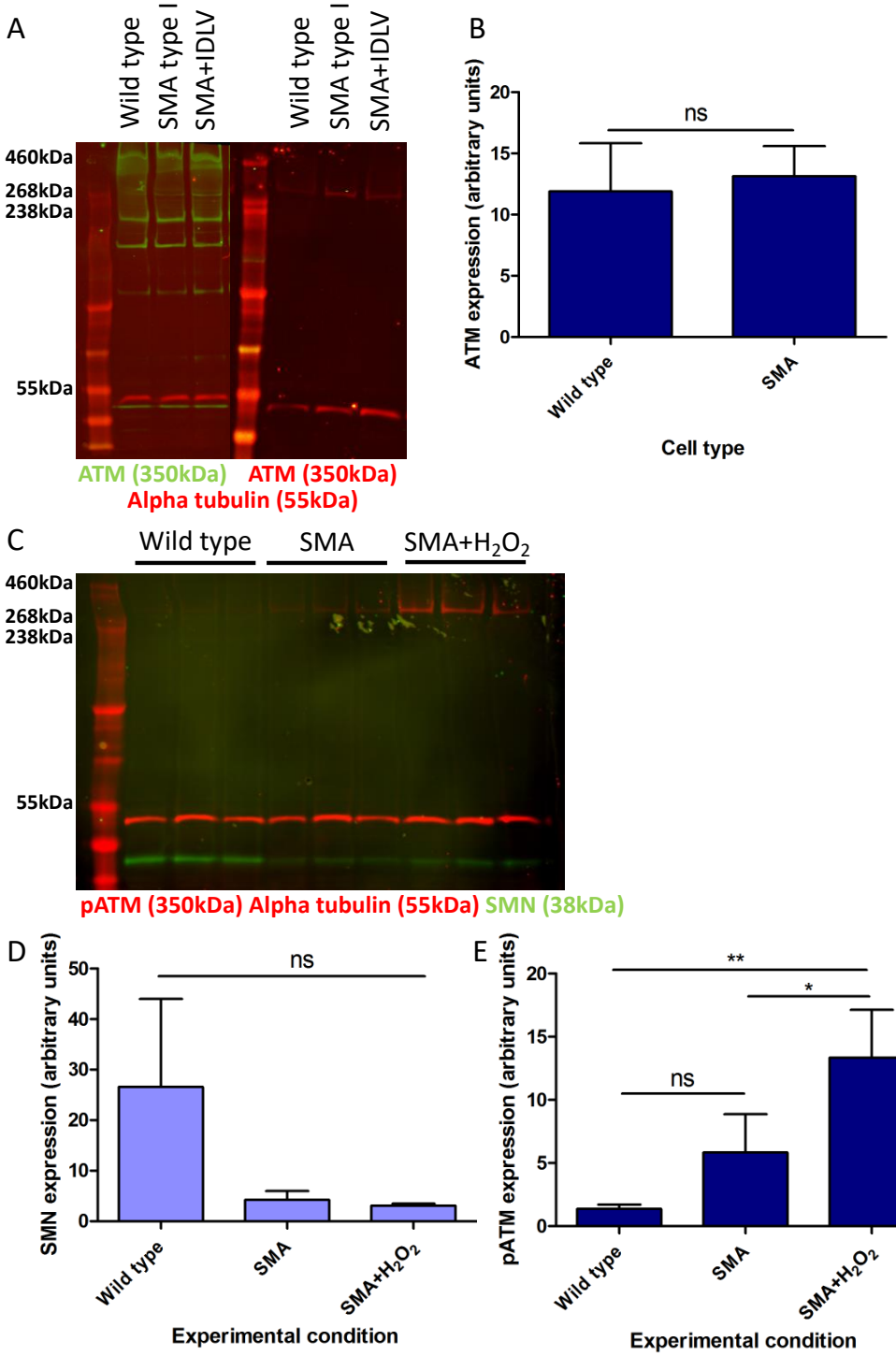


***Figure 7.15 ATM and pATM in wild type and SMA type I fibroblasts.***

*(A) Western blots using protein lysates from wild type, SMA type I fibroblasts and SMA type I fibroblasts transduced with IDLV_CMV_*Co-hSMN1 *at MOI 75. The same samples were run twice and blotted using two antibodies against ATM (ab78 and ab32420) as the first showed non-specific bands. (B) Quantification of ATM expression from western blots using both antibodies (SMA+IDLV was not quantified); unpaired, two-tailed t-test, P=0.6662. (C) Western blots showing wild type, SMA type I fibroblasts and SMA type I fibroblasts treated with 200µM hydrogen peroxide for 2 hours prior to lysis. (D) SMN (P=0.0502) and (E) pATM were quantitated (wild type vs SMA+$H_2O_2$ P<0.01, SMA vs SMA+ $H_2O_2$ P<0.05); one-way ANOVAs with Dunnett's multiple comparison post-hoc tests.*

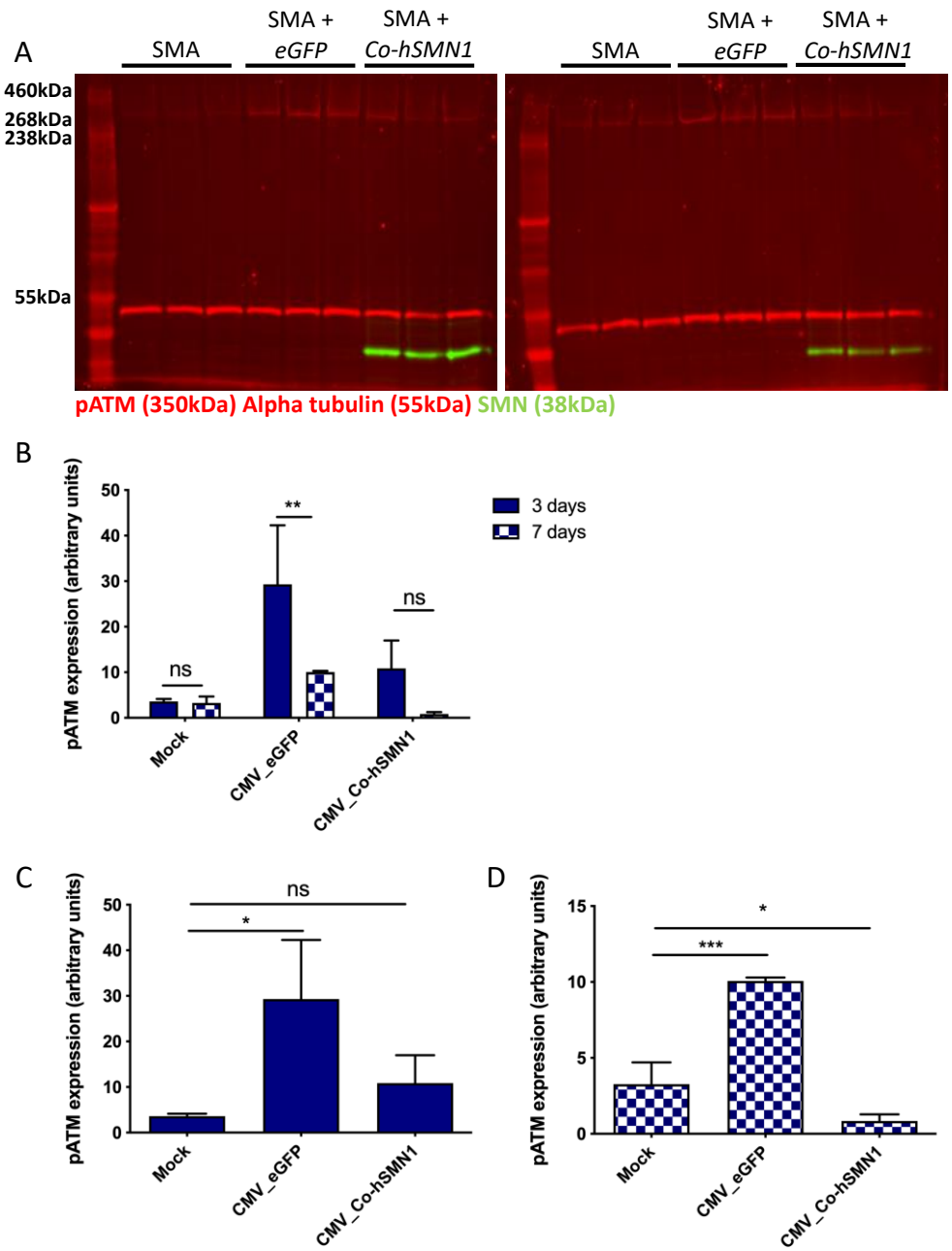


***Figure 7.16 The effect of delaying harvest following transduction on pATM protein expression.***

*SMA type I fibroblasts were transduced with either IDLV_CMV_*eGFP *or IDLV_CMV_*Co-hSMN1 *at MOI 75 and incubated for either 3 days (A left, C) or 7 days (A right, D) following transduction. SMN was detected as a positive control that transduction was successful, but this was not quantified. (B) Comparing pATM between the same sample at different time points revealed only significant changes in* eGFP*-transduced samples (mock P>0.9999,* eGFP *P=0.0053,* Co-hSMN1 *P=0.1794). (C,D) pATM was quantified at 3 (*eGFP *P=0.0160,* Co-hSMN1 *P=0.4983, compared to mock) and 7 days (*eGFP *P=0.0002,* Co-hSMN1 *P=0.0.256, compared to mock) and normalised to alpha tubulin. Data were analysed by (B) two-way ANOVA with Bonferroni multiple comparisons or (C,D) one-way ANOVA with Dunnett's multiple comparison post-test.*

Given the increase seen in pATM following IDLV transduction, it was hypothesised that this initial peak in pATM expression may be caused by the vectors entry into the cell and could mask any potential benefit from transduction with IDLV_CMV_*Co-hSMN1*. Therefore, a a second harvest point was implemented to see if the initial peak of pATM expression subsided once *Co-hSMN1* was expressed stably, potentially rescuing the phenotype. At 3 days post-transduction, pATM expression significantly increased in *eGFP*- but not *Co-hSMN1*-transduced samples, compared to mock (*eGFP* P=0.0160, *Co-hSMN1* P=0.4983; Figure 7.16C). At 7 days post-transduction pATM in IDLV_*eGFP* samples remained elevated compared to mock (P=0.0002; Figure 7.16D), but had decreased significantly since 3 days post-transduction (P=0.0053; Figure 7.16B). Interestingly, at 7 days post-transduction, pATM protein levels in IDLV_*Co-hSMN1* transduced samples decreased to that significantly lower than the mock (P=0.0256; Figure 7.16D), perhaps in agreement with the stated hypothesis that *Co-hSMN1* can reduce pATM to nearer wild type levels if given sufficient time. It is encouraging to see that IDLV_CMV_*Co-hSMN1* transduced samples showed consistently lower pATM than those transduced with a control *eGFP* vector, suggesting that the SMN produced by the IDLV has some benefit.

#### 7.4.2.2 SMA type I MNs

ATM and phosphorylated ATM western blots were completed in wild type and SMA type I MNs without transduction, as well as IDLV_CMV_*Co-hSMN1* transduced SMA type I MNs. Here, ATM or pATM expression was normalised to alpha tubulin rather than total protein as is normally done in MN samples; this was due to the lack of a goat anti-rabbit secondary antibody that could be detected in the green 800nm channel, necessitating the use of a secondary antibody visible in the red 700nm channel, the same as total protein. Alpha tubulin signal appeared very intense in ATM blots (Figure 7.17A), despite the same amount of protein being loaded on gels (15µg) and the same concentration of antibody (0.33µg/ml) as normally used. pATM blots were run subsequently to ATM, so a lower concentration of alpha-tubulin primary antibody was used (0.2µg/ml) was used to combat this excessive signal, improving quality of the blot (Figure 7.17B).

It was also necessary to use the PageRuler™ Prestained Plus protein ladder in ATM blots due to a lack of availability of the HiMark™ Prestained Protein Standard normally used at the time of the experiment. Unfortunately, the PageRuler™

Prestained Plus protein ladder's highest molecular weight band is 250kDa which is smaller than 350kDa ATM and pATM, but an indication of size could at least be drawn using this ladder and the same western blot running conditions as normal. Again, as pATM blots were run subsequently, the correct ladder was used here.

Initially, any difference in ATM and phosphorylated ATM levels between wild type and SMA type I MNs were assessed without transduction. Five out of six lines showed no difference in ATM expression to any other line with only 19-9-7T showing much higher levels (Figure 7.18A, $P<0.0001$); it is unknown why this was the case. No difference was seen in pATM expression across all six iPSC MNs lines (Figure 7.18A, $P>0.9999$).

Upon transduction of SMA type I MNs only, an increase in pATM expression was seen in all SMA type I MNs at 3 days post-transduction (Figure 7.18C, $P=0.0003$, $P<0.0001$, $P=0.0160$, respectively), but total ATM remained unchanged (Figure 7.18B). This pattern of increased pATM expression following transduction mirrored that seen in SMA type I fibroblasts in section 7.4.2.1 and Figure 7.16, suggesting this is conserved across cell types. Data from a later time point, such as 7 days post-transduction used earlier in this chapter, were unavailable for MNs.

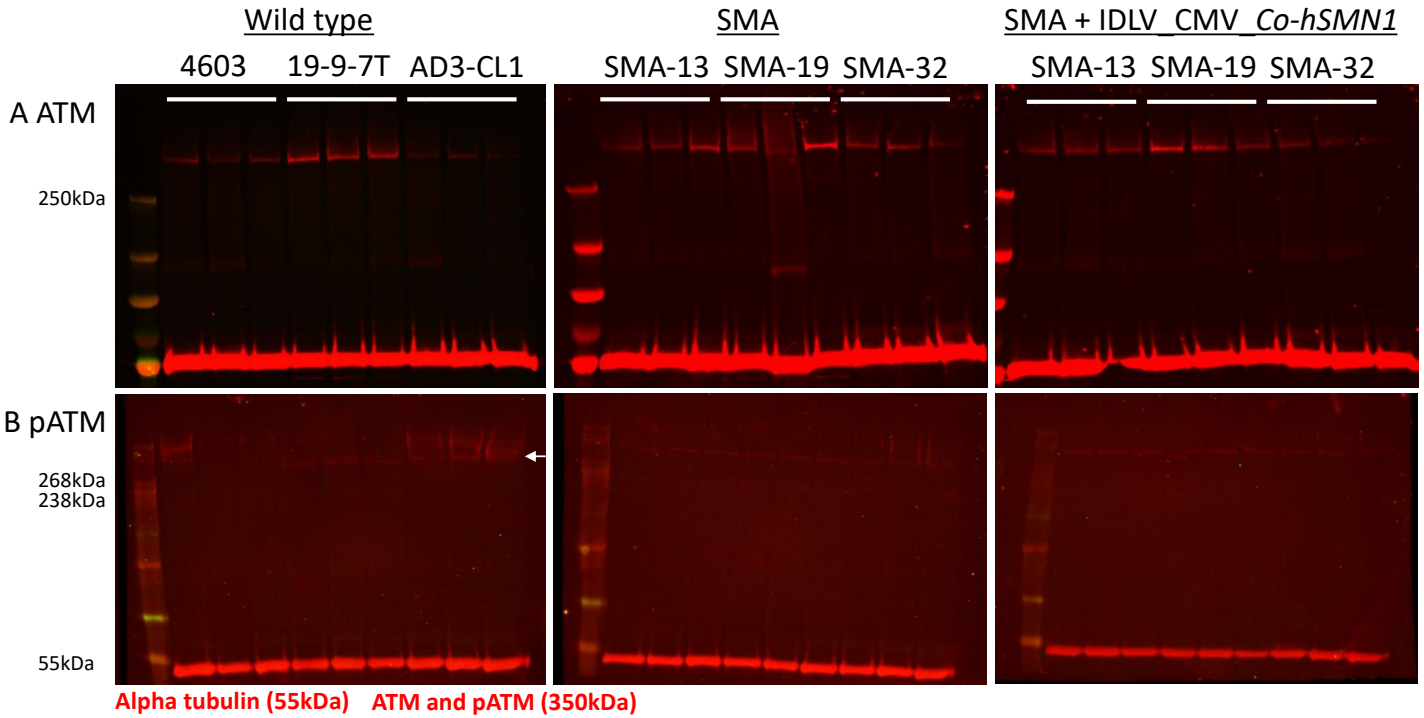


***Figure 7.17 ATM and pATM expression in wild type, SMA type I and SMA type I MNs transduced with IDLV_CMV_*Co-hSMN1.**

*Protein lysates from six MN lines, as well as IDLV_CMV_*Co-hSMN1 *MOI 75 transduced SMA type I MNs were run on western blots. (A) ATM and (B) pATM, indicated by an arrow in (B, left) signal was normalised to alpha tubulin. Total protein staining was not used as a loading control due to the nature of both ATM and pATM antibodies requiring a secondary antibody that is only detected in the 700nm (red) channel. (A) HiMark™ Prestained Protein Standard was unavailable at the time of the ATM western blot so PageRuler™ Prestained Plus protein ladder was used instead; unfortunately, this does not extend to proteins larger than 250kDa. (B) pATM western blots were later ran using HiMark™ Prestained Protein Standard, also with a lower concentration of rabbit anti-alpha tubulin antibody (0.2µg/ml compared to 0.33µg/ml) to reduce very high signal seen in (A).*

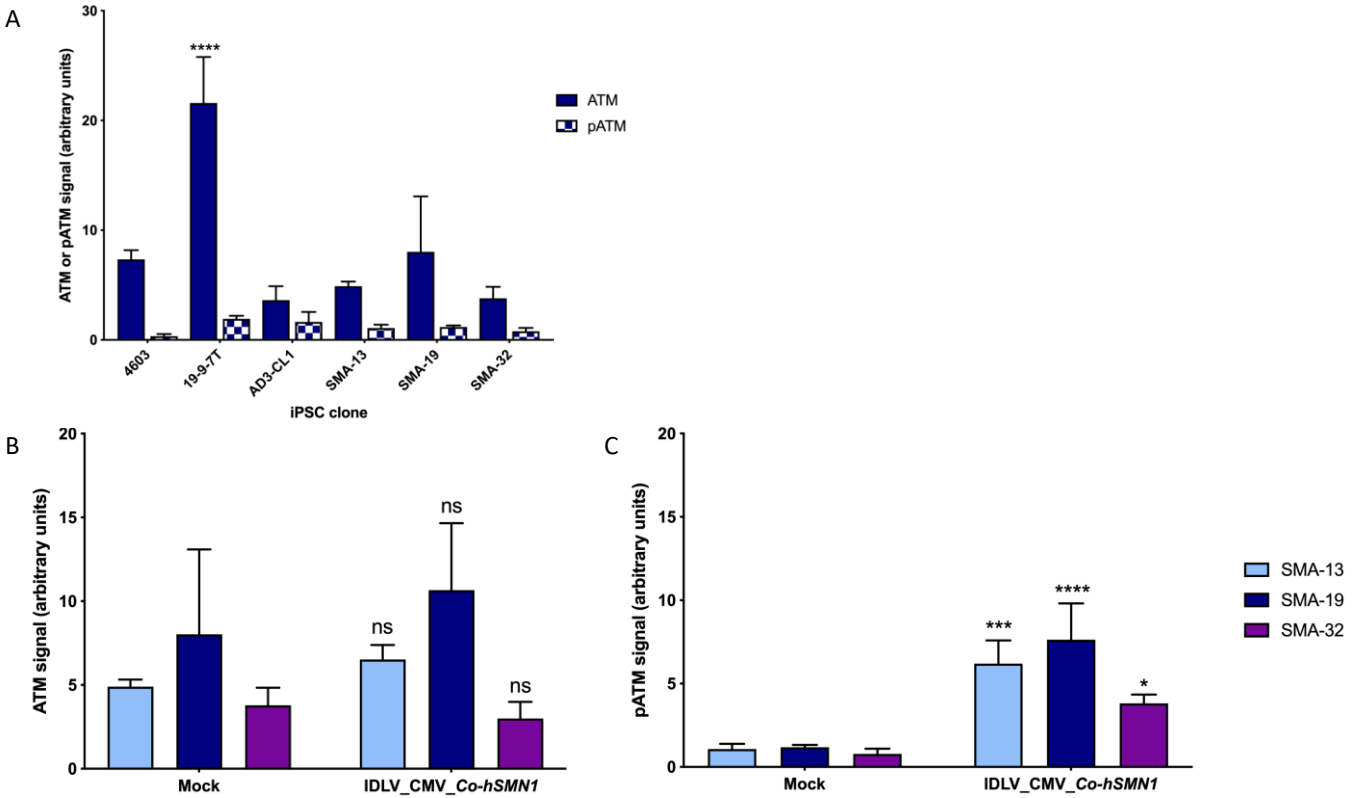


***Figure 7.18 Quantification of ATM and pATM in wild type, SMA type I and SMA type I MNs transduced with IDLV_CMV_Co-hSMN1.***

*(A) 19-9-7T ATM expression was significantly different from any other line's ATM expression (P<0.0001). pATM expression did not differ between all of the six lines tested (P>0.9999). The same values for SMA type I line's expression of ATM and pATM were used in (B) and (C) as mock samples. All western blots were run con-currently so that data could be shared across plots. (B) Within SMA type I MN lines, ATM expression was non-significantly different between mock samples and those transduced with IDLV_CMV_*Co-hSMN1 *at MOI 75 (SMA-13 P>0.9999, SMA-19 P=0.7778, SMA-32 P>0.9999). (C) pATM showed increased expression in transduced samples with a significant rise for SMA-13 (P=0.0025) and SMA-19 (P<0.0001), but only a trend for SMA-32 (P>0.9999). All statistical analyses were completed using two-way ANOVAs with Bonferroni multiple comparisons.*

## 7.5 Discussion

Firstly, an attempt to determine if transduction could improve MN survival was conducted. This involved the optimisation of a flow cytometric assay using two compounds that stained either apoptotic or dead cells. CellEvent™ Caspase-3/7 Green Detection Reagent has previously been used to detect apoptotic loss of MNs in long term culture following differentiation from ALS iPSCs (Bhinge et al., 2017). Here, transduction of MNs with IDLV_CMV_*Co-hSMN1* was implemented at either day 23 or day 28, representing immature, or mature MNs, respectively. A trend was seen for reducing SMN protein levels from day 23-32, and although transduction at either time point led to significant increases in SMN protein, the two were insignificantly different from one another. Perhaps even earlier transduction at the MNP stage (day 16) could have been able to induce some difference, but this was not tested here. However, results from the accompanying flow cytometry experiment were inconclusive. In retrospect, the use of flow cytometry to assess MN survival was perhaps not the most appropriate method of detection. Simpler methods of assessing MN cell numbers could have been employed, such as counting cells positive for MN markers, or those showing hallmark morphological features of MNs, at multiple time points and plotting the change in number over time. This would have generated preliminary data to confirm if MN cell numbers were indeed declining in SMA lines used in this project.

As the above assay provided no real insights into MN survival on a macroscopic level, a molecular approach was designed to assess proteins of interest involved in DNA damage and apoptotic pathways. The first of which was ATM and more importantly its phosphorylated form, pATM, which acts as a chief mobiliser of the above pathways. No differences in ATM expression was seen in both fibroblasts and MNs, between wild type and SMA, with the exception of particularly high ATM in the 19-9-7T MN line only. These results contrast to those seen in Kannan et al. (2018) where pATM was significantly increased in GM03813 and GM09677 fibroblasts (i.e. those that SMA-13 and SMA-19 iPSCs were derived from). Using the same protein lysate from 19-9-7T in the previous chapter (section 6.5.1) also provided the highest Gemin2 protein levels compared to any other line, but no difference in SMN was seen between 19-9-7T and other wild type MN lines. It is unclear why ATM and Gemin2 in 19-9-7T were unusually high. pATM showed a trend for increased levels in SMA fibroblasts, but no difference in MNs at all. pATM

could be further increased in SMA fibroblasts when treated with hydrogen peroxide at a dose that has previously been shown to have little effect on viability of cells or protein synthesis, but caused DNA synthesis to be abolished and exit from the cell cycle. This senescent phenotype with loss of replicative capacity was cumulative and irreversible (Chen and Ames, 1994).

It was hypothesised that should an increase in pATM be evident in SMA cells compared to wild type, as evidence of cellular stress, IDLV-mediated expression of SMN in SMA cells may bring down the pATM levels closer to normal. However, increases in pATM were in fact seen following transduction in both SMA type I fibroblasts and iPSC-derived MNs. It is also unclear whether the pATM increase in above experiments was due to the act of transduction alone, or if this was also mediated by the specific transgene expressed. Here, a trend was seen for increased pATM in cells transduced by *eGFP*- rather than *Co-hSMN1*-expressing vectors. Nevertheless, regardless of the transgene encoded, a reduction down to near wild type levels was not seen in any experiment conducted. Another group has published downregulation of DDR proteins following SMN restoration with an adenovirus (Kannan et al., 2018), but pATM was not measured specifically in this experiment, so it is unclear how this may have been affected by Ad transduction, or SMN restoration.

Naturally, cellular infection by viruses would activate innate immunity to prevent viral propagation. Host anti-viral factors may be activated upon lentiviral vector transduction of cells due to similarity of vector particles to those from an ancestral HIV-1 virus. VSV-G pseudotyped lentiviral vectors, such as those used in this project, rely on endocytosis to enter cells, potentially activating Toll-like receptors as they do so (Kajaste-Rudnitski and Naldini, 2015). The single stranded RNA vector genome, or double stranded RNA:DNA hybrids following reverse transcription, both act as pathogen-associated molecular patterns, alerting the cell to presence of the viral vector (Kajaste-Rudnitski and Naldini, 2015). This can also be exacerbated by plasmid contamination of laboratory-grade lentiviral vector preparations, despite best efforts to reduce these with DNaseI incubation, as employed here. Finally, 3$^{rd}$ generation lentiviral vectors lack pathogenic proteins such as Vpr, whose role normally is to counteract host anti-viral factors (Kajaste-Rudnitski and Naldini, 2015).

All of the above host anti-viral sensing mechanisms will act together to activate type I interferon (IFN) signaling and RNA interference mechanisms (Maillard et al., 2019) to prevent viral propagation, potentially resulting in the dampening of transduction efficiency and transgene expression. Similarly, conversion on IFN innate immunity will likely activate ATM. Both ATM and DNA-PKcs have been shown to be activated, in response to IFN-γ treatment (Morales et al., 2017). Since the activation of ATM is primarily mediated by its autophosphorylation, this will lead to an increase in the expression of pATM, possibly explaining the increased pATM seen following IDLV transduction in this chapter. Moreover, treatment with a Toll-like receptor 4 agonist (which could mimic activation caused by viral particles) and IFN-γ caused increases in γH2AX protein expression (Morales et al., 2017). Another group has found that unrepaired DNA lesions, such as those evidenced by the increased γH2AX foci in SMA fibroblasts seen in this chapter, primes the type I IFN system leading to enhanced anti-viral responses upon encounter with viral particles (Hartlova et al., 2015). This too would then exacerbate pATM increases and may lead to apoptosis of cells, as evidenced by increased cleaved caspase 3 signal. Future work should investigate these factors in response to IDLV transduction to determine if host anti-viral responses are indeed causing the observed changes in DNA damage response proteins.

It was postulated that perhaps the pATM increase mediated by activation of the DDR pathway, may peak shortly after transduction, but then settle again at a reduced level. Therefore, a delayed harvest at seven days post-transduction was also implemented as well as the normal three days post-transduction. Significantly increased pATM was shown in *eGFP*, but not *Co-hSMN1*, transduced samples compared to mock, in the short-term. However, analysis at a later time point suggested that pATM indeed decreases from its level at three days post-transduction, and in the case of *Co-hSMN1*-transduced cells, decreases to a level lower than in mock transduced cells. This suggests that restoring SMN protein levels by IDLV transduction can prove to be protective against DDR activation.

In this chapter it was shown that cleaved caspase 3 and γH2AX expression could be detected by immunofluorescence, but not western blotting. Despite other groups having managed to determine γH2AX levels by protein analysis (Hartlova et al., 2015, Kannan et al., 2018), this is not commonly used, with most literature opting for *in situ* methods such as immunofluorescence or immunocytochemistry (Yajima

et al., 2009, Jangi et al., 2017). Nevertheless, using immunofluorescence here a clear increase in both cleaved caspase 3 and γH2AX foci were seen in SMA cells compared to wild type, as expected from the literature (Parker et al., 2008, Sareen et al., 2012, Mutsaers et al., 2011, Jangi et al., 2017, Kannan et al., 2018). With this information a hypothesis was formed; if cleaved caspase 3 and γH2AX were increased as a result of SMN deficiency, it would be logical to expect a decrease in the expression of these proteins once SMN was restored, for example using lentiviral transduction.

However, no difference in cleaved caspase 3 was seen here. It is important to note a scoring system was devised here to quantitate cleaved caspase signal as it was not possible to count individual foci in cells that strongly expressed cleaved caspase 3. The use of this scoring system does come with the inherent limitation that scoring can be subjective, however attempts to limit this included setting reference nuclei with specific expression strengths that could be compared to all subsequent cells. Within transduced samples, some images showed stark differences in levels of apoptosis between neighbouring cells suggesting that adjacent cells are not uniformly affected by apoptosis-inducing factors. Should it be the case that some cells in a population do exhibit a very low level of cleaved caspase 3 following transduction, this may serve as evidence that rescue is possible in a subset of the population. It would be interesting to assess single cell responses on a larger scale, for example using flow cytometry. However, the intranuclear localisation of this protein would make this assay more challenging as flow cytometry is most often used to assess expression of cell surface markers.

The data presented in this chapter contrast to that in the literature. Transfection of PC12 rat adrenal medulla cells and Rat-1 fibroblasts with a *hSMN*-expressing plasmid was able to protect against apoptosis induced by trophic support withdrawal by 30%, improving cell viability to a level similar to transfection with the anti-apoptotic IAP-2 protein (Vyas et al., 2002). Adenoviral-expressed SMN has also been found to be protective against staurosporin-induced cell death, reducing the presence of TUNEL-positive cells exhibiting DNA fragmentation (Parker et al., 2008). Although *hSMN* transfection could not reduce cell death after UV irradiation or etopside treatment, it could lower the levels of p53-positive cells and prevent the release of cytochrome c immediately following insult (Vyas et al., 2002). SMN directly interacts with p53 via a domain encoded by exon 2 causing p53 to localise

within Cajal bodies bound to SMN (Figure 7.3); suggested as a mechanism to physically sequester p53 within a cellular compartment that inhibits it's function (Young et al., 2002). The delayed release of cytochrome c until 24 hours post-insult coincides with a significantly reduced intensity of the active p20 subunit of caspase 3, suggesting that SMN reduces caspase activation by delaying cytochrome c release (Vyas et al., 2002), a downstream consequence of p53 sequestration.

As it was unclear if cell death could be assessed by flow cytometry and as transduction did not improve cleaved caspase 3 signal, a marker of cellular apoptosis, a potential cause of cell death that could trigger the caspase cascade was assessed. Genomic instability caused by DNA DSBs is sensed by the MRN complex and this signal is transduced via ATM and downstream proteins such as H2AX (Figure 7.1). Transduction of this signal either leads to DNA repair by proteins such as BRCA1, or if damage is too severe, apoptosis. SMA fibroblasts have been found to have increased γH2AX expression here and elsewhere (Mutsaers et al., 2011, Jangi et al., 2017, Kannan et al., 2018). Primary SMA spinal cord neurons transduced with Ad_GFP_*SMN* has shown rescued expression of γH2AX (a marker of DSBs) and DNA-PKcs (a DNA repair protein) (Kannan et al., 2018), which had suggested that the presence of SMN can revert some molecular signatures of DNA damage. However, here, it was found that lentiviral mediated increase of SMN actually caused an increase in the proportion of cells that exhibited γH2AX foci, indicative of an increase in DNA DSBs. As stated earlier, lentiviral vector transduction is likely to trigger host anti-viral responses causing an increase in Toll-like receptor-transduced and type I IFN signaling, which when combined has been shown to induce increases in γH2AX expression (Hartlova et al., 2015).

The data presented in this chapter warrant further investigation of how IDLV_*Co-hSMN1* transduction leads to apparent increases in DNA damage-associated proteins, rather than restoring the low levels of these proteins that are present in wild type cells as was hypothesised. Assessment of DNA damage and apoptotic protein expression changes following *in vivo* administration of IDLVs would also be beneficial to determine if the patterns observed in this chapter are recapitulated in an animal model, or if these patterns are specifically seen *in vitro*. In the context of translating the use of IDLVs to animal models as a therapeutic strategy, the increases in DNA damage response proteins observed in this chapter pose a question of whether IDLV_*Co-hSMN1* administration would be as beneficial as

previously imagined. It is unclear at this time if the responses observed in this chapter are due to vector transduction itself, in which case analysis of the same proteins following transduction with a different vector, for example an integrating lentiviral vector, or an AAV vector, would be interesting, or if the supraphysiological levels of SMN induced by transduction could actually be detrimental in a system that has been severely lacking in SMN since development.

## 7.6 Conclusions

Taken together, the data presented here suggests that SMA cells exhibit molecular signatures associated with DNA damage and apoptosis such as significantly increased cleaved caspase 3 and γH2AX and a trend for increased pATM, despite no clear conclusions able to be drawn about their survival on a macroscopic level. The clear increase in pATM and γH2AX following transduction provides evidence that the vectors used here strongly activate the cell's DNA damage response pathways, potentially in response to host anti-viral mechanisms. Despite increases in both of these proteins, this did not translate to any difference in cellular apoptosis, as measured by cleaved caspase 3 signal. Further investigation into DNA damage response and apoptotic proteins following transduction is warranted.

# 8 Discussion and conclusions

## 8.1 Discussion

Spinal muscular atrophy is a devastating genetic disease that proves fatal by the age of two in the most severe cases. This disease has been the target for vast amounts of gene therapy research for almost two decades, culminating in the development and licensing approval of not one, but two, genetic therapies for SMA; Spinraza and Zolgensma.

Overall, this project aimed to further investigate SMA gene therapy approaches; analysing the pre-clinical development of the two licensed therapies whilst also developing a new strategy focusing on the delivery of the novel, sequence-optimised transgene *Co-hSMN1* within SMA *in vitro* systems. The novelty of the work presented in this thesis lies primarily in the development and testing of a human MN model for the assessment of integration-deficient lentiviral. Here IDLVs vectors were employed to safely express the novel *Co-hSMN1* transgene with much reduced risk of insertional mutagenesis, increasing the translatability of this gene therapy approach. The hypothesis stated that the expression of *Co-hSMN1* by viral vectors would increase SMN protein levels robustly across cell lines *in vitro* leading to an improved phenotype, something that if successful, could then be translated into an *in vivo* setting. In summary, the research presented here highlighted the following key findings.

Firstly, a meta-analysis was conducted to assess the current standing of pre-clinical SMA gene therapy. Meta-analyses, a term coined by Glass (Glass, 1976), provide the unique opportunity to integrate the findings of a collection of related studies, systematically reporting study design and characteristics, as well as incorporating heterogeneity between studies into overall conclusions (DerSimonian and Laird, 2015). To my knowledge, no other quantitative meta-analyses of gene therapies for SMA specifically have been performed, with only one systematic review compiling studies relating to antisense therapies in neurodegenerative and neuromuscular diseases (van der Bent et al., 2018). Here, it was found that administering gene therapy *in vivo* to various SMA models improved median survival significantly, but the manner in which the therapy was delivered fundamentally impacted the outcome. Specifically, the route and timing of therapeutic agent administration, the

model to which it was delivered and the therapeutic target were all found to significantly alter the efficacy of the treatment in question. It was also shown that pre-clinical efficacy was able to predict successful clinical translation of the six clinical trials assessing Spinraza (Chiriboga et al., 2016, Darras et al., 2019, Finkel et al., 2016, Finkel et al., 2017, Mercuri et al., 2018) and Zolgensma (Mendell et al., 2017). Here, no quantitative analysis was undertaken due to inconsistent reporting of clinical data within trials, but positive increases in HFMSE, HINE-2 and CHOP-INTEND motor function scales were reported frequently. This suggests improved responses in treatment groups, echoing the data from pre-clinical studies.

Secondly, extensive testing of IDLV and AAV9 vectors encoding *Co-hSMN1* under CMV, hSYN and hPGK promoters was completed in cell lines. These data revealed that IDLVs are able to transduce multiple cell lines and primary cells (HEK293T/17, Neuro2a, SH-SY5Y, CHO and wild type and SMA type I fibroblasts) with high efficiency, leading to increased SMN production and reformation of nuclear gems. The reformation of gems is an important endpoint suggesting that the SMN expressed from viral vectors is indeed functional and can localise to the correct subcellular compartment. These results are similar to those reported for lentiviral (Valori et al., 2010) and adenoviral (DiDonato et al., 2003) transduction, *SMN1* plasmid lipofection (Rashnonejad et al., 2016) and gene targeting (Feng et al., 2018) approaches. Analysis of SMN protein expression from each of the three transcriptionally controlled IDLVs showed that constitutive expression from the CMV promoter drove the highest SMN increases as was the case in a previous PhD project within this laboratory (Ali Mohammadi Nafchi, 2017), and also as expected from promoter comparisons in the literature (Damdindorj et al., 2014). The ubiquitous hPGK vectors and neuronal-specific hSYN vectors provided lower, but still significant improvements.

The data presented in this thesis build upon the successful implementation of gene therapy for SMA in many other laboratories, but provide further evidence of the efficacy of different approaches and vectors to target this disease, as well as the gold standard AAV9_*SMN1* published by many groups. Currently, limited use of lentiviral vectors to mediate *SMN* replacement for SMA has been reported *in vivo* (Azzouz et al., 2004) or *in vitro* (Valori et al., 2010). Lentiviral vectors have been used infrequently to rescue SMA phenotypes *in vitro*, for example, by expressing the SMA disease modifier Plastin3 (Alrafiah et al., 2018), or by siRNA downregulation of PTEN protein expression (Ning et al., 2010). *In vivo,* lentiviral

vectors would not be expected to induce widespread expression following a systemic injection, although some expression within the liver may bee seen after vascular delivery, instead inducing expression locally around the delivery site. When coupled with the fact that AAVs can express transgenes systemically and are able to efficiently cross the blood brain barrier (Foust et al., 2009), these vectors have often been favoured for *in vivo* gene therapy studies.

In contrast to the research suggesting that AAV9 vectors are successfully able to treat SMA *in vivo* (Foust et al., 2010, Valori et al., 2010, Passini et al., 2010, Dominguez et al., 2011), the data here suggest that *in vitro* lentiviral expression of *Co-hSMN1* was in fact superior to the AAV9 equivalent. Despite clear evidence of the *Co-hSMN1* transcript from both vectors within transduced cells, SMN increases were not detected following AAV9 transduction. To troubleshoot why transduction did not produce the expected SMN protein increases, various analyses were undertaken in an attempt to understand this surprising data. Increased SMN protein was only evident when the AAV9 transfer plasmid was transfected, or when cells were induced to exit the cell cycle prior to AAV9 transduction. The expression cassettes within IDLVs and AAV9s were designed to be equivalent with the exception of a CAG promoter in the AAV9 instead of a CMV in the IDLV. Since the CAG promoter is a chimera of CMV and elements from the chicken β-actin and β-globin genes and is thought to be more efficient than CMV, this does not wholly explain the data seen here. Although it is known that AAVs can efficiently transduce cells *in vitro* (Walker et al., 2017, Chandran et al., 2017, Iannitti et al., 2018) and successfully express transgenes relevant for gene therapy applications (Valori et al., 2010, Powis et al., 2016), no logical reasons for their inefficiency here could be found, despite extensive investigation.

Subsequently, a MN model of severe SMA was established by adapting and optimising a published protocol (Maury et al., 2015) that directs the differentiation of iPSCs into mature MNs. This optimised protocol was successfully employed to differentiate six iPSC lines (three wild type and three SMA type I), with all lines expressing markers of mature MNs such as SMI-32 and ChAT. SMA type I MNs recapitulated hallmarks of SMA *in vivo*, such as a lack of full length *SMN* transcripts and reduced SMN protein. These data echo the results seen in many other SMA iPSC MN studies (Ebert et al., 2009, Chang et al., 2011, Corti et al., 2012, Sareen et al., 2012, Yoshida et al., 2015, Nizzardo et al., 2015, Fuller et al., 2016, Powis et al., 2016). Using this iPSC MN model, transduction with IDLVs was able to increase

SMN protein production significantly but this could not rescue downstream Gemin2 protein levels.

Although every care was taken to remove intra-experiment variability by culturing and differentiating multiple iPSC lines simultaneously, obtaining biological replicates within iPSC MN lines and the use of three lines per genotype, it is important to note that inter-experiment variability may be present. Specifically, inter-experiment variability was seen when Gemin2 expression was rescued following transduction, with similar increases across the pilot and later experiments but differing significance levels seen in the SMA-32 line. Given the lengthy period of time necessary to grow and differentiate MNs (up to 8 weeks per round of differentiation), it was not always possible to repeat experiments independently using every iPSC line, representing an inherent limitation within this study. Despite this, data from MNs produced similar overall conclusions as those seen in cell lines earlier in this thesis, strengthening the argument that the emerging patterns were indeed robust despite the highlighted variability. Furthermore, these data suggest that translation of these vectors to *in vivo* systems would be advisable.

Finally, an aim of this thesis was to assess and attempt rescue of SMA phenotypes relating to DNA damage and apoptosis, something not well investigated prior to this. Although an improvement in MN survival could not be detected in short term experiments by flow cytometry, molecular analysis revealed that SMA cells show signatures of increased DNA damage and apoptosis, compared to wild type cells. Specifically, cleaved caspase 3 and γH2AX levels could not be rescued by IDLV_*Co-hSMN1* transduction, and in the case of γH2AX, actually exacerbated these further. These results contrasted with others seen in the literature where restoration of SMN was able to lower levels of cleaved caspase 3 (Vyas et al., 2002) and γH2AX (Kannan et al., 2018). However, some encouraging data were observed when analysis of pATM protein was undertaken. An initial increase in pATM was seen when assessed shortly after transduction, but with time, pATM levels decreased again. It was also observed that restoration of SMN protein levels by IDLV transduction could decrease pATM expression to below that of mock transduced cells, something that was not seen following control *eGFP* transduction, suggesting a protective effect of SMN.

It was hypothesised that the patterns observed may be due to IDLV transduction causing short-term host-anti viral responses to activate the DNA damage response (DDR) pathway molecules, further increasing their expression above that of SMA basal levels. However, it is important to note that unanswered questions still remain regarding how IDLV_*Co-hSMN1* transduction may impact a cell, and whether this will have both beneficial and detrimental effects. It would also be important to consider whether the data found here are conserved if other transgenes (not just the *eGFP* control used here) were expressed by IDLVs, determining if the increase in DDR is a general feature after IDLV transduction. These questions present avenues of investigation for future work.

Genetic therapies are now well established in the clinic for SMA, but limitations to these therapeutic strategies do exist. The data presented here add to those existing strategies by showing that lentiviral expression of *Co-hSMN1* is very efficient in both cell lines and iPSC MNs. The *in vitro* presented data here warrant *in vivo* testing of this approach to gain more insight into how this therapeutic approach may modulate survival *in vivo*. It is currently unclear whether the insights gained from DNA damage response experiments here would be similarly translated *in vivo*, and thus would be important to understand. To answer both of these questions, a collaboration with Melissa Bowerman (Keele University) has been forged where intraspinal injection of IDLVs expressing *Co-hSMN1* on the day of birth into *SMN2B/-* mice was agreed in principle. However, due to regulatory requirements and COVID-19 restrictions, this practical work has not yet been undertaken, but it is our hope that this will be completed in the near future.

A technical limitation apparent in this project that should be noted was the difficulty in undertaking immunofluorescence analysis of MNs. Primarily this was highlighted in section 5.5.2 when assessing markers of MN maturity, where the main problem encountered was the inability of cells to remain adherent to coverslips during fixation and antibody incubations or washes. Protocol optimisations following recommendations from colleagues were trialed but these did not lead to consistent successes. In chapter 5 it was suggested that variation within quality of MNs produced caused differing success rates when immunofluorescence protocols were applied. This was suggested as the same protocol could successfully be implemented, for example, in only one of two iPSC lines simultaneously differentiated or it was found that success was not line-specific as results varied between differentiation rounds of the same line. It is important to note that this

problem was only encountered some of the time and several successful experiments were completed, as evidenced in this thesis. However, due to the inconsistency encountered, experiments in MNs were not designed to be analysed by immunofluorescence wherever possible, for example necessitating the attempted optimisation of western blot detection of cleaved caspase 3 and γH2AX in chapter 7.

Another important limitation of this work to address, is that the SMA therapeutic field is saturated with therapies at various stages of development (see Figure 1.4 in section 1.1.4). It is therefore difficult to foresee if and how the IDLV_*Co-hSMN1* strategy developed here will progress further through translational studies and be distinguishable from those already further down the pipeline. Therefore, it is necessary to question how to best use this technology to maximise its potential benefits and indeed its worth to the SMA therapeutics field.

An ultimate goal for SMA gene therapies would be to correct the majority of pathologies occurring throughout the body. One potential approach to ensure maximal correction would be a combinatorial approach, as already proposed in the SMA field (Bowerman et al., 2017), perhaps using both an antisense oligonucleotide and a viral vector, or two viral vectors with different tropisms or temporal expression patterns. A dual viral vector approach would be optimal when using lentiviral vectors; an AAV may be used intravenously to address systemic pathologies whilst a lentivirus could reinforce expression in areas requiring particularly strong expression, for example within the spinal cord to address MN loss.

A second strategy to best use the IDLV_*Co-hSMN1* technology developed here would be to deliver these vectors pre-natally. *In utero* delivery of vectors favours widespread expression as the small size of the fetus, as well as the potential to transduce stem cells (Waddington et al., 2005), ensures maximal transduction. Secondly, if delivering vectors at a pre-symptomatic stage, the necessity for very fast-onset gene expression (provided by vectors such as self-complementary AAVs), is less important. All of these factors would suggest that lentiviral-based expression systems could be successful when treating diseases whose genesis occurs *in utero*. *In utero* delivery of an AAV9 for the treatment of SMA has only very recently been employed (Rashnonejad et al., 2019). However, this study showed only 44% of injected pups survived for the full gestation period with the authors citing this may have been caused by an inflammatory response to the AAV capsid. Patients receiving Zolgensma are required to have an anti-AAV9 antibody titre of

less than 1:50 (Mendell et al., 2017), with those above this value excluded from treatment. It is tempting to speculate that an alternative vector without the potential for inflammatory responses, could rectify the number of pups reaching full gestation, but no studies have been completed to confirm or refute this statement.

The translation from *in vitro* to *in vivo* is a key step in the pre-clinical development of any novel therapeutic agent, so the following experiments are proposed as future research based on this thesis. Firstly, administration of IDLVs on the day of birth in a severe SMA model would allow a comparison to AAV9 post-natal delivery studies already published, albeit an indirect comparison resulting from the direct CNS delivery of IDLVs, compared to intravenous delivery of AAVs. These experiments should assess any survival benefit, functional recovery of pups and biodistribution of *Co-hSMN1* expression. Following on from recently published data with eGFP labelling *in utero* (Ahmed et al., 2018), the biodistribution of both IDLVs and AAV9s following fetal delivery should be confirmed. Fetal delivery of vectors expressing *Co-hSMN1* is hypothesised to allow earlier correction of SMN deficiency pre-symptomatically, potentially preventing irreversible MN degeneration and development of the SMA phenotype. Understanding of transduction patterns of IDLVs and AAV9 *in utero* would then enable the potential for combined delivery of both vectors in an attempt to maximise therapeutic efficiency.

## 8.2 Conclusions

In conclusion, this project has summarised the state of SMA gene therapy within the vast amounts of literature published recently, highlighting the efficacy of genetic therapies in both pre-clinical and clinical trials. The laboratory-based data here have provided evidence that IDLV-mediated expression of a codon-optimised version of the *SMN1* gene can rescue SMN expression in multiple *in vitro* cell systems, including the tissue primarily affected in SMA; the motor neuron. An iPSC-derived MN differentiation protocol has been optimised to allow efficient generation of MNs within 28 days that recapitulate features of mature MNs *in vivo* as well as hallmarks of SMA disease. Furthermore, expression of *Co-hSMN1* can induce the reformation of gems within SMA type I cells, a downstream endpoint suggestive of functioning SMN protein. Finally, molecular analysis has revealed that DNA damage and apoptotic phenotypes in SMA type I cells is significantly higher than in wild type cells, but cannot be rescued by lentiviral transduction, however the reasons for this

are unclear. Taken together, these data add substantial evidence of the benefits of a gene therapy approach for SMA and present an alternative transgene and delivery system to those already in the SMA therapeutics pipeline.

# 9 References


*Abd Al Samid, M., Mcphee, J.S., Saini, J., Mckay, T.R., Fitzpatrick, L.M., Mamchaoui, K., Bigot, A., Mouly, V., Butler-Browne, G. & Al-Shanti, N. 2018. A functional human motor unit platform engineered from human embryonic stem cells and immortalized skeletal myoblasts. Stem Cells and Cloning-Advances and Applications, 11, 85-93.*

*Ahlskog, N., Hayler, D., Krueger, A., Kubinski, S., Claus, P., Hammond, S.M., Wood, M.J.A., Yanez-Munoz, R.J. & Bowerman, M. 2020. Muscle overexpression of Klf15 via an AAV8-Spc5-12 construct does not provide benefits in spinal muscular atrophy mice. Gene Therapy.*

*Ahmed, S.G., Waddington, S.N., Boza-Moran, M.G. & Yáñez-Muñoz, R.J. 2018. High-efficiency transduction of spinal cord motor neurons by intrauterine delivery of integration-deficient lentiviral vectors. Journal of Controlled Release, 273, 99-107.*

*Ali Mohammadi Nafchi, N. 2017. Gene therapy for the treatment of Spinal Muscular Atrophy. PhD Biology, Royal Holloway, University of London.*

*Almeida-Porada, G., Waddington, S., Chan, J.K.Y., Peranteau, W.H., Mackenzie, T. & Porada, C.D. 2019. In Utero Gene Therapy Consensus Statement from the IFeTIS. Molecular Therapy, 27.*

*Alrafiah, A., Karyka, E., Coldicott, I., Iremonger, K., Lewis, K.E., Ning, K. & Azzouz, M. 2018. Plastin 3 Promotes Motor Neuron Axonal Growth and Extends Survival in a Mouse Model of Spinal Muscular Atrophy. Mol Ther Methods Clin Dev, 9, 81-89.*

*Also-Rallo, E., Alias, L., Martinez-Hernandez, R., Caselles, L., Barcelo, M.J., Baiget, M., Bernal, S. & Tizzano, E.F. 2011. Treatment of spinal muscular atrophy cells with drugs that upregulate SMN expression reveals inter- and intra-patient variability. Eur J Hum Genet, 19, 1059-65.*

*Amirache, F., Lévy, C., Costa, C., Mangeot, P.E., Torbett, B.E., Wang, C.X., Nègre, D., Cosset, F.L. & Verhoeyen, E. 2014. Mystery solved: VSV-G-LVs do not allow efficient gene transfer into unstimulated T cells, B cells, and HSCs because they lack the LDL receptor. Blood, 123, 1422-1424.*

*Amoroso, M.W., Croft, G.F., Williams, D.J., O'keeffe, S., Carrasco, M.A., Davis, A.R., Roybon, L., Oakley, D.H., Maniatis, T., Henderson, C.E. & Wichterle, H. 2013. Accelerated High-Yield Generation of Limb-Innervating Motor Neurons from Human Stem Cells. Journal of Neuroscience, 33, 574-586.*

*Anderton, R.S., Meloni, B.P., Mastaglia, F.L., Greene, W.K. & Boulos, S. 2011. Survival of motor neuron protein over-expression prevents calpain-mediated cleavage and activation of procaspase-3 in differentiated human SH-SY5Y cells. . Neuroscience, 181, 226-233.*

*Andreassi, C., Angelozzi, C., Tiziano, F.D., Vitali, T., De Vincenzi, E., Boninsegna, A., Villanova, M., Bertini, E., Pini, A., Neri, G. & Brahe, C. 2004. Phenylbutyrate increases SMN expression in vitro: relevance for treatment of spinal muscular atrophy. Eur J Hum Genet, 12, 59-65.*

*Andreassi, C., Jarecki, J., Zhou, J., Coovert, D.D., Monani, U.R., Chen, X., Whitney, M., Pollok, B., Zhang, M., Androphy, E. & Burghes, A.H. 2001. Aclarubicin*

*treatment restores SMN levels to cells derived from type I spinal muscular atrophy patients. Hum Mol Genet, 10, 2841-9.*

*Andrews, P.W. 2006. The selfish stem cell. Nature Biotechnology, 24, 325-326.*

*Andrews, P.W., Ben-David, U., Benvenisty, N., Coffey, P., Eggan, K., Knowles, B.B., Nagy, A., Pera, M., Reubinoff, B., Rugg-Gunn, P.J. & Stacey, G.N. 2017. Assessing the Safety of Human Pluripotent Stem Cells and Their Derivatives for Clinical Applications. Stem Cell Reports, 9, 1-4.*

*Araujo, A., Araujo, M. & Swoboda, K.J. 2009. Vascular Perfusion Abnormalities in Infants with Spinal Muscular Atrophy. Journal of Pediatrics, 155, 292-294.*

*Armbruster, N., Lattanzi, A., Jeavons, M., Van Wittenberghe, L., Gjata, B., Marais, T., Martin, S., Vignaud, A., Voit, T., Mavilio, F., Barkats, M. & Buj-Bello, A. 2016. Efficacy and biodistribution analysis of intracerebroventricular administration of an optimized scAAV9-SMN1 vector in a mouse model of spinal muscular atrophy. Mol Ther Methods Clin Dev, 3, 16060.*

*Avery, S., Hirst, A.J., Baker, D., Lim, C.Y., Alagaratnam, S., Skotheim, R.I., Lothe, R.A., Pera, M.F., Colman, A., Robson, P., Andrews, P.W. & Knowles, B.B. 2013. BCL-XL Mediates the Strong Selective Advantage of a 20q11.21 Amplification Commonly Found in Human Embryonic Stem Cell Cultures. Stem Cell Reports, 1, 379-386.*

*Avexis. 2019. Overview of the Zolgensma clinical studies [Online]. Available: https://www.zolgensma.com/clinical-study [Accessed 21st October 2019].*

*Azzouz, M., Le, T., Ralph, G.S., Walmsley, L., Monani, U.R., Lee, D.C., Wilkes, F., Mitrophanous, K.A., Kingsman, S.M., Burghes, A.H. & Mazarakis, N.D. 2004. Lentivector-mediated SMN replacement in a mouse model of spinal muscular atrophy. J Clin Invest, 114, 1726-31.*

*Baccon, J., Pellizzoni, L., Rappsilber, J., Mann, M. & Dreyfuss, G. 2002. Identification and characterization of Gemin7, a novel component of the survival of motor neuron complex. Journal of Biological Chemistry, 277, 31957-31962.*

*Balabanian, S., Gendron, N.H. & Mackenzie, A.E. 2007. Histologic and transcriptional assessment of a mild SMA model. Neurological Research, 29, 413-424.*

*Barczak, W., Suchorska, W., Rubiś, B. & Kulcenty, K. 2015. Universal Real-Time PCR-Based Assay for Lentiviral Titration. Molecular Biotechnology, 57, 195-200.*

*Barral, S. & Kurian, M.A. 2016. Utility of Induced Pluripotent Stem Cells for the Study and Treatment of Genetic Diseases: Focus on Childhood Neurological Disorders. Frontiers in Molecular Neuroscience, 9.*

*Battaglia, G., Princivalle, A., Forti, F., Lizier, C. & Zeviani, M. 1997. Expression of the SMN gene, the spinal muscular atrophy determining gene, in the mammalian central nervous system. Human Molecular Genetics, 6, 1961-1971.*

*Baughan, T., Shababi, M., Coady, T.H., Dickson, A.M., Tullis, G.E. & Lorson, C.L. 2006. Stimulating full-length SMN2 expression by delivering bifunctional RNAs via a viral vector. Mol Ther, 14, 54-62.*

*Baughan, T.D., Dickson, A., Osman, E.Y. & Lorson, C.L. 2009. Delivery of bifunctional RNAs that target an intronic repressor and increase SMN levels in an animal model of spinal muscular atrophy. Hum Mol Genet, 18, 1600-11.*

*Bedi, P.K., Castro-Codesal, M.L., Featherstone, R., Albalawi, M.M., Alkhaledi, B., Kozyrskyj, A.L., Flores-Mir, C. & Maclean, J.E. 2018. Long-term Non-Invasive Ventilation in Infants: A Systematic Review and Meta-Analysis. Frontiers in Pediatrics, 6.*

*Benkhelifa-Ziyyat, S., Besse, A., Roda, M., Duque, S., Astord, S., Carcenac, R., Marais, T. & Barkats, M. 2013. Intramuscular scAAV9-SMN injection mediates widespread gene delivery to the spinal cord and decreases disease severity in SMA mice. Mol Ther, 21**,** 282-90.*

*Bergin, A., Kim, G., Price, D.L., Sisodia, S.S., Lee, M.K. & Rabin, B. 1997. Identification and characterization of a mouse homologue of the Spinal Muscular Atrophy-determining gene, survival motor neuron. Gene, 204**,** 47-53.*

*Bertini, E., Dessaud, E., Mercuri, E., Muntoni, F., Kirschner, J., Reid, C., Lusakowska, A., Comi, G.P., Cuisset, J.M., Abitbol, J.L., Scherrer, B., Ducray, P.S., Buchbjerg, J., Vianna, E., Van Der Pol, W.L., Vuillerot, C., Blaettler, T. & Fontoura, P. 2017. Safety and efficacy of olesoxime in patients with type 2 or non-ambulatory type 3 spinal muscular atrophy: a randomised, double-blind, placebo-controlled phase 2 trial. Lancet Neurology, 16**,** 513-522.*

*Besse, A., Astord, S., Marais, T., Roda, M., Giroux, B., Lejeune, F.X., Relaix, F., Smeriglio, P., Barkats, M. & Biferi, M.G. 2020. AAV9-Mediated Expression of SMN Restricted to Neurons Does Not Rescue the Spinal Muscular Atrophy Phenotype in Mice. Molecular Therapy, 28.*

*Bevan, A.K., Hutchinson, K.R., Foust, K.D., Braun, L., Mcgovern, V.L., Schmelzer, L., Ward, J.G., Petruska, J.C., Lucchesi, P.A., Burghes, A.H. & Kaspar, B.K. 2010. Early heart failure in the SMNDelta7 model of spinal muscular atrophy and correction by postnatal scAAV9-SMN delivery. Hum Mol Genet, 19**,** 3895-905.*

*Bhinge, A., Namboori, S.C., Zhang, X., Van Dongen, A.M.J. & Stanton, L.W. 2017. Genetic correction of SOD1 mutant iPSCs reveals ERK and JNK activated AP1 as a driver of neurodegeneration in Amyotrophic Lateral Sclerosis. Stem cell reports, 8**,** 856-869.*

*Blackford, A.N. & Jackson, S.P. 2017. ATM, ATR, and DNA-PK: The Trinity at the Heart of the DNA Damage Response. Molecular Cell, 66**,** 801-817.*

*Bogdanik, L.P., Osborne, M.A., Davis, C., Martin, W.P., Austin, A., Rigo, F., Bennett, C.F. & Lutz, C.M. 2015. Systemic, postsymptomatic antisense oligonucleotide rescues motor unit maturation delay in a new mouse model for type II/III spinal muscular atrophy. Proc Natl Acad Sci U S A, 112**,** E5863-72.*

*Borghese, L., Dolezalova, D., Opitz, T., Haupt, S., Leinhaas, A., Steinfarz, B., Koch, P., Edenhofer, F., Hampl, A. & Brustle, O. 2010. Inhibition of notch signaling in human embryonic stem cell- derived neural stem cells delays G1/S phase transition and accelerates neuronal differentiation in vitro and in vivo. Stem Cells, 28**,** 955-964.*

*Bowerman, M., Anderson, C.L., Beauvais, A., Boyl, P.P., Witke, W. & Kothary, R. 2009. SMN, profilin IIa and plastin 3: A link between the deregulation of actin dynamics and SMA pathogenesis. Molecular and Cellular Neuroscience, 42**,** 66-74.*

*Bowerman, M., Becker, C.G., Yáñez-Muñoz, R.J., Ning, K., Wood, M., Gillingwater, T.H. & Talbot, K. 2017. Therapeutic strategies for spinal muscular atrophy: SMN and beyond. Disease Models & Mechanisms, 10, 943-954.*

*Bowerman, M., Murray, L.M., Beauvais, A., Pinheiro, B. & Kothary, R. 2012. A critical smn threshold in mice dictates onset of an intermediate spinal muscular atrophy phenotype associated with a distinct neuromuscular junction pathology. Neuromuscular Disorders, 22, 263-276.*

*Bowerman, M., Murray, L.M., Scamps, F., Schneider, B.L., Kothary, R. & Raoul, C. 2018. Pathogenic commonalities between spinal muscular atrophy and amyotrophic lateral sclerosis: Converging roads to therapeutic development. Eur J Med Genet, 61, 685-698.*

*Boza-Moran, M.G. 2012. Modelling SMA using induced pluripotent stem cells from a discordant affected family., Royal Holloway, University of London.*

*Briese, M., Richter, D.U., Sattelle, D.B. & Ulfig, N. 2006. SMN, the Product of the Spinal Muscular Atrophy-Determining Gene, Is Expressed Widely but Selectively in the Developing Human Forebrain. The Journal of Comparative Neurology, 497, 808-816.*

*Brimble, S.N., Sherrer, E.S., Uhl, E.W., Wang, E., Kelly, S., Merill, A.H.J., Robbins, A.J. & Schulz, T.C. 2007. The Cell Surface Glycosphingolipids SSEA-3 and SSEA-4 Are Not Essential for Human ESC Pluripotency. Stem Cells, 25, 54-62.*

*Buning, H., Braun-Falco, M. & Hallek, M. 2004. Progress in the use of adeno-associated viral vectors for gene therapy. Cells Tissues Organs, 177, 139-150.*

*Burger, C., Nguyen, F.N., Deng, J. & Mandel, R.J. 2005. Systemic mannitol-induced hyperosmolality amplifies rAAV2-mediated striatal transduction to a greater extent than local co-infusion. Molecular Therapy, 11, 327-331.*

*Burnett, B.G., Munoz, E., Tandon, A., Kwon, D.Y., Sumner, C.J. & Fischbeck, K.H. 2009. Regulation of SMN Protein Stability. Molecular and Cellular Biology, 29, 1107-1115.*

*Butera, S. 2018. CAR-T: trailblazing the path from clinical development to the clinic. Gene Therapy, 25, 163-164.*

*Campbell, L., Hunter, K.M., Mohaghegh, P., Tinsley, J.M., Brasch, M.A. & Davies, K.E. 2000. Direct interaction of Smn with dp103, a putative RNA helicase: a role for Smn in transcription regulation? Human Molecular Genetics, 9, 1093-1100.*

*Caron, L., Kher, D., Lee, K.L., Mckernan, R., Dumevska, B., Hidalgo, A., Li, J., Yang, H., Main, H., Ferri, G., Petek, L.M., Poellinger, L., Miller, D.G., Gabellini, D. & Schmidt, U. 2016. A Human Pluripotent Stem Cell Model of Facioscapulohumeral Muscular Dystrophy-Affected Skeletal Muscles. Stem Cell Translational Medicine, 5, 1145-1161.*

*Carr, D.J., Wallace, J.M., Aitken, R.P., Milne, J.S., Mehta, V., Martin, J.F., Zachary, I.C., Peebles, D.M. & David, A.L. 2014. Uteroplacental Adenovirus Vascular Endothelial Growth Factor Gene Therapy Increases Fetal Growth Velocity in Growth-Restricted Sheep Pregnancies. Human Gene Therapy, 25, 375-384.*

*Chan, J.K.Y., Gil-Farina, I., Johana, N., Rosales, C., Tan, Y.W., Ceiler, J., Mcintosh, J., Ogden, B., Waddington, S.N., Schmidt, M., Biswas, A., Choolani, M., Nathwani, A.C. & Mattar, C.N.Z. 2019. Therapeutic expression of human clotting factors IX and X following adeno-associated viral vector-mediated*

*intrauterine gene transfer in early-gestation fetal macaques. Faseb Journal, 33, 3954-3967.*

*Chandran, J.S., Sharp, P.S., Karyka, E., Aves-Cruzeiro, J.M.D., Coldicott, I., Castelli, L., Hautbergue, G., Collins, M.O. & Azzouz, M. 2017. Site Specific Modification of Adeno-Associated Virus Enables Both Fluorescent Imaging of Viral Particles and Characterization of the Capsid Interactome. Scientific Reports, 7.*

*Chang, T., Zheng, W., Tsark, W., Bates, S., Huang, H., Lin, R.J. & Yee, J.K. 2011. Phenotypic Rescue of Induced Pluripotent Stem Cell-Derived Motoneurons of a Spinal Muscular Atrophy Patient. Stem Cells, 29, 2090-2093.*

*Chansel-Debordeaux, L., Bourdenx, M., Dovero, S., Grouthier, V., Dutheil, N., Espana, A., Groc, L., Jimenez, C., Bezard, E. & Dehay, B. 2017. In utero delivery of rAAV2/9 induces neuronal expression of the transgene in the brain: towards new models of Parkinson's disease. Gene Therapy, 24, 801-809.*

*Charroux, B., Pellizzoni, L., Perkinson, R.A., Shevchenko, A., Mann, M. & Dreyfuss, G. 1999. Gemin3: a novel DEAD box protein that interacts with SMN, the spinal muscular atrophy gene product, and is a component of gems. Journal of Cell Biology, 147, 1181-1194.*

*Charroux, B., Pellizzoni, L., Perkinson, R.A., Yong, J., Shevchenko, A., Mann, M. & Dreyfuss, G. 2000. Gemin4. A novel component of the SMN complex that is found in both gems and nucleoli. Journal of Cell Biology, 148, 1177-1186.*

*Chauhan, D.P., Srivastava, A.S., Moustafa, M.E., Shenouda, S. & Carrier, E. 2004. In utero gene therapy: prospect and future. Current Pharmaceutical Design, 10, 3663-3672.*

*Chen, Q. & Ames, B.N. 1994. Senescence-like growth arrest induced by hydrogen-peroxide in human-diploid fibroblast F65 cells. PNAS USA, 91, 4130-4134.*

*Chiriboga, C. 2020. JEWELFISH: Safety and Pharmacodynamic Data in Non-Naive Patients with Spinal Muscular Atrophy Receiving Treatment with Risdiplam. Cure SMA Research and Clinical Care Virtual Sessions. Virtual.*

*Chiriboga, C.A., Swoboda, K.J., Darras, B.T., Iannaccone, S.T., Montes, J., De Vivo, D.C., Norris, D.A., Bennett, C.F. & Bishop, K.M. 2016. Results from a phase 1 study of nusinersen (ISIS-SMNRx) in children with spinal muscular atrophy. Neurology, 86, 890-897.*

*Cho, S., Moon, H., Loh, T.J., Oh, H.K., Cho, S., Choy, H.E., Song, W.K., Chun, J.S., Zheng, X. & Shen, H. 2014. hnRNP M facilitates exon 7 inclusion of SMN2 pre-mRNA in spinal muscular atrophy by targeting an enhancer on exon 7. Biochim Biophys Acta, 1839, 306-15.*

*Coady, T.H. & Lorson, C.L. 2010. Trans-splicing-mediated improvement in a severe mouse model of spinal muscular atrophy. J Neurosci, 30, 126-30.*

*Coovert, D.D., Le, T.T., Morris, G.E., Man, N.T., Kralewski, M., Sendtners, M. & Burghes, A.H.M. 2000. Does the survival motor neuron protein (SMN) interact with Bcl-2? Journal of Medical Genetics, 37, 536-539.*

*Corey, D.R. 2017. Nusinersen, an antisense oligonucleotide drug for spinal muscular atrophy. Nature Neuroscience, 20, 497-499.*

*Corti, S., Nizzardo, M., Simone, C., Falcone, M., Nardini, M., Ronchi, D., Donadoni, C., Salani, S., Riboldi, G., Magri, F., Menozzi, G., Bonaglia, C., Rizzo, F., Bresolin, N. & Comi, G.P. 2012. Genetic correction of human induced pluripotent stem*

*cells from patients with spinal muscular atrophy. Sci Transl Med, 4, 165ra162.*

*D'ydewalle, C., Ramos, D.M., Pyles, N.J., Ng, S.Y., Gorz, M., Pilato, C.M., Ling, K.R., Kong, L.L., Ward, A.J., Rubin, L.L., Rigo, F., Bennett, C.F. & Sumner, C.J. 2017. The Antisense Transcript SMN-AS1 Regulates SMN Expression and Is a Novel Therapeutic Target for Spinal Muscular Atrophy. Neuron, 93, 66-79.*

*Dabbous, O., Maru, B., Jansen, J.P., Lorenzi, M., Cloutier, M., Guerin, A., Pivneva, I., Wu, E.Q., Arjunji, R., Feltner, D. & Sproule, D.M. 2019. Survival, Motor Function, and Motor Milestones: Comparison of AVXS-101 Relative to Nusinersen for the Treatment of Infants with Spinal Muscular Atrophy Type 1. Advances in Therapy, 36, 1164-1176.*

*Dai, G., Xu, Q., Luo, R., Gao, J.F., Chen, H., Deng, Y., Li, Y.Q., Wang, Y.Q., Yuan, W.Z. & Wu, X.S. 2015. Atorvastatin treatment improves effects of implanted mesenchymal stem cells: meta-analysis of animal models with acute myocardial infarction. Bmc Cardiovascular Disorders, 15.*

*Damdindorj, L., Karnan, S., Ota, A., Hossain, E., Konishi, Y., Hosokawa, Y. & Konishi, H. 2014. A Comparative Analysis of Constitutive Promoters Located in Adeno-Associated Viral Vectors. . Plos One, 9.*

*Darras, B.T., Chiriboga, C.A., Iannaccone, S.T., Swoboda, K.J., Montes, J., Mignon, L., Xia, S.T., Bennett, C.F., Bishop, K.M., Shefner, J.M., Green, A.M., Sun, P., Bhan, I., Gheuens, S., Schneider, E., Farwell, W., De Vivo, D.C., Castro, D., Cowie, M., Gilbreath, H., Johnson, S., Kauk, M., Khan, M., Mcelroy, E., Kneirbein, E.N., Nelson, L., Smith, L., Trest, S., Aziz-Zaman, S., Cappell, J., Constantinescu, A., Cruz, R., Dastgir, J., Dunaway, S., Holuba, N., Khandji, A.G., Kramer, S., Marra, J., Ortiz-Miller, C., Popolizio, M., Salazar, R., Sanabria, L., Sproule, D.M., Weimer, L., Berde, C., Binalsheikh, I., Graham, R., Kang, P., Koka, A., Landrigan, M., Liew, W., Markowitz, J., Paldino, M., Prabhu, S., Sethna, N., Yang, E., Butterfield, R., Dibella, D., Dixon, M., Gibson, S., Howard, E., Jensen, B., Johnson, N.E., Lei, D., Mayne, K., Murphy, K.J., Newcomb, T.M., Niu, S., Page, M., Pucillo, E., Ramos, C., Rao, A., Rausch, N.M., Redd, W.C., Villanueva, S.R., Davis, J.R., Sakonji, A., Smart, A.L., Sorenson, S., Stevens, A., Tennyson, R., Trussell, D.V., Wood, J.L., Workman, M.J., Grp, I.C.S. & Grp, I.C.S. 2019. Nusinersen in later-onset spinalmuscular atrophy Long-term results from the phase 1/2 studies. Neurology, 92, E2492-E2506.*

*David, A.L., Torondel, B., Zachary, I., Wigley, V., Nader, K.A., Mehta, V., Buckley, S.M.K., Cook, T., Boyd, M., Rodeck, C.H., Martin, J. & Peebles, D.M. 2008. Local delivery of VEGF adenovirus to the uterine artery increases vasorelaxation and uterine blood flow in the pregnant sheep. Gene Therapy, 15, 1344-1350.*

*Day, J. 2020. SUNFISH Part 1: 24-month Safety and Exploratory Outcomes of Risdiplam (RG7916) Treatment in Patients with Type 2 or 3 Spinal Muscular Atrophy (SMA). Cure SMA Research and Clinical Care Virtual Sessions. Virtual.*

*Delanote, V., Vandekerckhove, J. & Gettemans, J. 2005. Plastins: versatile modulators of actin organization in (patho)physiological cellular processes,. Acta Pharmacologica Sinica, 26, 769–779.*

*Deml, L., Bojak, A., Steck, S., Graf, M., Wild, J., Schirmbeck, R., Wolf, H. & Wagner, R. 2001. Multiple effects of codon usage optimization on expression and immunogenicity of DNA candidate vaccines encoding the human immunodeficiency virus type 1 Gag protein. Journal of Virology, 75, 10991-11001.*

*Dersimonian, R. & Laird, N.M. 1986. Meta-analysis in clinical trials. Controlled Clinical Trials, 7, 177-188.*

*Dersimonian, R. & Laird, N.M. 2015. Meta-analysis in clinical trials revisted. Contemperary Clinical Trials, 45, 139-145.*

*Deveraux, Q.L., Roy, N., Stennicke, H.R., Van Arsdale, T., Zhou, Q., Srinivasula, S.M., Alnemri, E.S., Salvesen, G.S. & Reed, J.C. 1998. IAPs block apoptotic events induced by caspase-8 and cytochrome c by direct inhibition of distinct caspases. Embo Journal, 17, 2215-2223.*

*Deymeer, F., Serdaroglu, P., Parman, Y. & Poda, M. 2008. Natural history of SMA IIIb - Muscle strength decreases in a predictable sequence and magnitude. Neurology, 71, 644-649.*

*Di Tomaso, M.V., Basso, S., Lafon-Hughes, L., Saona, G., Lopez-Carro, B., Reyes-Abalos, A.L. & Liddle, P. 2014. Spontaneous and Bleomycin-Induced γ H2AX Signals in CHO9 Metaphase Chromosomes. Advances in Bioscience and Biotechnology, 5, 603-616.*

*Didonato, C.J., Chen, X.N., Noya, D., Korenberg, J.R., Nadeau, J.H. & Simard, L.R. 1997. Cloning, characterisation and copy number of the murine survival motor neuron gene: homolog of the spinal muscular atrophy-determining gene. Genome Research, 7, 339-352.*

*Didonato, C.J., Parks, R.J. & Kothary, R. 2003. Development of a gene therapy strategy for the restoration of survival motor neuron protein expression: implications for spinal muscular atrophy therapy. Hum Gene Ther, 14, 179-88.*

*Dittgen, T., Nimmerjahn, A., Komai, S., Licznerski, P., Waters, J., Margrie, T.W., Helmchen, F., Denk, W., Brecht, M. & Osten, P. 2004. Lentivirus-based genetic manipulations of cortical neurons and their optical and electrophysiological monitoring in vivo. Proceedings of the National Academy of Sciences of the United States of America, 101, 18206-18211.*

*Dolmetsch, R. & Geschwind, D.H. 2011. The human brain in a dish: the promise of iPSC-derived neurons. Cell, 145, 831-4.*

*Dominguez, E., Marais, T., Chatauret, N., Benkhelifa-Ziyyat, S., Duque, S., Ravassard, P., Carcenac, R., Astord, S., Pereira De Moura, A., Voit, T. & Barkats, M. 2011. Intravenous scAAV9 delivery of a codon-optimized SMN1 sequence rescues SMA mice. Hum Mol Genet, 20, 681-93.*

*Donadon, I., Bussani, E., Riccardi, F., Licastro, D., Romano, G., Pianigiani, G., Pinotti, M., Konstantinova, P., Evers, M., Lin, S., Ruegg, M.A. & Pagani, F. 2019. Rescue of spinal muscular atrophy mouse models with AAV9-Exon-specific U1 snRNA. Nucleic Acids Research, 47, 7618-7632.*

*Douglas, A.G. & Wood, M.J. 2013. Splicing therapy for neuromuscular disease. Mol Cell Neurosci, 56, 169-85.*

*Dragunow, M. 2008. The adult human brain in preclinical drug development. Nature Reviews Drug Discovery, 7, 659-666.*

*Draper, J.S., Pigott, C., Thomson, J.A. & Andrews, P.W. 2002. Surface antigens of human embryonic stem cells: changes upon differentiation in culture. Journal of Anatomy, 200, 249-258.*

*Dressman, D., Ahearn, M.E., Yariz, K.O., Basterrecha, H., Martinez, F., Palau, F., Barmada, M.M., Clark, R.D., Meindl, A., Wirth, B., Hoffman, E.P. & Baumbach-Reardon, L. 2007. X-linked infantile spinal muscular atrophy: Clinical definition and molecular mapping. Genetics in Medicine, 9, 52-60.*

*Du, Z.W., Chen, H., Liu, H., Lu, J., Qian, K., Huang, C.T.L., Xhong, X., Fan, F. & Zhang, S.C. 2015. Generation and expansion of highly pure neuron progenitors from human pluripotent stem cells. . Nature communications, 6, 6626.*

*Duque, S., Joussemet, B., Riviere, C., Marais, T., Dubreil, L., Douar, A.M., Fyfe, J., Moullier, P., Colle, M.A. & Barkats, M. 2009. Intravenous Administration of Self-complementary AAV9 Enables Transgene Delivery to Adult Motor Neurons. Molecular Therapy, 17, 1187-1196.*

*Duque, S.I., Arnold, W.D., Odermatt, P., Li, X.H., Porensky, P.N., Schmelzer, L., Meyer, K., Kolb, S.J., Schumperli, D., Kaspar, B.K. & Burghes, A.H.M. 2015. A Large Animal Model of Spinal Muscular Atrophy and Correction of Phenotype. Annals of Neurology, 77, 399-414.*

*Duval, S. & Tweedie, R. 2000. Trim and fill: A simple funnel-plot-based method of testing and adjusting for publication bias in meta-analysis. Biometrics, 56, 455-463.*

*Eaton, S.L., Roche, S.L., Llavero Hurtado, M., Oldknow, K.J., Farquharson, C., Gillingwater, T.H. & Wishart, T.M. 2013. Total protein analysis as a reliable loading control for quantitative fluorescent western blotting. PLoS One, 8, e72457.*

*Ebert, A.D., Yu, J., Rose, F.F., Jr., Mattis, V.B., Lorson, C.L., Thomson, J.A. & Svendsen, C.N. 2009. Induced pluripotent stem cells from a spinal muscular atrophy patient. Nature, 457, 277-80.*

*Edens, B.M., Ajroud-Driss, S., Ma, L. & Ma, Y.C. 2015. Molecular mechanisms and animal models of spinal muscular atrophy. Biochimica Et Biophysica Acta-Molecular Basis of Disease, 1852, 685-692.*

*Egger, M., Smith, G.D., Schneider, M. & Minder, C. 1997. Bias in meta-analysis detected by a simple, graphical test. Bmj-British Medical Journal, 315, 629-634.*

*Elshafay, A., Hieu, T.H., Doheim, M.F., Kassem, M.a.M., Eldoadoa, M.F., Holloway, S.K., Abo-Elghar, H., Hirayama, K. & Huy, N.T. 2019. Efficacy and Safety of Valproic Acid for Spinal Muscular Atrophy: A Systematic Review and Meta-Analysis. CNS Drugs, 33, 239-250.*

*Ema 2020. New gene therapy to treat spinal muscular atrophy (corrected).*

*Engberg, N., Kahn, M., Petersen, D.R., Hansson, M. & Serup, P. 2010. Retinoic acid synthesis promotes development of neural progenitors from mouse embryonic stem cells by suppressing endogenous, Wnt-dependent nodal signaling. Stem Cells, 28, 1498-1509.*

*Engelman, A. 1999. In vivo analysis of retroviral integrase structure and function. In: MARAMOROSCH, K., MURPHY, F. A. & SHATKIN, A. J. (eds.) Advances in Virus Research.*

*Fan, Q.W., Iosbe, I., Asou, H.H., Yanagisawa, K. & Michikawa, M. 2001. Expression and regulation of apoliporpotein E receptors in the cells of the central nervous system in culture: a review. Journal of the American Aging Association, 24, 1-10.*

*Faravelli, I., Bucchia, M., Rinchetti, P., Nizzardo, M., Simone, C., Frattini, E. & Corti, S. 2014. Motor neuron derivation from human embryonic and induced pluripotent stem cells: experimental approaches and clinical perspectives. Stem Cell Research & Therapy, 5.*

*Farrar, M.A., Park, S.B., Vucic, S., Carey, K.A., Turner, B.J., Gillingwater, T.H., Swoboda, K.J. & Kiernan, M.C. 2017. Emerging Therapies and Challenges in Spinal Muscular Atrophy. Annals of Neurology, 81, 355-368.*

*Farrelly-Rosch, A., Lau, C.L., Patil, N., Turner, B.J. & Shabanpoor, F. 2017. Combination of valproic acid and morpholino splice-switching oligonucleotide produces improved outcomes in spinal muscular atrophy patient-derived fibroblasts. Neurochem Int, 108, 213-221.*

*Fda. 2018. What is Gene Therapy? [Online]. Available: https://www.fda.gov/vaccines-blood-biologics/cellular-gene-therapy-products/what-gene-therapy [Accessed 22nd May 2020.*

*Feng, M., Liu, C., Xia, Y., Liu, B., Zhou, M., Li, Z., Sun, Q., Hu, Z., Wang, Y., Wu, L., Liu, X. & Liang, D. 2018. Restoration of SMN expression in mesenchymal stem cells derived from gene-targeted patient-specific iPSCs. J Mol Histol, 49, 27-37.*

*Ferri, A., Melki, J. & Kato, A.C. 2004. Progressive and selective degeneration of motoneurons in a mouse model of SMA. Neuroreport, 15, 275-280.*

*Finkel, R.S., Chiriboga, C.A., Vajsar, J., Day, J.W., Montes, J., De Vivo, D.C., Yamashita, M., Rigo, F., Hung, G., Schneider, E., Norris, D.A., Xia, S., Bennett, C.F. & Bishop, K.M. 2016. Treatment of infantile-onset spinal muscular atrophy with nusinersen: a phase 2, open-label, dose-escalation study. Lancet, 388, 3017-3026.*

*Finkel, R.S., Mercuri, E., Darras, B.T., Connolly, A.M., Kuntz, N.L., Kirschner, J., Chiriboga, C.A., Saito, K., Servais, L., Tizzano, E., Topaloglu, H., Tulinius, M., Montes, J., Glanzman, A.M., Bishop, K., Zhong, Z.J., Gheuens, S., Bennett, C.F., Schneider, E., Farwell, W. & De Vivo, D.C. 2017. Nusinersen versus Sham Control in Infantile-Onset Spinal Muscular Atrophy. N Engl J Med, 377, 1723-1732.*

*Finkelshtein, D., Werman, A., Novick, D., Barak, S. & Rubinstein, M. 2013. LDL receptor and its family members serve as the cellular receptors for vesicular stomatitis virus. PNAS, 110, 7306-7311.*

*Fitzsimons, H.L. & During, M.J. 2005. Design and optimization of expression cassettes including promoter choice and regulatory elements. In: KAPLITT, M. G. (ed.) Gene Therapy of the Central Nervous System: From Bench to Bedside. Elsevier.*

*Foecking, M.K. & Hofstetter, H. 1986. Powerful and versatile enhancer-promoter unit for mammalian expression vectors. . Gene, 45, 101-105.*

*Foust, K.D., Nurre, E., Montgomery, C.L., Hernandez, A., Chan, C.M. & Kaspar, B.K. 2009. Intravascular AAV9 preferentially targets neonatal neurons and adult astrocytes. Nat Biotechnol, 27, 59-65.*

*Foust, K.D., Wang, X.Y., Mcgovern, V.L., Braun, L., Bevan, A.K., Haidet, A.M., Le, T.T., Morales, P.R., Rich, M.M., Burghes, A.H.M. & Kaspar, B.K. 2010. Rescue of the spinal muscular atrophy phenotype in a mouse model by early postnatal delivery of SMN. Nature Biotechnology, 28, 271-U126.*

*Frattini, E., Ruggieri, M., Salani, S., Faravelli, I., Zanetta, C., Nizzardo, M., Simone, C., Magri, F. & Corti, S. 2015. Pluripotent stem cell-based models of spinal muscular atrophy. Molecular and Cellular Neuroscience, 64, 44-50.*

*Fuller, H.R., Mandefro, B., Shirran, S.L., Gross, A.R., Kaus, A.S., Botting, C.H., Morris, G.E. & Sareen, D. 2016. Spinal muscular atrophy patient iPSC-derived motor neurons have reduced expression of proteins important in neuronal development. Frontiers in Cellular Neuroscience, 9, 506.*

*Gabanella, F., Butchbach, M.E.R., Saieva, L., Carissimi, C., Burghes, A.H.M. & Pellizzoni, L. 2007. Ribonucleoprotein Assembly Defects Correlate with Spinal Muscular Atrophy Severity and Preferentially Affect a Subset of Spliceosomal snRNPs. Plos One, 2.*

*Gangwani, L., Mikrut, M., Theroux, S., Sharma, M. & Davis, R.J. 2001. Spinal muscular atrophy disrupts the interaction of ZPR1 with the SMN protein. Nature Cell Biology, 3, 376-383.*

*Gao, G., Vandenberge, L.H., Alvira, M.R., Lu, Y., R., C., Zhou, X. & Wilson, J.M. 2004. Clades of Adeno-associated viruses are widely disseminated in human tissues. . Journal of Virology, 78, 6381-6388.*

*Gaspar, H.B., Parsley, K.L., Howe, S., King, D., Gilmour, K.C., Sinclair, J., Brouns, G., Schmidt, M., Von Kalle, C., Barington, T., Jakobsen, M.A., Christensen, H.O., Al Ghonaium, A., White, H.N., Smith, J.L., Levinsky, R.J., Ali, R.R., Kinnon, C. & Thrasher, A.J. 2004. Gene therapy of X-linked severe combined immunodeficiency by use of a pseudotyped gammaretroviral vector. Lancet, 364, 2181-2187.*

*Geib, T. & Hertel, K.J. 2009. Restoration of full-length SMN promoted by adenoviral vectors expressing RNA antisense oligonucleotides embedded in U7 snRNAs. PLoS One, 4, e8204.*

*Gibson, C.L. & Murphy, S.P. 2010. Benefits of histone deacetylase inhibitors for acute brain injury: a systematic review of animal studies. Journal of Neurochemistry, 115, 806-813.*

*Giesemann, T., Rathke-Hartlieb, S., Rothkegel, M., Bartsch, J.W., Buchmeier, S., Jockusch, B.M. & Jockusch, H. 1999. A role for polyproline motifs in the spinal muscular atrophy protein SMN. Profilins bind to and colocalize with smn in nuclear gems. Journal of Biological Chemistry, 274, 37908–37914.*

*Gilliam, T.C., Brzustowicz, L.M., Castilla, L.H., Lehner, T., Penchaszadeh, G.K., R.J., D., Byth, B.C., Knowles, J., Hislop, J.E., Shapira, Y., Dubowitz, V., Munsat, T.L., Ott, J. & Davies, K.E. 1990. Gentic homogeneity between acute and chronic forms of spinal muscular atrophy. Nature, 345.*

*Glascock, J.J., Osman, E.Y., Wetz, M.J., Krogman, M.M., Shababi, M. & Lorson, C.L. 2012a. Decreasing disease severity in symptomatic, Smn(-/-);SMN2(+/+), spinal muscular atrophy mice following scAAV9-SMN delivery. Hum Gene Ther, 23, 330-5.*

*Glascock, J.J., Shababi, M., Wetz, M.J., Krogman, M.M. & Lorson, C.L. 2012b. Direct central nervous system delivery provides enhanced protection following*

*vector mediated gene replacement in a severe model of spinal muscular atrophy. Biochem Biophys Res Commun, 417, 376-81.*

*Glass, G.V. 1976. Primary, secondary, and meta-analysis of research. Educational Researcher, 5, 3-8.*

*Gong, Y., Klein Wolterink, R.G.L., Janssen, I., Groot, A.J., Bos, G.M.J. & Germeraad, W.T.V. 2020. Rosuvastatin Enhances VSV-G Lentiviral Transduction of NK Cells via Upregulation of the Low-Density Lipoprotein Receptor. Mol Ther Methods Clin Dev, 17, 634-646.*

*Goulet, B.B., Mcfall, E.R., Wong, C.M., Kothary, R. & Parks, R.J. 2013. Supraphysiological expression of survival motor neuron protein from an adenovirus vector does not adversely affect cell function. Biochem Cell Biol, 91, 252-64.*

*Gray, S.J., Foti, S.B., Schwartz, J.W., Bachaboina, L., Taylor-Blake, B., Coleman, J., Ehlers, M.D., Zylka, M.J., Mccown, T.J. & Samulski, R.J. 2011. Optimizing Promoters for Recombinant Adeno-Associated Virus-Mediated Gene Expression in the Peripheral and Central Nervous System Using Self-Complementary Vectors. Human Gene Therapy, 22, 1143-1153.*

*Gray, S.J. & Samulski, R.J. 2011. Vector design and considerations for CNS applications. In: GLORIOSO, J. (ed.) Gene vector design and application to treat nervous system disorders. Washington, DC: Society for Neuroscience.*

*Groen, E.J.N., Talbot, K. & Gillingwater, T.H. 2018. Advances in therapy for spinal muscular atrophy: promises and challenges. Nat Rev Neurol, 14, 214-224.*

*Gubitz, A.K., Feng, W. & Dreyfuss, G. 2004. The SMN complex. Experimental Cell Research, 296, 51-56.*

*Gubitz, A.K., Mourelatos, Z., Abel, L., Rappsilber, J., Mann, M. & Dreyfuss, G. 2002. Gemin5, a novel WD repeat protein component of the SMN complex that binds Sm proteins. Journal of Biological Chemistry, 277, 5631-5636.*

*Guo, X., Das, M., Rumsey, J., Gonzalez, M., Stancescu, M. & Hickman, J. 2010. Neuromuscular junction formation between human stem cell derived motoneurons and rat skeletal muscle in a defined system. . Tissue Engineering: Part C, 1, 1347-1355.*

*Gustafsson, C., Govindarajan, S. & Minshull, J. 2004. Codon bias and heterologous protein expression. Trends in Biotechnology, 22, 346-353.*

*Hacein-Bey-Abina, S., Von Kalle, C., Schmidt, M., Mcccormack, M.P., Wulffraat, N., Leboulch, P., Lim, A., Osborne, C.S., Pawliuk, R., Morillon, E., Sorensen, R., Forster, A., Fraser, P., Cohen, J.I., De Saint Basile, G., Alexander, I., Wintergerst, U., Frebourg, T., Aurias, A., Stoppa-Lyonnet, D., Romana, S., Radford-Weiss, I., Gross, F., Valensi, F., Delabesse, E., Macintyre, E., Sigaux, F., Soulier, J., Leiva, L.E., Wissler, M., Prinz, C., Rabbitts, T.H., Le Deist, F., Fischer, A. & Cavazzana-Calvo, M. 2003. LMO2-associated clonal T cell proliferation in two patients after gene therapy for SCID-X1. Science, 302, 415-419.*

*Haidich, A.B. 2010. Meta-analysis in medical research. Hippokratia, 14, 29-37.*

*Hamdan, F.F., Mousa, A. & Ribeiro, P. 2002. Codon optimization improves heterologous expression of a Schistosoma mansoni cDNA in HEK293 cells. Parasitology Research, 88, 583-586.*

*Hamilton, G. & Gillingwater, T.H. 2013. Spinal muscular atrophy: going beyond the motor neuron. Trends in Molecular Medicine, 19, 40-50.*

*Hammond, S.M., Hazell, G., Shabanpoor, F., Saleh, A.F., Bowerman, M., Sleigh, J.N., Meijboom, K.E., Zhou, H., Muntoni, F., Talbot, K., Gait, M.J. & Wood, M.J. 2016. Systemic peptide-mediated oligonucleotide therapy improves long-term survival in spinal muscular atrophy. Proc Natl Acad Sci U S A, 113, 10962-7.*

*Han, Z.Y., Hendrickson, E.A., Bremner, T.A. & Wyche, J.H. 1997. A sequential two-step mechanism for the production of the mature p17:p12 form of caspase-3 in vitro. Journal of Biological Chemistry, 272, 13432-13436.*

*Hao, L.T., Burghes, A.H.M. & Beattie, C.E. 2011. Generation and Characterization of a genetic zebrafish model of SMA carrying the human SMN2 gene. Molecular Neurodegeneration, 6.*

*Hao, L.T., Duy, P.Q., Jontes, J.D., Wolman, M., Granato, M. & Beattie, C.E. 2013. Temporal requirement for SMN in motoneuron development. Human Molecular Genetics, 22, 2612-2625.*

*Hao, L.T., Fuller, H.R., Lam, L.T., Le, T.T., Burghes, A.H.M. & Morris, G.E. 2007. Absence of gemin5 from SMN complexes in nuclear Cajal bodies. Bmc Cell Biology, 8.*

*Hartlova, A., Erttmann, S.F., Raffi, F.a.M., Schmalz, A.M., Resch, U., Anugula, S., Lienenklaus, S., Nilsson, L.M., Kroeger, A., Nilsson, J.A., Ek, T., Weiss, S. & Gekara, N.O. 2015. DNA Damage Primes the Type I Interferon System via the Cytosolic DNA Sensor STING to Promote Anti-Microbial Innate Immunity. Immunity, 42, 332-343.*

*Hayler, D. 2017. Optimisation of viral delivery of SMN1 for the therapy of spinal muscular atrophy. MSc Biological Sciences, Royal Holloway, University of London.*

*Hedlund, E., Karlsson, M., Osborn, T., Ludwig, W. & Isacson, O. 2010. Global gene expression profiling of somatic motor neuron populations with different vulnerability identify molecules and pathways of degeneration and protection. Brain, 133, 2313-2330.*

*Hermes, K., Schneider, P., Krieg, P., Dang, A.T., Huttner, K. & Schneider, H. 2014. Prenatal Therapy in Developmental Disorders: Drug Targeting via Intra-Amniotic Injection to Treat X-Linked Hypohidrotic Ectodermal Dysplasia. Journal of Investigative Dermatology, 134, 2985-2987.*

*Hirst, T.C., Vesterinen, H.M., Sena, E.S., Egan, K.J., Macleod, M.R. & Whittle, I.R. 2013. Systematic review and meta-analysis of temozolomide in animal models of glioma: was clinical efficacy predicted? British Journal of Cancer, 108, 64-71.*

*Hoffman, J. 1891. Ueber chronische spinale Muskelatophie im Kindersalter. . Deutsch Ztschv f Nerrenh, 1, 95.*

*Holehonnur, R., Lella, S.K., Ho, A., Luong, J.A. & Ploski, J.E. 2015. The production of viral vectors designed to express large and difficult to express transgenes within neurons. Molecular Brain, 8, 12.*

*Hornburg, D., Drepper, C., Butter, F., Meissner, F., Sendtner, M. & Mann, M. 2014. Deep Proteomic Evaluation of Primary and Cell Line Motoneuron Disease*

*Models Delineates Major Differences in Neuronal Characteristics. Molecular & Cellular Proteomics, 13, 3410-3420.*

*Hosseinibarkooie, S., Peters, M., Torres-Benito, L., Rastetter, R.H., Hupperich, K., Hoffmann, A., Mendoza-Ferreira, N., Kaczmarek, A., Janzen, E., Milbradt, J., Lamkemeyer, T., Rigo, F., Bennett, C.F., Guschlbauer, C., Buschges, A., Hammerschmidt, M., Riessland, M., Kye, M.J., Clemen, C.S. & Wirth, B. 2016. The Power of Human Protective Modifiers: PLS3 and CORO1C Unravel Impaired Endocytosis in Spinal Muscular Atrophy and Rescue SMA Phenotype. Am J Hum Genet, 99, 647-665.*

*Hou, P., Li, Y., Zhang, X., Liu, C., Guan, J., Li, H., Zhao, T., Ye, J., Yang, W., Liu, K., Ge, J., Xu, J., Zhang, Q., Zhao, Y. & Deng, H. 2013. Pluripotent Stem Cells Induced from Mouse Somatic Cells by Small-Molecule Compounds. Science, 341, 651-654.*

*Howe, S.J., Mansour, M.R., Schwarzwaelder, K., Bartholomae, C., Hubank, M., Kempski, H., Brugman, M.H., Pike-Overzet, K., Chatters, S.J., De Ridder, D., Gilmour, K.C., Adams, S., Thornhill, S.I., Parsley, K.L., Staal, F.J.T., Gale, R.E., Linch, D.C., Bayford, J., Brown, L., Quaye, M., Kinnon, C., Ancliff, P., Webb, D.K., Schmidt, M., Von Kalle, C., Gaspar, H.B. & Thrasher, A.J. 2008. Insertional mutagenesis combined with acquired somatic mutations causes leukemogenesis following gene therapy of SCID-X1 patients. Journal of Clinical Investigation, 118, 3143-3150.*

*Hsieh-Li, H.M., Chang, J.G., Jong, Y.J., Wu, M., H., Wang, N.M., Tsai, C.H. & Li, H. 2000. A mouse model for spinal muscular atrophy. Nature Genetics, 24, 66-70.*

*Hua, Y., Liu, Y.H., Sahashi, K., Rigo, F., Bennett, C.F. & Krainer, A.R. 2015. Motor neuron cell-nonautonomous rescue of spinal muscular atrophy phenotypes in mild and severe transgenic mouse models. Genes Dev, 29, 288-97.*

*Hua, Y., Sahashi, K., Rigo, F., Hung, G., Horev, G., Bennett, C.F. & Krainer, A.R. 2011. Peripheral SMN restoration is essential for long-term rescue of a severe spinal muscular atrophy mouse model. Nature, 478, 123-126.*

*Hua, Y.M., Vickers, T.A., Baker, B.F., Bennett, C.F. & Krainer, A.R. 2007. Enhancement of SMN2 Exon 7 inclusion by antisense oligonucleotides targeting the exon. Plos Biology, 5, 729-744.*

*Huangfu, D., Maehr, R., Guo, W., Eijkelenboom, A., Snitow, M., Chen, A.E. & Melton, D.A. 2008. Induction of pluripotent stem cells by defined factors is greatly improved by small-molecule compounds. Nat Biotechnol, 26, 795-7.*

*Hukriede, N.A., Joly, L., Tsang, M., Miles, J., Tellis, P., Epstein, J.A., Barbazuk, W.B., Li, F.N., Paw, B., Postlethwait, J.H., Hudson, T.J., Zon, L.I., Mcpherson, J.D., Chevrette, M., Dawid, I.B., Johnson, S.L. & Ekker, M. 1999. Radiation hybrid mapping of the zebrafish genome. PNAS USA, 96, 9745-9750.*

*Hunter, G., Roche, S.L., Somers, E., Fuller, H.R. & Gillingwater, T.H. 2014. The influence of storage parameters on measurement of survival motor neuron (SMN) protein levels: Implications for pre-clinical studies and clinical trials for spinal muscular atrophy. Neuromuscular Disorders, 24, 973-977.*

*Hutson, T.H., Verhaagen, J., Yáñez-Muñoz, R.J. & Moon, L.D. 2012. Corticospinal tract transduction: a comparison of seven adeno-associated viral vector serotypes and a non-integrating lentiviral vector. Gene Therapy, 19, 49-60.*

*Hwee, D.T., Kennedy, A.R., Hartman, J.J., Ryans, J., Durham, N., Malik, F.L. & Jasper, J.R. 2015. The small-molecule fast skeletal troponin activator, CK-2127107, improves exercise tolerance in a rat model of heart failure. Journal of Pharmacology and Experimental Therapeutics, 353, 159-168.*

*Iannitti, T., Scarrott, J.M., Likhite, S., Coldicott, I.R.P., Lewis, K.E., Heath, P.R., Higginbottom, A., Myszczynska, M.A., Milo, M., Hautbergue, G.M., Meyer, K., Kaspar, B.K., Ferraiuolo, L., Shaw, P.J. & Azzouz, M. 2018. Translating SOD1 Gene Silencing toward the Clinic: A Highly Efficacious, Off-Target-free, and Biomarker-Supported Strategy for fALS. Molecular Therapy-Nucleic Acids, 12, 75-88.*

*Ichida, J.K., Blanchard, J., Lam, K., Son, E.Y., Chung, J.E., Egli, D., Loh, K.M., Carter, A.C., Di Giorgio, F.P., Koszka, K., Huangfu, D., Akutsu, H., Liu, D.R., Rubin, L.L. & Eggan, K. 2009. A small-molecule inhibitor of tgf-Beta signaling replaces sox2 in reprogramming by inducing nanog. Cell Stem Cell, 5, 491-503.*

*Inada, E., Saitoh, I., Kubota, N., Iwase, Y., Murakami, T., Sawami, T., Yamasaki, Y. & Sato, M. 2019. Increased Expression of Cell Surface SSEA-1 is Closely Associated with Naive-Like Conversion from Human Deciduous Teeth Dental Pulp Cells-Derived iPS Cells. International Journal of Molecular Sciences, 20.*

*Iwahashi, H., Eguchi, Y., Yasuhara, N., Hanafusa, T., Matsuzawa, Y. & Tsujimoto, Y. 1997. Synergistic anti-apoptotic activity be- tween Bcl-2 and SMN implicated in spinal muscular atrophy. Nature, 390, 413-417.*

*Jablonka, S., Schrank, B., Kralewski, M., Rossoll, W. & Sendtner, M. 2000. Reduced survival motor neuron (Smn) gene dose in mice leads to motor neuron degeneration: an animal model for spinal muscular atrophy type III. Human Molecular Genetics, 9, 341-346.*

*Jacob, J. & Briscoe, J. 2003. Gli proteins and the control of spinal-cord patterning. EMBO Reports, 4, 761-765.*

*Jangi, M., Fleet, C., Cullen, P., Gupta, S.V., Mekhoubad, S., Chiao, E., Allaire, N., Bennett, C.F., Rigo, F., Krainer, A.R., Hurt, J.A., Carulli, J.P. & Staropoli, J.F. 2017. SMN deficiency in severe models of spinal muscular atrophy causes widespread intron retention and DNA damage. Proceedings of the National Academy of Sciences of the United States of America, 114, E2347-E2356.*

*Janzen, E., Mendoza-Ferreira, N., Hosseinibarkooie, S., Schneider, S., Hupperich, K., Tschanz, T., Grysko, V., Riessland, M., Hammerschmidt, M., Rigo, F., Bennett, C.F., Kye, M.J., Torres-Benito, L. & Wirth, B. 2018. CHP1 reduction ameliorates spinal muscular atrophy pathology by restoring calcineurin activity and endocytosis. Brain, 141, 2343-2361.*

*Jue, T.J., Hirst, T.C., Sena, E.S., Macleod, M.R. & Mcdonald, K.L. 2017. A SYSTEMATIC REVIEW AND META-ANALYSIS OF TOPOISOMERASE INHIBITION IN PRE-CLINICAL GLIOMA MODELS. Neuro-Oncology, 19, 59-59.*

*Kaifer, K.A., Villalon, E., Osman, E.Y., Glascock, J.J., Arnold, L.L., Cornelison, D.D.W. & Lorson, C.L. 2017. Plastin-3 extends survival and reduces severity in mouse models of spinal muscular atrophy. JCI Insight, 2, e89970.*

*Kajaste-Rudnitski, A. & Naldini, L. 2015. Cellular Innate Immunity and Restriction of Viral Infection: Implications for Lentiviral Gene Therapy in Human Hematopoietic Cells. Human Gene Therapy, 26, 201-209.*

*Kam, R.K.T., Deng, Y., Chen, Y. & Zhao, H. 2012. Retinoic acid synthesis and functions in early embryonic development. Cell & Bioscience, 2, 11.*

*Kannan, A., Bhatia, K., Branzei, D. & Gangwani, L. 2018. Combined deficiency of Senataxin and DNA-PKcs causes DNA damage accumulation and neurodegeneration in spinal muscular atrophy. Nucleic Acids Research, 46, 8326-8346.*

*Keil, J.M., Seo, J., Howell, M.D., Hsu, W.H., Singh, R.N. & Didonato, C.J. 2014. A short antisense oligonucleotide ameliorates symptoms of severe mouse models of spinal muscular atrophy. Mol Ther Nucleic Acids, 3, e174.*

*Kernochan, L.E., Russo, M.L., Woodling, N.S., Huynh, T.N., Avila, A.M., Fischbeck, K.H. & Sumner, C.J. 2005. The role of histone acetylation in SMN gene expression. Human Molecular Genetics, 14, 1171-1182.*

*Kerr, D.A., Nery, J.P., Traystman, R.J., Chau, B.N. & Hardwick, J.M. 2000. Survival motor neuron protein modulates neuron-specific apoptosis. Proceedings of the National Academy of Sciences of the United States of America, 97, 13312-13317.*

*Kim, J.K. & Monani, U.R. 2018. Augmenting the SMN Protein to Treat Infantile Spinal Muscular Atrophy. Neuron, 97, 1001-1003.*

*Kline, R.A., Kaifer, K.A., Osman, E.Y., Carella, F., Tiberi, A., Ross, J., Pennetta, G., Lorson, C.L. & Murray, L.M. 2017. Comparison of independent screens on differentially vulnerable motor neurons reveals alpha-synuclein as a common modifier in motor neuron diseases. Plos Genetics, 13.*

*Kong, L.L., Wang, X.Y., Choe, D.W., Polley, M., Burnett, B.G., Bosch-Marce, M., Griffin, J.W., Rich, M.M. & Sumner, C.J. 2009. Impaired Synaptic Vesicle Release and Immaturity of Neuromuscular Junctions in Spinal Muscular Atrophy Mice. Journal of Neuroscience, 29, 842-851.*

*Kubota, M., Sakakihara, Y., Uchiyama, Y., Nara, A., Nagata, T., Nitta, H., Ishimoto, K., Oka, A., Horio, K. & Yanagisawa, M. 2000. New ocular movement detector system as a communication tool in ventilator-assisted Werdnig-Hoffmann disease. Developmental Medicine and Child Neurology, 42, 61-64.*

*Kugelberg, E. & Welander, L. 1956. Heredo-familial juvenile muscular atrophy simulating muscular dystrophy. AMA Arch Neurol Psychiatry, 75, 500.*

*Kugler, S., Kilic, E. & Bahr, M. 2003. Human synapsin 1 gene promoter confers highly neuron-specific long-term transgene expression from an adenoviral vector in the adult rat brain depending on the transduced area. Gene Therapy, 10, 337-347.*

*Kugler, S., Meyn, L., Holzmuller, H., Gerhardt, E., Isenmann, S., Schulz, J.B. & Bahr, M. 2001. Neuron-specific expression of therapeutic proteins: Evaluation of different cellular promoters in recombinant adenoviral vectors. Molecular and Cellular Neuroscience, 17, 78-96.*

*Lai, J.I., Leman, L.J., Ku, S., Vickers, C.J., Olsen, C.A., Montero, A., Ghadiri, M.R. & Gottesfeld, J.M. 2017. Cyclic tetrapeptide HDAC inhibitors as potential therapeutics for spinal muscular atrophy: Screening with iPSC-derived neuronal cells. Bioorg Med Chem Lett, 27, 3289-3293.*

*Landfeldt, E., Edstrom, J., Sejersen, T., Tulinius, M., Lochmuller, H. & Kirschner, J. 2019. Quality of life of patients with spinal muscular atrophy: A systematic review. European Journal of Paediatric Neurology, 23, 347-356.*

*Le, T.T., Pham, L.T., Butchbach, M.E.R., Zhang, H.L., Monani, U.R., Coovert, D.D., Gavrilina, T.O., Xing, L., Bassell, G.J. & Burghes, A.H.M. 2005. SMN Delta 7, the major product of the centromeric survival motor neuron (SMN2) gene, extends survival in mice with spinal muscular atrophy and associates with full-length SMN. Human Molecular Genetics, 14, 845-857.*

*Lefebvre, S., Burgen, L., Reboullet, S., Clermont, O., Burlet, P., Viollet, L., Benichou, B., Cruaud, C., Millasseau, P., Zeviani, M., Le Paslier, D., Frezal, J., Cohen, D., Weissenbach, J., Munnich, A. & Melki, J. 1995. Identification and characterisation of a spinal muscular atrophy-determining gene. Cell, 80.*

*Lesbordes, J.C., Cifuentes-Diaz, C., Miroglio, A., Joshi, V., Bordet, T., Kahn, A. & Melki, J. 2003. Therapeutic benefits of cardiotrophin-1 gene transfer in a mouse model of spinal muscular atrophy. Hum Mol Genet, 12, 1233-9.*

*Li, H., Paes De Faria, J., Andrew, P., Nitarska, J. & Richardson, W.D. 2011a. Phosphorylation regulates OLIG2 cofactor choice and the motor neuron oligodendrocyte fate switch. Neuron, 69, 918-929.*

*Li, Y., Zhang, Q., Yin, X., Yang, W., Du, Y., Hou, P., Ge, J., Liu, C., Zhang, W., Zhang, X., Wu, Y., Li, H., Liu, K., Wu, C., Song, Z., Zhao, Y., Shi, Y. & Deng, H. 2011b. Generation of iPSCs from mouse fibroblasts with a single gene, Oct4, and small molecules. Cell Res, 21, 196-204.*

*Lin, T. & Wu, S. 2015. Reprogramming with Small Molecules instead of Exogenous Transcription Factors. Stem Cells International, 2015, 1-11.*

*Little, D., Valori, C.F., Mutsaers, C.A., Bennett, E.J., Wyles, M., Sharrack, B., Shaw, P.J., Gillingwater, T.H., Azzouz, M. & Ning, K. 2015. PTEN depletion decreases disease severity and modestly prolongs survival in a mouse model of spinal muscular atrophy. Mol Ther, 23, 270-7.*

*Liu, M., Hammers, D.W., Barton, E.R. & Sweeney, H.L. 2016. Activin Receptor Type IIB Inhibition Improves Muscle Phenotype and Function in a Mouse Model of Spinal Muscular Atrophy. PLoS One, 11, e0166803.*

*Liu, Q. & Dreyfuss, G. 1996. A novel nuclear structure containing the survival of motor neurons protein. The EMBO Journal, 15, 3555-3565.*

*Liu, Q., Fischer, F., Wang, F. & Dreyfuss, G. 1997. The spinal muscular atro- phy disease gene product, SMN, and its associated protein SIP1 are in a complex with spliceosomal snRNP proteins. Cell, 90, 1013-1021.*

*Locatelli, D., Terao, M., Fratelli, M., Zanetti, A., Kurosaki, M., Lupi, M., Barzago, M.M., Uggetti, A., Capra, S., D'errico, P., Battaglia, G.S. & Garattini, E. 2012. Human axonal survival of motor neuron (a-SMN) protein stimulates axon growth, cell motility, C-C motif ligand 2 (CCL2), and insulin-like growth factor-1 (IGF1) production. Journal of Biological Chemistry, 287, 25782–25794.*

*Long, C., Amoasii, L., Bassel-Duby, R. & Olson, E.N. 2016. Genome Editing of Monogenic Neuromuscular Diseases: A Systematic Review. JAMA Neurol, 73, 1349-1355.*

*Lorson, C.L. & Androphy, E.J. 1998. The domain encoded by exon 2 of the survival motor neuron protein mediates nucleic acid binding. Human Molecular Genetics, 7, 1269-1275.*

*Lorson, C.L., Hahnen, E., Androphy, E.J. & Wirth, B. 1999. A single nucleotide in the SMN gene regulates splicing and is responsible for spinal muscular atrophy. Proc Natl Acad Sci U S A, 96, 6307-11.*

*Lorson, C.L., Strasswimmer, J., Yao, J.M., Baleja, J.D., Hahnen, E., Wirth, B., Le, T., Burghes, A.H.M. & Androphy, E.J. 1998. SMN oligomerization defect correlates with spinal muscular atrophy severity. Nature Genetics, 19, 63-66.*

*Lorson, M.A., Spate, L.D., Samuel, M.S., Murphy, C.N., Lorson, C.L., Prather, R.S. & Wells, K.D. 2011. Disruption of the Survival Motor Neuron (SMN) gene in pigs using ssDNA. Transgenic Research, 20, 1293-1304.*

*Lu-Nguyen, N.B., Broadstock, M., Schliesser, M., Bartholomae, C., Von Kalle, C., Schmidt, M. & Yáñez-Muñoz, R.J. 2014. Transgenic expression from integration-deficient lentiviral vectors is neuroprotective in a rodent model of Parkinson Disease. Human Gene Therapy, 25, 631-641.*

*Lu-Nguyen, N.B., Broadstock, M. & Yáñez-Muñoz, R.J. 2015. Efficient expression of Igf-1 from lentiviral vectors protects in vitro but does not mediate behavioral recovery of a Parkinsonian lesion in rats. Human Gene Therapy, 26, 719-733.*

*Lyssiotis, C.A., Foreman, R.K., Staerk, J., Garcia, M., Mathur, D., Markoulaki, S., Hanna, J., Lairson, L.L., Charette, B.D., Bouchez, L.C., Bollong, M., Kunick, C., Brinker, A., Cho, C.Y., Schultz, P.G. & Jaenisch, R. 2009. Reprogramming of murine fibroblasts to induced pluripotent stem cells with chemical complementation of Klf4. Proc Natl Acad Sci U S A, 106, 8912-7.*

*Macleod, M.R., Mclean, A.L., Kyriakopoulou, A., Serghiou, S., De Wilde, A., Sherratt, N., Hirst, T., Hemblade, R., Bahor, Z., Nunes-Fonseca, C., Potluru, A., Thomson, A., Baginskitae, J., Egan, K., Vesterinen, H., Currie, G.L., Churilov, L., Howells, D.W. & Sena, E.S. 2015. Risk of Bias in Reports of In Vivo Research: A Focus for Improvement. Plos Biology, 13.*

*Madocsai, C., Lim, S.R., Geib, T., Lam, B.J. & Hertel, K.J. 2005. Correction of SMN2 Pre-mRNA splicing by antisense U7 small nuclear RNAs. Mol Ther, 12, 1013-22.*

*Maier, J.K.X., Lahoua, Z., Gendron, N.H., Fetni, R., Johnston, A., Davoodi, J., Rasper, D., Roy, S., Slack, R.S., Nicholson, D.W. & Mackenzie, A.E. 2002. The neuronal apoptosis inhibitory protein is a direct inhibitor of caspases 3 and 7. Journal of Neuroscience, 22, 2035-2043.*

*Maillard, P.V., Van Der Veen, A.G., Poirier, E.Z. & Reis E Sousa, C. 2019. Slicing and dicing viruses: antiviral RNA interference in mammals. Embo Journal, 38.*

*Markusic, D.M., Elferink, R.P.O. & Seppen, J. 2004. Baculovirus GP64 pseudotypes lentiviral vectors for improved hepatocyte transduction. Molecular Therapy, 9, S277.*

*Marquis, J., Kampfer, S.S., Angehrn, L. & Schumperli, D. 2009. Doxycycline-controlled splicing modulation by regulated antisense U7 snRNA expression cassettes. Gene Ther, 16, 70-7.*

*Martin, S.J. & Green, D.R. 1995. Protease activation during apoptosis: death by a thousand cuts? Cell, 82, 349-352.*

*Martinez-Hernandez, R., Soler-Botija, C., Also, E., Alias, L., Caselles, L., Gich, I., Bernal, S. & Tizzano, E.F. 2009. The Developmental Pattern of Myotubes in Spinal Muscular Atrophy Indicates Prenatal Delay of Muscle Maturation. Journal of Neuropathology and Experimental Neurology, 68, 474-481.*

*Maruyama, R., Touznik, A. & Yokota, T. 2018. Evaluation of Exon Inclusion Induced by Splice Switching Antisense Oligonucleotides in SMA Patient Fibroblasts. J Vis Exp.*

*Massaro, G., Mattar, C.N.Z., Wong, A.M.S., Sirka, E., Buckley, S.M.K., Herbert, B.R., Karlsson, S., Perocheau, D.P., Burke, D., Heales, S., Richard-Londt, A., Brandner, S., Huebecker, M., Priestman, D.A., Platt, F.M., Mills, K., Biswas, A., Cooper, J.D., Chan, J.K.Y., Cheng, S.H., Waddington, S.N. & Rahim, A.A. 2018. Fetal gene therapy for neurodegenerative disease of infants. Nature Medicine, 24, 1317-+.*

*Masu, Y., Wolf, E., Holtmann, B., Sendtner, M., Brem, G. & Thoenen, H. 1993. Disruption of the CNTF gene results in motor neuron degeneration. Nature, 365, 27-32.*

*Mattar, C.N.Z., Gil-Farina, I., Rosales, C., Johana, N., Tan, Y.Y.W., Mcintosh, J., Kaeppel, C., Waddington, S.N., Biswas, A., Choolani, M., Schmidt, M., Nathwani, A.C. & Chan, J.K.Y. 2017. In Utero Transfer of Adeno-Associated Viral Vectors Produces Long-Term Factor IX Levels in a Cynomolgus Macaque Model. Molecular Therapy, 25, 1843-1853.*

*Mattar, C.N.Z., Nathwani, A.C., Waddington, S.N., Dighe, N., Kaeppel, C., Nowrouzi, A., Mcintosh, J., Johana, N.B., Ogden, B., Fisk, N.M., Davidoff, A.M., David, A., Peebles, D., Valentine, M.B., Appelt, J.U., Von Kalle, C., Schmidt, M., Biswas, A., Choolani, M. & Chan, J.K.Y. 2011. Stable Human FIX Expression After 0.9G Intrauterine Gene Transfer of Self-complementary Adeno-associated Viral Vector 5 and 8 in Macaques. Molecular Therapy, 19, 1950-1960.*

*Maury, Y., Come, J., Piskorowski, R.A., Salah-Mohellibi, N., Chevaleyre, V., Peschanski, M., Martinat, C. & Nedelec, S. 2015. Combinatorial analysis of developmental cues efficiently converts human pluripotent stem cells into multiple neuronal subtypes. Nature Biotechnol, 33, 89-96.*

*Mavuluri, J., Beesetti, S., Surabhi, R., Kremerskothen, J., Venkatraman, G. & Rayala, S.K. 2016. Phosphorylation-Dependent Regulation of the DNA Damage Response of Adaptor Protein KIBRA in Cancer Cells. Molecular and Cellular Biology, 36, 1354-1365.*

*Mccarty, D.M. 2008. Self-complementary AAV Vectors; Advances and Applications. Molecular Therapy, 16, 1648-1656.*

*Mccarty, D.M., Fu, H., Monahan, P.E., Toulson, C.E., Naik, P. & Samulski, R.J. 2003. Adeno-associated virus terminal repeat (TR) mutant generates self-complementary vectors to overcome the rate-limiting step to transduction in vivo. Gene Therapy, 10, 2112-2118.*

*Mccarty, D.M., Young, S.M. & Samulski, R.J. 2004. Integration of adeno-associated virus (AAV) and recombinant AAV vectors. Annual Review of Genetics, 38, 819-845.*

*Mcwhorter, M.L., Monani, U.R., Burghes, A.H.M. & Beattie, C.E. 2003. Knockdown of the survival motor neuron (Smn) protein in zebrafish causes defects in motor axon outgrowth and pathfinding. Journal of Cell Biology, 162, 919-931.*

*Meergans, T., Hildebrandt, A.K., Horak, D., Haenisch, C. & Wendel, A. 2000. The short prodomain influences caspase-3 activation in HeLa cells. Biochemical Journal, 349, 135-140.*

*Mehta, V., Abi-Nader, K.N., Peebles, D.M., Benjamin, E., Wigley, V., Torondel, B., Filippi, E., Shaw, S.W., Boyd, M., Martin, J., Zachary, I. & David, A.L. 2012. Long-term increase in uterine blood flow is achieved by local overexpression of VEGF-A(165) in the uterine arteries of pregnant sheep. Gene Therapy, 19, 925-935.*

*Mehta, V., Abi-Nader, K.N., Shangaris, P., Shaw, S.W., Filippi, E., Benjamin, E., Boyd, M., Peebles, D.M., Martin, J., Zachary, I. & David, A. 2014. Local over-expression of VEGF-DΔNΔC in the uterine arteries of pregnant sheep results in long-term changes in uterine artery contractility and angiogenesis. PLoS ONE, 9, e100021.*

*Meilinger, D., Fellinger, K., Bultmann, S., Rothbauer, U., Bonapace, I.M., Klinkert, W.E.F., Spada, F. & Leonhardt, H. 2009. Np95 interacts with de novo DNA methyltransferases, Dnmt3a and Dnmt3b, and mediates epigenetic silencing of the viral CMV promoter in embryonic stem cells. Embo Reports, 10, 1259-1264.*

*Melki, J., Abdelhak, S., Sheth, P., Bachelot, M.F., Burlet, P., Marcadet, A., Aicardi, J., Barois, A., Carriere, J.P., Fardeau, M., Fontan, D., Ponsot, G., Billette, T., Angelini, C., Barbosa, C., Ferriere, G., Lanzi, G., Ottolini, A., Babron, M., Cohen, D., Hanauer, A., Clerget-Darproux, F., Lathrop, M., Munnich, A. & Frezal, J. 1990. Gene for proximal spinal muscular atrophies maps to chromosome 5q. Nature, 344, 767-768.*

*Mendell, J.R., Al-Zaidy, S., Shell, R., Arnold, W.D., Rodino-Klapac, L.R., Prior, T.W., Lowes, L., Alfano, L., Berry, K., Church, K., Kissel, J.T., Nagendran, S., L'italien, J., Sproule, D.M., Wells, C., Cardenas, J.A., Heitzer, M.D., Kaspar, A., Corcoran, S., Braun, L., Likhite, S., Miranda, C., Meyer, K., Foust, K.D., Burghes, A.H.M. & Kaspar, B.K. 2017. Single-Dose Gene-Replacement Therapy for Spinal Muscular Atrophy. N Engl J Med, 377, 1713-1722.*

*Mercuri, E., Darras, B.T., Chiriboga, C.A., Day, J.W., Campbell, C., Connolly, A.M., Iannaccone, S.T., Kirschner, J., Kuntz, N.L., Saito, K., Shieh, P.B., Tulinius, M., Mazzone, E.S., Montes, J., Bishop, K.M., Yang, Q., Foster, R., Gheuens, S., Bennett, C.F., Farwell, W., Schneider, E., De Vivo, D.C. & Finkel, R.S. 2018. Nusinersen versus Sham Control in Later-Onset Spinal Muscular Atrophy. N Engl J Med, 378, 625-635.*

*Meyer, K., Ferraiuolo, L., Schmelzer, L., Braun, L., Mcgovern, V., Likhite, S., Michels, O., Govoni, A., Fitzgerald, J., Morales, P., Foust, K.D., Mendell, J.R., Burghes, A.H.M. & Kaspar, B.K. 2015. Improving Single Injection CSF Delivery of AAV9-mediated Gene Therapy for SMA: A Dose-response Study in Mice and Nonhuman Primates. Molecular Therapy, 23, 477-487.*

*Meylemans, A. & De Bleecker, J. 2019. Current evidence for treatment with nusinersen for spinal muscular atrophy: a systematic review. Acta Neurologica Belgica, 119, 523-533.*

*Michiels, S., Piedbois, P., Burdett, S., Syz, N., Stewart, L. & Pignon, J.P. 2005. Meta-analysis when only the median survival times are known: A comparison with individual patient data results. International Journal of Technology Assessment in Health Care, 21, 119-125.*

*Miguel-Aliaga, I., Chan, Y.B., Davies, K.E. & Van Den Heuvel, M. 2000. Disruption of SMN function by ectopic expression of the human SMN gene in Drosophila. Febs Letters, 486, 99-102.*

*Miller, J.D., Ganat, Y.M., Kishinevsky, S., Bowman, R.L., Liu, B., Tu, E.Y., Mandal, P.K., Vera, E., Shim, J.W., Kriks, S., Taldone, T., Fusaki, N., Tomishima, M.J., Krainc, D., Milner, T.A., Rossi, D.J. & Studer, L. 2013. Human iPSC-Based Modeling of Late-Onset Disease via Progerin-Induced Aging. Cell Stem Cell, 13, 691-705.*

*Miyazaki, J., Takaki, S., Araki, K., Tashiro, F., Tominaga, A., Takatsu, K. & Yamamura, K. 1989. Expression vector system based on the chicken β-actin promoter directs efficient production of interleukin-5. Gene, 79, 269-277.*

*Mohseni, J., Zabidi-Hussin, Z. & Sasongko, T.H. 2013. Histone deacetylase inhibitors as potential treatment for spinal muscular atrophy. Genetics and Molecular Biology, 36, 299-307.*

*Monani, U.R. 2005. Spinal muscular atrophy: a deficiency in a ubiquitous protein; a motor neuron specific disease. Neuron, 48, 885-896.*

*Monani, U.R., Lorson, C.L., Parsons, D.W., Prior, T.W., Androphy, E.J., Burghes, A.H.M. & Mcpherson, J.D. 1999. A single nucleotide difference that alters splicing patterns distinguishes the SMA gene SMN1 from the copy gene SMN2. Human Molecular Genetics, 8, 1177-1183.*

*Monani, U.R., Sendtner, M., Coovert, D.D., Parsons, D.W., Andreassi, C., Le, T.T., Jablonka, S., Schrank, B., Rossol, W., Prior, T.W., Morris, G.E. & Burghes, A.H.M. 2000. The human centromeric survival motor neuron gene (SMN2) rescues embryonic lethality in Smn(-/-) mice and results in a mouse with spinal muscular atrophy. Human Molecular Genetics, 9, 333-339.*

*Morales, A.J., Carrero, J.A., Hung, P.J., Tubbs, A.T., Andrews, J.M., Edelson, B.T., Calderon, B., Innes, C.L., Paules, R.S., Payton, J.E. & Sleckman, B.P. 2017. A type I IFN-dependent DNA damage response regulates the genetic program and inflammasome activation in macrophages. Elife, 6.*

*Mourelatos, Z., Abel, L., Yong, J.S., Kataoka, N. & Dreyfuss, G. 2001. SMN interacts with a novel family of hnRNP and spliceosomal proteins. Embo Journal, 20, 5443-5452.*

*Munsat, T.L. & Davies, K.E. 1992. International SMA Consortium Meeting. Bonn, Germany: Neuromuscul Disord.*

*Murray, L.M., Beauvais, A., Gibeault, S., Courtney, N.L. & Kothary, R. 2015. Transcriptional profiling of differentially vulnerable motor neurons at pre-symptomatic stage in the Smn(2b-) mouse model of spinal muscular atrophy. Acta Neuropathologica Communications, 3.*

*Murray, L.M., Comley, L.H., Thomson, D., Parkinson, N., Talbot, K. & Gillingwater, T.H. 2008. Selective vulnerability of motor neurons and dissociation of pre- and post-synaptic pathology at the neuromuscular junction in mouse models of spinal muscular atrophy. Human Molecular Genetics, 17, 949-962.*

*Mutsaers, C.A., Wishart, T.M., Lamont, D.J., Riessland, M., Schreml, J., Comley, L.H., Murray, L.M., Parson, S.H., Lochmuller, H., Wirth, B., Talbot, K. & Gillingwater, T.H. 2011. Reversible molecular pathology of skeletal muscle in spinal muscular atrophy. Human Molecular Genetics, 20, 4334-4344.*

*Nguyen, H.T., Geens, M., Mertzanidou, A., Jacobs, K., Heirman, C., Breckpot, K. & Spits, C. 2014. Gain of 20q11.21 in human embryonic stem cells improves cell*

*survival by increased expression of Bcl-xL. Molecular Human Reproduction, 20, 168-177.*

*Nicolas, C.T., Allen, K.L., Du, Z., Guthman, R.M., Kaiser, R., Hickey, R.D. & Lillegard, J.B. In utero correction of hereditary tyrosinemia type 1 in mice through liver-directed lentiviral gene therapy. European Society of Gene and Cell Therapy, 2017 Berlin, Germany. Human Gene Therapy, A70.*

*Nicolas, C.T., Vanlith, C.J., Allen, K.L., Du, Z., Guthman, R.M., Kaiser, R.A., Hillin, L.G., Hickey, R.D. & Lillegard, J.B. 2018. In utero liver-directed lentiviral gene therapy cures a pig model of hereditary tyrosinemia type 1. Human Gene Therapy, 29, A27-A28.*

*Nikolic, J., Belot, L., Raux, H., Legrand, P., Gaudin, Y. & Albertini, A.A. 2018. Structural basis for the recognition of LDL-receptor family members by VSV glycoprotein. Nature Communications, 9.*

*Ning, K., Drepper, C., Valori, C.F., Ahsan, M., Wyles, M., Higginbottom, A., Herrmann, T., Shaw, P., Azzouz, M. & Sendtner, M. 2010. PTEN depletion rescues axonal growth defect and improves survival in SMN-deficient motor neurons. Human Molecular Genetics, 19, 3159-3168.*

*Nizzardo, M., Simone, C., Dametti, S., Salani, S., Ulzi, G., Pagliarani, S., Rizzo, F., Frattini, E., Pagani, F., Bresolin, N., Comi, G. & Corti, S. 2015. Spinal muscular atrophy phenotype is ameliorated in human motor neurons by SMN increase via different novel RNA therapeutic approaches. Sci Rep, 5, 11746.*

*Nizzardo, M., Simone, C., Salani, S., Ruepp, M.D., Rizzo, F., Ruggieri, M., Zanetta, C., Brajkovic, S., Moulton, H.M., Muehlemann, O., Bresolin, N., Comi, G.P. & Corti, S. 2014. Effect of combined systemic and local morpholino treatment on the spinal muscular atrophy Delta7 mouse model phenotype. Clin Ther, 36, 340-56.e5.*

*Nizzardo, M., Taiana, M., Rizzo, F., Benitez, J.A., Nijssen, J., Allodi, I., Melzi, V., Bresolin, N., Comi, G.P., Hedlund, E. & Corti, S. 2020. Synaptotagmin 13 is neuroprotective across motor neuron diseases. Acta Neuropathologica, 139, 837-853.*

*Nlend, R.N. & Schumperli, D. 2012. Antisense genes to induce exon inclusion. Methods Mol Biol, 867, 325-47.*

*NöLle, A., Zeug, A., Van Bergeijk, J., TöNges, L., Gerhard, R., Brinkmann, H., Al Rayes, S., Hensel, N., Schill, Y., Apkhazava, D., Jablonka, S., O'mer, J., Srivastav, R.K., Baasner, A., Lingor, P., Wirth, B., Ponimaskin, E., Niedenthal, R., Grothe, C. & Claus, P. 2011. The spinal muscular atrophy disease protein SMN is linked to the Rho-kinase pathway via profilin. Human Molecular Genetics, 20, 4865–4878.*

*Novartis 2017. Novartis Releases Update on LMI070 (Branaplam) Clinical Trial.*

*Oates, E.C., Reddel, S., Rodriguez, M.L., Gandolfo, L.C., Bahlo, M., Hawke, S.H., Lamande, S.R., Clarke, N.F. & North, K.N. 2012. Autosomal dominant congenital spinal muscular atrophy: a true form of spinal muscular atrophy caused by early loss of anterior horn cells. Brain, 135, 1714-1723.*

*Odermatt, P., Trub, J., Furrer, L., Fricker, R., Marti, A. & Schumperli, D. 2016. Somatic Therapy of a Mouse SMA Model with a U7 snRNA Gene Correcting SMN2 Splicing. Mol Ther, 24, 1797-1805.*

*Ogawa, C., Usui, K., Aoki, M., Ito, F., Itoh, M., Kai, C., Kanamori-Katayama, M., Hayashizaki, Y. & Suzuki, H. 2007. Gemin2 plays an important role in stabilizing the survival of motor neuron complex. Journal of Biological Chemistry, 282, 11122-11134.*

*Olivan, S., Calvo, A.C., Rando, A., Herrando-Grabulosa, M., Manzano, R., Zaragoza, P., Tizzano, E.F., Aquilera, J. & Osta, R. 2016. Neuroprotective Effect of Non-viral Gene Therapy Treatment Based on Tetanus Toxin C-fragment in a Severe Mouse Model of Spinal Muscular Atrophy. Front Mol Neurosci, 9, 76.*

*Oprea, G.E., KröBer, S., Mcwhorter, M.L., Rossoll, W., MüLler, S., Krawczak, M., Bassell, G.J., Beattie, C.E. & Wirth, B. 2008. Plastin 3 is a protective modifier of autosomal recessive spinal muscular atrophy. Science, 320, 524–527.*

*Osman, E.Y., Bolding, M.R., Villalon, E., Kaifer, K.A., Lorson, Z.C., Tisdale, S., Hao, Y., Conant, G.C., Pires, J.C., Pellizzoni, L. & Lorson, C.L. 2019. Functional characterization of SMN evolution in mouse models of SMA. Scientific Reports, 9.*

*Osman, E.Y., Miller, M.R., Robbins, K.L., Lombardi, A.M., Atkinson, A.K., Brehm, A.J. & Lorson, C.L. 2014. Morpholino antisense oligonucleotides targeting intronic repressor Element1 improve phenotype in SMA mouse models. Hum Mol Genet, 23, 4832-45.*

*Osman, E.Y., Washington, C.W., Kaifer, K.A., Mazzasette, C., Patitucci, T.N., Florea, K.M., Simon, M.E., Ko, C.P., Ebert, A.D. & Lorson, C.L. 2016. Optimization of Morpholino Antisense Oligonucleotides Targeting the Intronic Repressor Element1 in Spinal Muscular Atrophy. Molecular Therapy, 24, 1592-1601.*

*Osman, E.Y., Yen, P.F. & Lorson, C.L. 2012. Bifunctional RNAs targeting the intronic splicing silencer N1 increase SMN levels and reduce disease severity in an animal model of spinal muscular atrophy. Mol Ther, 20, 119-26.*

*Owen, N., Zhou, H.Y., Malygin, A.A., Sangha, J., Smith, L.D., Muntoni, F. & Eperon, I.C. 2011. Design principles for bifunctional targeted oligonucleotide enhancers of splicing. Nucleic Acids Research, 39, 7194-7208.*

*Pacak, C.A., Mah, C.S., Thattaliyath, B.D., Conlon, T.J., Lewis, M.A., Cloutier, D.E., Zolotukhin, I., Tarantal, A.F. & Byrne, B.J. 2006. Recombinant adeno-associated virus serotype 9 leads to preferential cardiac transduction in vivo. Circulation Research, 99, E3-E9.*

*Palacino, J., Swalley, S.E., Song, C., Cheung, A.K., Shu, L., Zhang, X., Van Hoosear, M., Shin, Y., Chin, D.N., Keller, C.G., Beibel, M., Renaud, N.A., Smith, T.M., Salcius, M., Shi, X., Hild, M., Servais, R., Jain, M., Deng, L., Bullock, C., Mclellan, M., Schuierer, S., Murphy, L., Blommers, M.J., Blaustein, C., Berenshteyn, F., Lacoste, A., Thomas, J.R., Roma, G., Michaud, G.A., Tseng, B.S., Porter, J.A., Myer, V.E., Tallarico, J.A., Hamann, L.G., Curtis, D., Fishman, M.C., Dietrich, W.F., Dales, N.A. & Sivasankaran, R. 2015. SMN2 splice modulators enhance U1-pre-mRNA association and rescue SMA mice. Nat Chem Biol, 11, 511-7.*

*Pao, P.W., Wee, K.B., Yee, W.C. & Dwipramono, Z.A. 2014. Dual Masking of Specific Negative Splicing Regulatory Elements Resulted in Maximal Exon 7 Inclusion of SMN2 Gene. Molecular Therapy, 22, 854-861.*

*Papazova, D.A., Oosterhuis, N.R., Gremmels, H., Van Koppen, A., Joles, J.A. & Verhaar, M.C. 2015. Cell-based therapies for experimental chronic kidney*

*disease: a systematic review and meta-analysis. Disease Models & Mechanisms, 8, 281-293.*

*Park, G.H., Maeno-Hikichi, Y., Awano, T., Landmesser, L.T. & Monani, U.R. 2010. Reduced Survival of Motor Neuron (SMN) Protein in Motor Neuronal Progenitors Functions Cell Autonomously to Cause Spinal Muscular Atrophy in Model Mice Expressing the Human Centromeric (SMN2) Gene. Journal of Neuroscience, 30, 12005-12019.*

*Parker, G.C., Li, X.L., Anguelov, R.A., Toth, G., Cristescu, A. & Acsadi, G. 2008. Survival motor neuron protein regulates apoptosis in an in vitro model of spinal muscular atrophy. Neurotoxicity Research, 13, 39-48.*

*Passini, M.A., Bu, J., Richards, A.M., Kinnecom, C., Sardi, S.P., Stanek, L.M., Hua, Y.M., Rigo, F., Matson, J., Hung, G., Kaye, E.M., Shihabuddin, L.S., Krainer, A.R., Bennett, C.F. & Cheng, S.H. 2011. Antisense Oligonucleotides Delivered to the Mouse CNS Ameliorate Symptoms of Severe Spinal Muscular Atrophy. Science Translational Medicine, 3.*

*Passini, M.A., Bu, J., Richards, A.M., Treleaven, C.M., Sullivan, J.A., O'riordan, C.R., Scaria, A., Kells, A.P., Samaranch, L., San Sebastian, W., Federici, T., Fiandaca, M.S., Boulis, N.M., Bankiewicz, K.S., Shihabuddin, L.S. & Cheng, S.H. 2014. Translational fidelity of intrathecal delivery of self-complementary AAV9-survival motor neuron 1 for spinal muscular atrophy. Hum Gene Ther, 25, 619-30.*

*Passini, M.A., Bu, J., Roskelley, E.M., Richards, A.M., Sardi, S.P., O'riordan, C.R., Klinger, K.W., Shihabuddin, L.S. & Cheng, S.H. 2010. CNS-targeted gene therapy improves survival and motor function in a mouse model of spinal muscular atrophy. J Clin Invest, 120, 1253-64.*

*Patitucci, T.N. & Ebert, A.D. 2016. SMN deficiency does not induce oxidative stress in SMA iPSC-derived astrocytes or motor neurons. Human Molecular Genetics, 25, 514–523.*

*Pattali, R., Mou, Y.C. & Li, X.J. 2019. AAV9 Vector: a Novel modality in gene therapy for spinal muscular atrophy. Gene Therapy, 26, 287-295.*

*Pearn, J. 1980. Classification of spinal muscular atrophies. The Lancet, 315, 919-922.*

*Pellizzoni, L., Baccon, J., Rappsilber, J., Mann, M. & Dreyfuss, G. 2002. Purification of native survival of motor neurons complexes and identifi- cation of Gemin6 as a novel component. Journal of Biological Chemistry, 277, 7540-7545.*

*Peluffo, H., Foster, E., Ahmed, S.G., Lago, N., Hutson, T.H., Moon, L., Yip, P., Wanisch, K., Caraballo-Miralles, V., Olmos, G., Llado, J., Mcmahon, S.B. & Yanez-Munoz, R.J. 2013. Efficient gene expression from integration-deficient lentiviral vectors in the spinal cord. Gene Therapy, 20, 645-57.*

*Peters, J.L., Sutton, A.J., Jones, D.R., Abrams, K.R. & Rushton, L. 2006. Comparison of two methods to detect publication bias in meta-analysis. Jama-Journal of the American Medical Association, 295, 676-680.*

*Philippe, S., Sarkis, C., Barkats, M., Mammeri, H., Ladroue, C., Petit, C., Mallet, J. & Serguera, C. 2006. Lentiviral vectors with a defective integrase allow efficient and sustained transgene expression in vitro and in vivo. Proceedings of the National Academy of Sciences of the United States of America, 103, 17684-17689.*

*Pool, M., Thiemann, J., Bar-Or, A. & Fournier, A.E. 2008. NeuriteTracer: a novel ImageJ plugin for automated quantification of neurite outgrowth. Journal of Neuroscience Methods, 168, 134-139.*

*Porensky, P.N. & Burghes, A.H.M. 2013. Antisense Oligonucleotides for the Treatment of Spinal Muscular Atrophy. Human Gene Therapy, 24, 489-498.*

*Porensky, P.N., Mitrpant, C., Mcgovern, V.L., Bevan, A.K., Foust, K.D., Kaspar, B.K., Wilton, S.D. & Burghes, A.H.M. 2012. A single administration of morpholino antisense oligomer rescues spinal muscular atrophy in mouse. Human Molecular Genetics, 21, 1625-1638.*

*Powis, R.A., Karyka, E., Boyd, P., Come, J., Jones, R.A., Zheng, Y., Szunyogova, E., Groen, E.J., Hunter, G., Thomson, D., Wishart, T.M., Becker, C.G., Parson, S.H., Martinat, C., Azzouz, M. & Gillingwater, T.H. 2016. Systemic restoration of UBA1 ameliorates disease in spinal muscular atrophy. JCI Insight, 1, e87908.*

*Prusty, A.B., Meduri, R., Prusty, B.K., Vanselow, J., Schlosser, A. & Fischer, U. 2017. Impaired spliceosomal UsnRNP assembly leads to Sm mRNA down-regulation and Sm protein degradation. Journal of Cell Biology, 216, 2391.*

*Pruszak, J., Ludwig, W., Blak, A., Alavian, K. & Isacson, O. 2009. CD15, CD24, and CD29 Define a Surface Biomarker Code for Neural Lineage Differentiation of Stem Cells. Stem Cells, 27, 2928-2940.*

*Qin, J.Y., Zhang, L., Clift, K.L., Hulur, I., Xiang, A.P., Ren, B.Z. & Lahn, B.T. 2010. Systematic Comparison of Constitutive Promoters and the Doxycycline-Inducible Promoter. Plos One, 5.*

*Qomi, S.B., Asghari, A., Salmaninejad, A. & Mojarrad, M. 2019. Spinal Muscular Atrophy and Common Therapeutic Advances. Fetal and Pediatric Pathology, 38, 226-238.*

*Ramser, J., Ahearn, M.E., Lenski, C., Yariz, K.O., Hellebrand, H., Von Rhein, M., Clark, R.D., Schmutzler, R.K., Lichtner, P., Hoffman, E.P., Meindl, A. & Baumbach-Reardon, L. 2008. Rare missense and synonymous variants in UBE1 are associated with X-linked infantile spinal muscular atrophy. American Journal of Human Genetics, 82, 188–193.*

*Rare Disease Uk. 2020. What is a rare disease? [Online]. Available: https://www.raredisease.org.uk/what-is-a-rare-disease/ [Accessed 10th June 2020.*

*Rashnonejad, A., Chermahini, G.A., Gunduz, C., Onay, H., Aykut, A., Durmaz, B., Baka, M., Su, Q., Gao, G.P. & Ozkinay, F. 2019. Fetal Gene Therapy Using a Single Injection of Recombinant AAV9 Rescued SMA Phenotype in Mice. Molecular Therapy, 27, 2123-2133.*

*Rashnonejad, A., Gunduz, C., Susluer, S.Y., Onay, H., Durmaz, B., Bandehpour, M. & Ozkinay, F. 2016. In vitro gene manipulation of spinal muscular atrophy fibroblast cell line using gene-targeting fragment for restoration of SMN protein expression. Gene Ther, 23, 10-7.*

*Ratni, H., Ebeling, M., Baird, J., Bendels, S., Bylund, J., Chen, K.S., Denk, N., Feng, Z., Green, L., Guerard, M., Jablonski, P., Jacobsen, B., Khwaja, O., Kletzl, H., Ko, C.P., Kustermann, S., Marquet, A., Metzger, F., Mueller, B., Naryshkin, N.A., Paushkin, S.V., Pinard, E., Poirier, A., Reutlinger, M., Weetall, M., Zeller, A., Zhao, X. & Mueller, L. 2018. Discovery of Risdiplam, a Selective Survival of*

*Motor Neuron-2 ( SMN2) Gene Splicing Modifier for the Treatment of Spinal Muscular Atrophy (SMA). Journal of Medicinal Chemistry, 61, 6501-6517.*

*Re, S., Dogan, A.A., Ben-Shachar, D., Berger, G., Werling, A.M., Walitza, S. & Grunblatt, E. 2018. Improved Generation of Induced Pluripotent Stem Cells From Hair Derived Keratinocytes - A Tool to Study Neurodevelopmental Disorders as ADHD. Frontiers in Cellular Neuroscience, 12, 11.*

*Rekling, J.C., Funk, G.D., Bayliss, D.A., Dong, X.W. & Feldman, J.L. 2000. Synaptic central of motoneuronal excitability. Physiological Reviews, 80, 767-852.*

*Ricciardi, A.S., Bahal, R., Farrelly, J.S., Quijano, E., Bianchi, A.H., Luks, V.L., Putman, R., Lopez-Giraldez, F., Coskun, S., Song, E., Liu, Y.F., Hsieh, W.C., Ly, D.H., Stitelman, D.H., Glazer, P.M. & Saltzman, W.M. 2018. In utero nanoparticle delivery for site-specific genome editing. Nature Communications, 9.*

*Riessland, M., Kaczmarek, A., Schneider, S., Swoboda, K.J., Lohr, H., Bradler, C., Grysko, V., Dimitriadi, M., Hosseinibarkooie, S., Torres-Benito, L., Peters, M., Upadhyay, A., Biglari, N., Krober, S., Holker, I., Garbes, L., Gilissen, C., Hoischen, A., Nurnberg, G., Nurnberg, P., Walter, M., Rigo, F., Bennett, C.F., Kye, M.J., Hart, A.C., Hammerschmidt, M., Kloppenburg, P. & Wirth, B. 2017. Neurocalcin Delta Suppression Protects against Spinal Muscular Atrophy in Humans and across Species by Restoring Impaired Endocytosis. Am J Hum Genet, 100, 297-315.*

*Robbins, K.L., Glascock, J.J., Osman, E.Y., Miller, M.R. & Lorson, C.L. 2014. Defining the therapeutic window in a severe animal model of spinal muscular atrophy. Hum Mol Genet, 23, 4559-68.*

*Rochette, C.F., Gilbert, N. & Simard, L.R. 2001. SMN gene duplication and the emergence of the SMN2 gene occurred in distinct hominids: SMN2 is unique to Homo sapiens. Human Genetics, 108, 255-266.*

*Rogakou, E.P., Boon, C., Redon, C. & Bonner, W.M. 1999. Megabase chromatin domains involved in DNA double-strand breaks in vivo. Journal of Cell Biology, 146, 905-915.*

*Rogakou, E.P., Pilch, D.R., Orr, A.H., Ivanova, V.S. & Bonner, W.M. 1998. DNA double-stranded breaks induce histone H2AX phosphorylation on serine 139. Journal of Biological Chemistry, 273, 5858-5868.*

*Rossidis, A.C., Stratigis, J.D., Chadwick, A.C., Hartman, H.A., Ahn, N.J., Li, H.Y., Singh, K., Coons, B.E., Li, L., Lv, W.J., Zoltick, P.W., Alapati, D., Zacharias, W., Jain, R., Morrisey, E.E., Musunuru, K. & Peranteau, W.H. 2018. In utero CRISPR-mediated therapeutic editing of metabolic genes. Nature Medicine, 24, 1513-+.*

*Rossoll, W., Jablonka, S., Andreassi, C., Kroning, A.K., Karle, K., Monani, U.R. & Sendtner, M. 2003. Smn, the spinal muscular atrophy-determining gene product, modulates axon growth and localization of beta-actin mRNA in growth cones of motoneurons. Journal of Cell Biology, 163, 801-812.*

*Roy, N., Mahadevan, M.S., Mclean, M., Shutler, G., Yaraghi, Z., Farahani, R., Baird, S., Besnerjohnston, A., Lefebvre, C., Kang, X.L., Salih, M., Aubry, H., Tamai, K., Guan, X.P., Ioannou, P., Crawford, T.O., Dejong, P.J., Surh, L., Ikeda, J.E., Korneluk, R.G. & Mackenzie, A. 1995. THE GENE FOR NEURONAL APOPTOSIS INHIBITORY PROTEIN IS PARTIALLY DELETED IN INDIVIDUALS WITH SPINAL MUSCULAR-ATROPHY. Cell, 80, 167-178.*

*Rudnik-Schoneborn, S., Heller, R., Berg, C., Betzler, C., Grimm, T., Eggermann, T., Eggermann, K., Wirth, R., Wirth, B. & Zerres, K. 2008. Congenital heart disease is a feature of severe infantile spinal muscular atrophy. Journal of Medical Genetics, 45, 635-638.*

*Rudnik-Schoneborn, S., Vogelgesang, S., Armbrust, S., Graul-Neumann, L., Fusch, C. & Zerres, K. 2010. DIGITAL NECROSES AND VASCULAR THROMBOSIS IN SEVERE SPINAL MUSCULAR ATROPHY. Muscle & Nerve, 42, 144-147.*

*Russell, D.W. & Kay, M.A. 1999. Adeno-associated virus vectors and hematology. Blood, 94, 864-+.*

*Sakuma, T., Barry, M.A. & Ikeda, Y. 2012. Lentiviral vectors: basic to translational. Biochemical Journal, 443, 603-618.*

*Samulski, R.J. & Muzyczka, N. 2014. AAV-Mediated Gene Therapy for Research and Therapeutic Purposes. In: ENQUIST, L. W. (ed.) Annual Review of Virology.*

*Samulski, R.J., Zhu, X., Xiao, X., Brook, J.D., Housman, D.E., Epstein, N. & Hunter, L.A. 1991. TARGETED INTEGRATION OF ADENOASSOCIATED VIRUS (AAV) INTO HUMAN CHROMOSOME-19. Embo Journal, 10, 3941-3950.*

*Sances, S., Bruijn, L.I., Chandran, S., Eggan, K., Ho, R., Klim, J.R., Livesey, M.R., Lowry, E., Macklis, J.D., Rushton, D., Sadegh, C., Sareen, D., Wichterle, H., Zhang, S.C. & Svendsen, C.N. 2016. Modeling ALS with motor neurons derived from human induced pluripotent stem cells. Nature Neuroscience, 19, 542-553.*

*Sandrock, A.W. & Farwell, W. 2019. Comparisons Between Separately Conducted Clinical Trials: Letter to the Editor Regarding Dabbous O, Maru B, Jansen JP, Lorenzi M, Cloutier M, Guérin A, et al. Adv Ther (2019) 36(5):1164–76. doi:10.1007/s12325-019-00923-8. Advances in Therapy, 36, 2979-2981.*

*Sareen, D., Ebert, A.D., Heins, B.M., Mcgivern, J.V., Ornelas, L. & Svendsen, C.N. 2012. Inhibition of Apoptosis Blocks Human Motor Neuron Cell Death in a Stem Cell Model of Spinal Muscular Atrophy. Plos One, 7.*

*Scarpato, R., Castagna, S., Aliotta, R., Azzara, A., Ghetti, F., Filomeni, E., Giovannini, C., Pirillo, C., Testi, S., Lombardi, S. & Tomei, A. 2013. Kinetics of nuclear phosphorylation (-H2AX) in human lymphocytes treated in vitro with UVB, bleomycin and mitomycin C. Mutagenesis, 28, 465-473.*

*Schmutz, J., Martin, J., Terry, A., Couronne, O., Grimwood, J., Lowry, S., Gordon, L.A., Scott, D., Xie, G., Huang, W., Hellsten, U., M., T.-G., X., S. & Prabhakar S. Aerts A., A.M., Bajorek E., Black S., Branscomb E., Caoile C., Challacombe J.F., Chan Y.M., Denys M., Detter J.C., Escobar J., Flowers D., Fotopulos D., Glavina T., Gomez M., Gonzales E., Goodstein D., Grigoriev I., Groza M., Hammon N., Hawkins T., Haydu L., Israni S., Jett J., Kadner K., Kimball H., Kobayashi A., Lopez F., Lou Y., Martinez D., Medina C., Morgan J., Nandkeshwar R., Noonan J.P., Pitluck S., Pollard M., Predki P., Priest J., Ramirez L., Retterer J., Rodriguez A., Rogers S., Salamov A., Salazar A., Thayer N., Tice H., Tsai M., Ustaszewska A., Vo N., Wheeler J., Wu K., Yang J., Dickson M., Cheng J.-F., Eichler E.E., Olsen A., Pennacchio L.A., Rokhsar D.S., Richardson P., Lucas S.M., Myers R.M., Rubin E.M. 2004. The DNA sequence and comparitive analysis of human chromosome 5. Nature, 431, 268-274.*

*Schneider, H., Faschingbauer, F., Schuepbach-Mallepell, S., Korber, I., Wohlfart, S., Dick, A., Wahlbuhl, M., Kowalczyk-Quintas, C., Vigolo, M., Kirby, N., Tannert,*

*C., Rompel, O., Rascher, W., Beckmann, M.W. & Schneider, P. 2018. Prenatal Correction of X-Linked Hypohidrotic Ectodermal Dysplasia. New England Journal of Medicine, 378, 1604-1610.*

*Schrank, B., Gotz, R., Gunnersen, J.M., Ure, J.M., Tokya, K.V., Smith, A.G. & Sendtner, M. 1997. Inactivation of the survival motor neuron gene, a candidate for human spinal muscular atrophy, leads to massive cell death in early mouse embryos. PNAS USA, 94, 9920-9925.*

*Sendtner, M., Schmalbruch, H., Stockli, K.A., Kreutzberg, G.W. & Thoenen, H. 1992. Ciliary neurotrophic factor prevents degeneration of motor neurons in mouse mutant progressive motor neuronopathy. Nature, 358, 502-504.*

*Servais, L. 2020. FIREFISH Part 2: Efficacy and Safety of Risdiplam (RG7916) in Infants with Type 1 Spinal Muscular Atrophy. Cure SMA Research and Clinical Care Virtual Meeting. Virtual.*

*Setola, V., Terao, M., Locatelli, D., Bassanini, S., Garattini, E. & Battaglia, G. 2007. Axonal-SMN (a-SMN), a protein isoform of the survival motor neuron gene, is specifically involved in axonogenesis. Proceedings of the National Academy of Sciences of the United States of America, 104, 1959-1964.*

*Shababi, M., Glascock, J. & Lorson, C. 2011. Combination of SMN Trans -Splicing and a Neurotrophic Factor Increases the Life Span and Body Mass in a Severe Model of Spinal Muscular Atrophy. Human Gene Therapy, 22, 135-144.*

*Shababi, M., Habibi, J., Ma, L., Glascock, J.J., Sowers, J.R. & Lorson, C.L. 2012. Partial restoration of cardio-vascular defects in a rescued severe model of spinal muscular atrophy. J Mol Cell Cardiol, 52, 1074-82.*

*Shabanpoor, F., Hammond, S.M., Abendroth, F., Hazell, G., Wood, M.J.A. & Gait, M.J. 2017. Identification of a Peptide for Systemic Brain Delivery of a Morpholino Oligonucleotide in Mouse Models of Spinal Muscular Atrophy. Nucleic Acid Therapeutics, 27, 130-+.*

*Shafey, D., Cote, P.D. & Kothary, R. 2005. Hypomorphic Smn knockdown C2C12 myoblasts reveal intrinsic defects in myoblast fusion and myotube morphology. Experimental Cell Research, 311, 49-61.*

*Shahryari, A., Jazi, M.S., Mohammadi, S., Nikoo, H.R., Nazari, Z., Hosseini, E.S., Burtscher, I., Mowla, S.J. & Lickert, H. 2019. Development and Clinical Translation of Approved Gene Therapy Products for Genetic Disorders. Frontiers in Genetics, 10.*

*Shangaris, P., Loukogeorgakis, S., Jackson, L., Wang, W., Blundell, M., Liu, S.R., Subramaniam, S., Eaton, S., Antoniou, M., Stuckey, D., Schmidt, M., Thrasher, A., Ryan, T., De Coppi, P. & David, A. 2017. In Utero Gene Therapy (IUGT) Using GLOBE Lentiviral Vector Phenotypically Corrects the Heterozygous Humanized Mouse Mode and Its Progress Can Be Monitored Using MRI Techniques. Reproductive Sciences, 24, 74A-74A.*

*Sheth, P., Abdelhak, S., Bachelot, M.F., Burlet, P., Masset, P., Hillaire, D., Clerget-Darproux, F., Frezal, J., Lathrop, M., Munnich, A. & Melki, J. 1991. Linkage analysis in spinal muscular atrophy by six closely flanking markers on chromosome 5. American Journal of Human Genetics, 48, 764-768.*

*Shorrock, H.K., Gillingwater, T.H. & Groen, E.J.N. 2018. Overview of Current Drugs and Molecules in Development for Spinal Muscular Atrophy Therapy. Drugs, 78, 293-305.*

*Simon, C.M., Van Alstyne, M., Lotti, F., Bianchetti, E., Tisdale, S., Watterson, D.M., Mentis, G.Z. & Pellizzoni, L. 2019. Stasimon Contributes to the Loss of Sensory Synapses and Motor Neuron Death in a Mouse Model of Spinal Muscular Atrophy. Cell Reports, 29, 3885-+.*

*Simonsohn, U., Nelson, L.D. & Simmons, J.P. 2014. p-Curve and Effect Size: Correcting for Publication Bias Using Only Significant Results. Perspectives on psychological science : a journal of the Association for Psychological Science, 9, 666-681.*

*Singh, N.K., Singh, N.N., Androphy, E.J. & Singh, R.N. 2006. Splicing of a critical exon of human survival motor neuron is regulated by a unique silencer element located in the last intron. Molecular and Cellular Biology, 26, 1333-1346.*

*Singh, N.N., Howell, M.D., Androphy, E. & Singh, R.N. 2017a. How the discovery of ISS-N1 led to the first medical therapy for spinal muscular atrophy. Gene Therapy, 24, 520-526.*

*Singh, N.N., Howell, M.D., Androphy, E.J. & Singh, R.N. 2017b. How the discovery of ISS-N1 led to the first medical therapy for spinal muscular atrophy. Gene Therapy, 24, 520-526.*

*Singh, N.N., Lawler, M.N., Ottesen, E.W., Upreti, D., Kaczynski, J.R. & Singh, R.N. 2013. An intronic structure enabled by a long-distance interaction serves as a novel target for splicing correction in spinal muscular atrophy. Nucleic Acids Res, 41, 8144-65.*

*Singh, N.N., Lee, B.M., Didonato, C.J. & Singh, R.N. 2015a. Mechanistic principles of antisense targets for the treatment of spinal muscular atrophy. Future Med Chem, 7, 1793-808.*

*Singh, N.N., Lee, B.M. & Singh, R.N. 2015b. Splicing regulation in spinal muscular atrophy by an RNA structure formed by long-distance interactions. Ann N Y Acad Sci, 1341, 176-87.*

*Singh, R.N., Howell, M.D., Ottesen, E.W. & Singh, N.N. 2017c. Diverse role of survival motor neuron protein. Biochemica et Biophysica Acta, 1860, 299-315.*

*Sleigh, J.N., Gillingwater, T.H. & Talbot, K. 2011. The contribution of mouse models to understanding the pathogenesis of spinal muscular atrophy. Dis Model Mech, 4, 457-67.*

*Spencer, R., Ambler, G., Brodszki, J., Diemert, A., Figueras, F., Gratacos, E., Hansson, S.R., Hecher, K., Huertas-Ceballos, A., Marlow, N., Marsal, K., Morsing, E., Peebles, D., Rossi, C., Sebire, N.J., Timms, J.F., David, A.L. & Consortium, E. 2017. EVERREST prospective study: a 6-year prospective study to define the clinical and biological characteristics of pregnancies affected by severe early onset fetal growth restriction. Bmc Pregnancy and Childbirth, 17.*

*Stabley, D.L., Harris, A.W., Holbrook, J., Chubbs, N.J., Lozo, K.W., Crawford, T.O., Swoboda, K.J., Funanage, V.L., Wang, W.L., Mackenzie, W., Scavina, M., Sol-Church, K. & Butchbach, M.E.R. 2015. SMN1 and SMN2 copy numbers in cell lines derived from patients with spinal muscular atrophy as measured by array digital PCR. Molecular Genetics & Genomic Medicine, 3, 248-257.*

*Swanson, A.M., Rossi, C.A., Ofir, K., Mehta, V., Boyd, M., Barker, H., Ledwozyw, A., Vaughan, O., Martin, J., Zachary, I., Sebire, N., Peebles, D.M. & David, A. 2016. Maternal Therapy with Ad.VEGF-A165 Increases Fetal Weight at Term*

*in a Guinea-Pig Model of Fetal Growth Restriction. Human Gene Therapy, 27, 997-1007.*

*Swoboda, K.J. 2014. SMN-targeted therapeutics for spinal muscular atrophy: are we SMArt enough yet? Journal of Clinical Investigation, 124, 487-490.*

*Swoboda, K.J., Prior, T.W., Scott, C.B., Mcnaught, T.P., Wride, M.C., Reyna, S.P. & Bromberg, M.B. 2005. Natural history of denervation in SMA: Relation to age, SMN2 copy number, and function. Annals of Neurology, 57, 704-712.*

*Takahashi, K., Tanabe, K., Ohnuki, M., Narita, M., Ichisaka, T., Tomoda, K. & Yamanaka, S. 2007. Induction of pluripotent stem cells from adult human fibroblasts by defined factors. Cell, 131, 861-72.*

*Takahashi, K. & Yamanaka, S. 2006. Induction of pluripotent stem cells from mouse embryonic and adult fibroblast cultures by defined factors. Cell, 126, 663-76.*

*Takaku, M., Tsujita, T., Horikoshi, N., Takizawa, Y., Qing, Y., Hirota, K., Ikura, M., Takeda, S. & Kurumizaka, H. 2011. Purification of the human SMN-GEMIN2 complex and as- sessment of its stimulation of RAD51-mediated DNA recombination reactions. Biochemistry, 50, 6797–6805.*

*Talbot, K. & Tizzano, E.F. 2017. The clinical landscape for SMA in a new therapeutic era. Gene Ther, 24, 529-533.*

*Tarantal, A.F., Lee, C.C.I., Martinez, M.L., Asokan, A. & Samulski, R.J. 2017. Systemic and Persistent Muscle Gene Expression in Rhesus Monkeys with a Liver De-Targeted Adeno-Associated Virus Vector. Human Gene Therapy, 28, 385-+.*

*Thermo Fisher. 2020. CellEvent™ Caspase-3/7 Green Detection Reagent [Online]. Available: https://www.thermofisher.com/order/catalog/product/C10423#/C10423 [Accessed 1st June 2020.*

*Thomsen, D.R., Stenberg, R.M., Goins, W.F. & Stinski, M.F. 1984. Promoter-regulatory region of the major immediate early gene of human Cytomegalovirus. . Proceedings of the National Academy of Sciences of the United States of America-Biological Sciences, 81, 659-663.*

*Tierney, J.F., Stewart, L.A., Ghersi, D., Burdett, S. & Sydes, M.R. 2007. Practical methods for incorporating summary time-to-event data into meta-analysis. Trials, 8.*

*Touznik, A., Maruyama, R., Hosoki, K., Echigoya, Y. & Yokota, T. 2017. LNA/DNA mixmer-based antisense oligonucleotides correct alternative splicing of the SMN2 gene and restore SMN protein expression in type 1 SMA fibroblasts. Sci Rep, 7, 3672.*

*Touznik, A., Maruyama, R. & Yokota, T. 2018. In Vitro Evaluation of Antisense-Mediated Exon Inclusion for Spinal Muscular Atrophy. Methods Mol Biol, 1828, 439-454.*

*Tsai, L.K., Chen, C.L., Ting, C.H., Lin-Chao, S., Hwu, W.L., Dodge, J.C., Passini, M.A. & Cheng, S.H. 2014. Systemic administration of a recombinant AAV1 vector encoding IGF-1 improves disease manifestations in SMA mice. Mol Ther, 22, 1450-1459.*

*Ulloa, F. & Briscoe, J. 2007. Morphogens and the control of cell proliferation and patterning in the spinal cord. Cell Cycle, 6, 2640-2649.*

*Umegaki-Arao, N., Pasmooij, A.M.G., Itoh, M., Cerise, J.E., Guo, Z.Y., Levy, B., Gostynski, A., Rothman, L.R., Jonkman, M.F. & Christiano, A.M. 2014.*

*Induced pluripotent stem cells from human revertant keratinocytes for the treatment of epidermolysis bullosa. Science Translational Medicine, 6, 10.*

*Vaidya, S. & Boes, S. 2018. Measuring quality of life in children with spinal muscular atrophy: a systematic literature review. Quality of Life Research, 27, 3087-3094.*

*Valori, C.F., Ning, K., Wyles, M., Mead, R.J., Grierson, A.J., Shaw, P.J. & Azzouz, M. 2010. Systemic delivery of scAAV9 expressing SMN prolongs survival in a model of spinal muscular atrophy. Sci Transl Med, 2, 35ra42.*

*Van Alstyne, M. 2020. Gain of Toxic Function by Long-Term SMN Overexpression in the Mouse Motor Circuit. Cure SMA Research and Clinical Care Virtual Meeting. Virtual.*

*Van Der Bent, M.L., Da Silva, O.P., Van Luijk, J., Brock, R. & Wansink, D.G. 2018. Assisted delivery of antisense therapeutics in animal models of heritable neurodegenerative and neuromuscular disorders: a systematic review and meta-analysis. Scientific Reports, 8.*

*Vera, E. & Studer, L. 2015. When rejuvenation is a problem: challenges of modeling late-onset neurodegenerative disease. Development, 142, 3085-3089.*

*Verma, I.M. & Weitzman, M.D. 2005. Gene therapy: twenty-first century medicine. Annual Review of Biochemistry, 74, 711-738.*

*Vesterinen, H.M., Sena, E.S., Egan, K.J., Hirst, T.C., Churolov, L., Currie, G.L., Antonic, A., Howells, D.W. & Macleod, M.R. 2014. Meta-analysis of data from animal studies: A practical guide. Journal of Neuroscience Methods, 221, 92-102.*

*Vicario-AbejóN, C., FernáNdez-Moreno, C., Pichel, J.G. & De Pablo, F. 2004. Mice lacking IGF-I and LIF have motoneuron deficits in brain stem nuclei. Neuroreport, 15, 2769-2772.*

*Vigna, E. & Naldini, L. 2000. Lentiviral vectors: excellent tools for experimental gene transfer and promising candidates for gene therapy. Journal of Gene Medicine, 2, 308-316.*

*Villalon, E., Kline, R.A., Smith, C.E., Lorson, Z.C., Osman, E.Y., O'day, S., Murray, L.M. & Lorson, C.L. 2019. AAV9-Stathmin1 gene delivery improves disease phenotype in an intermediate mouse model of spinal muscular atrophy. Human Molecular Genetics, 28, 3742-3754.*

*Viollet, L., Bertrandy, S., Bueno Brunialti, A.L., Lefebvre, S., Burlet, P., Clermont, O., Cruaud, C., Guenet, J., Munnich, A. & Melki, J. 1997. cDNA isolation, expression and chromosomal localisation of the mouse surival motor neuron gene (Smn). Genomics, 40, 185-188.*

*Vyas, S., Bechade, C., Riveau, B., Downward, J. & Triller, A. 2002. Involvement of survival motor neuron (SMN) protein in cell death. Human Molecular Genetics, 11, 2751-2764.*

*Waddington, S.N., Kennea, N.L., Buckley, S.M.K., Gregory, L.G., Themis, M. & Coutelle, C. 2004. Fetal and neonatal gene therapy: benefits and pitfalls. Gene Therapy, 11, S92-S97.*

*Waddington, S.N., Kramer, M.G., Hernandez-Alcoceba, R., Buckley, S.M.K., Themis, M., Coutelle, C. & Prieto, J. 2005. In utero gene therapy: current challenges and perspectives. Molecular Therapy, 11, 661-676.*

*Waldman, Y.Y., Tuller, T., Shlomi, T., Sharan, R. & Ruppin, E. 2010. Translation efficiency in humans: tissue specificity, global optimization and differences between developmental stages. Nucleic Acids Research, 38, 2964-2974.*

*Walker, C., Herranz-Martin, S., Karyka, E., Liao, C.Y., Lewis, K., Elsayed, W., Lukashchuk, V., Chiang, S.C., Ray, S., Mulcahy, P.J., Jurga, M., Tsagakis, I., Iannitti, T., Chandran, J., Coldicott, I., De Vos, K.J., Hassan, M.K., Higginbottom, A., Shaw, P.J., Hautbergue, G.M., Azzouz, M. & El-Khamisy, S.F. 2017. C9orf72 expansion disrupts ATM-mediated chromosomal break repair. Nature Neuroscience, 20, 1225-+.*

*Walter, L.M., Deguise, M.O., Meijboom, K.E., Betts, C.A., Ahlskog, N., Van Westering, T.L.E., Hazell, G., Mcfall, E., Kordala, A., Hammond, S.M., Abendroth, F., Murray, L.M., Shorrock, H.K., Prosdocimo, D.A., Haldar, S.M., Jain, M.K., Gillingwater, T.H., Claus, P., Kothary, R., Wood, M.J.A. & Bowerman, M. 2018. Interventions Targeting Glucocorticoid-Kruppel-like Factor 15-Branched-Chain Amino Acid Signaling Improve Disease Phenotypes in Spinal Muscular Atrophy Mice. EBioMedicine, 31, 226-242.*

*Wan, H.W.Y., Carey, K.A., D'silva, A., Vucic, S., Kiernan, M.C., Kasparian, N.A. & Farrar, M.A. 2020. Health, wellbeing and lived experiences of adults with SMA: a scoping systematic review. Orphanet Journal of Rare Diseases, 15.*

*Wang, D., Tai, P.W.L. & Gao, G.P. 2019. Adeno-associated virus vector as a platform for gene therapy delivery. Nature Reviews Drug Discovery, 18, 358-378.*

*Wang, J. & Dreyfuss, G. 2001. A cell system with targeted disruption of the SMN gene - Functional conservation of the SMN protein and dependence of gemin2 on SMN. Journal of Biological Chemistry, 276, 9599-9605.*

*Warnock, J.N., Daigre, C. & Al-Rubeai, M. 2011. Introduction to Viral Vectors. Methods in Molecular Biology. Clifton, N.J.*

*Werdnig, G. 1890. Ueber einem Fall von Dystrophiae musculorum mit positivenen Ruckenmakefunde. Wien Med Wochenschr, 40, 1798.*

*Wijngaarde, C.A., Blank, A.C., Stam, M., Wadman, R.I., Van Den Berg, L.H. & Van Der Pol, W.L. 2017. Cardiac pathology in spinal muscular atrophy: a systematic review. Orphanet Journal of Rare Diseases, 12.*

*Wishart, T.M., Mutsaers, C.A., Riessland, M., Reimer, M.M., Hunter, G., Hannam, M.L., Eaton, S.L., Fuller, H.R., Roche, S.L., Somers, E., Morse, R., Young, P.J., Lamont, D.J., Hammerschmidt, M., Joshi, A., Hohenstein, P., Morris, G.E., Parson, S.H., Skehel, P.A., Becker, T., Robinson, I.A., Becker, C.G., Wirth, B. & Gillingwater, T.H. 2014. Dysregulation of ubiquitin homeostasis and β-catenin signaling promote spinal muscular atrophy. The Journal of Clinical Investigation, 124, 1821-1834.*

*Wolstencroft, E.C., Mattis, V., Bajer, A.A., Young, P.J. & Lorson, C.L. 2005. A non-sequence-specific requirement for SMN protein activity: the role of aminoglycosides in inducing elevated SMN pro- tein levels. Human Molecular Genetics, 14, 1199-1210.*

*Workman, E., Kalda, C., Patel, A. & Battle, D.J. 2015. Gemin5 Binds to the Survival Motor Neuron mRNA to Regulate SMN Expression. Journal of Biological Chemistry, 290, 15662-15669.*

*Yajima, H., Lee, K.J., Zhang, S.C., Kobayashi, J. & Chen, B.P.C. 2009. DNA Double-Strand Break Formation upon UV-Induced Replication Stress Activates ATM and DNA-PKcs Kinases. Journal of Molecular Biology, 385, 800-810.*

*Yáñez-Muñoz, R.J., Balaggan, K.S., Macneil, A., Howe, S.J., Schmidt, M., Smith, A.J., Buch, P., Maclaren, R.E., Anderson, P.N., Barker, S.E., Duran, Y., Bartholomae, C., Von Kalle, C., Heckenlively, J.R., Kinnon, C., Ali, R.R. & Thrasher, A.J. 2006. Effective gene therapy with nonintegrating lentiviral vectors. Nature Medicine, 12, 348-53.*

*Yi, H., Xie, B., Liu, B., Wang, X., Xu, L., Liu, J., Li, M., Zhong, X. & Peng, F. 2018. Derivation and Identification of Motor Neurons from Human Urine-Derived Induced Pluripotent Stem Cells. Stem Cells International, 3628578.*

*Yoshida, M., Kitaoka, S., Egawa, N., Yamane, M., Ikeda, R., Tsukita, K., Amano, N., Watanabe, A., Morimoto, M., Takahashi, J., Hosoi, H., Nakahata, T., Inoue, H. & Saito, M.K. 2015. Modeling the Early Phenotype at the Neuromuscular Junction of Spinal Muscular Atrophy Using Patient-Derived iPSCs. Stem cell reports, 4, 561-568.*

*Young, P.J., Day, P.M., Zhou, J., Androphy, E.J., Morris, G.E. & Lorson, C.L. 2002. A direct interaction between the survival motor neuron protein and p53 and its relationship to spinal muscular atrophy. Journal of Biological Chemistry, 277, 2852-2859.*

*Young, P.J., Man, N.T., Lorson, C.L., Le, T.T., Androphy, E.J., Burghes, A.H.M. & Morris, G.E. 2000. The exon 2b region of the spinal muscular atrophy protein, SMN, is involved in self-association and SIP1 binding. Human Molecular Genetics, 9, 2869-2877.*

*Yu, J., Vodyanik, M.A., Smuga-Otto, K., Antosiewicz-Bourget, J., Frane, J.L., Tian, S., Nie, J., Jonsdottir, G.A., Ruotti, V., Stewart, R., Slukvin, I.I. & Thomson, J.A. 2007. Induced pluripotent stem cell lines derived from human somatic cells. Science, 318, 1917-1920.*

*Zhang, H.L.L., Pan, F., Hong, D., Shenoy, S.M., Singer, R.H. & Bassell, G.J. 2003. Active transport of the survival motor neuron protein and the role of exon-7 in cytoplasmic localization. Journal of Neuroscience, 23, 6627-6637.*

*Zhang, Q.J., Li, J.J., Lin, X., Lu, Y.Q., Guo, X.X., Dong, E.L., Zhao, M., He, J., Wang, N. & Chen, W.J. 2017. Modeling the phenotype of spinal muscular atrophy by the direct conversion of human fibroblasts to motor neurons. Oncotarget, 8, 10945-10953.*

*Zhang, Z., Pinto, A.M., Wan, L., Wang, W., Berg, M.G., Oliva, I., Singh, L.N., Dengler, C., Wei, Z. & Dreyfuss, G. 2013. Dysregulation of synaptogenesis genes antecedes motor neuron pathology in spinal muscular atrophy. PNAS USA, 110, 19348-19353.*

*Zhou, H., Janghra, N., Mitrpant, C., Dickinson, R.L., Anthony, K., Price, L., Eperon, I.C., Wilton, S.D., Morgan, J. & Muntoni, F. 2013. A novel morpholino oligomer targeting ISS-N1 improves rescue of severe spinal muscular atrophy transgenic mice. Hum Gene Ther, 24, 331-42.*

*Zhou, H.Y., Meng, J.H., Malerba, A., Catapano, F., Sintusek, P., Jarmin, S., Feng, L., Ngoc, L.N., Sun, L.W., Mariot, V., Dumonceaux, J., Morgan, J.E., Gissen, P., Dickson, G. & Muntoni, F. 2020. Myostatin inhibition in combination with*

*antisense oligonucleotide therapy improves outcomes in spinal muscular atrophy. Journal of Cachexia Sarcopenia and Muscle.*

*Zhou, H.Y., Meng, J.H., Marrosu, E., Janghra, N., Morgan, J. & Muntoni, F. 2015. Repeated low doses of morpholino antisense oligomer: an intermediate mouse model of spinal muscular atrophy to explore the window of therapeutic response. Human Molecular Genetics, 24, 6265-6277.*

*Zhou, M.J., Hu, Z.Q., Qiu, L.Y., Zhou, T., Feng, M., Hu, Q., Zeng, B.T., Li, Z., Sun, Q.R., Wu, Y., Liu, X.H., Wu, L.Q. & Liang, D.S. Seamless Genetic Conversion of SMN2 to SMN1 via CRISPR/Cpf1 and Single-Stranded Oligodeoxynucleotides in Spinal Muscular Atrophy Patient-Specific Induced Pluripotent Stem Cells. Human Gene Therapy.*

*Zufferey, R., Donello, J.E., Trono, D. & Hope, T.J. 1999. Woodchuck hepatitis virus posttranscriptional regulatory element enhances expression of transgenes delivered by retroviral vectors. Journal of Virology, 73, 2886-2892.*

*Zwetsloot, P.P., Vegh, A.M.D., Jansen, S.J., Van Hout, G.P.J., Currie, G.L., Sena, E.S., Gremmels, H., Buikema, J.W., Goumans, M.J., Macleod, M.R., Doevendans, P.A., Chamuleau, S.a.J. & Sluijter, J.P.G. 2016. Cardiac Stem Cell Treatment in Myocardial Infarction: A Systematic Review and Meta-Analysis of Preclinical Studies. Circulation Research, 118, 1223-1232.*

# 10 Appendix: Products

## 10.1 Cell culture

| Item | Source | Catalogue number |
|---|---|---|
| DMEM+Glutamax media | Fisher Scientific | 12077549 |
| Trypsin | Fisher Scientific | 11570626 |
| M199 Earle's salts media | Thermo Fisher Scientific | 31150022 |
| Fetal bovine serum | Life Technologies | 10270106 |
| Gentamicin | Thermo Fisher Scientific | 15710049 |
| Penicillin/Streptomycin | Thermo Fisher Scientific | 15140122 |
| FGF2 | Miltenyi Biotech | 130-093-838 |
| EGF | Miltenyi Biotech | 130-093-825 |
| Non-essential amino acids | Fisher Scientific | 11350912 |
| Opti-MEM | Fisher Scientific | 10149832 |
| Invitrogen™ Lipofectamine™ 2000 Transfection Reagent | Fisher Scientific | 12313563 |

### 10.1.1 iPSC culture and MN differentiation

| Item | Source | Catalogue number |
|---|---|---|
| mTESR1 media | Stem Cell Technologies | 85850 |
| DMEM/F12 media | Fisher Scientific | 11574546 |
| Neurobasal media | Fisher Scientific | 11560426 |
| B27 supplement 50x | Fisher Scientific | 11500446 |
| N2 supplement 100x | Fisher Scientific | 11520536 |
| Antibiotic-antimycotic 100x | Fisher Scientific | 15240062 |
| β-mercaptoethanol 1000x | Thermo Fisher Scientific | 31350010 |
| Ascorbic Acid | Sigma | A92902-25G |
| Chir99021 | Tocris Bioscience | 4423 |
| Compound C | Merck | 171261 |
| Retinoic Acid | Sigma | R2625 |
| SAG | Enzo Life Sciences | ALX-270-426-M001 |
| Laminin | Thermo Fisher Scientific | 23017015 |
| BDNF | Thermo Fisher Scientific | PHC7074 |
| GDNF | Thermo Fisher Scientific | PHC7045 |

| | | |
|---|---|---|
| DAPT | Tocris Bioscience | 2634 |
| Rock inhibitor | Miltenyi Biotech | 130-106-538 |
| CNTF | Thermo Fisher Scientific | PHC7015 |
| IGF1 | Thermo Fisher Scientific | PHG0071 |
| Matrigel | Fisher Scientific | 11573560 |
| Accutase | Life Technologies | A1110501 |
| Poly-ornithine | Sigma | P4957 |
| SYTOX™ AADvanced dead cell stain | Fisher Scientific | 10287064 |

## 10.2 Production and titration of IDLVs

| **Item** | **Source** | **Catalogue number** |
|---|---|---|
| TE buffer | Qiagen | 1018456 |
| HyPure™ cell culture grade water | GE | SH30529.02 |
| DNaseI | Promega | M6101 |
| Polybrene | Sigma | H-9268 |
| SensiMix SYBR No-ROX Mix | Bioline | QT650-05 |

## 10.3 Molecular biology

| **Bacteriological reagent** | **Source** | **Catalogue number** |
|---|---|---|
| LB broth | Sigma | 85850 |
| Agar | Sigma | A5306 |
| Ampicillin Sodium salt | Sigma | A9518 |
| Kanamycin Sulfate | Thermo Fisher Scientific | 11815024 |
| SOC medium | Fisher Scientific | BP9740 |
| T4 DNA ligase | NEB | EL0014 |
| XL10 Gold Ultracompetent cells | Stratagene | 200314 |

| **Restriction enzyme** | **Source** | **Catalogue number** |
|---|---|---|
| *Sal*I | Promega | R605A |
| *Eco*RI | NEB | R0107L |
| *Xho*I | Promega | R616A |
| *Bam*HI | Promega | R602A |

| | | |
|---|---|---|
| *Dde*I | Promega | R6291 |
| *Eco*NI | NEB | R0521S |
| *Sac*II | NEB | R0157S |
| *Sph*I | NEB | R3182 |
| *Xba*I | Promega | R618A |
| *Nco*I | Promega | R651F |
| *Nde*I | NEB | R0111S |
| *Fsp*I | NEB | R0135S |

| **Molecular biology reagent** | **Source** | **Catalogue number** |
|---|---|---|
| GoTaq G2 Flexi DNA Polymerase | Promega | M780A |
| 5X Green GoTaq Flexi buffer | Promega | M891A |
| 5X Colourless GoTaq Flexi buffer | Promega | M890A |
| Primers | Sigma | N/A |
| dNTPs | Promega | U1240 |
| Hyperladders 25bp-1kb | Bioline | Assorted |
| Gene Rulers | Thermo Fisher Scientific | Assorted |
| Agarose | Bioline | BIO-41026 |
| SensiMix SYBR No-ROX Mix | Bioline | QT650-05 |
| DNeasy Blood and Tissue Kit | Qiagen | 69506 |
| QIAprep Spin Miniprep Kit | Qiagen | 27104 |
| EndoFree Plasmid Maxi Kit | Qiagen | 12362 |

## 10.4 Immunofluorescence staining

| **Item** | **Source** | **Catalogue number** |
|---|---|---|
| DAPI | Sigma | D9542-1MG |
| Normal goat serum | Fisher Scientific | PCN5000 |
| Fluoromount™ Aqueous mounting medium | Sigma | F4680 |

For antibodies used in immunofluorescence staining, please see section 2.1.4.2.

## 10.5 Protein analysis

| Item | Source | Catalogue number |
|---|---|---|
| DC protein assay | BioRad | 5000112 |
| BSA 2mg/ml standard | BioRad | 5000206 |
| RIPA buffer | Fisher Scientific | 10017003 |
| Halt Protease Inhibitor Cocktail, EDTA-Free | Thermo Fisher Scientific | 78437 |
| Phosphatase inhibitor cocktail 3 | Sigma | P0044 |
| 4x loading buffer | Thermo Fisher Scientific | NP0007 |
| Reducing agent | Thermo Fisher Scientific | NP0009 |
| Antioxidant | Thermo Fisher Scientific | NP0005 |
| NuPAGE™ Tris-Acetate SDS 20x running buffer | Thermo Fisher Scientific | LA0041 |
| NuPAGE™ 20x transfer buffer | Thermo Fisher Scientific | NP0006 |
| Mini-Protean 4-15% TGX pre-cast gels | BioRad | 4561083 |
| NuPAGE™ 3-8% Tris-Acetate pre-cast gels | Thermo Fisher Scientific | EA037BBOX |
| Amersham™ Protran™ premium nitrocellulose membrane (0.45µm) | Sigma | GE10600003 |
| Amersham™ Protran™ NC nitrocellulose membrane (0.2µm) | Fisher Scientific | *GE10600001* |
| Immobilon-FL PVDF membrane (0.45µm) | Merck Millipore | IPFL00010 |
| REVERT total protein stain and wash | LiCor | 926-11015 |
| Odyssey blocking buffer | LiCor | 927-40000D |
| PageRuler™ Plus Pre-stained Protein Ladder | Thermo Fisher Scientific | 26619 |
| HiMark™ Pre-stained Protein Standard | Thermo Fisher Scientific | LC5699 |

For antibodies used in western blots, please see section 2.1.4.1.